BAW-10227-A
February 2000

Evaluation of Advanced Cladding and Structural Material (M5) in PWR Reactor Fuel

FRAMATOME COGEMA FUELS

BAW-10227-A
February 2000

Evaluation of Advanced Cladding and Structural Material (M5) in PWR Reactor Fuel

Non Proprietary Version

by

David B. Mitchell
Bert M. Dunn

Framatome Cogema Fuels
3315 Old Forest Road
P.O. Box 10935
Lynchburg, Virginia 24506-0935

ACKNOWLEDGEMENTS

The authors would like to express their appreciation to J.P. Mardon, J. Thomazet, and G. Wissinger for significant technical contributions, and to M. Bale, G. Garner, B. Julien, T. Miles and A. Le Bourhis for their participation in the program that produced this document.

UNITED STATES
NUCLEAR REGULATORY COMMISSION
WASHINGTON, D.C. 20555-0001

February 4, 2000

Mr. T. A. Coleman, Vice President
Government Relations
Framatome Cogema Fuels
3315 Old Forest Road
P. O. Box 10935
Lynchburg, Virginia 24506-0935

SUBJECT: REVISED SAFETY EVALUATION (SE) FOR TOPICAL REPORT BAW-10227P: "EVALUATION OF ADVANCED CLADDING AND STRUCTURAL MATERIAL (M5) IN PWR REACTOR FUEL" (TAC NO. M99903)

Dear Mr. Coleman:

By letter dated December 14, 1999, the Nuclear Regulatory Commission (NRC) staff issued the SE for Framatome Topical Report BAW-10227P, "Evaluation of Advanced Cladding and Structural Material (M5) in PWR Reactor Fuel." Subsequently, Framatome informed the NRC staff that a statement in the SE related to Framatome's small-break loss-of-coolant accident (SBLOCA) and large-break loss-of-coolant accident (LBLOCA) methodologies had unintentionally restricted the methodologies application to M5. Section 7 of the December 14, 1999, SE states, "The limitations and conditions identified in past SEs for the Framatome SBLOCA and LBLOCA models continue to apply." The SE for Topical Report BAW-10166P, "BEACH - Best Estimate Analysis Core Heat Transfer - A Computer Program for Reflood Heat Transfer," Revision 2, dated August 13, 1990, concluded that for analysis where cladding swell exceeds 20 percent, but the fuel does not rupture, the user should justify the acceptability of the methodology. For M5 fuel, cladding swell greater than 20 percent can occur at the extremes of the calculations.

By letter dated January 14, 2000, Framatome provided additional information to justify applicability of the LOCA methodologies to approximately 57 percent cladding swell. The staff accepts that the previous limit of 20 percent cladding swell for Framatome LOCA methodologies may be raised to 57 percent, as is documented in the revised SE (Enclosed) for BAW-10227P. Revision bars denote the changes from the SE dated December 14, 1999. The attached SE also contains minor editorial changes, and clarifies the staff's review of Framatome's evaluation models as they incorporate the material properties of M5 fuel. The staff's review of Revision 4 to Topical Report BAW-10164, "RELAP5MOD2-B&W, An Advanced Computer Program for Light Water Reactor LOCA and Non-LOCA Transient Analysis," which was provided in your submittals dated April 23 and September 24, 1999, will be provided under a separate cover.

The staff has completed its review of the subject report submitted by Framatome Cogema Fuels (FCF) by letter dated September 30, 1997, and the additional information submitted by letters dated February 5, April 23, July 29, September 24, and October 20, 1999, and January 14, 2000. On the basis of our review, the staff finds the subject report to be acceptable for referencing in license applications to the extent specified and under the limitations stated in the enclosed SE.

Licensees who reference this topical report as part of fuel reload submittals should also submit exemption requests with regard to the provisions of 10 CFR 50.46, 10 CFR 50.44, and other applicable regulations that are relevant to particular fuel cladding materials.

The NRC staff will not repeat its review of the matters described in FCF Topical Report BAW-10227P, and found acceptable, when the report appears as a reference in license applications, except to ensure that the material presented applies to the specific plant involved. The NRC staff's acceptance applies only to the matters described in FCF Topical Report BAW-10227P.

In accordance with procedures established in NUREG-0390, the NRC staff requests that FCF publish accepted versions of the report, including the safety evaluation, in proprietary and non-proprietary forms within 3 months of receipt of this letter. The accepted versions shall incorporate this letter and the enclosed SE between the title page and the abstract and an -A (designating accepted) following the report identification symbol. The accepted versions shall also incorporate all communications between FCF and the NRC staff during this review.

Should our acceptance criteria or regulations change so that our conclusions as to the acceptability of the report are no longer valid, applicants referencing this topical report will be expected to revise and resubmit their respective documentation, or submit justification for the continued applicability of the topical report without revision of their respective documentation.

Sincerely,

Stuart A. Richards, Director
Project Directorate IV & Decommissioning
Division of Licensing Project Management
Office of Nuclear Reactor Regulation

Project No. 693

Enclosure: Safety Evaluation

cc w/encl: See next page

UNITED STATES
NUCLEAR REGULATORY COMMISSION
WASHINGTON, D.C. 20555-0001

REVISED SAFETY EVALUATION BY THE OFFICE OF NUCLEAR REACTOR REGULATION

TOPICAL REPORT BAW-10227P

"EVALUATION OF ADVANCED CLADDING AND STRUCTURAL MATERIAL (M5) IN PWR REACTOR FUEL"

FRAMATOME COGEMA FUELS, INC.

1.0 INTRODUCTION

Framatome Cogema Fuels (FCF) has submitted to the U.S. Nuclear Regulatory Commission (NRC) a topical report entitled "Evaluation of Advanced Cladding and Structural Material (M5) in PWR Reactor Fuel," BAW-10227P (Reference 1), for review and approval. This report provides the licensing basis for the FCF advanced cladding and structural material, designated M5, and requests full batch implementation of this material for their Mark-B (15X15 fuel array) fuel design for B&W type reactors, and Mark-BW (15X15 and 17X17 fuel arrays) designs for Westinghouse type reactors. This submittal further requests full batch implementation of this material up to the currently approved rod-average burnup level of 62 GWd/MTU for the Mark B design and 60 GWd/MTU for Mark BW designs (Reference 2).

It should be explained that Framatome Cogema Fuels was previously named the B&W Fuel Company (BWFC), a part of B&W Nuclear Technologies, and prior to BWFC was named Babcock & Wilcox (B&W). Some of the references in this safety evaluation (SE) refer to these different company names depending on the date the reference was generated.

Pacific Northwest National Laboratory (PNNL) has acted as a consultant to the NRC in this review. As a result of the NRC staff's and their PNNL consultants' review of the topical report, the NRC sent a two-part list of questions to FCF. The first part (Reference 3) addressed Sections 1 through 6 and Appendices A and B of the report that discussed M5 properties and models generally associated with normal operation. The second list of questions (Reference 4) addressed Appendices C, D, E, and G of the report that discussed cladding rupture, ballooning, flow blockage, and high temperature oxidation models used in loss-of-coolant accident (LOCA) analyses. Both sets of questions (References 3 and 4) requested additional data that support the M5 material property and cladding performance models, additional information about the data provided, assumptions used in model development, and to provide example licensing analyses. FCF partially responded to the first list of questions in Reference 5 and provided the remaining responses to the second list in Reference 6. FCF submitted a revised M5 creep model in Reference 7. FCF also supplied additional information (Reference 8) to support their responses to questions for some of the original request for additional information (RAI). In Reference 9, FCF supplied information on their new axial growth methodology and a commitment to obtain additional M5 data up to currently approved burnup levels.

This report consists of nine sections, Section 1 - Introduction, Section 2 - M5 Material Properties, Section 3 - Fuel System Damage, Section 4 - Fuel Rod Failure, Section 5 - Fuel Coolability, Section 6 - Fuel Surveillance, Section 7- M5 LOCA Evaluation, Section 8 - Conclusions, and Section 9 - References. Section 2, as the title implies, addresses the M5 material properties, while Sections 3, 4, 5, 6, and 7 address licensing requirements identified in Section 4.2 of the Standard Review Plan (SRP) (Reference 10) for fuel designs. Some of the licensing requirements identified in Section 4.2 of the SRP require fuel performance properties or models be used to demonstrate that design criteria or limits are met. Therefore, subsections of Section 2 will refer to Sections 3, 4, 5, 6, and 7 and vice versa.

Section 4.2 of the SRP states that fuel system safety review must provide assurance that (1) the fuel system is not damaged as a result of normal operation and anticipated operational occurrences (AOOs), (2) fuel system damage is never so severe as to prevent control rod insertion when it is required, (3) the number of fuel rod failures is not underestimated for postulated accidents, and (4) coolability is always maintained. A "not damaged" fuel system is defined as fuel rods that do not fail, fuel system dimensions that remain within operational tolerances, and functional capabilities that are not reduced below those assumed in the safety analysis. Objective 1, above, is consistent with General Design Criterion (GDC) 10 (10 CFR Part 50, Appendix A) (Reference 11), and the design limits that accomplish this are called specified acceptable fuel design limits (SAFDLs). "Fuel rod failure" means that the fuel rod leaks and that the first fission product barrier (the cladding) has, therefore, been breached. However, the staff recognizes that it is not possible to avoid all fuel rod failures during normal operation, and reactor coolant cleanup systems are installed to deal with a small number of leaking rods. Fuel rod failures must be accounted for in the dose analysis required by 10 CFR Part 100 (Reference 12) for postulated accidents. "Coolable geometry" means, in general, that the fuel assembly retains its rod-bundle geometrical configuration with adequate coolant channels to permit removal of residual heat for a design-basis accident. The general requirements to maintain control rod insertability and core coolability appear repeatedly in the GDC (e.g., GDC 27 and 35). Specific coolability requirements for the LOCA are given in 10 CFR Part 50, Section 50.46 (Reference 13).

In order to assure that the above stated objectives are met, and to follow the format of Section 4.2 of the SRP, Sections 3, 4, and 5 of this SE cover the following three major categories: (1) fuel system damage mechanisms, which are most applicable to normal operation and AOOs, (2) fuel rod failure mechanisms, which apply to normal operation, AOOs, and postulated accidents, and (3) fuel coolability, which are applied to postulated accidents. Specific fuel damage or failure mechanisms are identified under each of these categories in Section 4.2 of the SRP. This SE discusses, under each fuel damage or failure mechanism listed in the SRP, the FCF design limits, analysis methods and data used to demonstrate that the SAFDLs are met up to the rod-average burnup levels of 62 GWd/MTU for Mark B and 60 GWd/MTU for Mark BW designs.

The purpose of the FCF design criteria or limits (defined in Reference 14) is to provide limiting values that prevent fuel damage or failure and fuel coolability/control rod insertability for postulated accidents with respect to each mechanism. The FCF design criteria remain the same as defined in Reference 14 for fuel designs with the M5 alloy. The staff reviewed whether FCF has adequate data to demonstrate that fuel designs using M5 cladding and structural

material can operate satisfactorily up to rod-average burnups of 62 GWd/MTU for Mark B and 60 GWd/MTU for Mark BW designs as defined by the SAFDLs for normal operation, AOOs and postulated accidents.

Section 7.0 of this SE addresses the changes to the emergency core cooling system (ECCS) evaluation models to account for M5 cladding. This section covers calculated results, sensitivities, and compliance with 10 CFR 50.46.

2.0 M5 MATERIAL PROPERTIES

The M5 material properties addressed in this section are in general, applicable to properties under normal operation and AOOs, but some such as fuel thermal conductivity, thermal expansion, heat capacity, $\alpha \rightarrow \beta$ phase transformation, and emissivity up to fuel melting are also applicable to design basis accidents. Other properties that are unique to accident conditions, such as cladding rupture, ballooning, flow blockage, and high temperature oxidation, are addressed in Sections 4 and 5 of this SE. The properties addressed in this section, along with FCF analysis methodology, are used to demonstrate that FCF fuel designs meet the SAFDLs defined in Sections 3, 4, and 5 of this SE.

2.1 Specific Gravity (Density)

The FCF value for specific gravity of the M5 alloy is interpolated from the measured values reported for pure reactor grade zirconium and that reported for the zirconium - 2.5 percent niobium alloy. The specific gravity for these two materials are within 10 percent of each other and, therefore, little change in specific gravity is expected. In addition, a 1 or 2 percent error in the specific gravity will not impact fuel performance analyses and, therefore, the interpolated values are satisfactory. The NRC staff concludes that the FCF value for M5 specific gravity is acceptable for M5 licensing applications up to currently approved burnup levels.

2.2 Coefficient of Thermal Expansion

FCF has proposed (Reference 6) a different coefficient of thermal expansion for M5 cladding than presented in the original submittal (Reference 1) based on new FCF dilatometry measurements in the radial, azimuthal, and axial directions with a reference point of 20°C (Reference 8). These results demonstrate that there is a small difference from Zr-4 and a larger difference in contraction in the $\alpha+\beta$ phase region. The $\alpha+\beta$ region is the phase transition region where both α and β phases are present, while $\alpha \rightarrow \beta$ represents the α to β phase transformation process. Due to the contraction in the $\alpha+\beta$ phase region there is a significant change in slope of the expansion coefficient in this region that once again changes to a more positive slope when the β phase transition is complete. Examination of the FCF data and correlations for M5 expansion demonstrates that the M5 correlation for expansion in the α and β phase regions matches the data very well, but the transition point between the α phase and the $\alpha+\beta$ phase is not consistent with the new revised FCF $\alpha \rightarrow \beta$ phase transformation temperatures (see Section 2.17 of this SE). The FCF correlation for M5 thermal expansion shows the $\alpha \rightarrow \beta$ phase transition beginning at a temperature approximately 60°C before the new proposed FCF phase transformation temperature for the start of the $\alpha \rightarrow \beta$ phase region. The M5 expansion model cannot be correct if the FCF $\alpha \rightarrow \beta$ phase transformation temperature is correct.

This is not a problem for fuel performance analyses at normal cladding operating temperatures but is an issue for transients that achieve high cladding temperatures such as for LOCA, i.e., that reach the α-β phase transformation temperatures.

The staff asked FCF about this inconsistency and what the impact would be on LOCA analyses, based on the current FCF assumption that the cladding contracts 60°C below the actual point of contraction. FCF responded that this would have a very small impact on the LOCA analyses because this will only change the gap size by a very small amount and in turn the gap conductance by a very small amount. The NRC staff agrees that the impact on LOCA analyses is small.

The NRC staff concludes that the FCF correlation for M5 thermal expansion (Reference 6) is acceptable for M5 licensing applications up to currently approved burnup levels.

2.3 Thermal Conductivity

The thermal conductivity relationship submitted in Reference 1 was modified in the first response to questions (Reference 5) because additional data became available. However, Reference 5 did not provide the data used for supporting the new modified thermal conductivity relationship. The staff asked FCF to supply this new data, and FCF provided it in Reference 8. The FCF data demonstrated that the modified relationship given in References 5 and 8 was a satisfactory representation of measured M5 thermal conductivity similar to the relationship used for Zircalloy-4 (Zr-4). Therefore, the NRC staff concludes that the modified thermal conductivity relationship in References 5 and 8 is acceptable for M5 licensing applications up to currently approved burnup levels.

2.4 Heat Capacity

The heat capacity relationship submitted in Reference 1 was modified in Reference 6 based on proprietary data from Commissariat a l'Energie Atomique (CEA) testing in the α and β region for M5 material, and Russian open literature data (References 15, 16, and 17) from material similar to M5. The FCF correlation for heat capacity in the α region is based on the average of the Russian and CEA data. The FCF correlation for heat capacity in the β region is based on combining the average of the Russian data with the average of the CEA data. The average of the two data sets were used to determine the mean heat capacity in the β region in order to provide equal weighting between the two data sources (CEA and Russian).

The heat capacity in the α+β region was determined from the CEA measured data in this temperature range. The uncertainty in M5 heat capacity in these three temperature ranges is approximately 8 percent. Since the uncertainty in M5 heat capacity is considered in the safety analyses, the NRC staff concludes that the FCF heat capacity correlations for M5 are acceptable for licensing analyses with M5 cladding up to currently approved burnup levels.

2.5 Emissivity

The emissivity for M5 does not change much within the temperature range of interest for LOCA and safety analyses and, therefore, is represented as a constant value, as is currently the case for Zr-4. Reference 1 stated there was little difference between Zr-4 and M5 emissivity. However, Reference 6 states that the emissivity value for M5 material is larger than for Zr-4 based on recent data. The staff examined the data and found the new M5 emissivity value to be a satisfactory representation of M5 emissivity, which varies a small amount within the temperature range of application. Because cladding radiation heat transfer is not a dominant mechanism for a fuel rod and the variation of emissivity within the range of application is small, the use of the FCF constant value of cladding emissivity on LOCA and safety analyses is acceptable. The NRC staff concludes that the Reference 6 value for emissivity is acceptable for licensing applications with M5 cladding up to currently approved burnup levels.

2.6 Oxidation

The M5 application that results in the most severe oxidation environment for both normal operation and accident operation is the fuel cladding. Cladding oxidation for normal operation and LOCA is discussed in Sections 3.4 and 5.1, respectively.

2.7 Ultimate Tensile Strength

The ultimate tensile strength (UTS) is used by FCF to determine the stress intensity limits for the assembly guide thimbles for seismic-LOCA and other assembly loading analyses based on guidelines established in Section III of the American Society of Mechanical Engineers (ASME) Boiler & Pressure Vessel Code (Reference 18). FCF was asked to provide the M5 UTS correlation with temperature used for licensing analyses and a comparison to data. These were provided in Reference 8 and demonstrated that the M5 axial UTS correlation conservatively bounds the unirradiated M5 data. The M5 UTS increases significantly (a factor of 1.4 to 1.9) and quickly with burnup (less than 10 GWd/MTU) compared to the unirradiated values. The use of unirradiated M5 UTS offers additional conservatism in FCF analyses. The NRC staff concludes that the FCF unirradiated UTS bounding correlation is conservative and, therefore, acceptable for licensing applications with M5 cladding up to currently approved burnup levels.

2.8 Yield Strength (0.2 Percent Offset)

The Reference 1 model for predicting M5 yield strength (0.2 percent offset) is based on unirradiated cladding data and was found to overpredict the unirradiated M5 data by up to 10 percent within given temperature ranges used for FCF analyses. A new yield strength model, provided in Reference 8, was found to be in much better agreement with, or conservative with relation to, the unirradiated M5 yield strength data. In general, the use of unirradiated values for yield strength is conservative for determining the cladding stress limits that are discussed in Sections 3.1 and 5.4 of this SE. This is because yield stress values for recrystalized zirconium base alloys increase by nearly a factor of 2 or greater following short term irradiation. FCF has provided measurements of M5 yield strength as a function of burnup that demonstrates it increases by a factor of 3 or more compared to unirradiated values within less than 10 GWd/MTU burnup. It is concluded that the FCF model for unirradiated yield

strength is very conservative for determining in-reactor M5 strength. The NRC staff concludes that the FCF unirradiated yield strength correlation is acceptable for licensing applications with M5 cladding up to currently approved burnup levels.

2.9 Ductiltity

Cladding ductility needs to be retained to avoid brittle failures. Generally, irradiation and hydride formation (due to corrosion) have been found to decrease the ductility of zirconium alloys (References 19, 20, and 21). The NRC does not have a specific minimum limit on cladding ductility; however, Section 4.2 of the SRP (Reference 10) suggests a limit for total (elastic + plastic) cladding uniform strain of 1 percent that should not be exceeded during normal operation and AOOs. Therefore, the SRP would suggest a minimum total strain capability of at least 1 percent in order to prevent cladding failure below the 1 percent strain limit.

FCF was asked (Reference 3) to supply measured strains from tensile and burst tests of both unirradiated and irradiated M5 cladding. FCF supplied (Reference 5) the requested data for unirradiated cladding and cladding that was irradiated to fuel rod burnups of 10, 20, and 38 GWd/MTU. The tensile data demonstrated reasonably high strains compared to Zr-4 strain data. The biaxial burst test data demonstrated that uniform plastic strains were below 1 percent for the irradiated M5 cladding with only one data point for total elongation strain and this datum was above 1 percent strain. The uniform strains from both the tensile and biaxial tests do not appear to decrease with increasing burnup but appeared to be uniform within the burnup range of the data, i.e., 10 to 38 GWd/MTU. In addition, further M5 burst strain data have recently been obtained by FCF at a rod-average burnup of 43 GWd/MTU that is consistent with the lower burnup FCF strain data for M5. This suggests that there is no further decrease in ductility with burnup within the range of the FCF data for M5. The M5 uniform strains from the biaxial tests are on average lower than those observed on similar Zr-4 test specimens at similar burnup levels but they are within the lower bounds of the Zr-4 data. In addition, the biaxial ultimate tensile strengths for the irradiated cladding were only slightly higher than the measured yield strengths indicating that total strains were low. The staff asked FCF why total elongation strain was measured on only one irradiated burst test specimen, and also asked FCF to provide micrographs of the fracture surfaces at high magnification to demonstrate ductility in the failure location. FCF responded that they had difficulty in measuring total strains on these burst specimens and did not have any high magnifications of the failure surfaces of these specimens.

FCF noted that the burst tests of the M5 cladding demonstrated total (elastic + plastic) uniform strain capability greater than 1 percent using the measured yield strengths for this data and, therefore, M5 meets the 1 percent strain limit suggested in the SRP. The NRC staff confirmed that the M5 burst test specimens met the 1 percent (elastic + plastic) strain limit by a small margin.

FCF was also asked (Reference 3) to supply in-reactor power ramp test data (including total measured strains) from irradiated rods with M5 cladding. FCF responded that they had performed 5 ramp tests (rods with burnups between 25 to 30 GWd/MTU) with some rods resulting in failure and others remaining intact. The failure threshold in terms of rod powers and delta power change for these rods were found to be similar to those observed for FCF Zr-4 fuel

rods. The plastic strains for the failed rods with M5 cladding were below 1 percent strain but the total (elastic + plastic) calculated strains remained above 1 percent. It is noted that low strains are also seen in power ramp tested Zr-4 rods because the cesium and iodine released during these power ramps promote cracking of the cladding on the inside surface. FCF was also asked to supply micrographs of the failure surfaces of the ramped rods as well. These micrographs were supplied and demonstrated a crack surface at the cladding inner-diameter but then quickly transformed to ductile cupping for the failure surface. This indicates that the irradiated M5 cladding remained ductile outside of the inner diameter (ID) surface.

The NRC staff concludes that the M5 cladding meets the 1 percent strain criterion of SRP Section 4.2, and remains ductile up to the burnup range of current data (43 GWd/MTU), but notes that FCF needs to collect M5 tensile and burst test data (including uniform strain, total strain, and micrographs of the fracture surfaces at high magnification) up to currently approved burnup levels of 60 and 62 GWd/MTU for FCF designs. FCF has committed to collecting this data up to currently approved burnup levels (see Section 6, FUEL SURVEILLANCE). FCF has further committed to inform the NRC if they find either of the following in these M5 mechanical tests; (1) total (elastic + plastic) uniform strains falling below 1 percent, or (2) the micrographs showing brittle failure surfaces (Reference 9).

The NRC staff concludes that the M5 alloy has acceptable ductility for fuel rod strain licensing analyses of M5 cladding up to currently approved burnup levels based on FCFs commitment to collect further M5 strain data up to approved burnup levels.

2.10 Creep

In Reference 1, FCF proposed using their old Zr-4 creep model with an adjustment multiplication factor (less than 1.0) for determining M5 material creep, with the M5 material showing lower overall creep than Zr-4. It is noted that the M5 creep data is currently only from 4 irradiated rods from one plant and further creep data are planned from future fuel exams of lead test assemblies (LTAs). FCF will use this revised Zr-4 creep model for determining M5 creep in their current fuel performance code, TACO-3 (Reference 22). TACO-3 code comparisons of predicted creep to the M5 creep data demonstrates a significant scatter in the data but is considered to be a satisfactory comparison for its intended application in TACO-3. Therefore, the modified Zr-4 model (with an adjustment factor) to predict the M5 cladding creep is considered to be satisfactory for fuel performance calculations in TACO-3. It is noted that FCF has recently submitted a new fuel performance code for NRC review that may have a more sophisticated M5 creep model.

For creep collapse analysis, FCF proposed (Reference 1) to continue to use their Zr-4 creep model for creep collapse (with no adjustment factors, e.g., a multiplication factor of 1.0) because they believed that this model would remain conservative for this application. However, FCF developed a new M5 creep model that was submitted in Reference 7. FCF discovered that the Zr-4 creep model was slightly less conservative than the new M5 creep model at moderate-to-high burnup levels for determining rod internal pressure limits (no fuel cladding gap reopening is allowed) and for cladding collapse analyses. The greater predicted creep in M5 at high burnups is due to the fact that the M5 creep data shows a smaller amount of in-reactor primary creep (transient) resulting in a larger secondary (steady-state) creep rate,

proportionately, than observed for their standard Zr-4 creep data and model. The secondary creep rate is important for both determining the FCF rod pressure limits (based on the limit for gap reopening) and cladding collapse for their fuel designs at high burnup levels. The new M5 creep model conservatively ignores primary creep by assuming that all the creep observed is secondary creep. This will typically result in an underprediction of cladding creep data early-in-life and an overprediction later-in-life which is conservative for determining the rod pressure limit and cladding collapse at high burnup levels. This new M5 creep model has been compared to the M5 creep data from the 4 irradiated rods and found to provide a small underprediction of the first cycle data (from two rods) and a larger overprediction of the second cycle data that demonstrates the conservatism in the M5 creep model at higher burnup levels. In addition, there were two creep data from two third cycle rods (measured at the fuel rod ends where the gap has not closed) that were significantly overpredicted by the new M5 model that further demonstrates the conservatism in the M5 creep model.

The standard error for this new M5 model was significantly smaller than the standard error for Zr-4 creep model, but the Zr-4 model was based on a much larger data base with rods from several different reactors. The standard error for the new M5 creep model is also significantly smaller than that for the Zr-4 model modified for M5 based on the limited M5 data. However, due to the small amount of M5 cladding creep data from which their new M5 creep model is based, FCF intends to continue to use the more conservative standard error based on the Zr-4 creep model and standard Zr-4 creep data for determining the upper bound uncertainty in M5 creep. FCF's conservative assumptions of no primary creep in their new M5 creep model and the use of the standard error from the standard Zr-4 model offers sufficient conservatisms for calculating the FCF rod pressure limits and cladding collapse. The previous approval of FCF's rod pressure analysis methodology (Reference 23) concluded that the conservatisms in the FCF fuel swelling model plus those in the creep model were sufficient to compensate for the potential difference between compressive versus tensile creep that has been proposed by others (References 24 and 25).

The NRC staff concludes that the use of the modified Zr-4 creep model (multiplication factor for M5) for modeling M5 creep in TACO-3 is acceptable for licensing applications with M5 cladding up to currently approved burnup levels. The NRC staff further concludes that the use of the new M5 creep model (Reference 7) and uncertainites (i.e, the uncertainties of the M5 model are assumed to be the same as those from the Zr-4 model and data) are acceptable for determining rod pressure limits (see Section 3.8 of this SE) and for cladding collapse (see Section 4.2 of this SE) licensing analyses with M5 cladding up to currently approved burnup levels.

2.11 Poisson's Ratio

FCF uses a constant value for Poisson's ratio with temperature that is consistent with the value used for Zr-4. The FCF constant value for Poisson's ratio has been compared to data for M5 and a similar Zr-1 percent Nb alloy and shown to agree well with this data (Reference 6). The NRC staff concludes that FCF's value of Poisson's ratio for M5 is acceptable for licensing applications with M5 cladding up to currently approved burnup levels.

2.12 Modulus of Elasticity

In Reference 1, FCF proposed that the Zircaloy correlations for modulus of elasticity used in RELAP5 (Reference 26) and TACO-3 (Reference 22) be used for the M5 alloy. The difference in elastic modulus between Zircaloy and M5 materials is expected to be similar. However, FCF submitted a new correlation for M5 modulus of elasticity in References 5 and 8 with measured data up to 350 °C. This new M5 correlation is intended to be used in both the RELAP5 and TACO-3 codes, where the former is used for accident analyses (LOCA) and the latter for analyses related to normal operation and AOOs.

PNNL's comparison between FCF's correlation to that recommended in MATPRO-11 (Reference 27) for Zr-4 demonstrated very good agreement up to 400 °C and then started to become slightly larger with a higher value at 1000 °C than the MATPRO Zircaloy correlation. This higher value is within the scatter of the data for Zircalloy's modulus of elasticity and is considered to be acceptable. In addition, for the maximum temperatures used for LOCA analyses, the elastic strains are small compared to either thermal expansion strains in the 700°C to 1000°C range or strain due to plastic deformation in the 1000°C to 1200°C range. Therefore, a small variation in modulus of elasticity has a negligible impact on LOCA analysis results. The impact of the modulus of elasticity is of greater significance at normal operating reactor temperatures; in this region the M5 modulus of elasticity is nearly identical to the MATPRO Zircaloy correlation. The NRC staff concludes that the M5 modulus of elasticity correlation proposed in References 5 and 8 is acceptable for licensing applications with M5 cladding up to currently approved burnup levels.

2.13 Hardness (Meyer's)

Meyer hardness is used in calculating the contact conductance between the fuel and cladding when the fuel-to-cladding gap is closed. FCF utilizes the MATPRO-11 (Reference 27) correlation for Zircaloy-4 Meyer hardness for the M5 alloy. Generally, the Meyer hardness of an alloy is related to the yield strength of the alloy. The M5 alloy has a significantly lower unirradiated yield strength than Zr-4 but hardens quickly with irradiation. The M5 irradiated yield strength in the tensile direction is nearly 70 percent of that for irradiated Zr-4 and similar to Zr-4 for the biaxial pressure tests. Therefore, the Meyer hardness for irradiated M5 cladding is most likely a little lower than for irradiated Zr-4 cladding. The consequence of having an overprediction of Meyer hardness for M5 cladding would be a lower contact conductance and higher fuel temperatures. For those analyses where contact conductance occurs higher fuel temperatures result in more conservative results. The NRC staff concludes that the FCF correlation for Meyer hardness is conservative and, therefore, acceptable for licensing applications with M5 cladding up to currently approved burnup levels.

2.14 Growth

Generally both fuel assembly and fuel rod growth have been shown to be linear with fast fluence (E> 1 mev) for Zr-4 and Zr-2 alloys and similar behavior is expected for the M5 alloy; however, as noted below the M5 fuel rod growth appears to saturate at high fluences (greater than 8×10^{21} n/cm^2) based on a limited data base.

M5 guide tube/thimble (assembly) growth needs to be evaluated to prevent the assembly holddown springs from bottoming out that would result in assembly and fuel rod bowing (see Section 3.7 of this SE). FCF has presented upper tolerance and lower tolerance limits (UTL and LTL, respectively) for both Zr-4 and M5 assembly (guide tube/thimble) growth. FCF has over 80 assembly measurements of assembly growth with Zr-4 guide tubes for assembly burnups up to 58 GWd/MTU. Currently, FCF has only two data points for M5 guide tube growth at an assembly burnup of 22 GWd/MTU. The UTL curve for M5 assembly growth is very conservative compared to the two data points while the LTL curve is adequately conservative. FCF has committed to collecting further assembly growth data for M5 guide tubes in North Anna up to currently approved burnup levels (see Section 6, FUEL SURVEILLANCE). The NRC staff concludes that the M5 guide tube/thimble (assembly) growth model is acceptable for licensing applications with M5 guide tubes/thimbles up to currently approved burnup levels based on FCFs commitment to collect further M5 assembly growth data up to approved burnup levels. M5 cladding irradiation axial growth needs to be considered in the TACO 3 fuel performance code (Reference 22). FCF presented a correlation for rod growth as a function of burnup with upper and lower bounds along with measured rod growth data up to a fluence of approximately 10×10^{21} n/cm^2 (E> 1 MeV) (this fluence translates to a burnup of approximately 52 GWd/MTU). Another datum point with a fluence of 11.8×10^{21} n/cm^2 (burnup of 61 GWd/MTU), which was added to this rod growth data in Reference 5, lies significantly below the mean of the M5 growth curve. Based on the limited amount of data (7 to 9 data) to date above a fast fluence of 8×10^{21} n/cm^2 there appears to be a saturation in the M5 growth. This would suggest that FCF's upper bound for axial growth is indeed bounding up to 61 GWd/MTU. The NRC staff concludes that the M5 fuel rod (cladding) growth model is acceptable for licensing applications with M5 cladding up to currently approved burnup levels.

2.15 Hydrogen Pickup Fraction

In Reference 1, FCF provided a hydrogen pickup fraction that was more than a factor of 2 lower than that observed in Zr-4; however, the data only extended to a burnup of 38 GWd/MTU (with less than 20μm of oxide thickness) and showed a higher fraction at burnups greater than 20 GWd/MTU. FCF was asked (Reference 3) about the higher pickup fraction in the data at burnups greater than 20 GWd/MTU than the FCF assumed value in Reference 1. FCF responded (Reference 5) that the Reference 1 pickup fraction was based on early results of pickup fraction, and in Reference 5 FCF revised the pickup fraction upwards to a larger value, but was still considerably lower than the fraction measured for Zr-4 (0.15, Reference 28). The data in References 27 and 28 for Zr-4 demonstrated that the hydrogen pickup fraction continued to increase with increasing oxide thickness (and burnup) until a thickness between 50 and 60μm was achieved. The hydrogen pickup fraction for the M5 alloy may be lower than that observed for Zr-4, but based on past experience with Zr-4 the pickup fraction will increase with increasing oxide thickness until a thickness between 50 to 60μm is achieved. Currently, FCF has measured hydrogen content on cladding with only oxide thicknesses (less than 20μm). Considering the lack of data beyond 35 GWd/MTU, the NRC staff recommended that FCF continue collecting data and use a pickup fraction of 0.10, which is close to the maximum M5 pickup fraction, to compensate for the burnup effect. Based on FCF's commitment to collect further hydrogen pickup fraction data up to approved burnup levels (see Section 6, FUEL SURVEILLANCE), the NRC staff concludes that the hydrogen pickup fraction is acceptable for

use in licensing applications (see Section 4.1) with M5 cladding up to currently approved burnup levels.

2.16 Stress Corrosion Cracking

The NRC currently has no requirements related to stress corrosion cracking (SCC) of fuel assembly components other than the total uniform 1 percent strain limit discussed in Section 2.2 of this SE. However, FCF has performed SCC sensitivity testing on M5 and compared it to their Zr-4 material. The tests were out-of-reactor ring tensile tests with nearly constant strain rate on unirradiated cladding in a mixture of argon gas and iodine vapor. These tests demonstrated that the M5 alloy was less susceptible to SCC (higher ductility) than their standard Zr-4 alloy.

2.17 α-β Phase Transformation Temperatures

The α-β transformation temperatures are not listed by FCF as a separate material property for the M5 alloy. The transformation temperatures have been singled out in this review because of their importance in interpreting some M5 material properties (because these properties change during and following the transformation to the β phase) and behavior. Some of the M5 material properties that change are thermal expansion, heat capacity, rupture and ballooning. Therefore, it is important to know the temperature range of this phase transformation.

The NRC staff asked FCF about the α-β phase transformation temperatures provided in their original submittal (Reference 1), and the data from which the initiation and the completion of the transformation temperatures were obtained, because the phase change started at a lower temperature and completed at a higher temperature than had been previously observed for similar zirconium alloys. FCF responded (Reference 5) that they had since obtained better test data of the α-β transformation temperatures, and provided the new phase transformation temperatures, the data and testing methods. The newly revised FCF transformation temperatures agreed very well with other NRC proprietary information on similar zirconium alloys. The FCF test data also suggested that the initial transformation and completion of the transformation temperatures were dependent on the heating rate, i.e., the kinetics of the phase transformation impact the transformation temperatures. This shift to higher transformation temperatures is also observed in their cladding ballooning (strain) data and models (see Section 5.3). The NRC staff asked FCF about whether this should be explicitly modeled (currently it is implicitly modeled for LOCA ballooning because the effect is inherent in the data). FCF stated that while the data qualitatively demonstrates a kinetic effect on the transformation temperature, FCF currently does not have sufficient data to model the kinetics quantitatively. The NRC staff agrees with FCF's assessment of the data and modeling capabilities.

The NRC staff concludes that the FCF α-β transformation temperatures are acceptable for use in licensing applications with M5 cladding up to currently approved burnup levels.

3.0 FUEL SYSTEM DAMAGE

The design criteria presented in this section should not be exceeded during normal operation including AOOs. The evaluation portion of each damage mechanism evaluates the analysis

methods and analyses used by FCF to demonstrate that the design criteria are not exceeded during normal operation, including AOOs, for their Mark-B and Mark-BW designs.

3.1 Stress

Bases/Criteria - In keeping with the GDC 10 SAFDLs, fuel damage criteria for cladding stress should ensure that fuel system dimensions remain within operational tolerances and that functional capabilities are not reduced below those assumed in the safety analysis. The FCF design criteria for fuel rod cladding and assembly stresses are based on unirradiated yield and ultimate tensile strengths to determine the stress limits for all M5 applications. The M5 yield and ultimate tensile strengths are discussed in Sections 2.7 and 2.8 of this SE and found to be acceptable. The use of unirradiated values is conservative because irradiation has been shown to increase the yield and ultimate tensile strengths for M5 and other zirconium alloys. These criteria are consistent with the acceptance criteria established in Section 4.2 of the SRP and have been previously approved in Reference 14. The NRC staff concludes that these stress criteria are acceptable for licensing analyses with M5 cladding up to currently approved burnup levels.

Evaluation - The stress analyses for FCF fuel assembly components and fuel rod cladding are based on standard stress analysis methods including finite-element analysis. FCF will utilize the same analysis methods for M5 material as previously used and approved for Zr-4 (Reference 14). Pressure and temperature inputs to the stress analyses are chosen so that the operating conditions for all normal operation and AOOs are enveloped. The cladding wall thicknesses are reduced to those minimum values allowed by fabrication specifications and further reduced to allow for corrosion on the inside and outside diameter. FCF uses the cladding corrosion from COROSO2 (see Section 3.5) to determine corrosion on the outside diameter. The NRC staff concludes that the FCF design analysis methods for stress analyses for M5 materials are consistent with the guidelines in Section 4.2 of the SRP and are acceptable for licensing applications with M5 cladding up to currently approved burnup levels.

3.2 Strain

Bases/Criteria - The FCF design criteria for fuel rod cladding strain is that the maximum uniform hoop strain (elastic plus plastic) shall not exceed 1 percent. This criteria is intended to preclude excessive cladding deformation from normal operation and AOOs. This is the same criterion for cladding strain that is used in Section 4.2 of the SRP and has previously been approved in Reference 14.

The material property that could have a significant impact on the cladding strain limit is cladding ductility. The strain criterion could be impacted if cladding ductility were decreased, as a result of in-reactor operation, to levels that would allow cladding failure without the 1 percent cladding strain criteria being exceeded under normal operation and AOOs.

As noted in Section 2.9 of this SE, FCF has collected ductility data from irradiated M5 cladding with burnups up to 43 GWd/MTU. These data demonstrate that M5 ductility exceeds the 1 percent total (elastic + plastic) uniform strain requirement and, therefore, has adequate ductility. In addition, FCF has committed to collecting additional M5 ductility data up to currently

approved burnup levels (see Section 6.0). The NRC staff concludes that FCF's 1 percent strain criterion is applicable to M5 cladding up to currently approved burnup levels based on FCF's commitment to continue to collect M5 ductility data up to approved burnup levels.

Evaluation - Reference 1 stated that the TACO-3 fuel performance code (Reference 22) is used for cladding strain analyses. FCF uses conservative bounding values for input to TACO-3 for this calculation including worst case fabrication tolerances, pressure differentials and power histories (including AOOs). Total strain as calculated by TACO-3 is strictly a function of fuel expansion and is not dependent on yield or ultimate tensile strength and, therefore, the use of M5 cladding is not expected to have a significant impact on cladding strain analyses. FCF was asked to provide an example 1 percent strain analysis with M5 cladding properties. FCF provided the results of an example strain analyses in Reference 5 for both M5 and Zr-4 cladding properties that demonstrated nearly identical results. This fuel performance code has been previously reviewed and approved by NRC up to a rod-average burnup of 62 GWd/MTU. The NRC staff concludes that the FCF analysis methodology for 1 percent cladding strain is applicable to M5 cladding up to currently approved burnup levels.

3.3 Strain Fatigue

Bases/Criteria - The FCF design criterion for cladding strain fatigue is that the cumulative fatigue usage factor be less than 0.9 when a minimum safety factor of 2 on the stress amplitude or a minimum safety factor of 20 on the number of cycles, whichever is the most conservative, is imposed in accordance with the O'Donnell and Langer design curve (Reference 28) for fatigue usage. This criterion is consistent with SRP Section 4.2 and has previously been approved in Reference 14. The NRC staff concludes that FCF's design criterion for cladding strain fatigue is applicable to M5 cladding up to currently approved burnup levels.

Evaluation - FCF has stated that the O'Donnell and Langer curve for irradiated Zircaloy (Reference 29), which includes a safety factor of 2 on stress amplitude or a factor of 20 on cycles (whichever is the more conservative), is conservative in relation to strain fatigue of M5 cladding. The staff asked FCF to supply their strain fatigue data for M5 cladding, and FCF supplied unirradiated M5 data in Reference 8. Examination of the M5 strain fatigue data demonstrates that the total strains from these tests are consistent with the unirradiated Zr-2 strain fatigue data of O'Donnell and Langer; therefore, M5 strain fatigue appears to be consistent with the O'Donnell and Langer curves for unirradiated Zr-2, 3, and 4. However, FCF uses the irradiated strain fatigue curve, with a safety factor of 2 on stress amplitude or a factor of 20 on cycles, from O'Donnell and Langer because it is more conservative than the unirradiated curve. The use of this curve and safety factor is conservative for determining M5 strain fatigue life. FCF introduces further conservatisms in this analysis by using the minimum, as-fabricated cladding thickness and subtracting metal loss based on the maximum calculated oxide layer thickness (Reference 2). The NRC staff concludes that FCF's analysis methodology for strain fatigue is conservative and, therefore, applicable to M5 cladding up to currently approved burnup levels.

3.4 Fretting Wear

Bases/Criteria - Fretting wear is a concern for fuel, burnable poison rods, and guide tubes. Fretting, or wear, may occur on the fuel and/or burnable rod cladding surfaces in contact with the spacer grids if there is a reduction in grid spacing loads in combination with small amplitude, flow induced, vibratory forces. Guide tube wear may result when there is flow induced motion between the control rod ends and the inner wall of the guide tube.

The FCF design criterion against fretting wear is that the fuel design shall provide sufficient support to limit fuel rod vibration and cladding fretting wear. This criterion is consistent with SRP Section 4.2 and has previously been approved in Reference 14. The NRC staff concludes that FCF's design criterion for cladding fretting wear is applicable to M5 cladding up to currently approved burnup levels.

Evaluation - Fretting wear resistance for the M5 alloy should be similar to standard Zr-4 material. In addition, the mechanisms for fretting wear such as grid spring relaxation loads and flow vibration are dependent on the spacer spring design and material, and spacer grid design flow characteristics rather than the cladding material.

As a result, FCF performs out-of-reactor vibration and wear tests (for more than 1000 hours) of a full assembly in a flow loop, and performs post-irradiation visual examination of LTAs to verify satisfactory fretting wear performance. This is performed by FCF when a significant change is made to the spacer springs, spacer grids or flow characteristics of an assembly design (Reference 14).

Therefore, a change in cladding material should not have a significant impact on fretting wear in current FCF fuel designs. The NRC staff concludes that the FCF test methodology for verifying fretting wear is applicable to M5 cladding up to currently approved burnup levels.

3.5 Oxidation and Crud Buildup

Bases/Criteria - Section 4.2 of the SRP identifies cladding oxidation and crud buildup as potential fuel system damage mechanisms. The SRP does not establish specific limits on cladding oxidation and crud but does specify that their effects be accounted for in the thermal and mechanical analyses performed for the fuel. Recent out-of-reactor measured elastic and plastic cladding strain values from high burnup cladding from two PWR fuel vendors (References 19, 20, and 21) have shown a decrease in Zr-4 cladding ductilities when oxide thicknesses begin to exceed 100μm. As a result, the NRC staff has encouraged fuel vendors to establish a maximum oxide thickness limit of 100μm. FCF has adopted this oxide thickness limit (Reference 2). The NRC staff finds this oxide limit acceptable for M5 cladding based on FCF's commitment to continue to collect oxide thickness and ductility data up to current burnup levels.

Evaluation - M5 corrosion is modeled by FCF using the same model with a different activation energy, COROSO2 (Reference 2), as used for their standard Zr-4 cladding. FCF has provided a large amount of M5 corrosion thickness data (maximum oxide measurement from over 370 rods and/or cycles where some rods have one measurement per cycle of operation) for

burnups up to 53 GWd/MTU. The COROSO2 model (with M5 activation energy) comparisons to this data demonstrate that there is a reasonable agreement with the data with a small degree of predictive conservatism (higher oxide thickness) at high burnup levels. In response to a question on whether additional data had been obtained since the publication of the topical report, FCF responded (Reference 6) that they recently collected oxidation data from an M5 clad fuel rod that was reconstituted into a Zr-4 LTA that achieved a rod average burnup of 63 GWd/MTU. This M5 clad fuel rod achieved a maximum fuel rod corrosion thickness that was less than half the FCF limit on corrosion thickness.

Cladding oxidation is generally the most severe in plants with high coolant outlet temperatures and those with aggressive power histories (i.e., those plants that drive the fuel at high heat fluxes for long periods of time). Examination of the plants from which the FCF M5 corrosion data was collected has revealed that a significant amount of the data is from plants with high outlet temperatures. Some of the data is from fuel with a more aggressive operating history as well. However, the highest burnup data is from a plant with a lower outlet temperature and an operating history that was not particularly aggressive. FCF has committed to continue to collect data up to currently approved burnup levels from plants with higher outlet temperatures and more aggressive operating histories.

The NRC staff concludes that the FCF corrosion model for M5 cladding is acceptable for application to licensing analyses up to currently approved burnup levels, based on FCF's commitment to continue to collect M5 corrosion and ductility data up to approved burnup levels.

3.6 Rod Bowing

Bases/Criteria - Fuel and burnable poison rod bowing are phenomena that alter the design-pitch dimensions between adjacent rods. Bowing affects local nuclear power peaking and the local heat transfer to the coolant. Rather than place design limits on the amount of bowing that is permitted, the effects of bowing are included in the departure from nucleate boiling (DNB) analysis by a DNB ratio penalty when rod bow is greater than a predetermined amount. This methodology for rod bow is consistent with SRP Section 4.2 and has previously been approved in Reference 14. Thus the NRC staff concludes that FCF's rod bowing methodology is acceptable for licensing analyses with M5 cladding up to currently approved burnup levels.

Evaluation - Rod bowing has been found to be dependent on rod axial growth, the distance between grid spacers, the rod moment of inertia, flux distribution and other assembly design characteristics. FCF has indicated in their submittal (Reference 1) that they will continue to use the approved rod bow methodology (used for their standard Zr-4 cladding) for the M5 cladding. FCF has not presented any rod bowing data for M5 cladding to indicate that the approved Zr-4 methodology will envelope M5 rod bow; however, they have stated they intend to collect rod bow data from LTAs with M5 cladding in calendar years 2000 and 2001 up to extended burnup levels. FCF has argued that M5 cladding should have less rod bowing than their standard Zr-4 cladding at a given burnup level because axial rod growth is less for M5 cladding. The NRC staff agrees that rod bow will most likely be less at a given burnup level but it is necessary to confirm this and to also confirm that rod bow with M5 cladding saturates at high burnup levels, similar to what has been observed in Zr-4 cladding.

The NRC staff concludes that the use of FCF's approved rod bow methodology for M5 cladding is acceptable for application to licensing analyses up to currently approved burnup levels, based on FCF's commitment to collect M5 rod bow data up to high burnup levels to confirm that the M5 rod bow is enveloped by the Zr-4 rod bow model.

3.7 Axial Growth

Bases/Criteria - The FCF design basis for axial growth is that adequate clearance be maintained between the rod ends and the top and bottom nozzles to accommodate the differences in the growth of fuel rods and the growth of the fuel assembly. Similarly, for assembly growth, FCF has a design basis that axial clearance between core plates and the bottom and top assembly nozzles should allow sufficient margin for fuel assembly irradiation growth during the assembly lifetime to prevent the holddown spring in the assembly upper end fitting from going solid at cold shutdown. These criteria are consistent with SRP Section 4.2 and have previously been approved in Reference 14. Thus the NRC staff concludes that the FCF design basis is acceptable for licensing analyses with M5 cladding up to currently approved burnup levels.

Evaluation - FCF provides an initial fuel rod-to-nozzle growth gap in their fuel assembly designs to allow for differential irradiation growth and thermal expansion between the fuel rod cladding and the fuel assembly guide thimble tubes. If this gap were to close, an interference fit would develop that would result in fuel rod bowing. An interference fit can develop because the fuel rod cladding grows faster than the assembly guide tubes in the axial direction. FCF uses an upper tolerance limit (UTL) 95/95 (at least 95 percent probability, at a 95 percent confidence level) minimum gap model that bounds their shoulder gap data (the minimum measured gap closure per assembly is used), along with worst case fabrication tolerances and thermal expansion, to preclude interference during operation. This is a new methodology proposed by FCF for fuel assemblies with Zr-4 (cold-worked stress relief annealed) cladding and Zr-4 (fully annealed) guide tubes (Zr-4/Zr-4), with M5 cladding and Zr-4 (fully annealed) guide tubes (M5/Zr-4), and with M5 cladding and M5 guide tubes (M5/M5). Consequently, FCF has 3 UTL gap closure models for these three assembly combinations (i.e., Zr-4/Zr-4, M5/Zr-4, and M5/M5). The gap closure model for Zr-4/Zr-4 is based on a large data base with burnups up to 54 GWd/MTU, while the M5/Zr-4 closure model is based on measurements from approximately 19 individual assembly/cycles (minimum of approximately 56 gap measurements per assembly/cycle) with burnups up to 39 GWd/MTU. The M5/M5 model is only based on the minimum gap from 112 measurements from two assemblies after only one cycle of irradiation (approximately 22 GWd/MTU). Additional M5/M5 data will be obtained after two cycles of irradiation (approximately 45 GWd/MTU assembly burnup), scheduled in March of 2000, and three cycle data (approximately 55 GWd/MTU), scheduled in September 2001. FCF is also committed to obtaining gap closure data from M5/Zr-4 assembly up to currently approved burnup limits (see Section 6 on FUEL SURVEILLANCE). The NRC staff concludes that the FCF minimum gap closure models are acceptable for application to licensing analyses up to currently approved burnup levels, based on FCF's commitment to continue to collect Zr-4/M5 and M5/M5 gap closure data up to currently approved burnup levels.

In like manner FCF designs the holddown springs for the assembly to prevent the holddown spring from bottoming out on reactor-internals assuming maximum assembly growth and worst case tolerances. FCF utilizes upper bound 95/95 tolerance lines of their axial assembly growth data, along with worst case fabrication dimensions or 95/95 dimensional tolerances (when available), to assure that the holddown spring will not bottom out at end-of-life (EOL). As noted in Section 2.14 of this SE, FCF has presented UTL models for both Zr-4 and M5 assembly (guide tube/thimble) growth. FCF has over 80 assembly measurements of assembly growth with Zr-4 guide tubes for assembly burnups up to 58 GWd/MTU. Currently, FCF has only two data points for M5 guide tube growth at an assembly burnup of 22 GWd/MTU. The UTL curve for M5 assembly growth is very conservative compared to the two data points. FCF has committed to collecting further assembly growth data for M5 guide tubes in North Anna up to currently approved burnup levels (see Section 6, FUEL SURVEILLANCE). The NRC staff concludes that the Zr-4 and M5 UTL guide tube/thimble (assembly) growth models are acceptable for licensing applications up to currently approved burnup levels, based on FCF's commitment to continue to collect M5 assembly (guide tube) growth data up to approved burnup levels.

3.8 Rod Internal Pressure

Bases/Criteria - Rod internal pressure is a driving force for, rather than a direct mechanism of, fuel system damage that could contribute to the loss of dimensional stability and cladding integrity. To preclude fuel damage, SRP Section 4.2 presents a rod pressure limit of maintaining rod pressures below system pressure. The FCF design basis for the fuel rod internal pressure is that the fuel system will not be damaged due to excessive fuel rod internal pressure and FCF has established the "Fuel Rod Pressure Criterion" (Reference 23) to provide assurance that this design basis is met. The internal pressure of the FCF lead fuel rod in the reactor is limited to a value below that which could cause (1) the diametral gap to increase due to outward cladding creep during steady-state operation, and (2) extensive DNB propagation to occur. This FCF design basis and the associated limits have been approved by the NRC (Reference 23). The use of M5 cladding impacts the internal pressure limit because M5 cladding creep is different than that observed for their standard Zr-4. The M5 cladding creep model (with Zr-4 model upper bound uncertainties) is discussed in Section 2.10 of this SE and found to be acceptable for use in determining the rod pressure limits up to the currently approved burnup levels. The only difference in the rod pressure limit methodology for M5 cladding is the use of the new M5 creep model.

Evaluation - FCF utilizes the TACO-3 fuel performance code (Reference 22) for predicting EOL fuel rod pressures to verify that they do not exceed the FCF "Fuel Rod Pressure Criterion" during normal operation and AOOs. The FCF rod pressure analysis methodology has not changed other than the use of M5 properties in TACO-3. The use of M5 cladding will not significantly change the TACO-3 prediction of rod pressures; however, the change in the following material properties will have a small impact on the rod pressure analyses: thermal expansion, thermal conductivity, creep, poison's ratio, modulus of elasticity, and axial growth. These properties have all been reviewed and found acceptable in Sections 2.2, 2.3, 2.10, 2.11, 2.12, and 2.14, respectively.

The NRC staff concludes that the FCF analysis methodology, using TACO-3 and M5 properties, for determining rod internal pressures for rods with M5 cladding is acceptable up to currently approved burnup levels.

4.0 FUEL ROD FAILURE

In the following paragraphs, fuel rod failure thresholds and analysis methods for the failure mechanisms listed in the SRP will be reviewed. When the failure thresholds are applied for normal operation, including AOOs, they are used as limits (and hence SAFDLs) since fuel failure under those conditions should not occur according to the traditional conservative interpretation of GDC 10. When these thresholds are used for postulated accidents, fuel failures are permitted, but they must be accounted for in the dose assessments required by 10 CFR Part 100. The basis for establishing these failure thresholds is thus established by GDC 10 and Part 100, and only the threshold values and the analysis methods used to assure the thresholds are met will be reviewed below.

4.1 Hydriding

Bases/Criteria - Internal hydriding as a cladding failure mechanism is precluded by controlling the level of hydrogen impurities in the fuel during fabrication; this is generally an early-in-life failure mechanism. Internal hydriding is not impacted by the use of M5 cladding and, therefore, will not be discussed further in this SE.

External hydriding of M5 cladding due to waterside corrosion is the other source and is limited by FCF's 100μm limit on oxide thickness, as discussed in Section 3.5 of this SE.

Evaluation - FCF controls internal hydriding by taking statistical samples following pellet fabrication, prior to loading the pellets in the fuel rods, and confirming that hydrogen is below a specified level. Therefore, no analyses are necessary other than to confirm that the statistical pellet sampling shows that hydrogen is below the specified level. The use of M5 cladding does not impact the internal hydriding. The staff considers this acceptable.

4.2 Cladding Collapse

Bases/Criteria - If axial gaps in the fuel pellet column were to occur due to fuel densification, the potential would exist for the cladding to collapse into a gap (i.e., flattening). Because of the large local strains that would result from collapse, the cladding is then assumed to fail. It is an FCF design criterion that cladding collapse is precluded during the fuel rod design lifetime. This design basis is the same as that in the SRP and has been previously approved (Reference 14). This design criteria is not affected by the use of M5 cladding. The NRC staff concludes that this FCF design criterion is acceptable for licensing analyses with M5 cladding up to currently approved burnup levels.

Evaluation - The FCF analytical models for evaluating cladding creep collapse are the approved CROV and TACO-3 computer codes (References 30 and 22). The application of these codes to calculating creep collapse is discussed in Reference 30. The TACO-3 code will include the M5 material property models discussed in Section 2.0 of this SE. As discussed in Section 2.10

of this SE, the new M5 creep model (Reference 7) is more conservative for calculating creep collapse in CROV than the old Zr-4 creep model originally used in CROV. Therefore, FCF has adopted the more conservative M5 creep model, along with the Zr-4 model uncertainties, for use in determining the upper bound creep for use in CROV for cladding collapse analyses. The NRC staff concludes that the use of the TACO-3 and CROV codes with the appropriate M5 material property models is acceptable for creep collapse analyses for fuel rods with M5 cladding up to currently approved burnup levels.

4.3 Overheating of Cladding

Bases/Criteria - The FCF design criterion for the prevention of fuel failures due to overheating is that there will be at least 95 percent probability, at a 95 percent confidence level, (95/95) that DNB will not occur on a fuel rod during normal operation and AOOs. This design limit is consistent with the thermal margin criterion of the SRP guidelines and has previously been approved. This design criterion is not affected by the use of M5 cladding. The NRC staff concludes that this FCF design criterion is acceptable for licensing analyses with M5 cladding up to currently approved burnup levels.

Evaluation - As stated in SRP Section 4.2, adequate cooling is assumed to exist when the thermal margin criterion to limit DNB, or boiling transition, in the core is satisfied. The impact of the use of M5 cladding on DNB is small and related to the small change in gap conductance (due to differences in gap size from M5 creep down and thermal expansion) and M5 thermal conductivity. Other than the small changes in M5 material properties the FCF methodology for evaluating DNB has not changed. These M5 properties have been reviewed by the NRC staff in Section 2.0 of this SE and found to be acceptable for use in FCF licensing analyses up to currently approved burnup levels.

4.4 Overheating of Fuel Pellets

Bases/Criteria - To preclude overheating of fuel pellets, FCF design criterion is that no fuel centerline melting is allowed for normal operation and AOOs. This design criterion is the same as given in SRP Section 4.2 and has previously been approved (Reference 14). This design criterion is not affected by the use of M5 cladding. The NRC staff concludes that this FCF design criterion is acceptable for licensing analyses with M5 cladding up to currently approved burnup levels.

Evaluation - FCF utilizes the approved TACO-3 (Reference 22) fuel performance code to determine the maximum linear heat generation rate (LHGR) at which a given fuel design will not achieve fuel melting at a 95 percent probability at a 95 percent confidence level. This FCF analysis methodology has previously been found to be acceptable up to a rod-average burnup of 62 GWd/MTU (Reference 30). FCF was asked to provide an example fuel melting analysis with M5 cladding properties. In Reference 5, FCF provided example fuel melting analyses for both M5 and Zr-4 cladding that demonstrated nearly identical results. Therefore, the small changes in M5 cladding properties has an insignificant impact on fuel melting analyses. The NRC staff concludes that the use of the TACO-3 code with the appropriate M5 material property models is acceptable for fuel melting analyses for fuel rods with M5 cladding up to currently approved burnup levels.

4.5 Pellet-Cladding Interaction (PCI)

Bases/Criteria As indicated in SRP Section 4.2, there are no generally applicable criteria for PCI failure. However, two acceptable criteria of limited application are presented in the SRP for PCI: (1) less than 1 percent transient-induced cladding strain, and (2) no centerline fuel melting. Both of these limits are used by FCF as discussed in Sections 3.2 and 4.4 of this SE and, therefore, have been addressed by FCF.

Evaluation - As noted earlier, FCF utilizes the TACO-3 (Reference 22) code to show that their fuel meets both the cladding strain and fuel melting criteria. The NRC staff concludes that this code is acceptable per the recommendations in Sections 3.2 and 4.4 of this SE.

4.6 Cladding Rupture

Bases/Criteria - There are no specific design limits associated with cladding rupture other than the 10 CFR Part 50, Appendix K (Reference 31) requirement that the incidence of rupture not be underestimated. A cladding rupture temperature correlation must be used in the LOCA emergency core cooling system (ECCS) analysis. The cladding rupture temperature for M5 cladding is similar to Zr-4; however, FCF has elected to collect M5 cladding rupture temperature data versus hoop stress at various heating rates similar to what was done for Zr-4 in NUREG-0630 (Reference 32). The M5 rupture temperature model will be discussed in the Evaluation section below.

Evaluation - FCF has collected a large amount of M5 cladding rupture temperature data at slow and fast heating rates. The slow heating rate data (between 2 to 15°C/sec) determined rupture temperatures at stresses between 1 to 13.5 Ksi (kilo-pounds per square inch). The fast heating rate (25 to 100°C/sec) determined rupture temperatures at stresses between 1 to 10.5 Ksi. FCF has developed a new correlation for rupture temperature as a function of cladding hoop stress and heating rate in Reference 8 that is slightly different from the original submittal. The resulting rupture curves from this correlation are very similar to the NUREG-0630 curves with the exception that they have a steeper decrease in rupture temperature with stress at stresses below 5 Ksi (which was a characteristic of the M5 data). In addition, these rupture curves appear to span the breadth of the M5 data very similar to how the NUREG-0630 curves spanned the breadth of the Zr-4 rupture data. PNNL and the NRC staff have examained the M5 rupture correlation and data and agree that the correlation (1) is a reasonable relationship with the data, (2) is similar to the NUREG-0630 curves, and (3) meets the intent of Appendix K of 10 CFR 50.46 that the degree of swelling and incidence of rupture not be underestimated. The NRC staff concludes that the FCF rupture correlation for M5 cladding is accetable for determining rupture temperatures for LOCA ECCS analyses up to currently approved burnup levels.

4.7 Fuel Rod Mechanical Fracturing

Bases/Criteria - The term "mechanical fracture" refers to a fuel rod defect that is caused by an externally applied force such as a hydraulic load or a load derived from core-plate motion. The design limit proposed by FCF to prevent fracturing is that the stresses due to postulated accidents in combination with the normal steady-state fuel rod stresses should not exceed the

yield strength of the components in their fuel assemblies. This design criterion for fuel rod mechanical fracturing is consistent with the SRP guidelines, and has previously been approved (Reference 14). While the yield strength has changed for M5 cladding, as discussed in Section 2.8 of this SE, the FCF design criterion has not changed. Therefore, the design criterion is not affected by the use of M5 cladding. The NRC staff concludes that this FCF design criterion is acceptable for licensing analyses with M5 cladding up to currently approved burnup levels.

Evaluation - The mechanical fracturing analysis is done as a part of the seismic-and-LOCA loading analysis. A discussion of the seismic-and-LOCA loading analysis is given in Section 5.4 of this SE.

5.0 FUEL COOLABILITY

For postulated accidents in which severe fuel damage might occur, core coolability must be maintained as required by several GDCs (e.g., GDC 27 and 35). In the following paragraphs, limits and methods to assure that coolability is maintained are discussed for the severe damage mechanisms listed in the SRP.

5.1 Fragmentation of Embrittled Cladding

Bases/Criteria - The most severe occurrence of cladding oxidation and possible fragmentation during a postulated accident is the result of a LOCA. In order to reduce the effects of cladding oxidation during a LOCA, FCF uses a limiting criterion of 2200°F on peak cladding temperature (PCT) and a limit of 17 percent on maximum cladding oxidation as prescribed by 10 CFR 50.46. These criteria are consistent with SRP criteria and have previously been approved (Reference 14). FCF has performed high-temperature oxidation and quenching tests with M5 cladding to demonstrate that the 2200°F (1204°C) PCT and 17 percent oxidation limits protected the cladding against embrittlement and prevent the oxidation from becoming autocatalytic. This was demonstrated by FCF by heating M5 (Zr-4 was also tested) cladding to high temperatures of 1100, 1200, and 1300°C for various times and quickly (less than one second) quenching the cladding in a cold water bath (discussed in Appendix G of Reference 1). The cladding was removed from the bath and tested under pressure for leaks and oxide thickness measured. These tests demonstrated that failure did not occur until 20 to 25 percent of the cladding was oxidized, which is nearly identical to the test results for Zr-4 cladding in this test and other similar tests available to NRC, and no autocatalytic oxidation was observed. These FCF tests confirm that the 2200°F PCT and 17 percent oxidation criteria are conservative for M5 cladding in order to prevent cladding embrittlement and fragmentation during a LOCA. The NRC staff concludes that this FCF design criterion is acceptable for LOCA licensing analyses with M5 cladding up to currently approved burnup levels.

Evaluation - FCF uses approved LOCA evaluation models along with the Baker-Just correlation, as required by 10 CFR Part 50 Appendix K, for demonstrating compliance with the 2200 °F PCT and 17 percent oxidation criteria for the fuel cladding during a LOCA. FCF has performed high-temperature oxidation tests for M5 cladding (Appendix D of Reference 1) to confirm that the Baker-Just oxidation correlation remains conservative in relation to M5 high-temperature oxidation. The FCF high temperature oxidation tests were performed in super heated flowing

steam where the sample (both M5 and Zr-4) was inductively heated to temperatures of 1050, 1150, and 1250°C for various times. The measured oxidation rates for the M5 samples were significantly lower than those for the Zr-4 samples at 1050°C; however, at 1150 and 1250°C the oxidation rates were nearly identical. A comparison of M5 measured values to Baker-Just predictions demonstrated that the Baker-Just correlation remained conservative for temperatures typically calculated for LOCA. The staff asked FCF (Reference 4) to provide Arrehenius plots of the high-temperature oxidation data in order to provide a measure of bias and uncertainty in the data. FCF provided these plots (Reference 6) which demonstrated only small uncertainties and essentially no biases in the data. The FCF data demonstrates that high-temperature oxidation of the M5 alloy is bounded by the Baker-Just correlation and that the Appendix K requirement for the use of Baker-Just remains conservative in relation to the use of M5.

FCF provided example LOCA analyses (Appendix F of Reference 1) with M5 and Zr-4 cladding at beginning-of-life (BOL) and at a burnup of 40 GWd/MTU to demonstrate that the results were only slightly different between M5 and Zr-4.

The staff noted that the peak oxidation values calculated by FCF (Table F-3) for 40 GWd/MTU did not appear to include the initial oxidation that resulted from normal steady-state operation. It is noted that NRC Information Notice (IN) 98-29, dated August 28,1998, stated that initial oxidation thickness should be included in the peak oxidation calculated for LOCA to demonstrate compliance with 10 CFR 50.46 (17 percent oxidation criterion). In response to the staff's questions, FCF stated that while initial oxidation was included in the LOCA analysis at 40 GWd/MTU, the value was significantly lower than what would be the measured oxidation at a burnup of 40 GWd/MTU. FCF noted that the generic issue of whether to include initial oxidation in the 17 percent criterion is being disputed by NEI and fuel vendors. FCF further noted that they have committed to NRC to check their LOCA analyses to provide assurance that the 17 percent oxidation criterion will not be exceeded if such an approach were required by the NRC. The staff concludes that this generic issue is independent of the review of the subject topical report and will not be considered in this SE.

The NRC staff concludes that the Baker-Just correlation is conservative for determining high temperature M5 oxidation for LOCA analyses and, therefore is acceptable for LOCA ECCS analyses up to currently approved burnup levels.

5.2 Violent Expulsion of Fuel

Bases/Criteria - In a severe reactivity insertion accident (RIA), such as a control rod ejection accident, large and rapid deposition of energy in the fuel could result in melting, fragmentation, and dispersal of fuel. The mechanical action associated with fuel dispersal might be sufficient to destroy the fuel cladding and rod bundle geometry and to provide significant pressure pulses in the primary system. To limit the effects of an RIA event, Regulatory Guide 1.77 (Reference 33) recommends that the radially-averaged energy deposition at the hottest axial location be restricted to less than 280 cal/g. In addition, the fuel failure limit is the onset of DNB for determining the dose consequences of an RIA. The limiting RIA event for FCF fuel designs is a control rod ejection accident.

FCF's safety criteria for the control rod ejection accident is that the radial average peak fuel enthalpy for the hottest fuel rod shall not exceed 280 cal/g. This is identical to the guidance in SRP Section 4.2 and Regulatory Guide 1.77 (References 10 and 33). It is noted that the NRC staff is currently reviewing the 280 cal/gm limit and the limit for fuel failure may be decreased for fuel at high burnups. Recent RIA testing has indicated the fuel expulsion and fuel failure may occur before the 280 cal/gm limit and the onset of DNB, respectively (References 34 and 35). However, further testing and evaluation is needed to better establish new limits. The fuel expulsion and failure limits for an RIA may decrease in the future, but the current limits continue to be accepted by the staff and the use of M5 cladding is not expected to significantly impact these safety criteria. The NRC staff concludes that the FCF RIA criteria are valid for licensing applications up to currently approved burnup levels.

Evaluation - FCF verifies that this acceptance criterion is met for each fuel cycle through design and cycle specific analyses, and by limiting the ejected rod worth. The industry and NRC have both done preliminary evaluations of the worst impact of both a lower enthalpy limit for fuel expulsion and lower failure limit at current burnup limits. These very conservative analyses indicate that maximum enthalpies for high burnup rods are at least a factor of three lower than the current 280 cal/gm limit and violent expulsion is unlikely. In addition, the dose consequences are within those specified in 10 CFR Part 100. The use of M5 cladding has little impact on fuel expulsion and failure (compared to the use of Zr-4) as long as the cladding remains ductile under the operating conditions of this event (see Section 2.9 of this SE on Ductility). The impact of the use of M5 cladding on DNB is small due to the small changes in M5 material properties (as noted in Section 4.3 of this SE) and the FCF approved methodology for evaluating RIAs has not changed. The M5 properties have been reviewed by the NRC staff (see Section 2 of this SE) and found to be acceptable for use in FCF licensing analyses up to currently approved burnup levels.

5.3 Clad Ballooning

Bases/Criteria - Zircaloy cladding will balloon (swell) under certain combinations of temperature, heating rate, and stress during a LOCA. There are no specific design limits associated with cladding ballooning other than the 10 CFR Part 50 Appendix K requirement that the degree of swelling not be underestimated. To meet the requirement of 10 CFR Part 50 Appendix K, the burst strain and the flow blockage resulting from cladding ballooning must be taken into account in the overall LOCA analysis. Cladding ballooning is a result of high-temperature creep and deformation of the cladding. The M5 alloy has different high-temperature creep and deformation characteristics than Zr-4. As a result, FCF has developed new ballooning and flow blockage models for M5 cladding similar to the methodology developed in NUREG-0630 for Zr-4 and Zr-2 cladding (recommended in SRP Section 4.2). These FCF ballooning and flow blockage models for M5 will be discussed in the Evaluation section below.

Evaluation - The M5 cladding has different high-temperature creep characteristics and different $\alpha-\beta$ transformation temperatures than Zr-4 cladding and, therefore, the cladding burst strain and flow blockage models developed in NUREG-0630 (Reference 32) for Zr-4 cladding are not applicable to M5 cladding. Therefore, FCF performed single-rod (with M5 cladding) ballooning tests in the EDGAR test facility and measured cladding strains as a function of temperature for fast and slow heating rates, similar to what was done in NUREG-0630 for Zr-4. FCF also

performed single-rod ballooning tests and measured cladding burst strains for Zr-4 cladding using the same EDGAR facility, equipment and methodology as used for M5 cladding. The staff has compared the FCF Zr-4 burst strain results to the results in NUREG-0630 and found that the FCF measured strains were greater for both fast and slow heating rates and at all temperatures in the α and β regions. This would indicate that either the FCF Zr-4 cladding has higher creep rates than the Zr-4 cladding used in the NUREG-0630 tests or that the EDGAR test facility results in conservatively higher measured strains than the facility used in NUREG-0630 burst tests. Also a comparison of the M5 and Zr-4 measured burst strains from the EDGAR facility demonstrates that the M5 cladding has lower burst strains and, therefore, less strain capability than Zr-4. The NRC staff concludes that the single-rod strain data collected in the EDGAR facility are in general more conservative than the single-rod data used in NUREG-0630 and, therefore, are acceptable for use in developing M5 cladding ballooning and flow blockage models.

Single rod burst strains need to be translated to flow blockage in an actual fuel assembly (bundle). The flow blockage model in NUREG-0630 relied on three bundle tests (performed by Oak Ridge) under simulated LOCA heating (two bundles at fast and one bundle at slow heating rates) to relate the single rod burst strain data to the measured bundle flow blockages. FCF has not performed their own bundle tests with M5 cladding but instead has relied on the three Oak Ridge bundle tests from Appendix A of NUREG-0630 to model the relationship between single-rod burst and pre-rupture strains, and assembly flow blockages.

There are differences between the FCF methodology for calculating M5 cladding flow blockage and the flow blockage model developed in NUREG-0630 from single-rod burst strains. FCF has measured the burst strains at the rupture location, as discussed above, the same as in NUREG-0630, but in addition they have also measured the strain remote from the rupture location (20 mm on both sides of the rupture location) from their single-rod EDGAR tests. They assume that the axial strains decrease exponentially away from the $\pm$ 20 mm rupture location, and this exponential function is derived from the axial measured strains of the individual rods in the Oak Ridge bundle tests from NUREG-0630. FCF has further assumed that, in addition to the burst strains, the remote strain (referred to by FCF as pre-rupture strain or just pre-strain) also makes a major contribution to assembly flow blockage. NUREG-0630 also recognized that axial strains remote from the failure location, and also strains in non-failed rods, significantly contributed to the flow blockage in a bundle (assembly). NUREG-0630 assumed that the pre-rupture strains were proportional to the burst strains, and used a proportionality constant to relate the single-rod burst strains to bundle flow blockage (which was based on the flow blockages measured in the bundle tests). FCF was asked why a similar assumption was not also made for M5 cladding. FCF responded that M5 pre-rupture strains were not always the same proportionality to burst strains within all temperature ranges and, therefore, this assumption was not valid for M5 cladding.

The following discussions will be divided up into subsections in order to evaluate each component of the FCF methodology for calculating assembly flow blockage with M5 cladding. The first subsection will discuss the general characteristics of high-temperature strain data for zirconium alloys for background information for interpreting the Zr-4 and M5 data. The second subsection will discuss the adequacy of the FCF single rod burst strain curves (for fast and slow heating rates) used for calculating the extent of M5 assembly flow blockage. The third

subsection will discuss the adequacy of the FCF pre-rupture strain curves (for fast and slow heating rates) also used for calculating the extent of M5 assembly flow blockage. The fourth subsection will address the adequacy of the overall FCF methodology for calculating assembly flow blockage with M5 cladding.

5.3.1 General Characteristics of High Temperature Zirconium Alloy Strains

It is important to understand the general characteristics of the trends of burst and pre-rupture strain data as a function of high temperature in zirconium alloys. This is because the zirconium $\alpha \rightarrow \beta$ phase transformation temperatures have a significant impact on the shape of the burst strain data and, therefore, in the development of strain curves. The Zr-4 burst strain data and correlation in NUREG-0630 for both slow and fast heating rates has two strain peaks; one near the start of the $\alpha \rightarrow \beta$ phase transformation temperature, and the second peak near the completion of the β phase transformation temperature. Burst strains significantly decrease in the $\alpha+\beta$ phase region because ductility in this phase is significantly lower than in the pure α phase or the pure β phase. The burst strains in the pure β phase start to decrease at higher temperatures (above where the peak strain is observed) because of embrittlement due to oxidation. For the fast heating rate data there is generally a shift in the burst strain peaks to slightly higher temperatures than for the slow ramp data because the kinetics of the phase transformation are not fast enough to keep up with the fast heating rates. This information is important in understanding the results of the M5 burst strain data and in developing correlations from the data because there is a significant amount of scatter in this data (Zr-4 burst strain data also has considerable scatter) and several different curves could be drawn to represent this data without this background information.

5.3.2 Burst Strain (Slow and Fast Heating Rate) Curves

The FCF slow heating rate data base for M5 is fairly large in the α and $\alpha+\beta$ phase regions where it is principally applied in FCF LOCA analyses; however, there were only four data points in the pure β phase region. The original FCF burst strain curve for M5 cladding (Reference 1) either bounded or agreed with nearly all of the burst strain data for slow heating rates. The burst strain peak in the α phase was very near the temperature where the $\alpha \rightarrow \beta$ phase transformation starts but the second peak was at a considerably higher temperature (about 100 °C higher) than the temperature at which the β phase transformation is complete. This delta temperature difference is greater than what would be expected for slow heating rates. Consequently, FCF agreed (Reference 8) to shift the second burst strain peak to a lower temperature to better match the temperature at which the β phase transformation is complete. The shift in the temperature for this peak did not impact the agreement with the data in the β phase region. The NRC staff has reviewed the burst strain data and FCF slow heating rate curve for M5 cladding (Reference 8) and conclude that the FCF curves bound the majority of the burst strain data and, therefore, are conservative and acceptable.

The quantity and temperature range of the M5 fast heating rate data was considerably less than collected for the slow heating rate data. Nearly all of the fast heating rate data was located in a narrow temperature range (100 °C), where the $\alpha+\beta$ phase transformation takes place and displays low ductility (strains), although there were a couple of data taken in the higher temperature β phase region. The staff asked FCF about the lack of fast heating rate burst data

outside of the 100 °C range. FCF responded that this is the temperature range where the fast heating rates are calculated to occur for M5 fuel (using the M5 fast heating rate rupture temperature curves for LOCA analyses, as discussed in Section 4.6 of this SE). The location of the burst strain peaks in the α and β regions of the FCF fast heating rate curve, in relation to the α-β phase transformation temperatures, is consistent with what is observed for the Zr-4 burst strain curve found in NUREG-0630. The FCF fast heating rate curve either bounds or agrees well with the majority of fast heating rate data. The NRC staff has reviewed the FCF slow and fast heating rate burst strain curves for M5 cladding and concludes that the FCF curves bound the majority of the burst strain data and, therefore, are acceptable.

FCF has also developed a probability distribution function (PDF) for the axial position of cladding rupture. This PDF is based on the cladding temperature distribution between grids with the distribution being zero near the grid locations. Given a relatively even (constant) temperature distribution in the cladding, as conservatively assumed for LOCA burst strains, the location of the burst failure appears to be random based on the NUREG-0630 bundle tests. This PDF developed by FCF is a reasonably conservative estimate of the probability distribution of rupture locations within an assembly. The NRC staff has also reviewed the PDF used by FCF to determine the axial locations of rupture and concludes that they are reasonable and, therefore, acceptable.

5.3.3 Pre-Rupture Strain (Slow and Fast Heating Rate) Curves

The EDGAR test pre-rupture strain data and resulting FCF curves developed for the M5 cladding for both slow and fast heating rates have been examined. The pre-rupture strains were measured from the FCF single-rod burst tests. The corresponding temperature ranges for the pre-rupture strains are therefore, the same as for the burst strain data. Both the slow and fast heating rate curves, developed by FCF for predicting pre-rupture strains, assumed constant strains in the α and α+β phase regions, while examination of the slow heating rate data shows that higher strains were measured on average in the α phase than in the α+β phase. This is consistent with the higher strains observed in the α phase with the M5 burst strain data, the NUREG-0630 Zr-4 burst strain data, and the FCF Zr-4 pre-rupture strain data, compared to the lower strains observed in the α+β phase. In addition, the location of the β phase peak for both the slow and fast heating rate curves were at higher temperatures than observed for the peaks in the burst strain data, and at significantly higher temperatures than observed for the β phase transformation temperature. The staff asked FCF why these characteristics of the FCF pre-strain rupture curves did not match their own pre-rupture strain and burst data, and also did not match the strain behavior observed in other zirconium alloys.

FCF responded (Reference 8) with new pre-rupture strain (for slow and fast heating rates) curves with strain peaks in the α phase that provided much better agreement with the pre-rupture strain data. These new curves also shifted the peak strains for the β phase to better coincide with the peaks observed in the burst strain data and better agree with the β phase transformation temperature. The NRC staff has reviewed the M5 pre-rupture strain curves in Reference 8 and concludes that they are reasonable representations of M5 cladding strains at high cladding temperatures typical of LOCA and, therefore, are acceptable.

5.3.4 Overall Evaluation of Flow Blockage Methodology

For the LOCA analysis, FCF calculates burst and pre-rupture strains for all fuel rods in an assembly based on their cladding stresses and temperatures. Using these burst and pre-rupture strains, FCF calculates the geometry for all rods and resulting flow blockage in the assembly. While the individual models that make up the clad ballooning and flow blockage methodology have been reviewed in the above subsections and found to be conservative, this does not ensure that FCF's methodology for applying these models yields conservative and acceptable results. The only reference point for an acceptable flow blockage methodology is the methodology provided in NUREG-0630.

Consequently, the staff asked FCF to perform a direct comparison between the FCF methodology for determining flow blockage, the NUREG-0630 blockage curves for slow and fast heating rates, and the three Oak Ridge bundle blockage data provided in Appendix A of NUREG-0630.

FCF provided a comparison of their predicted blockage (local and assembly average blockage) results using their Zr-4 burst and pre-rupture strain curves, based on their EDGAR Zr-4 test results and their blockage methodology (Reference 8), to those predicted using NUREG-0630 curves and methodology. The FCF (Zr-4) predicted local flow blockage results for both slow and fast heating rates (Figures I-G.9 and I-G.10, respectively in Reference 8) demonstrated that the FCF methodology predicted greater assembly flow blockages at nearly all temperature ranges than was predicted by NUREG-0630 (blockage curves from Figures 14 and 15 in NUREG-0630). (The staff notes that the peak local blockage in the α phase predicted by the FCF methodology at the slow heating rates was only slightly greater than the local blockage predicted by NUREG-0630 in this temperature range.) In addition, FCF included comparisons to actual local flow blockage data from the three Oak Ridge bundle tests (References 36, 37 and 38) and from other bundle tests (Reference 32) to demonstrate that the FCF blockage methodology bounded all of this data. FCF has also provided assembly average flow blockage results for fast and slow heating rates (Figures I-G.7 and I-G.9, respectively, in Reference 8) to demonstrate similar conservatism between the FCF and NUREG-0630 blockage methodology for the local predicted FCF blockages. The NRC staff concludes that the FCF methodology for predicting clad ballooning (strains) and flow blockage are either as conservative or more conservative than the flow blockage model in NUREG-0630 (which is recommended for use by Section 4.2 of the SRP).

FCF has also argued that both the single-rod burst and bundle tests are conservative because they do not take into account the cladding hot spots as a result of asymmetric pellets and unheated surfaces in a commercial fuel assembly. These phenomena result in azimuthal temperature variations in the cladding that will limit cladding strains while the single rod and bundle tests have tried to eliminate any temperature variations to get the highest strains possible. The NRC staff agrees that there may be some conservatism built into the test data, but the temperature gradients in an actual assembly should not be large because part of the LOCA is nearly an adiabatic heatup which will tend to decrease temperature gradients.

The NRC staff concludes that the FCF methodology for determining M5 cladding ballooning and flow blockage is conservative for LOCA analyses and, therefore is acceptable for LOCA ECCS analyses up to currently approved burnup levels.

5.4 Fuel Assembly Structural Damage From External Forces

Bases/Criteria - Earthquakes and postulated pipe breaks in the reactor coolant system would result in external forces on the fuel assembly. Appendix A to SRP Section 4.2 states that the fuel system coolable geometry shall be maintained and damage should not be so severe as to prevent control rod insertion during seismic and LOCA events. FCF has adopted the SRP guidelines as their design bases and the use of M5 cladding does not alter these design bases.

Evaluation - FCF uses NRC-approved methodologies provided in Reference 14 for evaluating seismic and LOCA loads. The FCF methodology has not changed but part of the methodology requires using the yield and/or ultimate tensile strengths for the guide tubes/thimbles, as per ASME Section III of the Boiler Pressure Vessel Code (Reference 18). Should M5 alloy be used for the guide tubes/thimbles the M5 yield and ultimate tensile strengths will be used for this analysis. As noted in Sections 2.7 and 2.8 of this SE, the FCF relationships for yield and ultimate tensile strength for the M5 alloy are acceptable for licensing analyses. Therefore, the NRC staff concludes that the FCF methodology for seismic-and-LOCA loads using M5 yield and ultimate tensile strengths is acceptable up to currently approved burnup levels.

6.0 FUEL SURVEILLANCE

The staff asked FCF about what future fuel surveillance would be performed to verify satisfactory performance of the M5 alloy because very little data exists up to currently approved rod-average burnup levels of 62 GWd/MTU and 60 GWd/MTU for Mark-B and Mark-BW designs, respectively. FCF responded (Reference 8) that their LTA program consists of performing pool-side examinations of cladding oxide thickness, assembly length and bow, rod diameter (M5 creep data), rod length (growth measurement), guide tube oxide thickness, and rod extraction measurements along with visual examinations from 10 LTAs. It is noted that many of these LTAs represent only a partial loading of fuel rods with M5 cladding. In addition, FCF noted that they intend to perform hot cell examinations of individual M5 fuel rods to continue measuring mechanical properties, cladding hydrogen content, rod length, profileometry (cladding diameter), and oxide thicknesses. FCF was further asked about obtaining rod bow measurements because they currently do not have any rod bow data (see Section 3.6 of this SE). FCF responded (Reference 9) that they plan to perform rod bow measurements on the North Anna LTAs. FCF also stated that the pool-side measurements will include rod-shoulder to upper-tie-plate gap closure and M5 assembly growth (guide tube). Further, FCF stated that the hot cell laboratories will be asked to measure uniform and total strains of high burnup M5 cladding, along with micrographs of the failure surfaces in order to assess M5 ductility. FCF also committed (Reference 9) to obtain cladding strain, oxidation, hydride, rod bow, and axial growth (including shoulder gap closure) data up to the current approved rod-average burnup levels of 62 GWd/MTU and 60 GWd/MTU for Mark-B and Mark-BW designs, respectively.

The NRC staff concludes that the FCF fuel surveillance program for M5 alloy will address the current lack of data up to approved rod-average burnup levels of 62 GWd/MTU and 60 GWd/MTU for Mark-B and Mark-BW designs, respectively. Therefore, the NRC concludes that the FCF fuel surveillance program for M5 is acceptable.

7.0 LOCA EVALUATIONS WITH M5

BAW-10227-P, Appendix F, "M5 LOCA Evaluations," describes modifications in the use of Framatome approved large break loss-of-coolant accident (LBLOCA) and small break loss-of-coolant accident (SBLOCA) ECCS evaluation models to account for the presence of M5 fuel. Appendix F discusses the analysis methods, changes to the analysis methods to accommodate the presence of M5 fuel, sensitivity studies to show model convergence and conservatism, calculated results, and compliance with 10 CFR 50.46.

As discussed in other sections of this SE, the material properties of M5 are similar to those of other zirconium-based materials which have been previously licensed for use as cladding material. Based on this similarity, the staff finds it appropriately conservative to apply the criteria of 10 CFR 50.46 and 10 CFR Part 50, Appendix K when reviewing M5 fuel applications, including Appendix F of BAW-10227P. In performing this review, the staff has granted no exceptions in the application of these criteria. Although M5 is similar to Zircaloy, the criteria in the evaluation are specifically identified as appropriate for Zircaloy-clad fuel. Thus, exemptions must be obtained to allow application of those criteria to M5-clad fuel. Similarly, exemptions must be obtained to allow application of 10 CFR 50.44 dealing with hydrogen generation and combustible gas control to plants with M5-clad fuel.

BAW-10227-P, Appendix F, identifies changes in the use of the FCF LBLOCA and SBLOCA evaluation models to account for M5 material properties, including cladding conductivity, cladding creep, clad swelling, rupture deformation, and temperature. The material properties of M5 were found to be very similar to those of Zircaloy-4.

The Framatome models retain the methodology given in 10 CFR Part 50 Appendix K for the treatment of material properties, when prescribed by Appendix K and justified as suitably conservative. The retention of the Baker-Just equation for the calculation of metal/water reaction rate specified in Appendix K is such a case.

The swelling and rupture model for M5 cladding follows the approach of NUREG-0630 and meets the intent of NUREG-0630, as discussed in Section 4.6 of this SE. Section C.4 of BAW-10227P discusses post-LOCA droplet interaction modeling. Section C.4 indicates that the modeling of droplet interactions involves the thermodynamics of the fluid and the characteristics of the fuel, including its geometry. Sections 4.6 and 5.3 of this SE discuss M5 cladding deformation, including post-LOCA ballooning and rupture. These SE sections conclude that the fuel models in the FTI LOCA methodologies acceptably simulate M5 fuel performance, consistent with regulatory guidance.

The fluid thermodynamics models of the FTI LOCA methodologies are unchanged from those in the approved FTI LOCA analysis methodologies. The specific models which address droplet

interaction, including consideration of post-LOCA cladding deformation, are presented in the FTI Topical Report BAW-10166P Rev.2, "BEACH- Best Estimate Analysis Core Heat Transfer - A Computer Program for Reflood Heat Transfer," which was approved by letter dated August 13, 1990 (Reference 39), for analyses with Zircaloy cladding, with certain usage restrictions. From its review, the staff concluded that the FTI LOCA models, with the same usage restrictions except as addressed in this SE, that were approved for analyses assuming Zircaloy-clad fuel are acceptable for LOCA analyses assuming M5-clad fuel. This conclusion is based on the previous approvals of the LOCA models, the acceptability of the M5 fuel material characteristics modeling, the similarity of M5 and Zircaloy material properties, and the limited sensitivity of the analysis results to the difference in materials.

Although fuel pin cladding within a fuel assembly can swell prior to rupture creating a bulge that interferes with the local coolant passage, FTI LOCA evaluation models do not include flow diversion around this swelling until after a rupture has been calculated. This was found not to be non-conservative for cladding swell up to 20 percent, as is documented in the SE for the "BEACH" code (BAW-10166) dated August 13, 1990 (Reference 39). This SE concluded, "For any licensing analyses where cladding swell exceeds 20 percent, but does not rupture, the user should justify the acceptability." Calculated M5 fuel cladding swell can exceed 20 percent prior to rupture in LOCA analyses. In a letter dated January 14, 2000, FTI presented information from two reports, P. Ihle and K. Rust, "FEBA - Flooding Experiments with Blocked Arrays, Evaluation Report," KFK, 3657, March 1984, and Donald M. Ogden, "Review of FEBA Blockage Data," NUREG/CR-0048 Vol. 1, 11th Water Reactor Safety Research meeting, USNRC 1983, which indicate that omission of a pre-rupture swelling flow diversion model in FTI LOCA methodologies would not be non-conservative for calculated pre-rupture clad swelling of up to about 57 percent. Based on this information, the staff concludes that the previous limit of 20 percent cladding swell for FTI LOCA methodologies may be raised to 57 percent, and that a clad swelling flow diversion model may be omitted in LOCA analyses with FTI LOCA methodologies for calculated pre-rupture clad swelling of up to 57 percent. Above 57 percent pre-rupture clad swelling, the user must justify the acceptability.

The sensitivity studies performed demonstrated calculational stability and yielded expected results. The M5 calculated LOCA transient behavior showed modest quantitative differences from that of Zr-4, but the calculated behavior for LOCA transients with the two fuel types was very similar qualitatively.

In letters dated April 23 and September 24, 1999, Framatome also discussed the mechanics of incorporating correlations to accommodate M5 into its LOCA analysis codes and evaluation models. The staff finds that these are in accordance with regulatory guidance. The staff reviewed the RELAP5/MOD2-B&W model changes that reflect the properties of M5 fuel, and found them to be acceptable. The other changes to the model, which are not used in licensing calculations, are outside the scope of this review.

In its review of BAW-10227P, the staff considered each of the cladding property effects as a functional input to the analytical model and finds them acceptable (as is described in other sections of this SE).

The staff also considered LOCA analyses for M5-clad fuel co-resident with Zircaloy-clad fuel considering the possible effects of the differences in cladding properties, especially fuel swelling and rupture differences. The staff concluded that, because of the close similarity of M5 to Zircaloy, the effects of the differences on neighboring bundles would not be significant as long as the bundle geometries, including fuel dimensions and material surfaces, were alike. The staff, therefore, finds that when M5-clad fuel is co-resident with Zircaloy fuel, and fuel geometry and other properties that might affect fluid dynamics are alike, no mixed core penalty needs to be factored into the LOCA analyses performed with FCF's LOCA models for fuels clad with either M5 or Zircaloy.

The NRC staff concludes that the modifications to the use of the FCF SBLOCA and LBLOCA methodologies with M5 cladding and thimble tubes are in conformance with the requirements of 10 CFR Part 50, Appendix K and are, therefore, acceptable. The limitations and conditions identified in past SEs for the Framatome SBLOCA and LBLOCA models continue to apply.

8.0 CONCLUSIONS

The NRC staff has reviewed the FCF's advanced cladding and structural material, M5, for PWR fuel mechanical designs described in BAW-10227P. The NRC staff concludes that the M5 properties and mechanical design methodology, as defined in BAW-10227P and References 5, 6, 7, 8, and 9, are in accordance with SRP Section 4.2, 10 CFR 50.46, and 10 CFR Part 50 Appendix K and, therefore, are acceptable for fuel reload licensing applications up to rod average burnup levels of 62,000 MWd/MTU and 60,000 MWd/MTU for Mark B and Mark-BW fuel designs, respectively.

9.0 REFERENCES

1. Framatome Cogema Fuels. September 1997. Evaluation of Advanced Cladding and Structural Material (M5) in PWR Reactor Fuel. BAW-10227P, Framatome Cogema Fuels, Lynchburg, Virginia, transmitted by letter, J. H. Taylor (FCF) to U.S. NRC Document Control Desk, "Submittal of Topical Report BAW-10227P, Evaluation of Advanced Cladding and Structural Material in PWR Reactor Fuel," dated September 30, 1997, JHT/97-36.

2. B&W Fuel Company. June 1997. Extended Burnup Evaluation. BAW-10186P-A, B&W Fuel Company, Lynchburg, Virginia.

3. Letter, J. L. Birmingham, NRC, to C. F. McPhatter, Framatome Cogema Fuels, Request for Additional Information for Topical Report BAW-10227P, "Evaluation of Advanced Cladding and Structural Material in PWR Reactor Fuel," October 26, 1998.

4. Letter, J. L. Birmingham, NRC, to C. F. McPhatter, Framatome Cogema Fuels, Request for Additional Information for Topical Report BAW-10227P, "Evaluation of Advanced Cladding and Structural Material in PWR Reactor Fuel," January 29, 1999.

5. Letter, T. A. Coleman, Framatome Cogema Fuels, to U.S. NRC Document Control Desk, GR99-031.doc, February 5, 1999.

6. Letter, T. A. Coleman, Framatome Cogema Fuels, to U.S. NRC Document Control Desk, GR99-089.doc, April 23, 1999.

7. Letter, T. A. Coleman, Framatome Cogema Fuels, to U.S. NRC Document Control Desk, GR99-156.doc, July 29, 1999.

8. Letter, T. A. Coleman, Framatome Cogema Fuels, to U.S. NRC Document Control Desk, GR99-194.doc, September 24, 1999.

9. Letter, T. A. Coleman, Framatome Cogema Fuels, to U.S. NRC Document Control Desk GR-99-212.doc, October 20, 1999.

10. U.S. Nuclear Regulatory Commission. July 1981. "Section 4.2, Fuel System Design." Standard Review Plan for the Review of Safety Analysis Reports for Nuclear Power Plants - LWR Edition. NUREG-0800, Rev. 2, U.S. Nuclear Regulatory Commission, Washington, D.C.

11. United States Federal Register. "Appendix A, General Design Criteria for Nuclear Power Plants." In 10 Code of Federal Regulations (CFR), Part 50. U.S. Printing Office, Washington, D.C.

12. United States Federal Register. "Reactor Site Criteria." In 10 Code of Federal Regulations (CFR), Part 100. U.S. Printing Office, Washington, D.C.

13. United States Federal Register. In 10 Code of Federal Regulations (CFR), Part 50.46. U.S. Printing Office, Washington, D.C.

14. B&W Fuel Company. October 1999. Safety Criteria and Methodology for Acceptable Cycle Reload Analyses. BAW-10179P-A, Revision 3, B&W Fuel Company, Lynchburg, Virginia.

15. Lusternik V. E., Peletsky V. E., and Petrova I. I. 1993, "Experimental Study of Calorific Properties of Materials with Zirconium Base (Alloy E110) Used for Reactors," Teplofiz.Vys. Temp., Volume 31, No.4, pp. 560-564.

16. Lusternik V. E., Peletsky V. E., and Petrova I. I. 1993, "High Temperature Calorimetric Measurements of Zr-0.01Nb Alloy at Various Rates of Heating," High Temperatures -- High Pressures, Volume 25, pp. 539-543, Presented at the 13th European Conference on Thermophysical Properties Lisboa, Portugal, August 30- September 3, 1993.

17. Lusternik V. E., and Petrova I. I. 1997, "Investigation of the Thermophysical Properties of the Alloy Zr-0.01Nb by a Subsecond Pulse-Heating Technique," High Temperatures -- High Pressures, Volume 29, pp 373-378.

18. American Society of Mechanical Engineers. 1983 Edition. "Section III, Nuclear Power Plant Components." ASME Code. American Society of Mechanical Engineers, New York.

19. Garde, A. M. September 1986. Hot Cell Examination of Extended Burnup Fuel from Fort Calhoun. DOE/ET/34030-11, CEND-427, Combustion Engineering, Inc., Windsor, Connecticut.

20. Newman, L. W. et al. 1986. The Hot Cell Examination of Oconee Fuel Rods After Five Cycles of Irradiation. DOE/ET/34212-50 (BAW-1874), Babcock & Wilcox, Lynchburg, Virginia.

21. Garde, A. M. 1989. "Effects of Irradiation and Hydriding on the Mechanical Properties of Zircaloy-4 at High Fluence." In Zirconium in the Nuclear Industry: Eighth International Symposium, ASTM STP 1023, pp. 548-569, Eds. L.F.P. VanSwam and C. M. Eucken. American Society for Testing and Materials, Philadelphia, Pennsylvania.

22. Wesley, D. A., and K. J. Firth. October 1989. TACO-3 Fuel Pin Thermal Analysis Code. BAW-10162P-A, Babcock & Wilcox, Lynchburg, Virginia.

23. Wesley, D. A., D. A. Farnsworth and G. A. Meyer, July 1995. Fuel Rod Gas Pressure Criterion (FRGPC), BAW-10183P-A, B&W Fuel Company, Lynchburg, Virginia.

24. Garzarolli, F., H. Stehle, and E. Steinberg. 1996. "Behavior and Properties of Zircaloys in Power Reactors: A Short Review of Pertinent Aspects in LWR Fuel," ASTM 1295, pp. 12-32.

25. McGrath, M. A. 1998. "In-Reactor Creep Behavior of Zircaloy-2 Under Variable Loading Conditions," presented at the Annual Meeting on Nuclear Technology '98, The German Nuclear Society and The German Atomic Forum, Munchen Park Hilton, Munich Germany, May 26-28, 1998.

26. Framatome Technologies Incorporated. November 1992. RELAP5/MOD2-B&W - An Advanced Computer Program for Light Water Reactor LOCA and Non-LOCA Transient Analysis, BAW-10264P, Rev.1, Framatome Technologies Incorporated, Lynchburg, Virginia.

27. Hagrman, D. L., A. Reymann, and R. E. Mason. 1981. MATPRO-Version 11 (Revision 1): A Handbook of Materials Properties for Use in the Analysis of Light Water Reactor Fuel Rod Behavior, NUREG/CR-0497, Rev. 2, Prepared for the U.S. Nuclear Regulatory Commission by EG&G Idaho, Inc., Idaho Falls, Idaho.

28. Lanning D. D., C. E. Beyer, and C. L. Painter. 1997. FRAPCON-3: Modifications to Fuel Rod Material Properties and Performance Models for High Burnup Applications, NUREG/CR-6534, Volume 1 (PNNL-11513, Volume 1), Prepared for the U.S. Nuclear Regulatory Commission by Pacific Northwest National Laboratory, Richland, Washington.

29. O'Donnell, W. J., and B. F. Langer. 1964. "Fatigue Design Basis for Zircaloy Components." In Nuc. Sci. Eng. 20:1.

30. Miles, T., et. al., August 1995. Program to Determine In-Reactor Performance of B&W Fuel Cladding Creep Collapse, BAW-10084P-A Rev. 3, B&W Fuel Company, Lynchburg, Virginia.

31. United States Federal Register. "Appendix K.I.A, ECCS Evaluation Models." In 10 Code of Federal Regulations (CFR), Part 50. U.S. Printing Office, Washington, D.C.

32. Powers, D. A., and R. O. Meyer. April 1980. Cladding, Swelling, and Rupture Models for LOCA Analysis. NUREG-0630, U.S. Nuclear Regulatory Commission, Washington, D.C.

33. U.S. Nuclear Regulatory Commission. 1974. Assumptions Used for Evaluating a Control Rod Ejection Accident for Pressurized Water Reactors, Regulatory Guide 1.77, U.S. Nuclear Regulatory Commission, Washington D.C.

34. Schmitz, F., et. al., March 1996. " New Results from Pulse Test in the CABRI Reactor," Proceedings of the 23rd Water Reactor Safety Information Meeting October 23-25,1995.

35. Fuketa, T., et. al., March 1996. "New Results from the NSRR Experiments with High Burnup Fuel," Proceedings of the 23rd Water Reactor Safety Meeting, October 23-25, 1995.

36. Chapman, R. H. June 1978. Multirod Burst Test Program Progress Report for July-December 1977, NUREG/CR-0313, Oak Ridge National Laboratory, Oak Ridge, Tennessee.

37. Chapman, R. H. June 1979. Multirod Burst Test Program Progress Report for July-December 1978, NUREG/CR-00655, Oak Ridge National Laboratory, Oak Ridge, Tennessee.

38. Chapman, R. H. November 1979. Multirod Burst Test Program Progress Report for April-June 1979, NUREG/CR-1023, Oak Ridge National Laboratory, Oak Ridge, Tennessee.

39. Letter, A. C. Thadani, NRC, to J. M. Taylor, Babcock and Wilcox Nuclear Technologies, Acceptance for Referencing of Licensing Topical Report BAW-10166P, Revision 2, "BEACH - Best Estimate Analysis Core Heat Transfer, A Computer Program for Reflood Heat Transfer During LOCA," August 13, 1990.

Principal Contributors: S. L. Wu
F. R. Orr

Date: February 4, 2000

Framatome Cogema Fuels
Lynchburg, Virginia

Report BAW-10227-A

February 2000

Evaluation of Advanced Cladding and Structural Material (M5) in PWR Reactor Fuel

Key Words: Zirconium Alloy, Zr1Nb, Fuel Assembly Design, Fuel Rod Design, Pressurized Water Reactor, Performance under LOCA, Material Properties

ABSTRACT

This document contains the justification to use M5, a proprietary variant of Zr1Nb to replace Zircaloy-4 in the construction of fuel assembly components such as fuel rod cladding, guide tubes and spacer grids. This justification is required to support a request by Framatome Cogema Fuels for an exemption to, or a rule change to 10CFR50.46 to permit the use of M5 in addition to Zircaloy-4 and ZIRLO™. The use of M5 provides improvements in terms of lower corrosion, lower hydrogen pickup, lower axial growth and lower diametrical creep. These improvements will provide increased operating margin to the approved fuel rod burnup limits of 60 and 62 GWd/mtU for the Mark-BW and Mark-B fuel designs respectively.

This report is proprietary to Framatome Cogema Fuels (FCF). Alloy M5 was developed by FRAMATOME in France. Experimental data used in this report which is not in the public domain and some of the analytical models or correlations are the property of FRAMATOME.

CONTENTS

TABLES

FIGURES

1.0 INTRODUCTION AND SUMMARY

This document presents the results of Framatome Cogema Fuels evaluation of the use of the alloy M5 as an advanced cladding and structural material to replace Zircaloy-4 in PWR reactor fuel. M5 is a proprietary variant of Zr1Nb. In FCF fuel designs Zircaloy-4 is now used for the fuel rod cladding, end plugs, guide thimble tubes, instrumentation tubes and intermediate spacer grid strips. It is desired to replace these Zircaloy-4 parts with M5 parts to gain significant improvements in corrosion, hydrogen pickup, axial growth and diametral creep. To substitute M5 for Zircaloy-4 in fuel rod cladding requires that 10CFR50.46 be changed to include M5 as an approved material.

M5 has completed three cycles of irradiation in one U.S. reactor and is currently undergoing additional irradiation in two U.S. reactors. Eleven other commercial reactors in Europe have or are irradiating M5 fuel assembly parts. A maximum fuel rod burnup of 54.5 GWd/mtU has been achieved. The results show that the maximum fuel rod corrosion is 40 to 50% that of low tin Zircaloy-4 at higher burnups. Hydrogen pickup is a quarter of that experienced with Zircaloy-4. Similar improvements have been shown for the fuel assembly structural cage (guide thimbles and spacer grids). Ex-core and in-core testing have provided the data to formulate the properties for M5 presented in this report and used to perform the evaluations reported here.

The evaluations show that in most areas the use of M5 provides improved margins during normal operation (Condition I and II). M5 has also been evaluated for performance under accident conditions including LOCA. The basic material properties have been determined by a combination of testing and evaluation. These show that the present 10CFR50.46 criteria such as the 17% local maximum oxidation limit, the use of the Baker-Just metal-water reaction rate and the maximum allowable temperature of 2200 °F are still applicable when using M5. Based on test data changes were made to the material properties including those properties [c, d] These changes are described in Chapters 4 and Appendix A. Using these different material properties, LOCA evaluations were run to determine the impact of using M5. These evaluations show that the use of M5 does not require any reductions in operating limits to account for performance under LOCA conditions.

2.0 Fuel Assembly Mechanical Design

The use of M5 in fuel assembly fabrication is desired to provide an improvement in performance compared to Zircaloy-4. Although FCF fuel with Zircaloy-4 components has performed well to burnups approaching the licensed burnup limits, some of the Zircaloy-4 components are approaching design criteria in terms of allowable corrosion and hydrogen levels.[2-1] The improved corrosion, hydrogen pickup, growth and creep characteristics of M5 compared to Zircaloy-4 will provide increased margins and will form the basis for future burnup increases.

2.1 Fuel Assembly Design

Typical FCF fuel designs for the Mark-B and Mark-BW fuel assemblies are shown in Reference 2-1. Conversion from Zircaloy-4 to M5 involves only slight dimensional changes in guide tube and fuel rod lengths. The advanced Mark-BW (X1) lead test assemblies [2-2] under irradiation in North Anna 1 serve as an example. Table 2-1 compares the current Zircaloy-4 Mark-BW to the X1 LTA to demonstrate the changes. The primary changes are

The use of M5 for the structural material results in no changes to the basic analysis methods described in References 2-1, 2-2, 2-3 & 2-4.

2.2.1 Fuel Assembly Growth with M5 Structural Guide Thimbles

The use of M5 guide thimbles with FCF's present fuel assembly designs is expected to reduce fuel assembly growth due to irradiation. This prediction is based on the M5 database of fuel rod growth measurements and test reactor free growth measurements which have shown a reduced growth of approximately [c,d]relative to standard Zircaloy-4. In FCF fuel designs with the fuel rods in contact with the lower end fitting / bottom nozzle, the fuel assembly growth is coupled to the fuel rod growth. Measurements of shoulder gaps when evaluated against fuel assembly burnup typically show a slight and narrow range of shoulder gap closure with increasing exposure. Based on this coupling and the lower relative growth rate of M5 fuel rods and guide thimbles, the effective fuel assembly growth rate is expected to be [c,d]of that of fuel assemblies with Zircaloy-4 guide thimbles and fuel rods.

The four North Anna X1 LTAs which utilize M5 guide thimbles, will verify the growth behavior of M5 guide thimbles. These LTAs utilize M5 guide thimbles in the standard Mark-BW fuel assembly structure. Post irradiation examination (PIE) campaigns will be conducted on these fuel assemblies after each cycle of irradiation, including measurements of fuel assembly growth. The first of these PIEs is scheduled for [c,d] Similar measurements of M5 guide thimble growth are scheduled for M5 fuel assemblies being irradiated in Europe. Further details on these programs are given in Appendix E.

2.2.2 Fuel Assembly Structural Corrosion

The improved corrosion performance of M5 provides benefits to the structural components of the fuel assembly. For the fuel assembly structure, corrosion and the consequent hydrogen pickup result in a loss of material cross section to carry loads and a loss of ductility from high hydrogen concentrations. The buildup of hydrogen is of particular concern as structural components corrode on both surfaces (compared to the single sided corrosion of fuel rods). M5 provides improvements in both the general corrosion rate and the pickup of hydrogen. The general corrosion is approximately half that of low tin Zircaloy-4 and the hydrogen concentration is a one quarter of low tin Zircaloy-4 at high burnups. Figure 2-1 shows an example comparing the Mark-B (15x15) fuel assembly design using Zircaloy-4 and M5 guide tubes respectively. Guide tube oxide thickness and hydrogen pickup are plotted vs burnup for the two materials. It can be observed that there is a significant improvement in margins at the end of life with the M5 design. Similar improvements will be realized when using M5 for spacer grids.

2.2.3 Fuel Assembly Shipping and Handling

The fuel assembly is evaluated for performance during shipping and handling. The possible loads on the various components are evaluated and controls placed on acceleration the fuel can experience during shipping and on handling speeds during core loading and unloading. Accelerometers are part of each shipping container to assure that allowable acceleration limits are not exceeded. Typical acceleration limits applied to FCF fuel are:

Axial Acceleration	[	c, d	]
Horizontal Acceleration	[	c, d	]

The design requirements for the fuel assembly under normal operation are the same when using M5 components as when using Zircaloy-4. The criteria for buckling, applied loads and stresses for M5 components are the same for shipping and handling as in normal operation.

2.2.4 Fuel Assembly Normal Operating Analysis

The design requirements for the fuel assembly under normal operation are the same when using M5 components as when using Zircaloy-4. The design requirements for the M5 components will be reiterated here.

2.2.4.1 Spacer Grids

The M5 spacer grids (Intermediate Spacer Grid (ISG) and Mid Span Mixing Grid (MSMG)) must meet the following design requirements:

Dimensional requirements must be maintained during normal operation.

The ISG must also maintain adequate support to maintain the fuel rods in a coolable geometry under all conditions.

The maximum expected corrosion must be taken into account when determining the strength of the ISGs.

Hydrogen concentration must not exceed [c, d] to assure the ductility of the ISGs.

The mechanical characteristics of the grids (ISGs and MSMGs) are determined through testing. The types of characteristics determined from testing includes:

Dynamic Impact.

Static Crush.

Fuel Rod Slip Load.

Handling.

Fuel Assembly Corner to Corner Hang-up.

2.2.4.2 Guide Thimbles / Guide Tubes

Guide thimbles (Mark-BW) and guide tubes (Mark-B) provide an insertion path for the various control components (RCCAs, CRAs and BPRAs). The guide thimbles and guide tubes are similar in design except that the guide tubes do not have a reduced diameter region to act as a snubber for decelerating the movable control components following a SCRAM. Both guide thimbles and guide tubes are designed to the same requirements. For simplification only guide thimbles will be referred to in the following sections.

Guide thimbles are evaluated under normal operating conditions as specified in References 2-3 and 2-4. Typical normal operating conditions evaluated are Mechanical Design Flowrates (MDF), Pump Overspeed (PO) and SCRAM Loads.

2.2.5 Fuel Assembly Accident Analysis

The fuel assembly is evaluated for a series of potential accidents. These are:

Operation Base Earthquake (OBE). Allow continued safe operation of the fuel assembly following and OBE event by ensuring the fuel assembly components do not violate their dimensional requirements.

Safe Shutdown Earthquake (SSE). Ensure safe shutdown of the reactor by maintaining the overall structural integrity of the fuel assemblies, control rod insertability and a coolable geometry within the deformation limits consistent with the emergency core cooling system (ECCS) and safety analysis.

Loss of Coolant Accident (LOCA) or Combined LOCA/SSE. The fuel assembly must be design to allow for control rod insertion and to maintain a coolable geometry.

2.3 Extended Burnup Evaluation

The impact that the use of M5 has on extended burnup is that higher assembly burnups can be achieved due to the higher fuel rod burnups that can be realized with the lower corrosion of M5. Fuel that is limited by fuel rod corrosion in the range [c, d] maximum rod with Zircaloy-4 can be taken to the maximum approved rod limits of 60 and 62 GWd/mtU rod burnup for the Mark-BW and Mark-B fuel designs, respectively. The margin to criteria will be higher with the use of M5 due to lower corrosion and hydrogen pickup. Fuel assembly bow and guide thimble distortion are expected to be bounded by present FCF experience since the in-core growth and creep of M5 components will be lower compared to Zircaloy-4 components. The slight increase in burnup will not exceed the experience of other fuel assembly components such as the stainless steel end fittings, nozzles and Inconel 718 end grids and holddown springs in terms of burnup and neutron fluence.

Table 2-1 Fuel Assembly Design Comparison		
Parameter	Mark-BW	Mark-BW X1 LTA
Fuel Assembly Length, in.	[c,d]	[c,d]
Fuel Assembly Array	17x17	17x17
Number of End Spacer Grids	2	2
End Spacer Grid Material	Alloy 718	Alloy 718
Number of Intermediate Spacer Grids	6	6
Intermediate Spacer Grid Material	Zircaloy-4	[c,d]
Number of Midspan Mixing Grids	NA	[c,d]
Midspan Mixing Grid Material	NA	[c,d]
Guide Thimble Length, in.	[c,d]	[c,d]
Guide Thimble Dashpot Length, in.	[c,d]	[c,d]
Guide Thimble OD, in.	[c,d]	[c,d]
Guide Thimble ID, in.	[c,d]	[c,d]
Guide Thimble Dashpot OD, in.	[c,d]	[c,d]
Guide Thimble Dashpot ID, in.	[c,d]	[c,d]
Guide Thimble Material	Zircaloy-4	[c,d]
Shoulder Gap, in	[c,d]	[c,d]
Fuel Rod Length, in	[c,d]	[c,d]
Fuel Rod Cladding OD, in.	[c,d]	[c,d]
Fuel Rod Cladding ID, in.	[c,d]	[c,d]
Fuel Rod Cladding Material	Zircaloy-4	[c,d]
Fuel Pellet Diameter, in.	[c,d]	[c,d]
Fuel Stack Length, in	[c,d]	[c,d]

Figure 2-1Maximum Guide Tube Oxide Thickness and Hydrogen vs Burnup

Figure 2-1 is Proprietary

[c, d]

3.0 Fuel Rod Design Requirements and Analysis Results

The use of M5 for fuel rod cladding provides improvements in corrosion, creep and growth. This gives increased margins at current burnup limits and provides a basis to go to higher burnups. To illustrate this two rod designs using M5 have been developed and evaluated. Those two designs are shown in Table 3-1 along with the results of the evaluations.

Table 3-1
Representative M5 Fuel Rod Designs

Parameters and Conditions	Mark-B Ref 3-1	Mark-BW Ref 3-2
Design Parameters		
Array	15x15	17x17
Fuel Rod Length, inches Fuel Stack Length, inches Plenum Length, inches Plenum Volume, in^3 Annular Volume, in^3 Dish Volume, in^3 Cladding OD, inches Cladding ID, inches Pellet Diameter, inches Pellet -Clad Gap, inches Pellet density, %TD. Fill Gas Pressure, psia	[c, d]	[c, d]
Operating Conditions Core Average LHGR, kW/ft Core Inlet Temp, °F	[c, d]	[c, d]
End of Life Conditions Maximum Cladding Oxide Thickness at 65 GWd/mtU, μm Maximum Hydrogen Concentration at 65 GWd/mtU, ppm	[c, d]	[c, d]

In this section, the performance aspects covered in Reference 3-3 of the fuel rod under conditions I and II will be described. The standard FCF fuel rod analysis methods are detailed in References 3-4, 3-5 & 3-6. To evaluate M5 clad rods under these conditions, the following models must be revised.

Table 3-2
Model and Code Changes for M5 Use

Model	Codes Impacted	Calculations Impacted
[c, d]	[c, d]	[c, d]
[c, d]	[c, d]	[c, d]
[c, d]	[c, d]	[c, d]
[c, d]	[c, d]	[c, d]

The main factor that must be accounted for is the difference in material properties. This difference is due to the [c, d]current Zircaloy-4 cladding. In the next sections each analysis is discussed and evaluated using the M5 material properties. Details on the M5 material properties can be found in Chapter 5 and Appendix A.

3.1 Fuel Rod Cladding Corrosion and Hydriding

The corrosion of M5 has been measured through 54.5 GWd/mtU rod average burnup. Those results are shown in Figure 3-1. The corrosion of M5 is modeled using the same cladding corrosion model used for SRA Zircaloy-4 that is given in Reference 3-4 except that a different activation energy is used. In the COROS02 code the M5 oxide rate is calculated by the following formulas:

Pre Transition, for oxide layer growth up to the transition thickness in the range of 2 to 3 μm:

[c, d]

Post Transition, for oxide layer growth once the transition oxide thickness has been reached:

[c, d]

The constants are :

Constants	Standard Tin Zircaloy-4	Low Tin Zircaloy-4	Alloy-5
K pre (m^3/s)	[c,d]	[c,d]	[c,d]
Q pre (J/mol)	[c,d]	[c,d]	[c,d]
K post (m/s)	[c,d]	[c,d]	[c,d]
Q post (J/mol)	[c,d]	[c,d]	[c,d]

The performance of the COROS02 model in predicting M5 corrosion is shown in Figure 3-2. The hydrogen pickup of M5 is low [3-7]. The measured pickup for M5 fuel rods is shown in Figure 3-3. Based on this data a pickup of [c,d] is used in analysis. This pickup fraction and the M5 corrosion model were used to evaluate the two fuel rod designs. Those results are listed in Table 3-1 and shown in Figures 3-4 and 3-5. Also shown in those figures is the hydrogen concentration of the cladding.

3.2 Fuel Rod Internal Pressure

Fuel rod internal pressure is evaluated following the methods identified in References 3-4, 3-8 & 3-9. The only modification is that the creep model in TACO3 [3-8] is [c,d] A more complete description of M5 in-core creep is found in Appendix B. [c,d] The net effect is that very little change occurs in the burnup limit for rod pressure. [c,d]

3.3 Fuel Rod Cladding Stress and Buckling

The use of [c,d] The licensed method used by FCF evaluates fuel rods by determining the stress intensity and comparing that to a stress intensity limit Sm based on the ASME code [3-10]. Sm is set equal to the minimum unirradiated tensile yield strength of the cladding. For [c,d] FCF has used this method previously to license a limited number of fuel rods in three reactors [3-1, 3-2 & 3-11]. The limits and definitions of stress intensity are as follows:

Table 3-3
M5 Fuel Rod Stress Intensity Limits

	Compression		Tension	
Condition	Stress Intensity Limit	Stress Intensity Limit at 690 °F, ksi	Stress Intensity Limit	Stress Intensity Limit at 690 °F, ksi
Pm Primary membrane	[c,d]	[c,d]	Sm	[c,d]
Pm + Pb Primary membrane + Bending	[c,d]	[c,d]	1.5 Sm	[c,d]
Pm + Pb + Pl Primary membrane + Bending Local	[c,d]	[c,d]	1.5 Sm	[c,d]
Pm + Pb + Pl + Q Primary membrane + Bending Local + Local	[c,d]	[c,d]	3.0 Sm	[c,d]
Sm = [c]				

[

c,d

]

[

c, d

]

[c, d]

3.4 Fuel Rod Cladding Transient Strain

Reactor power must be controlled during Conditions I and II events to preclude the cladding strain exceeding 1% during a transient. To set operational limits to insure that centerline melting does not occur, an approved fuel performance code such as TACO3 is used to evaluate pellet/cladding strain as a function of a steady-state power history envelope with power transients superimposed until either a 1% maximum transient hoop strain or the fuel centerline melting temperature (LHRM) is reached. The operational transients imposed extend throughout a total rod-average burnup of 62,000 MWD/mtU. TACO3 models the effects of fission gas release, thermal expansion, irradiation growth, fuel densification and swelling, cladding creep, and elastic strain. The main impact of using M5 is the change

3.5 Fuel Centerline Melting Temperature

The reactor power must be controlled during Condition I and II events to preclude the centerline fuel temperature from reaching the melting point. To set operational limits to insure that centerline melting does not occur, the fuel rod power required to cause fuel centerline melt (LHRM) is determined using an approved fuel performance code. The main impact of using M5 [

c, d

]

3.6 Fuel Rod Cladding Fatigue

The fatigue analysis is performed with a conservative method and insures compliance with a design criterion of a cumulative fatigue usage factor of less than 0.9 for the fuel rod cladding.[3-3, 3-4 & 3-5] Procedures for the fatigue analysis follow those outlined in the ASME Boiler and Pressure Vessel Code [3-10], using the O'Donnel-Langer fatigue curve for irradiated Zircaloy[3-13] as a design basis. To determine the total fatigue usage factor of the cladding, all possible Condition I and II events are considered along with one condition III event. Conservatisms include cladding thickness, oxide layer buildup, external pressure, internal fuel rod pressure and pressure differential. The fatigue usage factors for MK-B and Mark-BW17 were calculated

using a [c, d] were calculated for the Mark-B and Mark-BW designs respectively.

Tests have been conducted by Framatome in France to determine the fatigue performance for M5. These tests have shown similar fatigue endurance performance for M5 compared to Zircaloy-4 with [c, d] Thus the fatigue utilization for M5 clad fuel rods will be similar to that for Zircaloy-4 clad fuel rods.

3.7 Fuel Rod Cladding Creep Collapse

The creep collapse is determined using the CROV computer code[3-14]. The creep collapse evaluations using the CROV code in reference 3-3 for Mark-B and Mark-BW designs both showed a creep collapse life of > 65 GWd/mtU. Since the creep rate of M5 is considerably slower than the standard [c, d] the creep collapse life of an M5 fuel rods is much greater than the standard rods and is not limiting at burnups up to 62 GWd/mtU.

3.8 Fuel Rod Axial Growth

The growth of the M5 fuel rods has been evaluated from measured growth data. Based on that data an M5 fuel rod will have a UTL growth rate of of the UTL for a Zircaloy-4 clad fuel rod. When an M5 fuel rod is used with M5 guide thimbles the result will be a shoulder gap closure rate similar to that observed in current FCF fuel designs. Figure 3-8 shows that shoulder gap closure for FCF fuel designs. [c, d] Figure 3-9 shows the growth rate of M5 fuel compared to Zircaloy-4 fuel rods in the same fuel assembly design.

3.9 Fuel Rod Bow

Fuel rod bow is driven by the irradiation growth of the fuel rods and friction with the supporting guide structure. Since M5 has lower growth than Zircaloy-4, M5 fuel rods are expected to have rod bow within the envelope established in references 3-4 & 3-16. Therefore, the performance and penalties established in references 3-4, 3-5 & 3-6 will apply to the M5 designs. This will be verified by the inspection of the X1 LTA assemblies under irradiation in North Anna 1.

Figure 3-1 M5 Maximum Oxide Thickness vs Burnup

Figure 3-1 is Proprietary

[d]

Figure 3-2 M5 Measured/Predicted Comparison

Figure 3-2 is Proprietary

[d]

Figure 3-3 M5 Hydrogen Pickup vs Burnup

Figure 3-3 is Proprietary

[d]

Figure 3-4 Predicted Maximum Oxide Thickness and Hydrogen Concentration vs Burnup, Mark-B

Figure 3-4 is Proprietary

[c,d]

Figure 3-5 Predicted Maximum Oxide Thickness and Hydrogen Concentration vs Burnup, Mark-BW

Figure 3-5 is Proprietary

[c,d]

Figure 3-6 Mark-BW X1 LTA Rod and Buckling Pressure vs Temperature

Figure 3-6 is Proprietary

[d]

Figure 3-7 M5 Yield Strength vs Local Burnup

Figure 3-7 is Proprietary

[d]

Figure 3-8 FCF Fuel Assembly Shoulder Gap Closure vs Burnup

Figure 3-8 is Proprietary

[c,d]

Figure 3-9 M5 Fuel Rod Growth vs Fast Fluence

Figure 3-9 is Proprietary

[d]

4. Accident Criteria and Evaluation

An assessment of the impact of the M5 alloy on the safety performance of nuclear fuel has been conducted. The material properties for M5 differ to varying degrees from those of currently approved cladding materials. The assessment presented in this section concludes that the results of accident evaluations will approximate those for current cladding and not comprise a decrease in the safety performance for plants using the M5 cladding. The use of the M5 alloy will have no significant adverse impact on the radiological doses calculated for those accidents wherein the release of radionuclides is postulated. The following characterizes the performance of the M5 alloy and the consequences of its use during LOCA and non-LOCA accidents.

4.1 Impact of M5 Fuel Rod Cladding on Non-LOCA Accident Analysis

The non-LOCA accident evaluations performed for licensing in the US can be divided into events with departure from nucleate boiling (DNB) acceptance criteria and events for which a specific parameter of the core or system is followed and compared to an acceptable value. Given a specified heat load the ability of the fuel assembly to remain below the threshold of DNB is primarily related to the mechanical configuration of the fuel assembly as opposed to the type of material employed. As demonstrated in Appendix A, the thermal conductivity is not affected by changes in minor alloying constituents and will not vary between M5 and Zircaloy. Within Section 3 it was demonstrated that the creep rate and axial growth of the M5 alloy is substantially less than that of Zircaloy-4. This means that, dependent on the extent of involvement of the M5 alloy in the fuel assembly design, fuel pins, grids, and/or guide tubes, the geometric changes due to exposure within the reactor will be smaller than those for Zircaloy. Thus, the effects of these changes, rod bow and control rod insertion time changes, will be improved and of less concern than for Zircaloy cladding. Thus, for the DNB related events there is no consequence of a switch from Zircaloy-4 to M5 other than an improved ability to control the fuel assembly performance and the results of these evaluations are the predicted mechanical configuration of the assembly and the plant system. Such events, as generally listed in the FSAR, are:

Uncontrolled RCCA Bank Withdrawal form a Subcritical Condition
Uncontrolled RCCA Bank Withdrawal at Power
Rod Cluster Control Assembly Misalignment
Uncontrolled Boron Dilution
Startup of an Inactive Reactor Coolant Loop
Spurious Operation of the Safety Injection System at Power
Loss of External Electrical Load
Excessive Heat Removal Due to Feedwater System Malfunctions
Excessive Load Increase Incident
Accidental Depressurization of the Reactor Coolant System
Accidental Depressurization of the Main Steam System
Main Steamline Rupture

Complete Loss of Reactor Coolant Flow
Single Reactor Coolant Pump Locked Rotor
Single RCCA Withdrawal at Full Power

For non-LOCA accident evaluations that do not involve DNB criteria, there is an effect of the M5 alloy if the transient involves the calculation of a detailed cladding temperature history with an excursion into the alpha/beta phase change temperature range. This effect is produced by the alteration over the alpha/beta phase change of the specific heat and thermal expansion, Appendix A. For M5 the phase change transition range initiates at approximately 690 C, while for Zircaloy the change initiates at approximately 825 C. Under typical conditions, both materials have transformed to 100 percent beta by approximately 980 C. The material properties prior to and following the phase change are essentially the same for Zircaloy and M5. Therefore, for transients that do not reach the transition temperature, no significant difference in results of predictions are expected. Further, the integrated effect of the phase change on the property is conserved over the phase change between the materials (Appendix A). The energy required to make the phase change, for example, is the same for both alloys but is consumed over a wider temperature range for M5. Thus, for transients wherein the temperature predictions transition into the M5 phase change range, there will be a slight effect on the cladding response. Because of the conservation of integrated effect across the phase change, transients that transition through the phase change will experience little change in result. It will be necessary to recalculate the temperature transients that enter or exceed the phase change range with M5 specific properties when licensing applications for M5 cladding are requested. These types of calculations have not been performed herein because they are dependent on the specific fuel assembly design and the specific plant systems and are not expected to demonstrate temperature differences of consequence.

As generally listed in the FSAR the non-DNB criteria events are:

Loss of Normal Feedwater
Loss of Offsite Power to the Station Auxiliaries
Spurious Operation of the Safety Injection System at Power
Steam Generator tube Rupture
Single Reactor Coolant Pump Locked Rotor
Fuel Handling Accident (Inside and Outside Containment)
Major Rupture of a Main Feedwater Line
Rupture of a Control Rod Drive Mechanism Housing (Rod Ejection).

Of these, the "Single Reactor Coolant Pump Locked Rotor" and the "Rupture of a Control Rod Drive Mechanism Housing" accidents are most likely to result in temperature transients that exceed the transition temperature.

In conclusion, there will be no effect of the M5 alloy cladding material on most of the non-LOCA safety analysis provided in plant FSARs. For those accident evaluations that produce cladding temperature responses that exceed the phase transition range,

approximately 700 C, a small impact on temperature response is expected and a revised calculation with M5 specific materials properties should be performed for batch licensing. The results of those calculations are not expected to differ substantially from Zircaloy-4 based calculations and no limiting criteria are expected to be challenged. Therefore, this alloy will have no adverse impact on the FCF fuel designs.

4.2 Impact of M5 Fuel Rod Cladding on LOCA Accident Analysis

Use of the M5 alloy as a cladding material for fuel assemblies interacts with the LOCA evaluation in several ways. The basic material properties of M5 differ from those of Zircaloy-4 to varying degrees over the range of the calculation. Of particular import are the creep behavior and the high temperature swelling and rupture behavior of the new material. Creep is reduced from that of Zircaloy-4 resulting in a different burnup dependency for the initial steady state-fuel temperatures. The swelling and rupture characteristics are similar to those of Zircaloy but shifted somewhat due to an alteration in the alpha/beta change temperatures for the material. Other changes involve the materials thermal heat capacity and the thermal expansion. An additional consideration is the applicability of the requirement of Appendix K of 10CFR50.46 to use the Baker/Just correlation for high temperature oxidation. Finally, the basic acceptance criteria of 10CFR50.46 must be verified as providing the appropriate degree of public protection when applied to the new cladding material.

4.2.1 Applicability of 10CFR50.46 Criteria

Two of the five criteria of 10CFR50.46 have the potential for interacting with the new cladding material.

1. 2200 F Peak Cladding Temperature (PCT) Limit This limit was established to maintain an acceptable margin to potential embrittlement of the cladding and assure a substantial margin to the true temperature at which the zirconium/water oxidation process becomes autocatalytic. FTI has determined that the M5 melt temperature and the cladding strength at 2200 F are such as to preserve the safety margins inherent in the application of this temperature to Zircaloy-4. Therefore, the 2200 F PCT limit is valid for the M5 cladding. Appendix G discusses the basis for this finding.

2. Maximum Local Oxidation < 17 Percent This limit was imposed on the calculation to prevent the brittle fracture of the fuel pin cladding during the reflood quench. For Zircaloy, the expected threshold for thermally induced brittle fracture is approximately 20 to 22 percent oxidation. Framatome has performed preliminary measurements of the brittle fracture limit for M5 with the result that the true limit [c, d]. Therefore,

the 17 percent criterion is valid for the M5 cladding. Appendix G discusses the basis for this finding.

3. Maximum Core Wide Oxidation < 1 Percent This limit was imposed to prevent the accumulation of a combustible amount of hydrogen within the reactor building. The criterion is imposed to prevent a difficulty with a system other than the cladding and is, therefore, not related to nor affected by the cladding material. Further, Framatome has determined that the high temperature oxidation behavior of M5 is essentially similar to that of Zircaloy and, since the small degree to which hydrogen is retained within the oxidized cladding is not considered in establishing the limit, both M5 and Zircaloy respond as hydrogen generators to the same extent. Thus, both realize the same conservative margin when the Baker/Just correlation is used to demonstrate adherence to the criterion. Therefore, the 1 percent criteria is valid for the M5 cladding. Appendix D discusses the high temperature oxidation performance of the M5 alloy.

4. The Core Geometry Shall Remain Amenable to Cooling The implication of this criterion is that the core shall remain in a condition that can be readily cooled by the type of short- and long-term cooling mechanisms provided by the plant ECCS. The goal of the criterion is not directly related to the cladding material such that the criterion applies equally well to all materials. Further, FTI has determined that the limiting blockage will remain below that which would compromise a coolable geometry. Therefore, the condition requirement applies and is valid for the M5 cladding. Appendices C and F provide discussions on the ability of M5 cladding to maintain a coolable geometry during LOCA.

5. Long-Term Core Cooling Shall Be Established This is a plant system requirement and not related to the cladding material. It is as valid for any cladding that could be used in a pressurized water reactor. Therefore, the criterion continues to be applicable with the M5 cladding.

4.2.2 Cladding Swelling and Rupture

Of significant importance to the licensing LOCA evaluations is the ability to describe the cladding swelling and rupture behavior at high temperature. Because M5 is a different alloy from the Zircaloy that has been used to develop correlations for the swelling and rupture behavior of cladding in current evaluation models and actually behaves somewhat differently than Zircaloy, a revised modeling and model basis for the material was developed. To facilitate the development, tests of cladding swelling and rupture were performed at the French CEA laboratory in Saclay, France. These tests, identified by the acronym EDGAR, were pressurized single pin, electrically heated rupture tests and measured both rupture deformation and the temperatures at which rupture would occur. The results of this testing were used to develop an M5 specific cladding swelling and

rupture model for use in the LOCA evaluation of this cladding. The model [redacted]. Appendix C fully describes the model developed. Appendix F provides representative LOCA calculations that incorporate the new model.

4.2.3 Cladding High Temperature Oxidation

Appendix K of 10CFR50.46 requires the application of the Baker/Just correlation for the modeling of high temperature oxidation during LOCA calculations. Appendix D provides the results of measurements of the high temperature oxidation rates for the M5 alloy that demonstrate that the Baker/Just correlation remains a conservative model for this material. In actuality the high temperature, greater than 1900 F, oxidation rates for M5 are substantially similar to those for Zircaloy. Therefore, the requirement of Appendix K is valid and the Baker/Just correlation will continue to be used within the LOCA evaluation models when fuel performance with the M5 cladding is being calculated.

4.2.4 Basic M5 Material Properties

The basic physical properties of the M5 alloy are quite similar to those of Zircaloy. However, some differences have been observed. These differences are of particular note for properties that relate to the materials phase change from the alpha crystalline structure to its beta structure. Appendix A presents the materials properties that have been used in the LOCA and safety analysis determinations presented in this report to characterize the performance of the M5 cladding. Not all of these properties have been experimentally measured but appropriate approximations based on available data are presented. The approximations are deemed sufficient for the demonstration of the material as a viable cladding for nuclear fuel pins. Appendix F provides representative LOCA calculations using the material properties given in Appendix A.

4.2.5 LOCA Performance of M5 Cladding

The LOCA performance of M5 cladding is provided for representative fuel designs in Appendix F. Calculations for both the Mark-B (B&W designed NSS fuel) and the Mark-BW (Westinghouse designed NSS fuel) are provided. The M5 cladding is shown to behave in a similar fashion to Zircaloy. The range of permissible design achieves acceptable LOCA performance. In particular the cladding temperatures and other criteria determinants vary only slightly from the reference Zircaloy cases. For some cases the peak cladding temperatures (PCT) may be slightly lower for M5 and in other cases or conditions the PCTs may be higher. One general observation is that the creep model for M5, Section 3.8, produces a slower creep down of the cladding onto the fuel pellet than for Zircaloy. This leads to lower fuel cladding gap conductivity for mid-life burnups and necessitates that burnup sensitivity studies be conducted for the first plant applications of the alloy.

The general conclusion from the work presented in Appendices C, D, F, and G, is that:

1. The criteria of 10CFR50.46 apply to the M5 alloy,

2. The modeling of the characteristics of the cladding has been developed in a conservative and appropriate way,

3. The cladding behavior during LOCA and the design ranges available are such that the LOCA criteria can be readily met by fuel assemblies incorporating the material, and

4. There is no LOCA related reason that the material should not be used in FCF fuel products.

4.3 Impact of M5 Fuel Rod Cladding on Radiological Dose Evaluations

The use of the M5 alloy will have no significant adverse impact on radiological doses, which may result from any accident involving the release of the radionuclides in the gap or fuel pellet. Safety analyses that evaluate radionuclide releases are done so using releases as defined in a given plant's FSAR. The releases for accidents such as the fuel handling accident (FHA) and the loss of cooling accident (LOCA) are independent of the cladding performance. A common assumption for the FHA is that all fuel rods of an assembly are damaged and release gap activity to the reactor coolant, whereas for the LOCA, all gap activity contained in the core is assumed released. The releases for LOCA and FHA are, therefore, arbitrary and depend only the licensed burnup of the fuel pins and assemblies contained in the plant core. In the case of a control rod ejection accident, it is conservatively assumed that all rods that undergo DNB fail and release gap activity. As stated in Section 4.1 the fuel DNB performance is not dependent on the material used in the cladding and thus the radiological consequences of this accident are not altered by the use of M5 cladding. The M5 alloy may, at some time in the future, facilitate an increase in the licensed burnup level but none is currently being sought and, therefore, there is no change to the radiological dose consequences of plant operation because of the use of M5 cladding.

5.0 M5 Material Properties

M5 is a proprietary variant of Zr1Nb. Like Zircaloy-4 and other zirconium alloys with small percentages of alloying agents it has a low cross section for thermal neutrons. Compared to Zircaloy-4, M5 shows less enhancement of corrosion, hydrogen pickup and growth due to in-core operation. It is to obtain the benefit of lower in-core corrosion, hydrogen pickup, growth and diametrical creep that FCF has evaluated M5 for PWR fuel application. In order to perform this evaluation, the significant material properties for M5 had to be identified and obtained from literature and testing. A complete listing of the significant material properties is given in Appendix A.

The significant differences between M5 and Zircaloy-4 are as follows:

M5 is only used in the [d]condition, both for guide thimble and for fuel rod cladding.

The transition from the α phase to the β phase occurs [d]while it is 825 C for Zircaloy-4.

The in-core corrosion rate of M5 is 50% that of Zircaloy-4. In the absence of a neutron flux, the corrosion rates for Zircaloy-4 and M5 are similar.

The hydrogen pickup fraction for M5 is 50% that of Zircaloy-4.

6 References

2-1. BAW-10186P-A, Extended-Burnup Evaluation, June 1997.

2-2. BAW-2272 Mark-BW17 Lead Test Assemblies for North Anna Power Station - Design Report, July 1996.

2-3. BAW-10179P-A, Safety Criteria and Methodology for Acceptable Cycle Reload Analyses, August 1993.

2-4. BAW-10172P-A "Mark-BW Mechanical Design Report." July 1988.

3-1. Jim Taylor to NRC, "Evaluation of M4 and M5 Cladding Alloys for TMI-1", May 2, 1995

3-2. BAW-2272 Mark-BW17 Lead Test Assemblies for North Anna Power Station - Design Report, July 1996.

3-3. Standard Review Plan, Section 4.2, NUREG-0800, Rev 2, U.S. Nuclear Regulatory Commission, July 1981.

3-4. BAW-10186P-A, Extended-Burnup Evaluation, June 1997.

3-5. BAW-10172P-A "Mark-BW Mechanical Design Report." July 1988.

3-6. BAW-10179P-A, Safety Criteria and Methodology for Acceptable Cycle Reload Analyses, August 1993.

3-7. J.P. Mardon, et al., Update on the Development of Advanced Zirconium Alloys for PWR Fuel Rod Performance, pg 405 to 412, Proceedings of The 1997 International Topical Meeting on LWR Fuel Performance, Portland Oregon, March 2-6, 1997.

3-8. D. A. Wesley and K. J. Firth, "TACO3 - Fuel Rod Thermal Analysis Code," BAW-10162P-A, August 1989.

3-9. D. A. Wesley, et. al., "Fuel Rod Gas Pressure Criterion (FRGPC)," BAW-10183P, July 1991.

3-10. ASME Code Section III," Nuclear Power Plant Components ", 1983 Edition.

3-11. BAW-2133P MARK-BW Advanced Claddings Fuel Rod Evaluation. March 1991.

3-12. Strength of Materials, Part II Advanced Theory and Problems, 3'rd ed, Timoshenko.

3-13. O'Donnell, W.J. and Langer, B.F."Fatigue Design Basis for Zircaloy Components." Nuclear Science and Engineering, Volume 20, pages 1-12.

3-14. BAW-10084P-A, Rev. 3, Program to Determine In-Reactor Performance of B&W Fuels--Cladding Creep Collapse--Revision 3, July 1995.

3-15. Fuel Rod Bowing in Babcock & Wilcox Fuel Designs, BAW-10147, Babcock & Wilcox , Lynchburg, Virginia, April 1981.

3-16. BAW-2294, Performance Summary of the Mark-BW Fuel Assembly Design, March 1997.

Appendix A

ALLOY M5 MATERIAL PROPERTIES

ALLOY M5 MATERIAL PROPERTIES

The following lists the material properties used for the M5 alloy, both for LOCA analysis and for normal operating conditions. Some of the properties used are extrapolations based on the known parameters for M5 and Zircaloy-4. Ongoing experimental programs are continuing to provide new data to compare to those extrapolations. As such information is obtained it will be evaluated and applicable analyses revised if the new data supports a change.

A.1 MATERIAL COMPOSITION AND CONDITION.

A.1.1 Alloy Composition

The nominal composition of the M5 alloy is 1.0% niobium, 0.125% oxygen with the balance being zirconium. The permitted range for these alloying elements is [c, d]niobium and [c, d]oxygen. The minor impurities are restricted to a maximum of [c, d] The composition is listed and compared to Zircaloy-4 in Table A-1

A.1.2 Material Condition

All components, (cladding, guide tubes, and grids) are specified in [c, d] The data presented below relates only to this condition. However, it should be noted that irradiation tends to strengthen zirconium alloys and many of the mechanical properties tend to new equilibrium values as a result of irradiation. This phenomenon appears to be independent of the original metallurgical condition so that the M5 mechanical properties are expected to be similar to those of Zircaloy-4 as a result of irradiation.

A.2 PHYSICAL PROPERTIES

A.2.1 Base Properties

A.2.1.1 Specific Gravity (Density)

The specific gravity of the M5 alloy is calculated as [c, d](Reference A-1)

A.2.1.2 Dimensional Controls

All material dimensions e.g. lengths, diameters, thickness, etc., are specified in the relevant FCF drawing or specification. These will generally be similar to dimensions used for Zircaloy cladding.

A.2.1.3 Surface Finish/Roughness

The surface finish defined by the drawings or specifications is used as the limiting criterion for design purposes. Measurements of the actual surface finish of M5 cladding are similar to those for Zircaloy 4 cladding.

A.2.2 Thermophysical Properties

A.2.2.1 Coefficient of Thermal Expansion

a) Alpha phase. - Thermal expansion coefficients of zirconium and its alloys vary both by direction, axial or circumferential, and by metallurgical state, alpha or beta phase. For the alpha phase, thermal expansion coefficients of a zirconium/1.17% niobium alloy have been referenced in the Thermophysical Properties Research Center (TPRC) at Purdue University (Reference A-2) and these have been compared with those for Zircaloy-4 obtained from Matpro. Both values agree well up to 1000 F (811 K) as seen in Figure A-1. Based on this agreement, the Matpro values used for Zircaloy (References A-3 and A-4) will also be used for the M5 alloy for the alpha phase.

b) Beta phase. - Figure A-1 shows that the gradients of the temperature/thermal expansion lines for the Zircaloy beta phase are essentially identical for both the axial and circumferential directions. This is to be expected for a cubic lattice. Since Matpro recommends that the coefficient of linear expansion for Zircaloy in the beta phase is taken to be that of pure zirconium (9.7×10^{-6} K^{-1}) the same assumption can be made for the M5 alloy.

c) Alpha/Beta phase change. - The only differences between the thermal expansion values for Zircaloy and M5 are during the alpha/beta transition period. For Zircaloy-4, the transition from the alpha to the beta phase occurs at approximately 1073K compared to 963K for M5. The contraction in the zirconium lattice cell during the phase change results in the rapid decrease in the thermal expansion term as shown in Figure A-1. Since zirconium is the major component of both Zircaloy and M5, it is reasonable to assume that the contraction will be the same for both alloys even though the change occurs at different temperatures. From Figure A-1, the expansion coefficient for Zircaloy at the initiation of the alpha/beta transition (1073K) is 0.353% in the axial direction and 0.514% in the circumferential direction. At the end of the transition (1274K) the respective values are 0.141% and 0.291%. The respective changes in values are thus 0.212% in the axial direction and 0.223% in the circumferential direction. Applying these latter values to the M5 case, which has expansion coefficients of 0.304% for the axial direction and 0.440% for the

circumferential direction prior to the alpha/beta phase change, the calculated M5 expansion coefficients for the beta phase are:

[c,d]

The above results are shown in graphical form in Figure A-1.

A.2.2.2 Thermal Conductivity

The thermal conductivity values used in the current RELAP5/MOD2-B&W, model for Zircaloy-4, Reference A-5, are shown in Figure A-2 together with the MATPRO formulation results, and the Purdue (TPRC) data for pure zirconium, Zircaloy-2, Zircalo-4 and a zirconium - 1.5% niobium alloy. The RELAP5 default curve is also included [c,d] Further, if the outlier Purdue C10[1] data is rejected, there is very good agreement between the thermal conductivity determinations regardless of alloy composition. Therefore the RELAP5 data is considered adequate to represent the thermal conductivity of the M5 alloy.

Note 1: The specimen "Zircaloy-4 (TPRC, C10)" had a higher impurity level and was heat treated for a number of hours before testing. These factors may have influenced the thermal conductivity value obtained.

A.2.2.3 Heat Capacity

Heat capacity is obtained from the specific heat/temperature relationship. Figure A-3 shows the data for Zircaloy-4 (RELAP5 model) and the proposed M5 model [c,d

]Examination of the TPRC database for zirconium and a zirconium-17.5% niobium alloy indicates that, although there is little difference in the heat capacities of the alloys before and after the phase change, there is a significant difference in the relationship during the phase change. Further examination of the data shows that the required energy for the phase change is constant and independent of the zirconium alloying element, therefore it is reasonable to predict that the total energy absorbed during the phase change is the same for both systems.

The temperatures selected for the phase change are 1098K to 1253K for Zircaloy-4 [c,d]

[c,d] It should be noted these temperatures do not represent equilibrium (or slow heating rate) conditions but are more representative of LOCA heating rates, see Appendix F. It is also recognized that the actual shape of the curves in Figure A-3 will be determined by the heating rate.

A.2.2.4 Emissivity

The clad emissivity of the interior and exterior surfaces of the M5 alloy is taken to be the same as that of Zircaloy -4 as used in RELAP5. This value is [c, d] The value is supported by emissivity data obtained on M5 cladding during the EDGAR test, see Appendix C, during the calibration of the optical pyrometers. These results gave an emissivity value between

A.2.2.5 Cladding Oxide Development.

Oxidation kinetics for the M5 alloy operating under normal conditions are discussed in section (A)4.1 and also in the Section 3.1 of the text.

The high temperature oxidation testing and characteristics of the M5 alloy are described in Appendix D. M5 high temperature oxidation is bounded by the Baker-Just Correlation.

A.3 MECHANICAL PROPERTIES

A.3.1 Tensile Strength

A.3.1.1 Ultimate Tensile Strength:

The ultimate tensile strength (UTS) for M5 has been established at various temperatures in the range of 25 to 400 C for both axial tensile and biaxial tests. Values obtained are very similar to those for [c, d] Some increase is observed with exposure to fast neutron fluence .

A.3.1.2 0.2% Offset Yield Strength

The yield strength for (YS) for M5 was obtained in the same tests used to establish the UTS. Figure A-4 shows the yield strength for both axial and biaxial conditions over the temperature range of 20 to 400 C. Significant increases are observed with exposure to fast neutron fluence (See figure 3-6 in section 3).

A.3.1.3 Ductility

The same testing which established the YS and UTS also provided ductility data. In the unirradiated condition the ductility is always greater than 10%. With irradiation the ductility decreases as the strength increases with less separation between the YS and UTS. However, irradiated cladding has ductility greater than 1%.

A.3.2 Creep

The M5 alloy has a significantly lower creep rate than SRA Zircaloy cladding. Details of the creep rates and a comparison to Zircaloy cladding are given in Appendix B. In-core creep of M5 is [c,d] that of the present FCF Zircaloy-4 cladding.

A.3.3 Poisson's Ratio

A value of [c, d] for Poisson's ratio

A.3.4 Modulus of Elasticity

The modulus of elasticity is used in determining deflections as a function of load, both for hand calculations and in various computer codes. The computer codes TACO3 (steady state fuel performance code, Reference A-6), CROV (Creep Collapse Code, Reference A-7) and RELAP5 (the LOCA thermal hydraulic Code) all have default values for the modulus of elasticity. Within RELAP5 the modulus for Zircaloy-4 is calculated using:

$$E_{R5} = \begin{cases} 1.088\times10^{11} - 5.475\times10^{7}\ T_c & 1090\ K \geq T_c \\ 1.017\times10^{11} - 4.827\times10^{7}\ T_c & 1240\ K \geq T_c > 1090\ K \\ 9.210\times10^{10} - 4.050\times10^{7}\ T_c & 2027\ K \geq T_c > 1240\ K \\ 1.0\times10^{10} & T_c > 2027\ K \end{cases}$$

where: E is in (Pa), and
T_c is in (^{o}K).

In TACO3, Reference A-6 the formulation for the modulus of Zircaloy-4 is separated into axial and hoop components as,

$$E_{T3,axial} = 1.0467\times10^{4}\ T_c^2 - 6.1949\times10^{7}\ T_c + 1.0284\times10^{11}$$
$$E_{T3,radial} = 1.6858\times10^{4}\ T_c^2 - 7.3431\times10^{7}\ T_c + 1.0857\times10^{11}$$

where: E is in (MPa), and
T_c is in (°K).

A test of the modulus conducted on a sample of M5 alloy by FCF resulted in

[c, d]

This curve is compared to the Zircaloy-4 correlation in Figure A-5. The results, up to approximately 700K, indicate that the RELAP5 Zircaloy-4 model provides a reasonable representation of the modulus for the M5 alloy. Therefore the default Zircaloy-4 model is used in the analyses detailed in Appendix F and in the TACO3 evaluations in Chapter 3. For the buckling strength of the cladding the modulus value determined by testing was used.

A.3.5 Hardness (Meyer's)

As discussed earlier, irradiation of zirconium alloys modifies the material structure, and results in similar values for the mechanical properties irrespective of original condition. The hardness of alloys tends to follow the mechanical properties with a direct correlation between the strength and hardness. On this basis it is reasonable to assume that the hardness value for irradiated M5 alloy will be similar to that of Zircaloy-4. This correlation, as used in RELAP5 is given by,

$$H = \text{Max}\{\exp[-2.5621\times10^{-8}\ T^3 + 4.3502\times10^{-5}\ T^2 - 2.6394\times10^{-2}\ T + 26.034],\ 1.0\times10^{5}\}$$

where H is the Meyer's Hardness, and
T is in °K

The curve of this relationship is shown in Figure A-6.

A.3.6 Growth

The growth model for M5 has been evaluated both in FCF fuel designs and in the Framatome AFA 2G fuel assembly designs used in Europe. FCF data shows the fuel rod growth for M5 is less than that of the standard FCF cladding. For Framatome AFA 2G fuel assemblies, the growth data is sufficient to define UTL, nominal and LTL growth laws. These laws are:

Nominal Growth:

[c,d]

Upper Growth Limit:

[c,d]

Lower Growth Limit:

[c,d]

Where:
L: Fuel rod length as a function of fluence.
L_0: Initial fuel rod length.
Φ: Average fuel rod fast fluence, E > 1 MeV.

The model is applicable up to fast fluences of [c,d] n/cm^2, E > 1 MeV.

A.4 CORROSION EFFECTS

A.4.1 Corrosion Rates

Autoclave testing of the alloy indicates that the corrosion rate is similar to that of Zircaloy-4 in the unirradiated condition when tested in accordance with the ASTM Standard G-2 test. However results from irradiated cladding shows that the corrosion rate of the alloy is much lower than that of Zircaloy-4 primarily because the irradiation enhancement factor associated with Zircaloy corrosion is very much reduced in the case of the M5 alloy. This can be observed in Figure 3-1 in Chapter 3.

The pre transition corrosion rate is considered to be the same as that for Zircaloy.

The post transition corrosion rate for Alloy-5 under irradiation is given by:-

[c, d]

Where:

ds/dt is the increase in oxide thickness (m/s)
A is a material constant (m/s)
R is the Universal gas Constant
Q is the Activation Energy (J/mole)
T is the metal/oxide interface temperature (°K)

Further details and example cases are given in section 3.1, chapter 3.

A.4.2 Hydrogen Pickup Fraction.

The hydrogen pickup fraction has been measured from hotcell testing of irradiated cladding over the burnup range of 9.2 to 38 GWd/mtU. The values for oxide thickness and hydrogen concentration were obtained by metallography. After evaluation of the data a design value of 6% pickup was determined. Values of hydrogen pickup fraction as a function of irradiation are given in Figure A-7 (Reference A-8) This shows a maximum hydrogen concentration of ppm at a burnup of GWd/mtU.

A.4.3 Stress Corrosion Cracking

The Stress corrosion cracking (SCC) performance of M5 has been established in ex-core testing and indirectly through ramp testing of refabricated fuel rods in experimental reactors. The testing has established that M5 fuel rod cladding has SCC threshholds the same or better than those of Zircaloy-4 cladding. The ex-core testing involves a slow tensile test at 350 C.

A.5 REFERENCES

A-1. Metals Handbook, Tenth Edition, Volume 2, Properties and Selection: Nonferrous Alloys and Special-Purpose Materials. ASM International. pp. 666.

A-2. Touloukain, Y.S., and Ho, C.Y. Thermophysical Properties of Materials, The TPRC Data Series, 1970.

A-3. NUREG/CR-0497, TREE-1280, Rev 1, "MATPRO-Version 11 (Revision 1) A Handbook of Materials Properties for Use in the Analysis of Light Water Reactor Fuel Rod Behavior," February, 1980, US Nuclear Regulatory Commission and US Department of Energy, Idaho Operations, Idaho Falls, Idaho.

A-4. NUREG/CR-0497, TREE-1280, Rev 2, "MATPRO-Version 11 (Revision 1) A Handbook of Materials Properties for Use in the Analysis of Light Water Reactor Fuel Rod Behavior," August, 1981, US Nuclear Regulatory Commission and US Department of Energy, Idaho Operations, Idaho Falls, Idaho.

A-5. FTI Topical report "RELAP5/MOD2-B&W - An Advanced Computer Program for Light Water Reactor LOCA and Non-LOCA Transient Analysis," BAW-10164P, Rev. 1, November, 1992.

A-6. D. A. Wesley and K. J. Firth, "TACO3 - Fuel Pin Thermal Analysis Code," BAW-10162P-A, August 1989.

A-7. BAW-10084P-A, Rev. 3, Program to Determine In-Reactor Performance of B&W Fuels--Cladding Creep Collapse--Revision 3, July 1995.

A-8. J.P. Mardon, et al., Update on the Development of Advanced Zirconium Alloys for PWR Fuel Rod Performance, pg 405 to 412, Proceedings of The 1997 International Topical Meeting on LWR Fuel Performance, Portland Oregon, March 2-6, 1997.

Table A-1 Alloy Chemistry							
Zircaloy-4	Sn wt %	Fe wt%	Cr wt %	O ppm	Nb wt %	C ppm	
Max	1.7	0.24	0.13	1600		270	
Min	1.2	0.18	0.07	900			
M5							
Max	[c, d]	[c, d]		[c, d]	[c, d]	[c, d]	
Min				[c, d]	[c, d]		

Figure A-1 Thermal Expansion vs Temperature

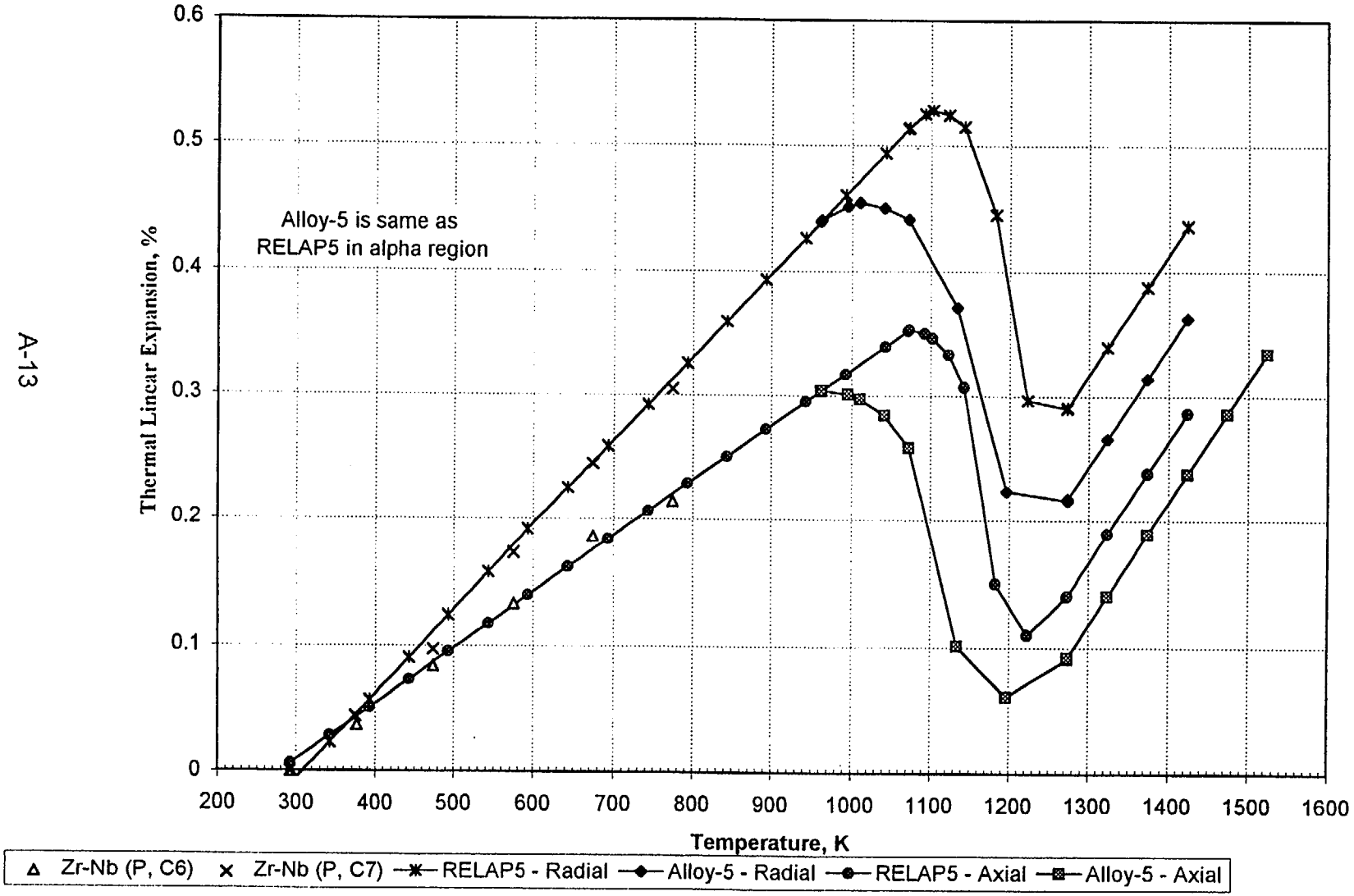

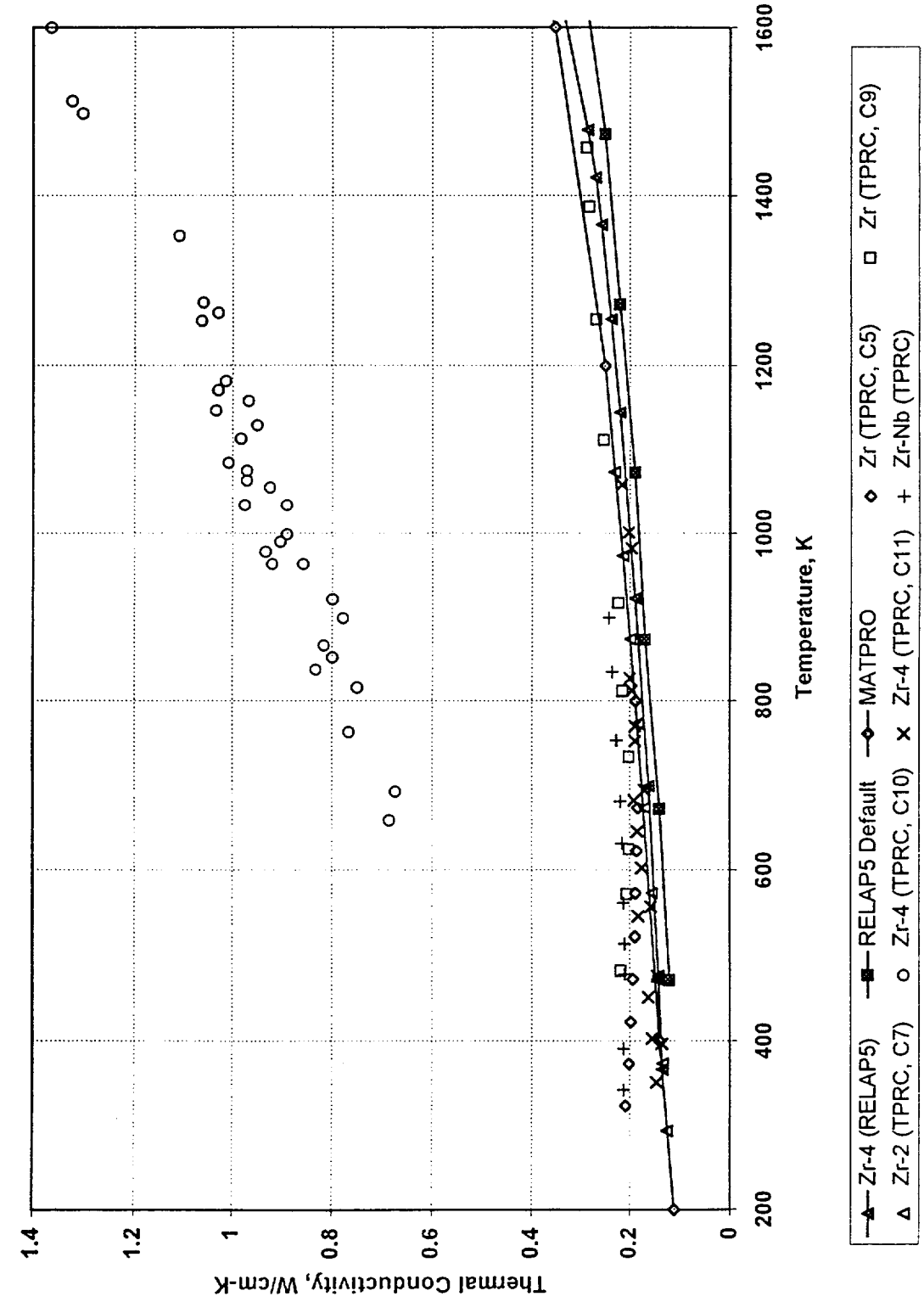

Figure A-2 Thermal Conductivity vs Temperature

Figure A-3 Specific Heat vs Temperature

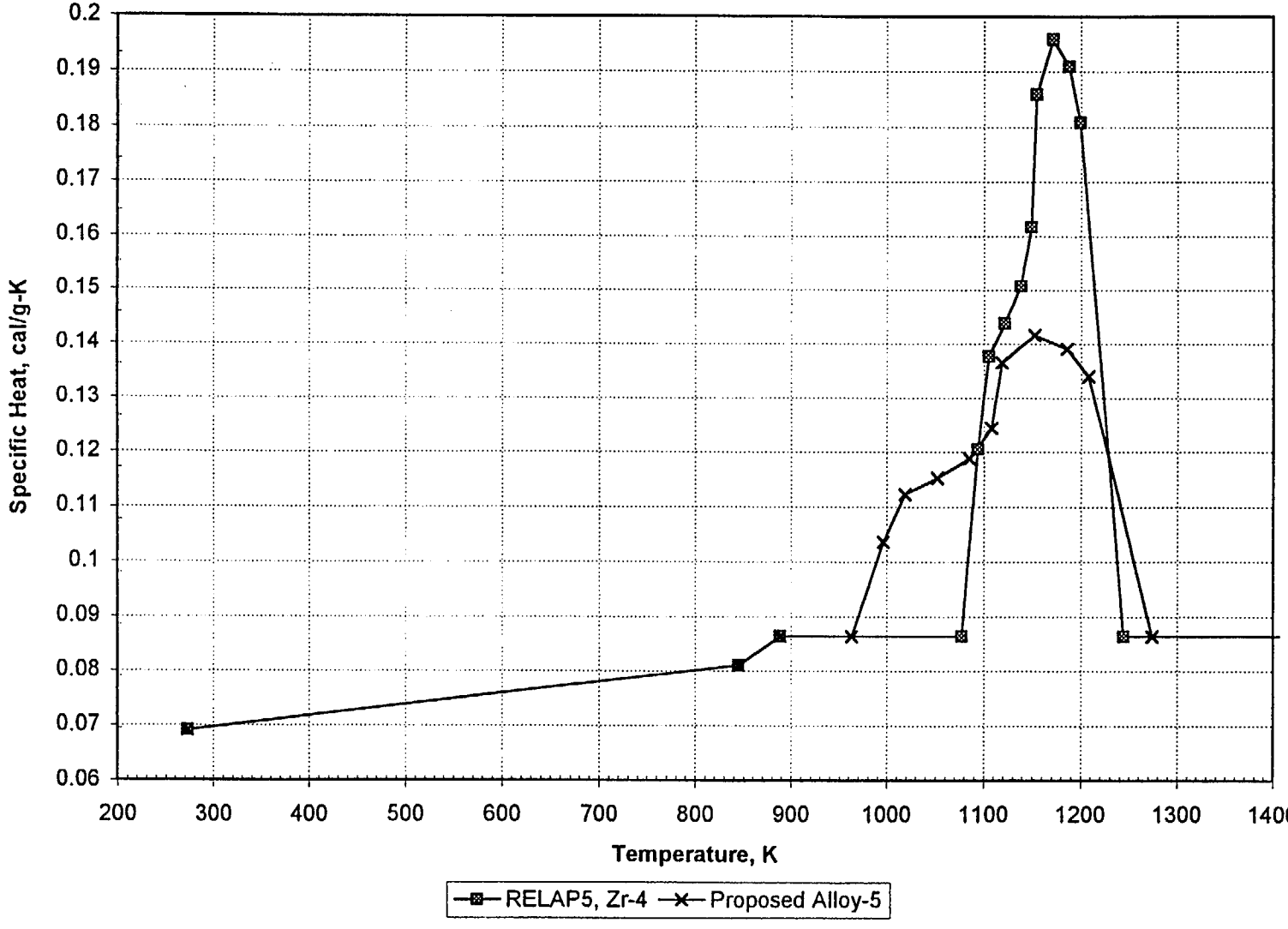

Figure A-4 M5 Yield Strength vs Temperature

Figure A-4 is Proprietary

[c, d]

Figure A-5 Young's Modulus vs Temperature

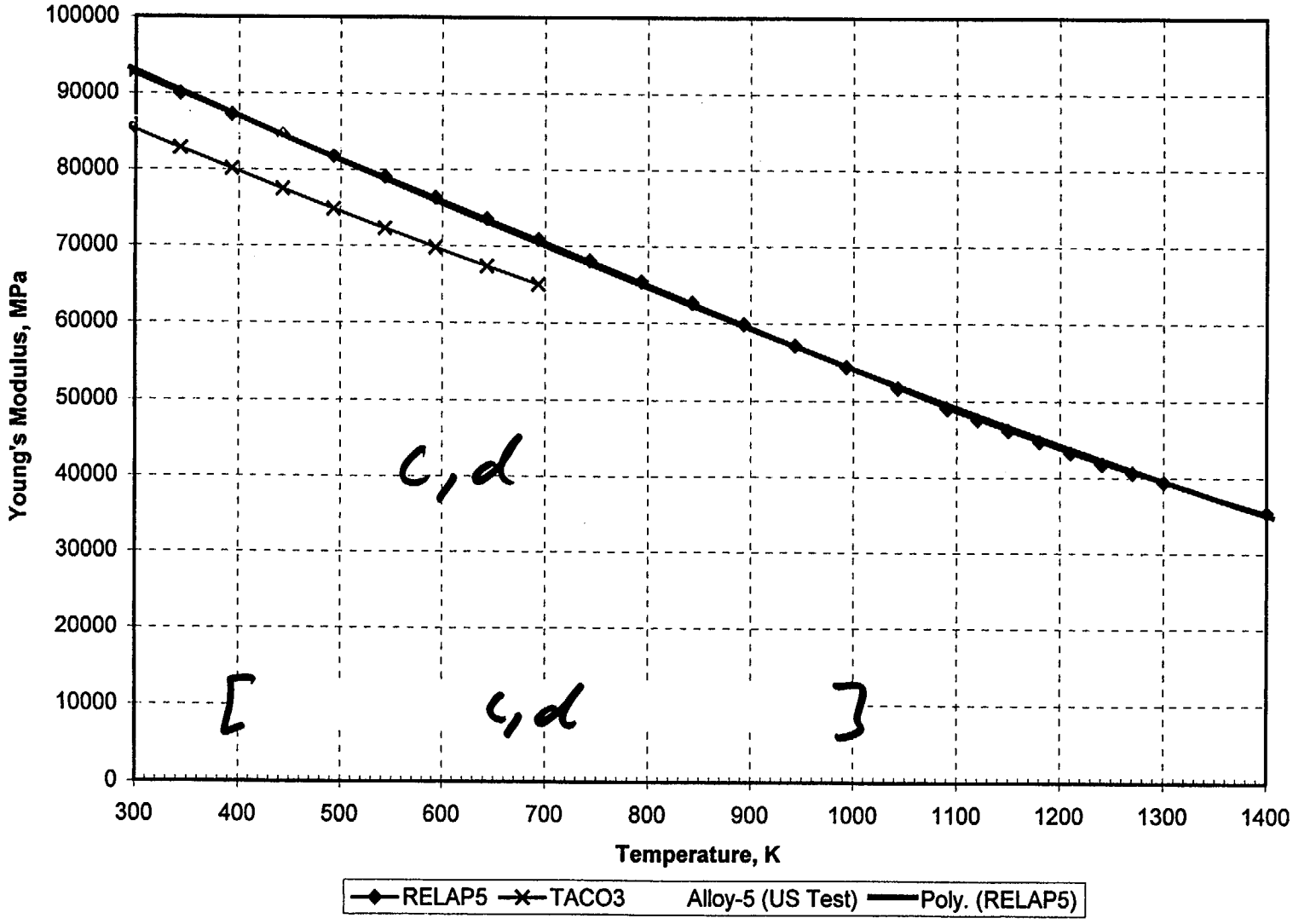

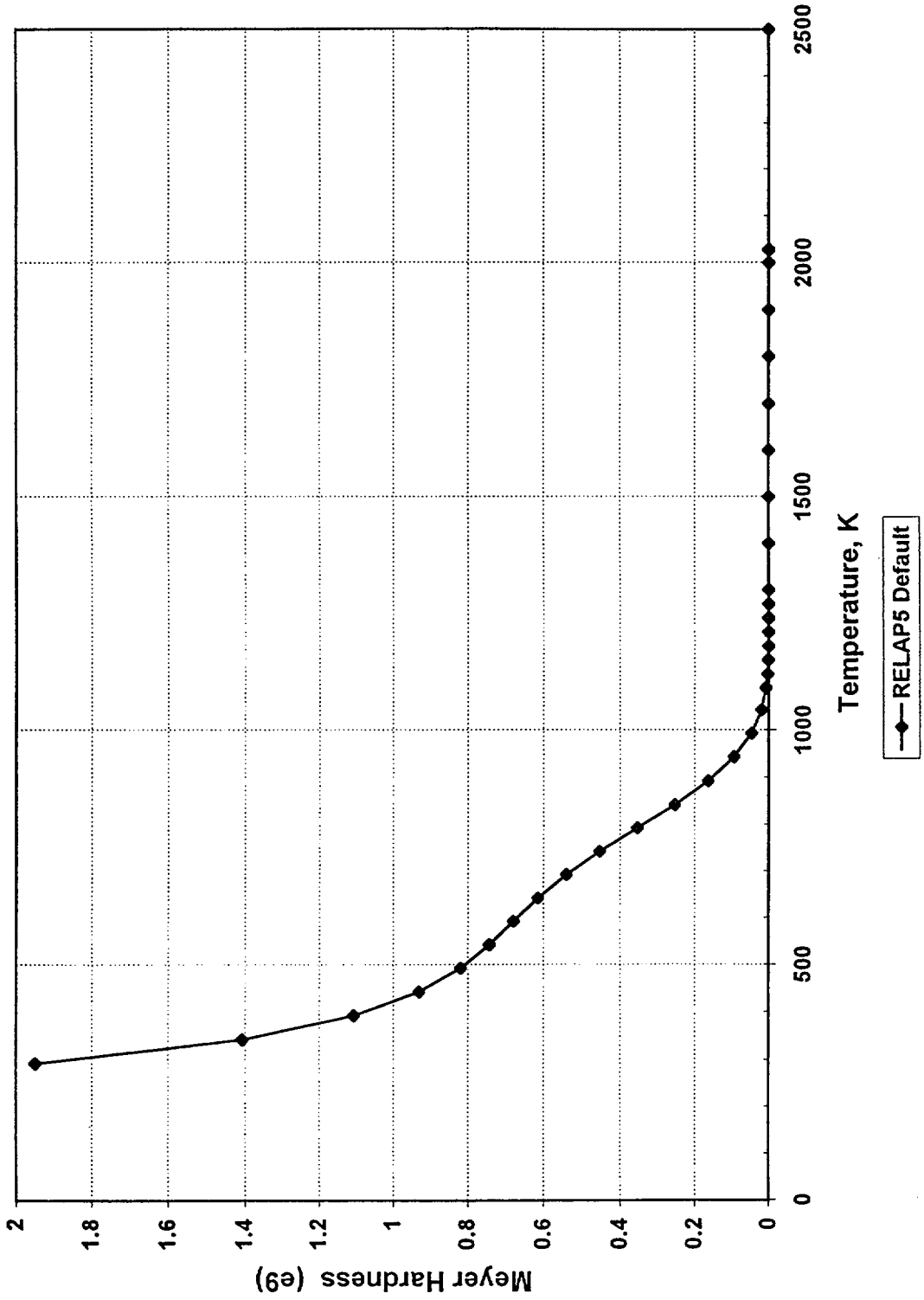

Figure A-6 Meyer's Hardness vs Temperature

Figure A-7 M5 Hydrogen Pickup vs Burnup

Figure is Proprietary

[c, d]

Appendix B

M5 In-Core Creep

M5 In-Core Creep

In the normal operational temperature and stress range of the fuel pin cladding, creep is a strong function of stress and fast neutron fluence with a weaker effect due to temperature. The modeling of the in-core creep of the fuel pin cladding is performed in the computer codes TACO3, FRGPC and CROV (References B-1, B-2 & B-3). The form of the models used for Zircaloy-4 are:

[c, d] Form used in FRGPC and CROV

[c, d] Form used in TACO3

To model M5 [

Creep testing has been performed where cladding segments were subjected to an internal pressure, and exposed in a test reactor to in-core temperatures and fast neutron fluxes. Measurements performed during this testing have provided the means to characterize both the standard
compared to the base FCF cladding.

In-Core Creep Multipliers by Cladding Type		
Cladding Alloy	Cladding Variant	Effective Creep Multiplier
[c, d]	[c, d]	[c, d]
[c, d]	[c, d]	[c, d]
[c, d]	[c, d]	[c, d]

In TACO3 the [

c, d

]

REFERENCES

B-1. D. A. Wesley and K. J. Firth, "TACO3 - Fuel Pin Thermal Analysis Code," BAW-10162P-A, August 1989.

B-2. D. A. Wesley, et. al., "Fuel Rod Gas Pressure Criterion (FRGPC)," BAW-10183P, July 1991.

B-3. BAW-10084P-A, Rev. 3, Program to Determine In-Reactor Performance of B&W Fuels--Cladding Creep Collapse--Revision 3, July 1995.

APPENDIX C

M5 HIGH TEMPERATURE SWELLING and RUPTURE MODEL

M5 HIGH TEMPERATURE SWELLING and RUPTURE MODEL

C.1 INTRODUCTION

The Framatome Technologies Incorporated (FTI) LOCA evaluation models, References C-1 and C-2, require the simulation and calculation of fuel cladding swelling and rupture. For Zircaloy-4, the LOCA modeling is based on NUREG-0630, Reference C-3. The models include provision for the determination of the occurrence of rupture as a function of the cladding surface temperature, the degree of swelling at the rupture location, and the amount of assembly average flow area reduction. The flow area reduction is also used to determine the amount of entrained water droplet mechanical inter-action within the fuel assembly at the location of rupture. This interaction causes droplet shattering which reduces vapor temperatures and increases cooling efficiency.

The NUREG-0630 model is based on Zircaloy-4 testing. M5 is a new material with differing creep characteristics and will behave differently during the high temperature strain and rupture of a LOCA. Because NUREG-0630 can not be applied without recognition of the differing behavior of M5, rupture testing at the CEA EDGAR facility in Saclay, France was conducted to determine M5 characteristics, Reference C-4. This Appendix presents the fuel cladding swelling and rupture model and materials data that have been developed by[c]approach.

The FTI swelling and rupture model is divided into the determination of individual pin characteristics, bundle flow blockage effects, and bundle fluid droplet interaction effects. Each of these, as related to the M5 material, is discussed in sequence within this Appendix. Also presented is a brief description of the EDGAR test facility and the results obtained for the M5 cladding.

C.2 INDIVIDUAL PIN CHARACTERISTICS

[c]

C.2.1 EDGAR Test Apparatus and Data

c, d

C.2.2 Fuel Pin Cladding Rupture Temperature Versus Stress

[

c, d

]

C.2.3 Fuel Pin Cladding Rupture Strain versus Rupture Temperature

[c, d]

C.2.4 Fuel Pin Cladding Strain Prior to Rupture and Remote from the Rupture Location

[C, d]

C.2.4.1 Fuel Pin Cladding Strain Prior to Rupture and Gap Heat Transfer

[C, d]

C.2.4.2 Fuel Pin Cladding Strain Prior to Rupture and Flow Blockage

c, d

[redacted]

[redacted]

c, d

C.3 BUNDLE FLOW BLOCKAGE CHARACTERISTICS

c, d

C.3.1 Assembly Simulation Effects

c, d

C.3.1.1 Axial Distribution of Rupture

C, d

c, d

C.3.1.2 Number of Fuel Pins in Simulation or Assembly

C, d

C.3.1.3 Unheated Surfaces and Pellet Simulation

C, d

[c,d]

C.3.2 The FTI Blockage Simulation Model

[c,d]

C.3.2.1 Blockage Limitation

[c,d]

c, d

c, d

[c, d]

C.3.2.2 Bundle Simulation Benchmarks

[c, d]

C.3.2.2.1 Benchmarks of the Chapman Bundle Tests

[c, d]

c, d

C.3.2.2.1 Benchmarks of the NUREG-0630 Blockage Calculation

c, d

[c, d]

C.3.2.3 Blockage Model Conservatisms

[c, d]

C.4 DROPLET INTERACTION MODELING

[c, d]

c, d

C.5 SUMMARY OF FTI M5 CLADDING SWELLING AND RUPTURE MODEL

c, d

C.6 REFERENCES

C-1. BAW-10168-A Rev. 3, RSG LOCA, BWNT Loss-of-Coolant Accident Evaluation Model for Recirculating Steam Generator Plants, B&W Nuclear Technologies, Lynchburg, Virginia, 1996.

C-2. BAW-10192-P, BWNT LOCA, BWNT Loss-of-Coolant Accident Evaluation Model for Once-Through Steam Generator Plants, B&W Nuclear Technologies, Lynchburg, Virginia, 1994.

C-3. D. A. Powers and R.O. Meyer. NUREG-0630, Cladding Swelling and Rupture Models for LOCA Analysis, U.S. Nuclear Regulatory Commission, Washington DC, 1980.

C-4. Letter J. Hivroz (CEA) to A. Le Bourhis (Framatome / TFP), Alliage M5. Transmission des resultats portant sur les essais de fluage et de rampe de temperature effectues sur le dispositif d'essai EDGAR, SRMA/97.391, July 3, 1997, Saclay, France, also included herein as Appendix A.

C-5. Note Technique SRMA 84-1346, EDGAR FROID - Gaines Framatome, Modelisation de la Deformation des Gaines en Ziracloy dans des Conditions d'un Accident de Perte de Refrigerant Primaire Critere de Rupture, Service de Recherches Metallurgiques Appliquees, Centre d'Etudes Nucleaires de Saclay, France, on file at Framatome Technologies Inc., Lynchburg, Virginia, as 38-1247171-00.

C-6. F.J. Erbacher and S. Leistikow, "Zircaloy Fuel Cladding Behavior in a Loss-of-Coolant Accident: A Review," Zircaloy in the Nuclear Industry, Seventh International Symposium, American Society for Testing and Materials, Philadelphia, Pennsylvania, 1987.

C-7. F. J. Erbacher et al, "Burst Criterion of Zircaloy Fuel Claddings in a Loss-of-Coolant Accident," Zirconium in the Nuclear Industry, Fifth Conference, ASTM STP 754, D. G. Franklin, Ed. American Society for Testing Materials, 1982, pp. 271-283.

C-8. D.G. Hardy, "High-Temperature Rupture Behavior of Zircaloy Tubing," CONF-730304, USAEC/TIC, Water-Reactor Safety, 1973.

C-9. BAW-10164-A Revision 3, RELAP5/MOD2-B&W, An Advanced Computer Code for Light Water Reactor LOCA and Non-LOCA Transient Analysis, B&W Nuclear Technologies, Lynchburg, Virginia, 1996.

C-10. NUREG/CR-0103, ORNL/NUREG/TM-200, Multirod Burst Test Program Progress Report for July-December 1997, Us Nuclear Regulatory Commission, Washington DC.

C-11. NUREG/CR-0655, ORNL/NUREG/TM-297, Multirod Burst Test Program Progress Report for July-December 1998, Us Nuclear Regulatory Commission, Washington DC.

C-12. NUREG/CR-1023, ORNL/NUREG/TM-351, Multirod Burst Test Program Progress Report for April-June 1999, Us Nuclear Regulatory Commission, Washington DC.

C-13. WA Fiveland and AR Barber, BW-4702, Rupture Characteristics of Zircaloy-4 Fuel Cladding Supplemental Report - Ruptured Clad Geometry, Babcock and Wilcox Company, Alliance, Ohio, February 1978.

C-14. D.A. Powers and R.O. Meyer, NUREG-0536, Evaluation of Simulated-LOCA Tests that Produced Large Fuel Cladding Ballooning, U.S. NRC, March 1979.

C-15. R.E. Williford and C.R. Hann, "Effects of Fill Gas Composition and Pellet Eccentricity," Battelle Northwest Laboratories Report, BNWL-2285, July 1977.

C-16. A.L. Lowe, jr. (Babcock and Wilcox Company) , letter to D.A. Powers (NRC), October 10, 1978, Available in file for USNRC Report, NUREG-0536, U.S. NRC.

Table C-1. EDGAR Swelling and Rupture, Slow Ramp Tests

	c,d						

			c,d				

Table C-2. EDGAR Swelling and Rupture, Fast Ramp Tests

	c,d						

Figure C-1 EDGAR Test Apparatus -- PROPRIETARY

[c,d]

Figure C-2 EDGAR Test Results Rupture Temperature versus Stress -- PROPRIETARY

[c,d]

Figure C-3 -- PROPRIETARY

[c, a]

Figure C-4 -- PROPRIETARY

[c, d]

Figure C-5 -- NONPROPRIETARY

[c, d]

Figure C-6 -- PROPRIETARY

[c,d]

Figure C-7 -- PROPRIETARY

[c,d]

Figure C-8 -- PROPRIETARY

[c, d]

Figure C-9 -- PROPRIETARY

[c,a]

Figure C-10.a Pin Strains in MBTP Bundle B-1 for Ruptures Just Above Lower Grid

PROPRIETARY

[c,a]

Figure C-10.b Pin Strains in MBTP Bundle B-1 for Ruptures Just Below Upper Grid

PROPRIETARY

[c,d]

Figure C-10.c Pin Strains in MBTP Bundle B-1 for Ruptures Above Upper Grid

PROPRIETARY

[c,d]

Figure C-11.a Pin Strains in MBTP Bundle B-2 for Ruptures Just Above Lower Grid

PROPRIETARY

{ c,d }

Figure C-11.b Pin Strains in MBTP Bundle B-2 for Ruptures Just Below Upper Grid

PROPRIETARY

[c,d]

Figure C-11.c Pin Strains in MBTP Bundle B-2 for Ruptures Above Upper Grid

PROPRIETARY

[c, d]

Figure C-12.a Pin Strains in MBTP Bundle B-3 for Ruptures Just Above Lower Grid

PROPRIETARY

[c, d]

Figure C-12.b Pin Strains in MBTP Bundle B-3 for Ruptures Just Below Upper Grid

PROPRIETARY

[c,d]

Figure C-13 Characterization of Axial Distribution of Strain for Ruptured M5 Cladding

PROPRIETARY

[a,d]

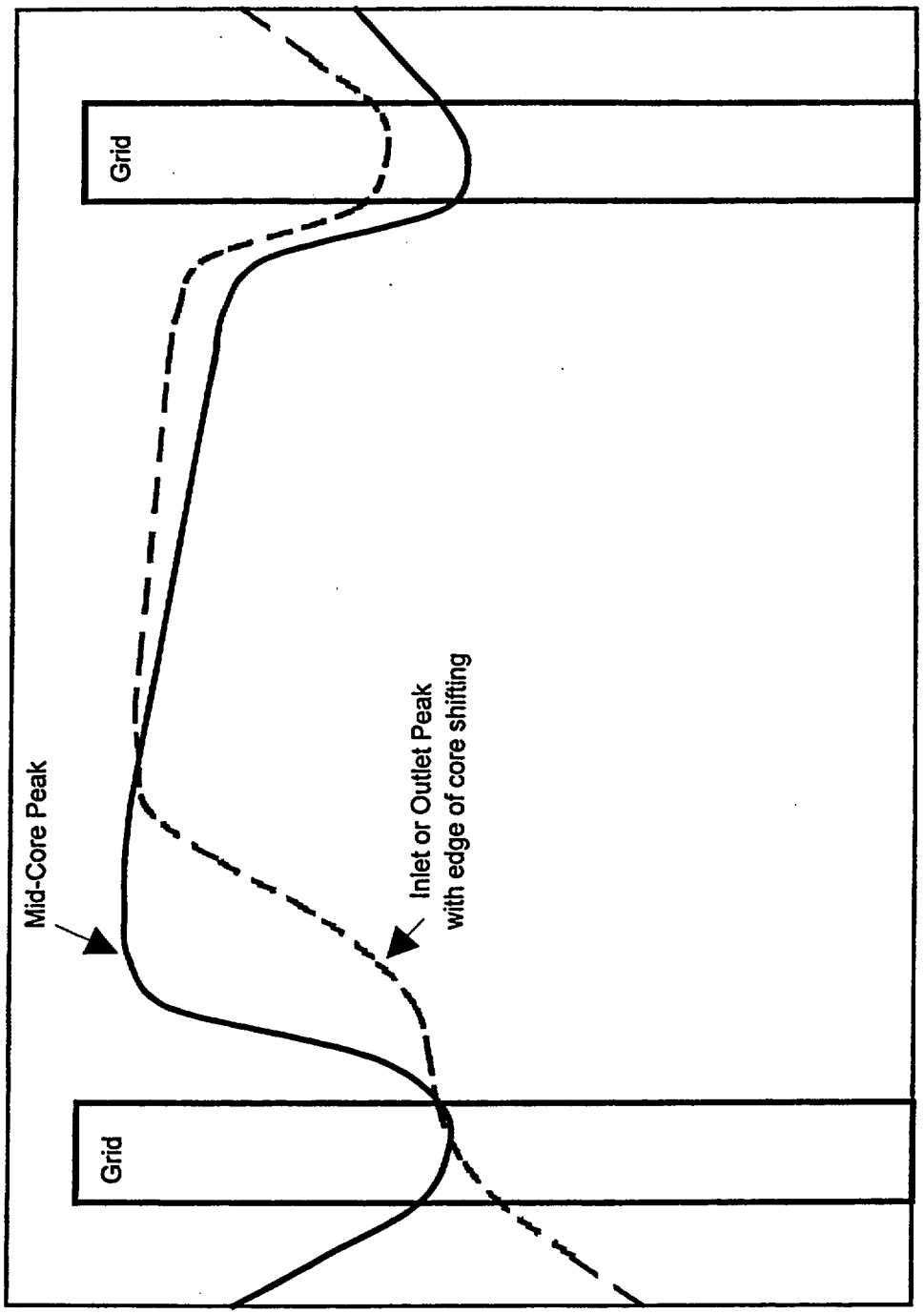

Figure C-14. Cladding Temperature Profiles for the B&W Designed NSS

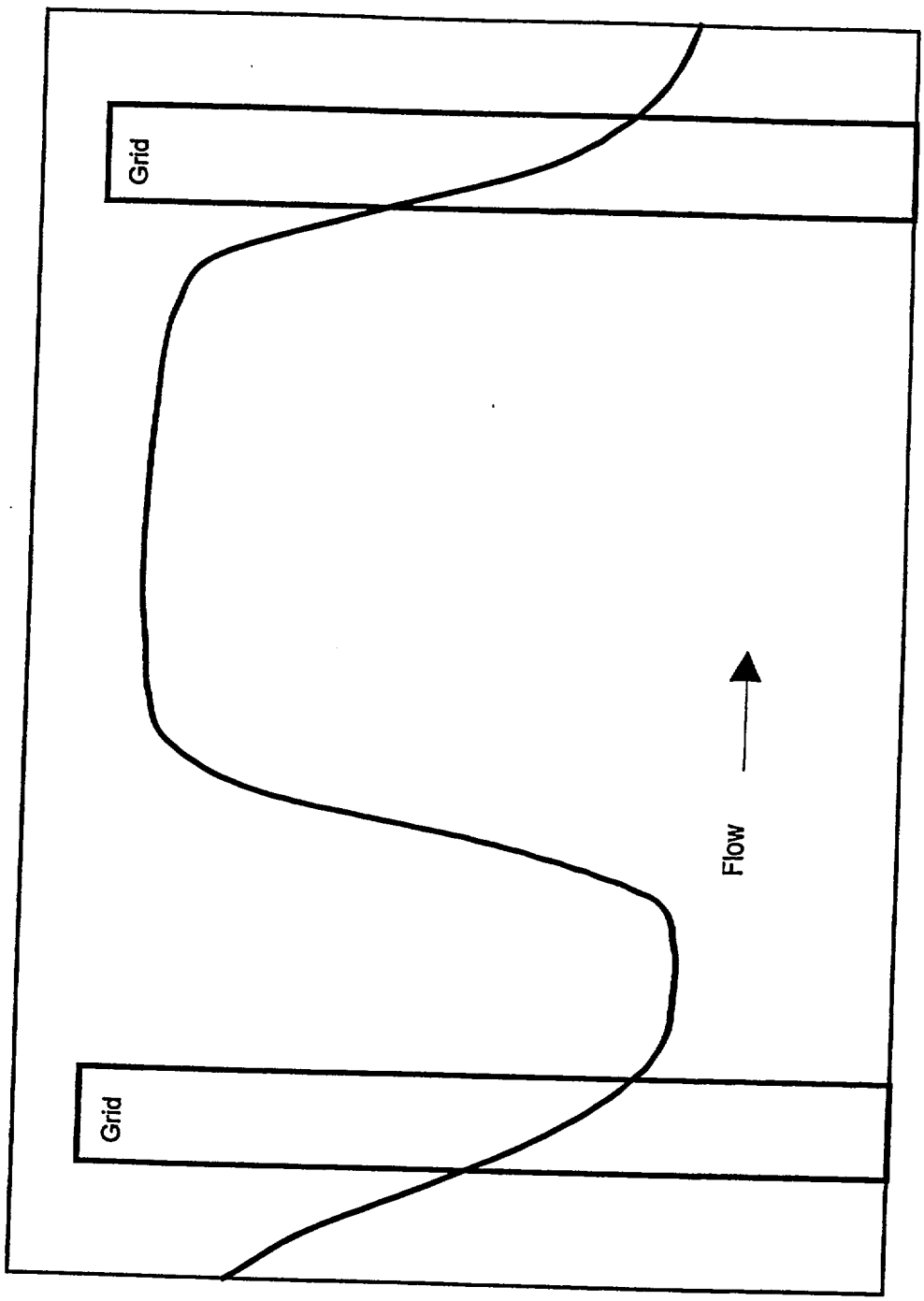

Figure C-15. Cladding Temperature Profile for NSSs with Recirculating Steam Generators

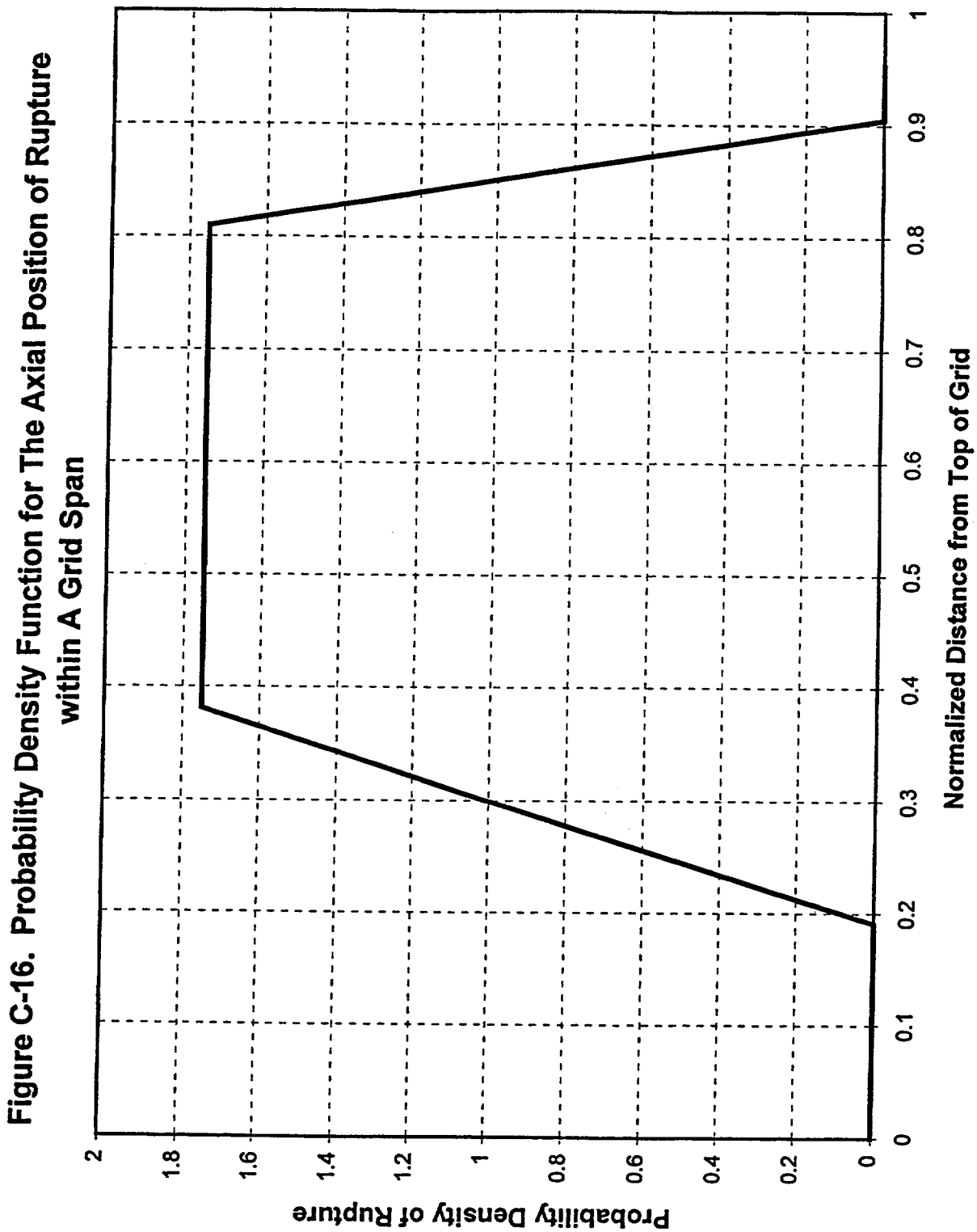

Figure C-16. Probability Density Function for The Axial Position of Rupture within A Grid Span

Figure C-17. Azimuthal Temperature Gradient Effect on Cladding Strain

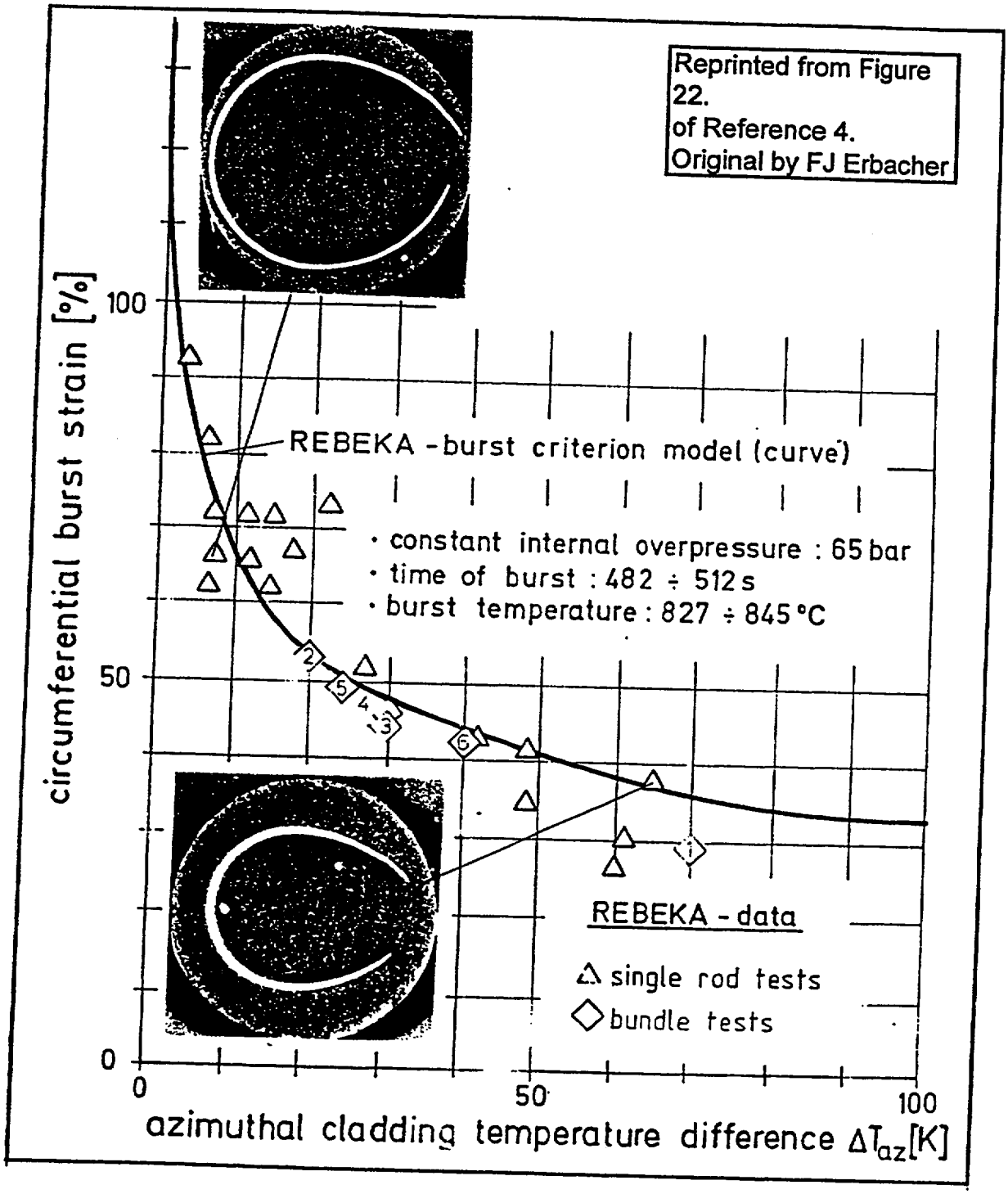

Figure C-18. Pin Rupture Strains for MBTP Tests B-1 and B-2

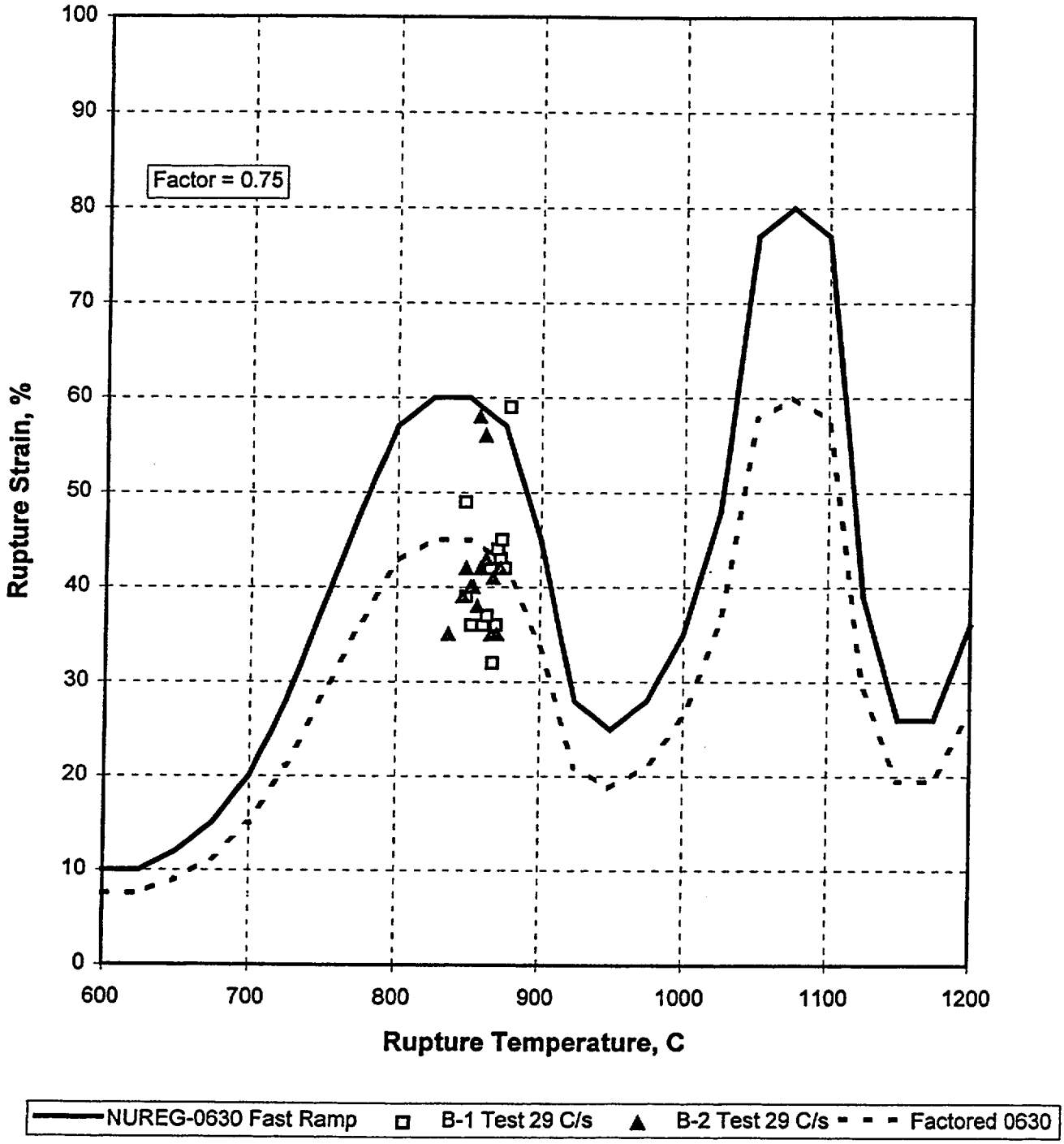

Figure C-19. Pin Rupture Strains for MBTP Test B-3

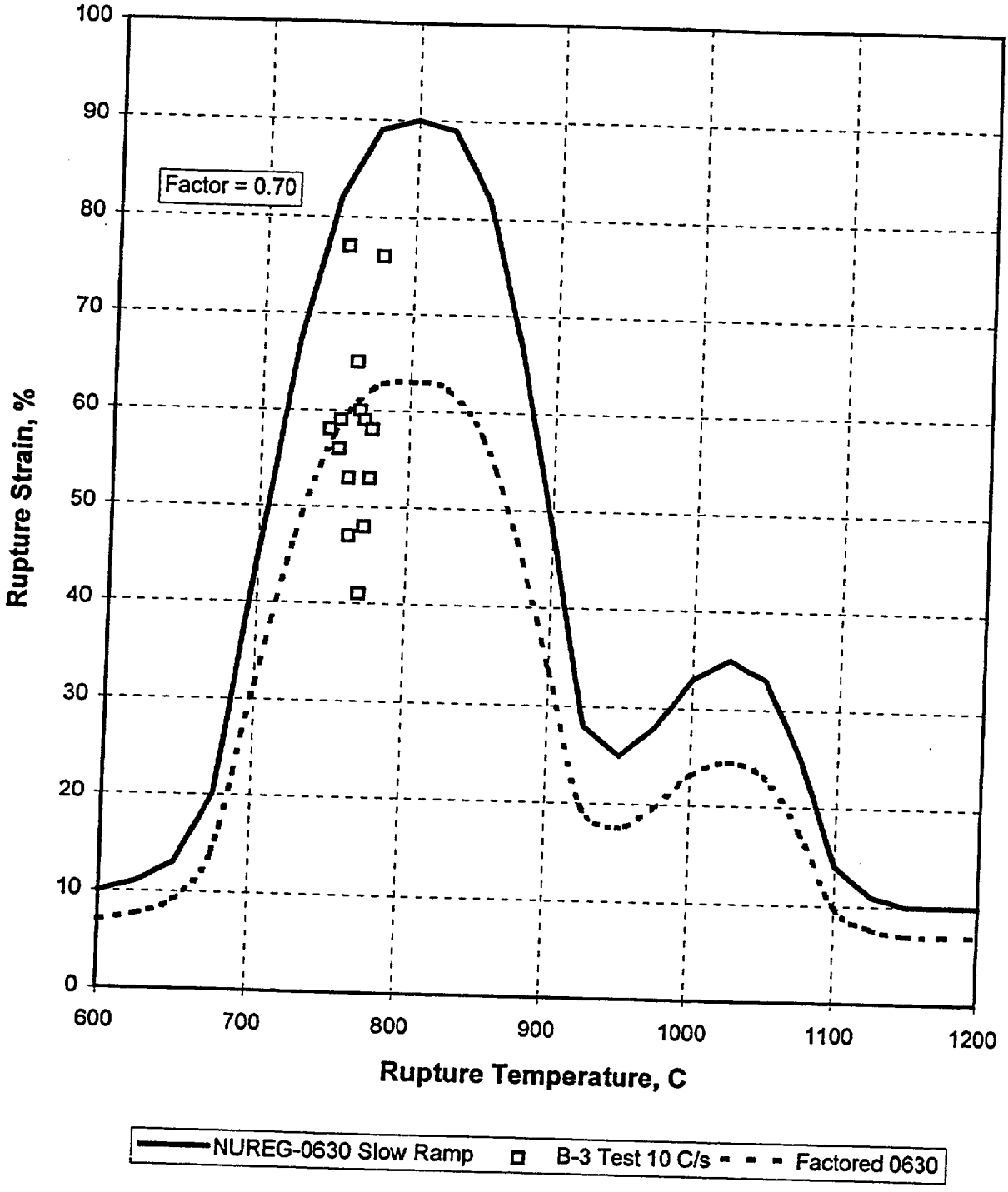

Figure C-20. MBTP Test B-1 Probability Density Function for Rupture Location

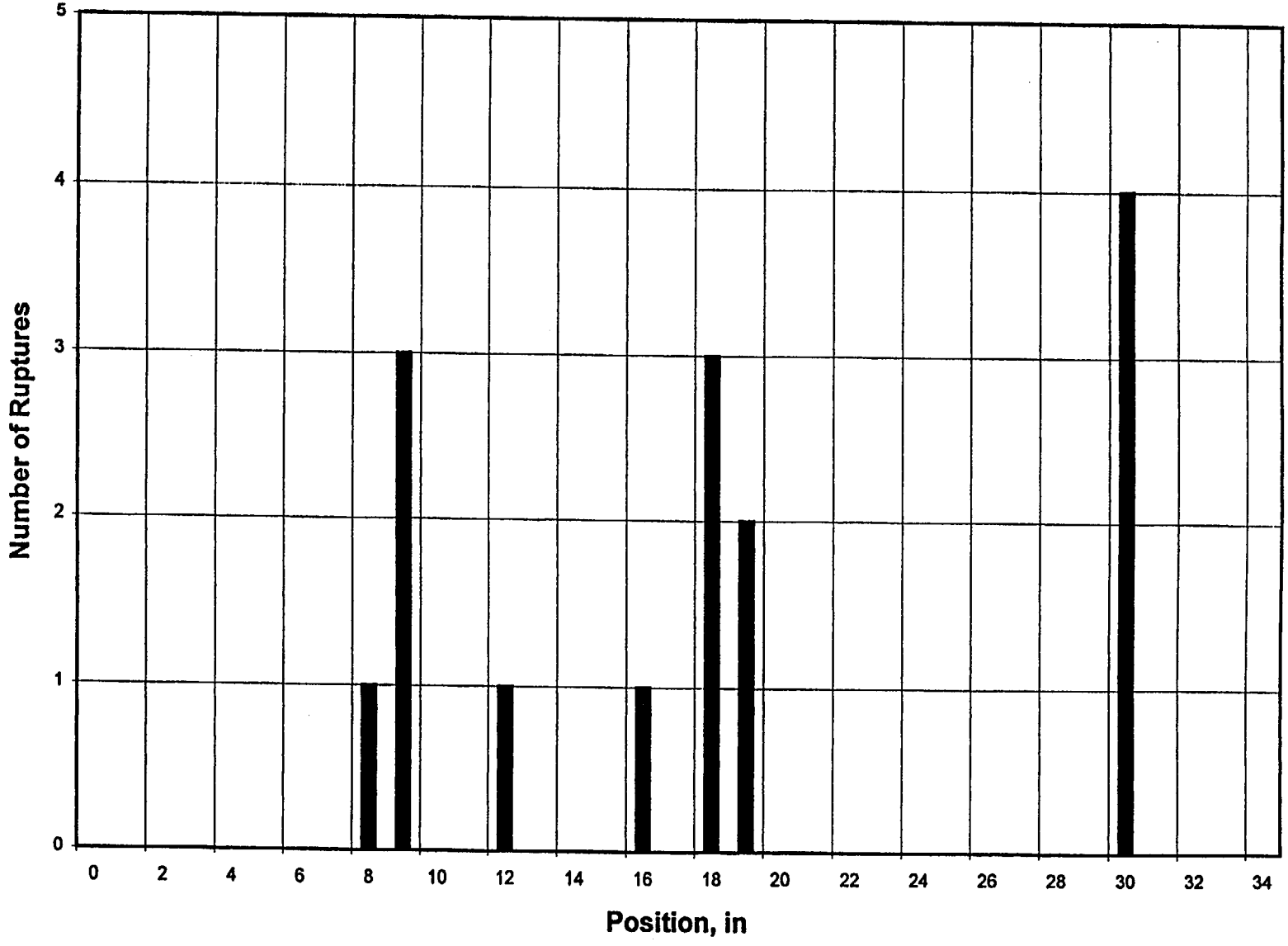

Figure C-21. MBTP Test B-2 Probability Density Function for Rupture Location

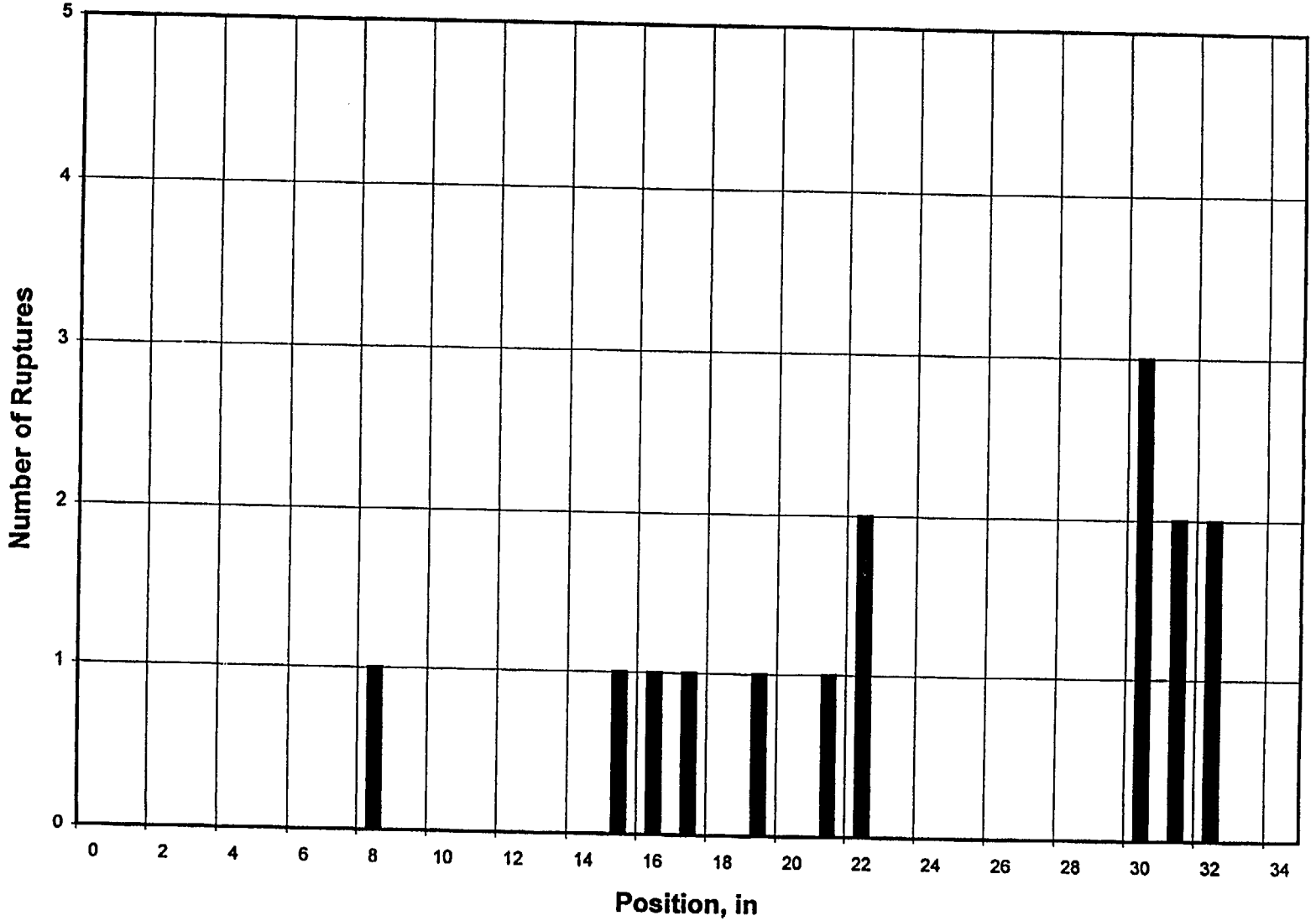

Figure C-22. MBTP Test B-3 Probability Density Function for Rupture Location

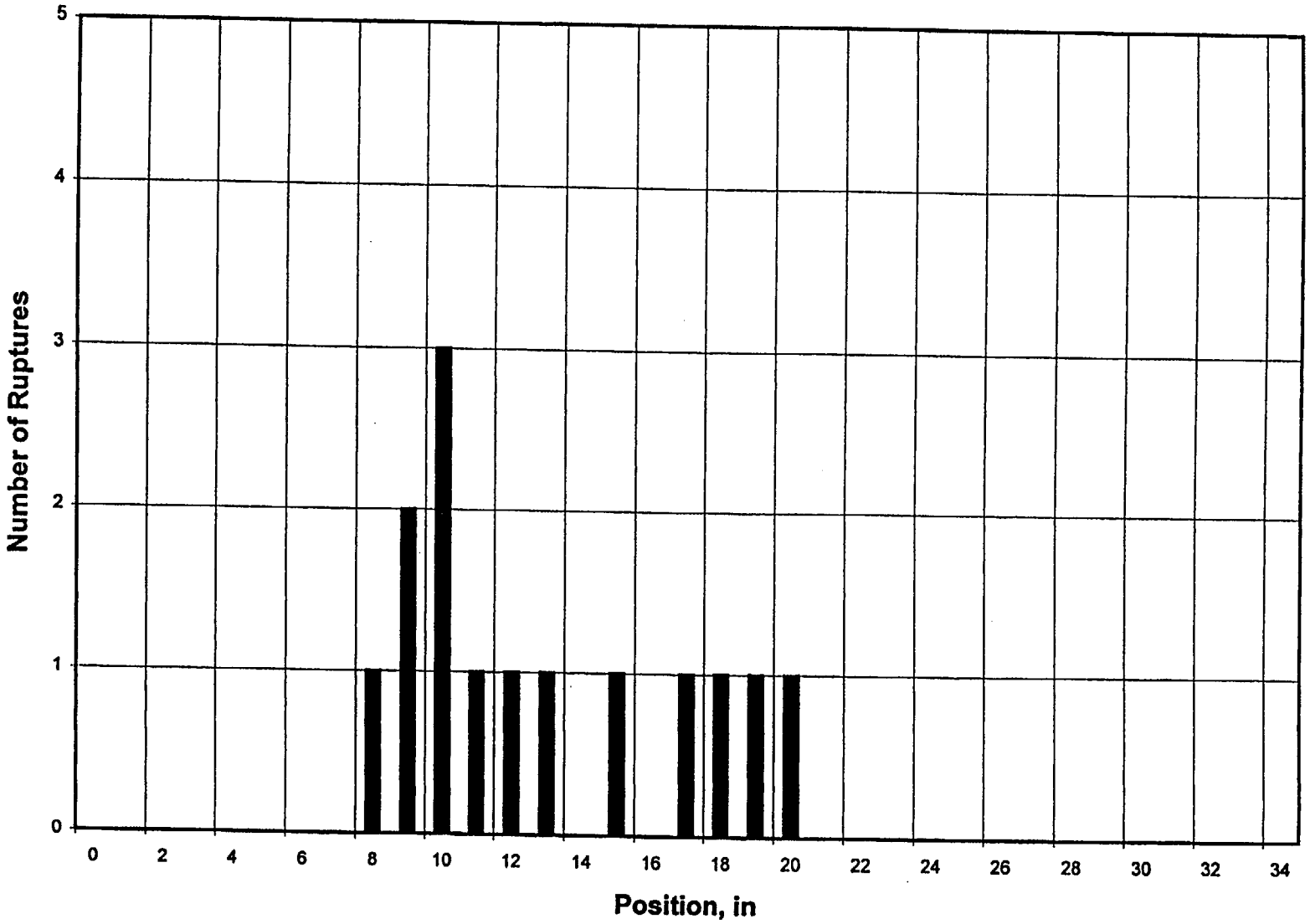

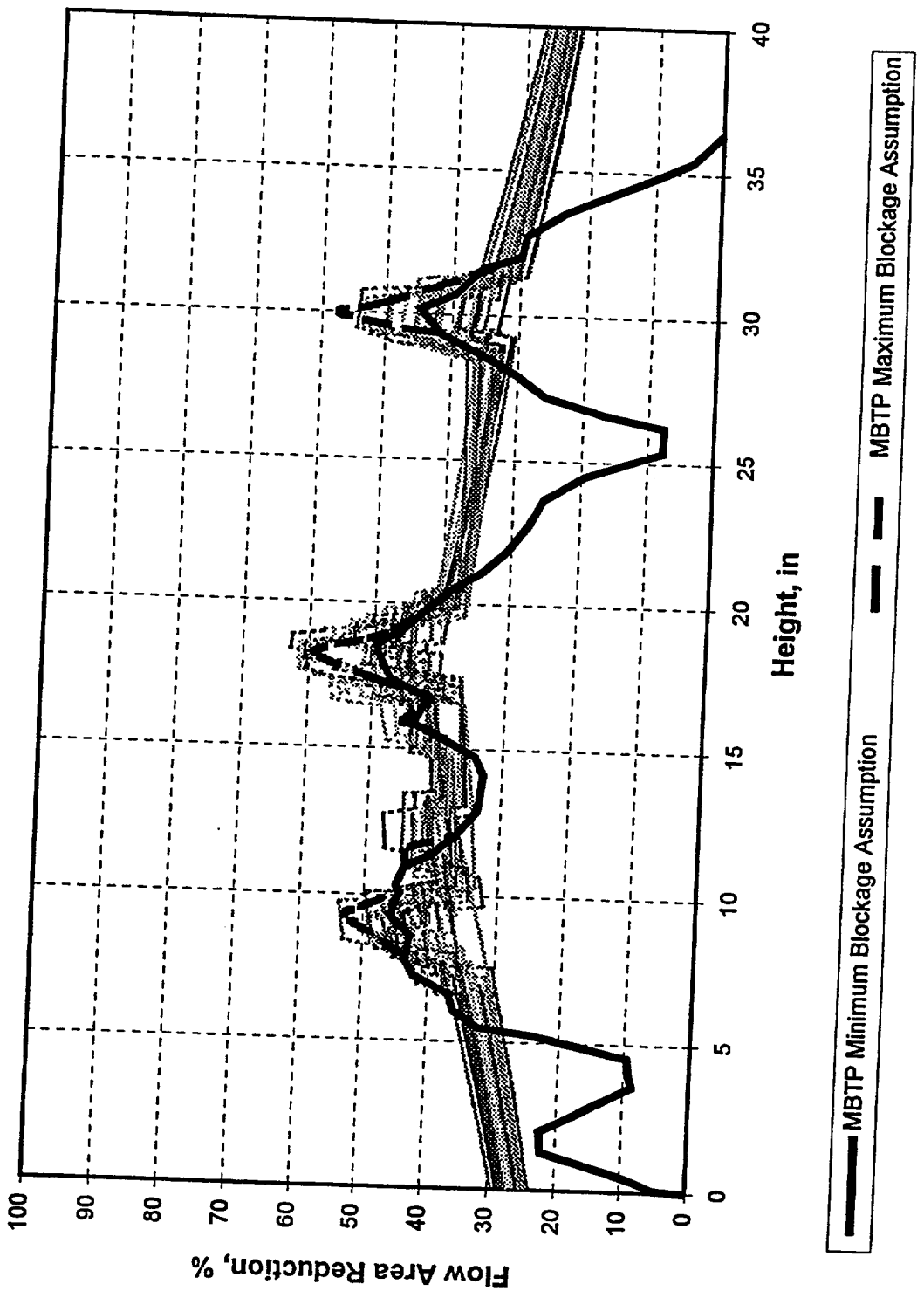

Figure C-23. Benchmark of MBTP Test B-1

Figure C-24. Benchmark of MBTP Test B-1 with All Rods Allowed to Strain

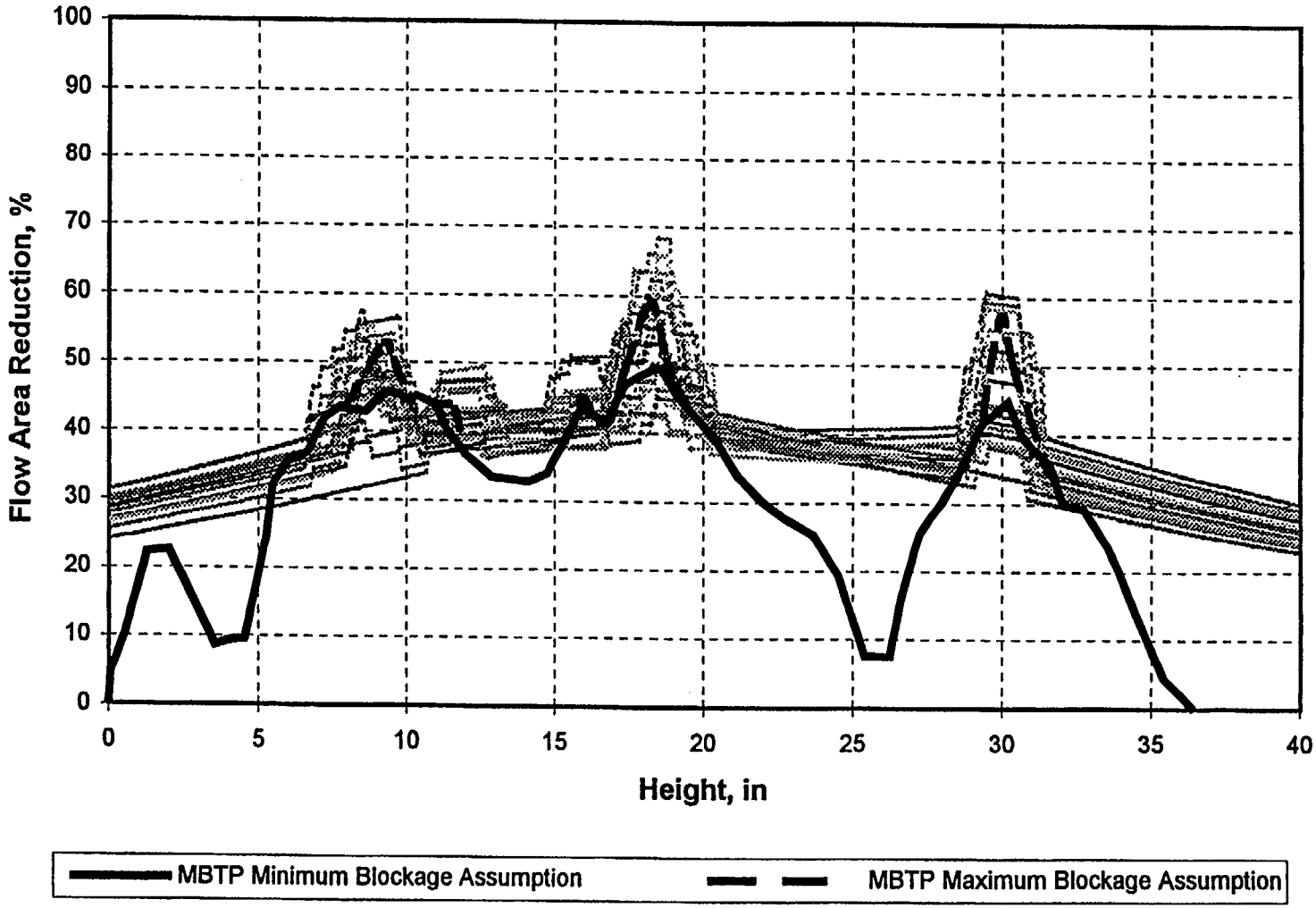

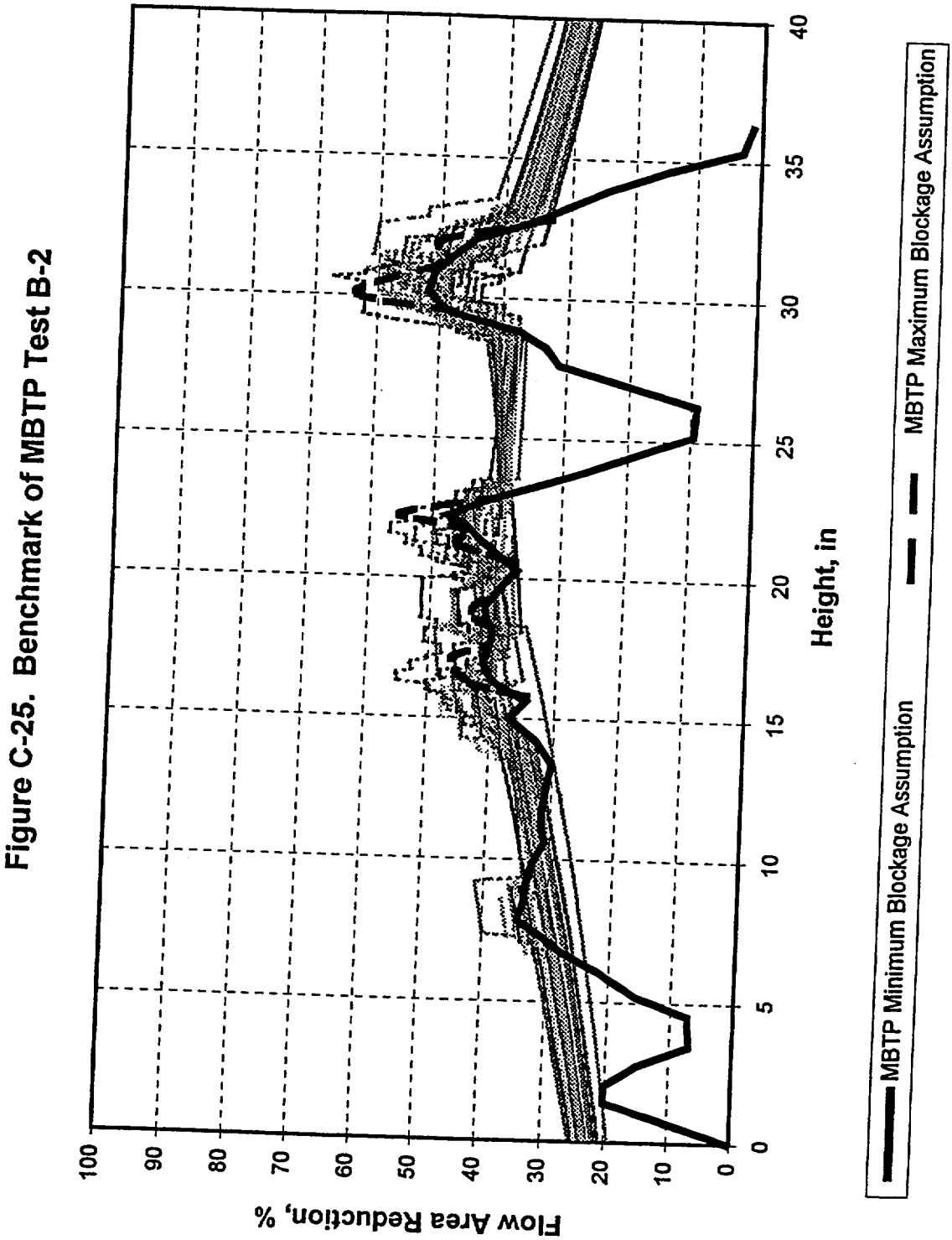

Figure C-25. Benchmark of MBTP Test B-2

Figure C-26. Benchmark of MBTP Test B-2 with All Rods Allowed to Strain

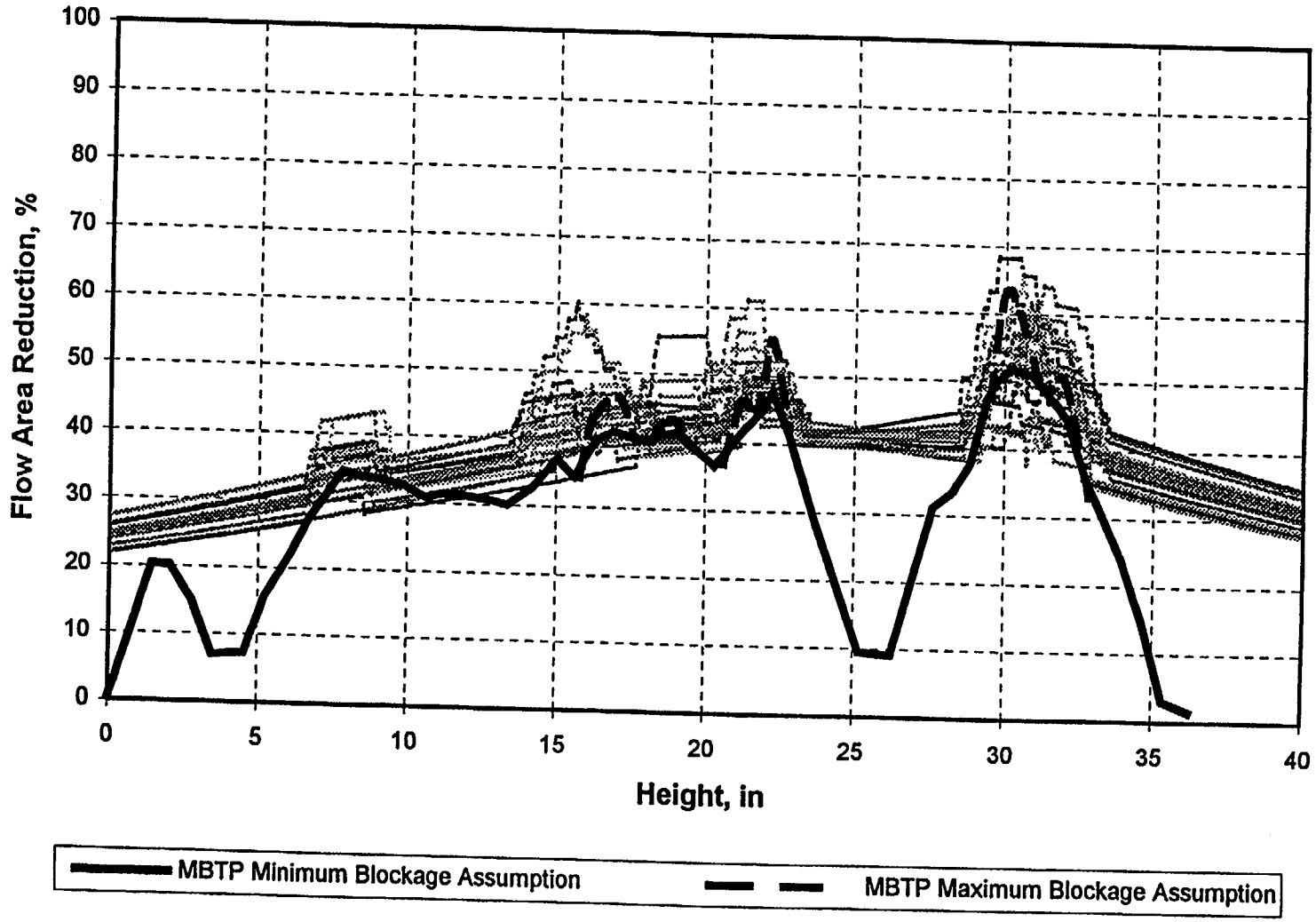

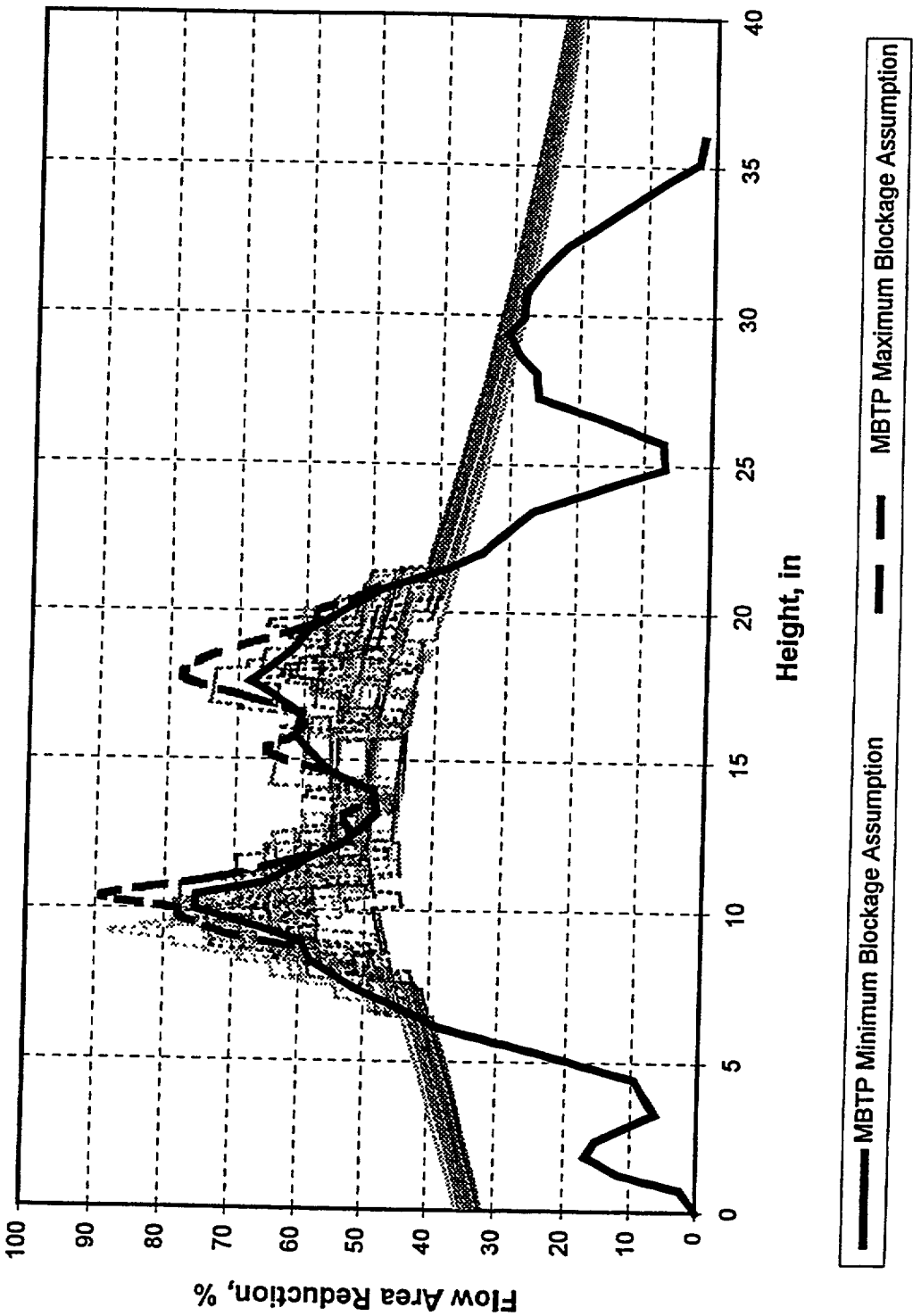

Figure C-27. Benchmark of MBTP Test B-3

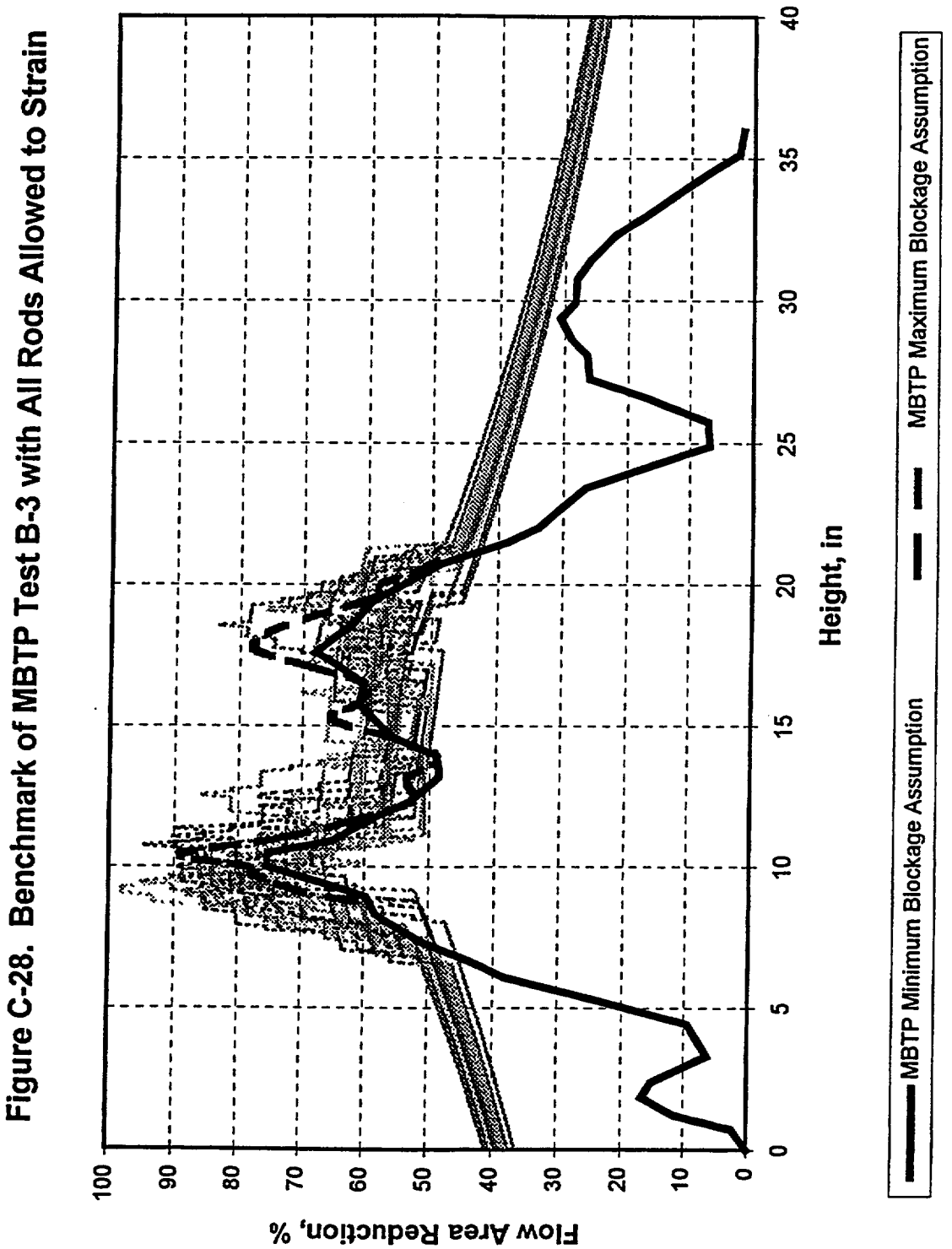
Figure C-28. Benchmark of MBTP Test B-3 with All Rods Allowed to Strain
Flow Area Reduction, %
100
90
80
70
60
50
40
30
20
10
0
Height, in
0
5
10
15
20
25
30
35
40
MBTP Minimum Blockage Assumption
MBTP Maximum Blockage Assumption

Figure C-29 -- PROPRIETARY

[c,d]

Figure C-30 -- PROPRIETARY

[c,a]

Figure C-31 -- PROPRIETARY

[c,a]

Figure C-32 -- PROPRIETARY

[c, a]

Figure C-33 -- PROPRIETARY

[a,c]

Figure C-34 -- PROPRIETARY

{c,d}

Figure C-35 -- PROPRIETARY

[c,d]

APPENDIX D

M5 HIGH TEMPERATURE OXIDATION TESTING

M5 HIGH TEMPERATURE OXIDATION TESTING

The Framatome Technologies Incorporated (FTI) LOCA evaluation models, References D-1 and D-2, and 10CFR50.46 Appendix K require the calculation of high temperature zirconium oxidation using the Baker/Just oxidation correlation. This appendix documents the results of an ongoing program to demonstrate that the Baker/Just correlation is conservative relative to the true oxidation performance of the M5 cladding material.

Oxidation tests on Zircaloy-4 and the M5 alloy have been conducted in the CINOG facility at the CEA laboratory in Grenoble, France. The facility is comprised of a high temperature steam source capable of bathing a short, up to 10 cm, tubing sample in steam for several thousand seconds, a power supply connected to an inductive coil for heating the sample, optical pyrometers for sample temperature measurement, and feedback controls that couple the temperature measurement with the power supply to provide for controlled heatup and the maintenance of a constant oxidation temperature. During testing the sample is positioned centrally within the heating coil. Steam flow is channeled over the exterior and the interior of the sample such that oxidation takes place on both surfaces relatively homogeneously. The heating coil is protected from the steam flow by a quartz tube surrounding the sample.

After the sample is positioned, superheated (250 C) steam flow is established and the sample is rapidly heated to the specified oxidation temperature. The steam flow is sufficient to insure that the oxidation is not steam limited except for the initial burning prior to the buildup of 1 or 2 microns of oxidation. The heating ramp rate is controlled at 20 C/s. Once the sample reaches the specified testing temperature, it is held at that temperature for a predetermined time. The oxidation times were selected to achieve total oxidation depths of 50, 100, and 200 microns. The use of a fast heating ramp minimizes the amount of off temperature oxidation incurred. A record of the actual temperature history is kept. Following the oxidation, the sample cools rapidly, minimizing any post period oxidation. A detailed test report is being prepared and will be available by January 1998.

This appendix reports the results of testing at three temperatures; 1050, 1150, and 1250 C. Both Zircaloy-4 and M5 tubing samples were tested and for each temperature samples were oxidized for three different times. Each test was performed three times to determine repeatability. Figures D-1 and D-2 provide the results of these tests for Zircaloy-4 and M5, respectively. Figures D-3, D-4, and D-5 present results of the Ziracloy-4 in comparison to M5 at each of the oxidation temperatures. At the lower of the temperatures, 1050 C, M5 oxidizes at a considerably lower rate than does Ziracloy-4. For the higher temperatures, the oxidation rate is essentially the same between the two alloys. Figures D-6 and D-7 compare the two alloys against the predictions of the Baker/Just correlation. The figures are arranged in the standard calculated versus measured format.

Data that lie above the median line have been conservatively predicted by the benchmarked correlation. As expected from the comparison figures M5 and Zircaloy demonstrate the same conservatism in Baker/Just for the upper temperatures and M5 is considerably more overpredicted at the lower temperatures.

Three considerations have been demonstrated by these tests. The high temperature oxidation of M5 can be conservatively evaluated with the Baker/Just correlation. The M5 alloy oxidizes [e , d

3. The prediction of high temperature oxidation by Baker/Just during LOCA calculations is slightly more conservative for M5 than it is for Zircaloy-4. Therefore, the Baker/Just correlation is appropriate and conservative for modeling, within an approved LOCA evaluation model as dictated by Appendix K to 10CFR50.46, of the high temperature oxidation of M5 alloy cladding.

REFERENCES

D-1. BAW-10168-A Rev. 3, RSG LOCA, BWNT Loss-of-Coolant Accident Evaluation Model for Recirculating Steam Generator Plants, B&W Nuclear Technologies, Lynchburg, Virginia, 1996.

D-2. BAW-10192-P, BWNT LOCA, BWNT Loss-of-Coolant Accident Evaluation Model for Once-Through Steam Generator Plants, B&W Nuclear Technologies, Lynchburg, Virginia, 1994.

D-1. High Temperature Oxidation of Zircaloy-4 Cladding -- PROPRIETARY

[c,d]

D-2. High Temperature Oxidation of M5 Cladding -- PROPRIETARY

[c, d]

D-3. Comparison of Zircaloy-4 and M5 Oxidation at 1050 C -- PROPRIETARY

[c,d]

D-4. Comparison of Zircaloy-4 and M5 Oxidation at 1150 C -- PROPRIETARY

[c,d]

D-5. Comparison of Zircaloy-4 and M5 Oxidation at 1250 C -- PROPRIETARY

[c,d]

D-6. Measured to Baker/Just Prediction of Oxidation for Zircaloy-4 -- PROPRIETARY

[c,d]

D-7. Measured to Baker/Just Prediction of Oxidation for M5 -- PROPRIETARY

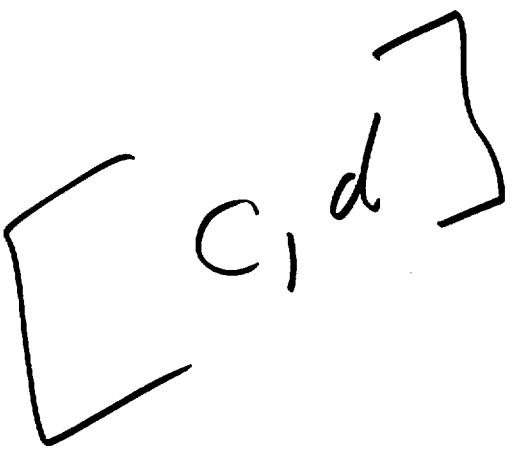

Appendix E

Summary of M5 In-core Irradiation and Planned Inspections

Summary of M5 In-core Irradiation and Planned Inspections

A total of 3061 M5 fuel rods have completed or are in operation in-core. This operation has achieved a maximum fuel rod burnup of 54.5 GWd/mtU[G1]. A total of 15 commercial reactors have been involved in this irradiation including three U.S. reactors. This in-core operation is summarized in Table E-1. Extensive examinations have been performed on the fuel rods involved in this irradiation. These exams include poolside measurements, hotcell measurements and testing, and refabrication of fuel rods and subsequent ramp testing in a experimental reactor.

The four Mark-BW X1 LTAs[G-2] in North Anna 1also [d]Full reload batches with M5 fuel rod cladding are planned in Europe in 1998 and in 1998/1999 in the U.S. [d] A summary of planned inspections in U.S. Plants is given in Table E-2.

REFERENCES

E-1. J.P. Mardon, et al., Update on the Development of Advanced Zirconium Alloys for PWR Fuel Rod Performance, page 405 to 412, Proceedings of The 1997 International Topical Meeting on LWR Fuel Performance, Portland Oregon, March 2-6, 1997.

E-2. BAW-2272 Mark-BW17 Lead Test Assemblies for North Anna Power Station - Design Report, July 1996.

Table E-1
M5 Experience

Reactor	Power Level MWt	# Fas In-Core	Core Height in.	Fuel Rod Array	Avg LHGR kW/ft	Vessel Exit Temp, C	# FAs with 5R/M5	Total # of 5R/M5 Fuel Rods	Cycles Achieved	Burnup Achieved GWd/mtU	Cycles Planned	Burnup Planned GWd/mtU
	2775	157	144.0	17x17	5.43	321	4	8	3	34		
	2775	157	144.0	17x17	5.43	321	2	8	5	55	6	63
	2775	157	144.0	17x17	5.43	322	2	6	3	40	4	46
	3411	193	144.0	17x17	5.43	327	2	7	3	39	3	39
	2775	157	144.0	17x17	5.43	321	4	48	3	33	4	44
	2893	157	144.0	17x17	5.67	327	4	1032			3	55
[c, d]	2568	177	140.6	15x15	5.80	319	2	8	1	13	3	55
	3800	193	168.0	17x17	5.19	324						
	3800	193	168.0	17x17	5.19	324	2	32				
	3800	193	168.0	17x17	5.19	324	2	32				
	1192	121	96.1	14x14	6.70	317	2	36	3	39	4	45
	3765	193	153.5	16x16	6.29	326	2	24	3	39		
	3765	193	153.5	16x16	6.29	326	4	48	3	38		
	3765	193	153.5	16x16	6.29	326	4	944				
	3850	193	153.5	18x18	6.43	326	1	300	2	31	3	44

Table E-2

Planned M5 U.S. Inspections

Plant/Cycle	Date	Purpose of Planned Inspections
[b]	[b]	[b]

Appendix F

M5 LOCA Evaluations

M5 LOCA Evaluations

F.1 INTRODUCTION

This appendix presents an evaluation of the LOCA performance of the M5 cladding alloy for Mark-B (B&W design NSSS fuel) and Mark-BW (Westinghouse design NSSS fuel) type fuel assemblies. To simulate the M5 cladding, the cladding material properties from Appendix A and the swelling and rupture model from Appendix C were employed in the appropriate evaluation model (Mark-B or Mark-BW). The cladding was shown to behave in a similar fashion to Zircaloy. The range of permissible design is such that acceptable LOCA performance is well within the achievable. In particular the cladding temperatures and other criteria determinants vary only slightly from the reference Zircaloy-4 cases. The only general observation made is that the creep model for M5, Section 3.8, produces a slower creep down of the cladding onto the fuel pellet than would be appropriate for Zircaloy-4. This leads to lower fuel cladding gap conductivity for middle of life burnups and necessitates that burnup sensitivity studies be conducted for the first plant applications of the alloy. An example of how the basic acceptance criteria of 10CFR50.46 will be met by the new material is also provided.

F.2 ANALYSIS METHODS

The LBLOCA analyses performed to support the licensing of the M5 cladding were conducted in accordance with the FTI once-through steam generator (OTSG) LOCA evaluation model (Reference F-1) for the Mark-B fuel assembly and the FTI recirculating steam generator (RSG) LOCA evaluation model (Reference F-2) for the Mark-BW fuel assembly. The evaluation of cladding temperature transients and local oxidation is performed with three computer codes, which are interconnected as depicted in Figure F-1. A brief summary of each code is provided in the following discussion.

RELAP5/MOD2-B&W (Reference F-3), a modified version of the INEL RELAP5/MOD2 code, calculates system thermal-hydraulics, core power generation, and the clad temperature response during blowdown. The REFLOD3B computer code (Reference F-4) simulates the thermal-hydraulic behavior of the primary system during the core refill and reflood phases of the LOCA in order to determine appropriate core flooding rates and upper and lower plenum conditions for input to BEACH. Finally, BEACH (Reference F-5), which is a RELAP5/MOD2-B&W core model with the reflood, fine-mesh rezoning option activated, determines the clad temperature response during the reflood period with input from REFLOD3B.

The plant noding diagrams that were developed in accordance with the appropriate evaluation model are shown in Figures F-2 through F-5 for the OTSG plant model and in Figures F-6 through F-8 for the RSG plant model.

F.3 CHANGES FOR M5 CLADDING

The LOCA modeling of M5 requires that the cladding materials properties be altered to values appropriate for the new material (Appendix A), that the initial fuel temperatures be changed, and that the high temperature swelling and rupture model of Appendix C be used. All of these considerations have been made in producing the example calculations presented within this appendix. The alteration of the materials properties merely required the determination of new values for input to the existing evaluation models. The swelling and rupture model, however, is somewhat more complex. FTI considers that [

e,d

].

Because M5 is a different alloy from the Zircaloy-4 that has been used to develop swelling and rupture correlations for the current evaluation models and actually behaves somewhat differently than Zircaloy-4, a revised modeling and model basis for the material were developed. To facilitate the development, tests of cladding swelling and rupture were performed at the French CEA laboratory in Saclay, France. These tests, identified by the acronym EDGAR, were pressurized single pin, electrically heated rupture tests and measured both rupture deformation and the temperatures at which rupture would occur. The results of this testing were used to develop an M5 specific cladding swelling and rupture model for use in the LOCA evaluation of this cladding. The model [

c,d

]. Appendix C fully describes the model developed.

The basic physical properties of the M5 alloy are quite similar to those for Zircaloy-4. However, some differences have been observed. These differences are of particular note for properties that relate to the materials phase change from its alpha crystalline structure to its beta structure. Appendix A presents the materials properties that have been used in the LOCA and safety analysis determinations presented in this report to characterize the performance of the M5 cladding. These properties have not been fully researched and determined but appropriate approximations, based on available data, are presented. The approximations are deemed sufficient for the demonstration of the material as a viable cladding for nuclear fuel pins.

Finally, the creep of M5 is reduced from that of Zircaloy-4 producing a slower creep down of the cladding onto the fuel pellet than would be appropriate for Zircaloy-4. This leads to lower fuel cladding gap conductivity for middle of life burnups which necessitated the burnup sensitivity studies provided herein and will require that these studies also be performed for the first plant applications of the alloy.

F.4 SENSITIVITY STUDIES

Various sensitivity studies performed with the evaluation models are required to demonstrate model convergence and conservatism. The studies can be divided into two categories: generic and plant specific. The generic studies are documented in the evaluation model reports, BAW-10192 (Reference F-1) and BAW-10168 (Reference F-2), for the OTSG and RSG plants, respectively. Those studies demonstrated results that are characteristic of the evaluation model--the codes and interfaces--and are not plant dependent. In as much as the use of the M5 cladding constitutes a fuel design change, and as such will not affect the system thermal-hydraulic calculations, its use does not alter the conclusions of the generic studies.

The plant specific studies, a time-in-life study for example, are performed to identify a limiting case to use in calculating the LOCA LHR limits based on the specific parameters of the plant design under consideration. In as much as the use of the M5 cladding constitutes a fuel design change, the plant specific studies must consider its use in determining limiting results.

F.5 COMPARISON OF CALCULATION RESULTS

Typically the LOCA evaluation is completed with a set of analyses to show compliance with 10CFR50.46 for the core power and peaking that will limit plant operation. While this report is not a plant specific application of either the OTSG or RSG EM, LOCA demonstration cases are presented to quantify the effects of the new cladding design. For each EM, a double ended guillotine break in the cold leg pump discharge piping with a discharge coefficient of 1.0 was analyzed. A comparison of results obtained using the base evaluation model methods with Zircaloy-4 cladding and the results obtained for an identical case using the M5 swelling and rupture model was made. The inputs and results are summarized in the following sections.

F.5.1 OTSG Evalutaion

F.5.1.1 Inputs and Assumptions

The OTSG evaluation considers a typical 177-LL plant, specifically TMI Unit-1. A case with a two foot power peak was selected, because this is typically the case that results in the least LOCA margin. Table F-1 identifies the inputs and assumptions used in the LBLOCA studies. The major plant operating parameters and boundary conditions used in the LOCA codes are:

1. Power Level - The analyses consider that the plant is operating at steady-state conditions with core thermal powers less than or equal to 2827 MWt (102% of 2772 MWt).

2. SG Tube Plugging - The tube flow area is based on the assumption that 20 percent of the broken loop and 10 percent of the intact loop tubes have been plugged on the primary side and removed from service. The higher number of plugged tubes in the broken loop produces increased resistance from the core to the break, which serves to decrease the positive core flows during the first portion of blowdown. The reduced core flows produce less heat transfer from the pins to the fluid resulting in higher fuel and cladding temperatures at the end of blowdown.

3. Total System Flow - The total reactor coolant system (RCS) flow, considering a unit-average tube plugging of 15 percent, is 137.3 Mlbm/hr. The total core bypass flow fraction is 7.5 percent of the RCS flow.

4. Fuel Parameters - The steady-state fuel pin parameters are calculated using a method and code (currently TACO3) that has been approved by the NRC for supplying inputs to the LOCA analysis (Reference F-6). The parameters used are consistent with, or bounded by, the core burnup conditions stated or simulated in the analysis. Parameters supplied to RELAP5/MOD2 as initial steady-state values include fuel volume-average temperatures, hot fuel and cladding dimensions, internal pin pressure, gap gas compositions, fuel radial source factors, fuel-clad mechanical contact pressures, hot pin plenum volumes, and rod average burnup. The M5 creep characteristics affect the predictions of this code as discussed in Section 3.8.

5. Emergency Core Cooling System - The ECCS flows are based on minimum ECCS flow (flow from one train).

6. Core Average Linear Heat Rate (LHR) - The core average LHR for the LOCA analyses performed at 102 percent of 2772 MWt is 6.4 kW/ft.

7. Moderator Density Reactivity - The moderator density reactivity coefficient is based on beginning-of-cycle conditions to minimize negative reactivity contributions. A zero moderator temperature coefficient (MTC) is used for all full-power cases. All cases use a representative end-of-life beta effective (0.0071) to slow the fission power shutdown.

8. Cladding Rupture Model - The cladding rupture model is based on NUREG-0630 for Zircaloy-4 cladding. The new swelling and rupture model discussed in Appendix C and Section 2.4 is used for the M5 cladding analyses.

F.5.1.2 Results

A comparison of results for LBLOCA cases performed at BOL using Zircaloy-4 and M5 cladding is shown in Figures F-9 through F-15. A summary of the important results is presented in Table F-2. The Zircaloy-4 rupture temperature is in the 875 to 900 C range. The M5 mechanical properties increase the calculated rupture temperature to the 900 to

925 C range. Subsequently, the M5 cladding rupture is delayed by approximately 1.5 seconds. Furthermore, the different rupture temperatures coupled with the different phase transition temperatures, [ ]. More specifically, the Zircaloy-4 rupture strain is decreasing with increased rupture temperature, whereas the M5 rupture strain is increasing with increased rupture temperature. The relative values are such that the flow blockage and additive loss coefficient are higher for the M5 cladding. However, the use of the EM changes required to model the M5 cladding do not otherwise alter the thermal-hydraulic predictions of the EM. Further, the resulting PCT and whole-core oxidation are not significantly different from the base EM that models Zircaloy-4.

A comparison of results for LBLOCA cases performed at 40 GWd/MTU using Zircaloy-4 and M5 cladding is shown in Figures F-16 through F-22. A summary of the important results is presented in Table F-3. For both claddings, the rupture temperature decreases with burnup. As noted at BOL, the Zircaloy-4 rupture strain is increasing with decreased rupture temperature, whereas the M5 rupture strain is decreasing with decreased rupture temperature. The relative values are such that the flow blockage and additive loss coefficient are higher for the Zircaloy-4 cladding. However, the use of the EM changes required to model the M5 cladding do not otherwise alter the thermal-hydraulic predictions of the EM. Further, the resulting PCT and whole-core oxidation are not significantly different from the base EM that models Zircaloy-4.

F.5.2 RSG Evaluation

F.5.2.1 Inputs and Assumptions

The RSG evaluation considers a cold upper head (T-cold) 193-FA Westinghouse 4-loop plant. A case with the power peaked near the ten foot elevation was selected, because this is typically the case that produces limiting results. Table F-4 identifies the inputs and assumptions used in the LBLOCA studies. The major plant operating parameters and boundary conditions used in the LOCA codes are:

1. Power Level - The plant is assumed to be operating in steady-state at 3479 MWT (102% of 3411 MWT).

2. SG Tube Plugging - The Steam Generator tube plugging level was set at 5 percent per generator.

3. Total System Flow - The initial RCS flow is 382,000 gpm.

4. Fuel Parameters - The discussion in BAW-10168 (Reference F-2, pp. A-15 and LA-148) demonstrates that fuel conditions at the beginning of life are the most severe for the LBLOCA evaluation of the Mark-BW FA.

5. Emergency Core Cooling System - The ECCS flows are based on the assumption of no single active failure (i.e. maximum injected flow). This assumption leads to the lowest possible containment pressure and lower core flooding rates.

6. Total Peaking Factor - A value of $F_Q = 2.5$ was used for the total peaking factor.

7. Moderator Density Reactivity - The moderator density reactivity coefficient is based on beginning-of-cycle conditions to minimize negative reactivity.

8. Cladding Rupture Model - The cladding rupture model is based on NUREG-0630 for Zircaloy-4 cladding. The new swelling and rupture model discussed in Appendix C and Section 2.4 is used for the M5 cladding analyses.

F.5.2.2 Results

A comparison of results for LBLOCA cases performed at BOL using Zircaloy-4 and M5 cladding is shown in Figures F-23 through F-29. A summary of the important results is presented in Table F-5. The M5 mechanical properties lead to a higher calculated rupture temperature that delays rupture by approximately 1.5 seconds. The higher rupture temperature and the new swelling and rupture model also predict a larger flow blockage and additive loss coefficient. However, the use of the EM changes required to model the M5 cladding do not otherwise alter the thermal-hydraulic predictions of the EM. Further, the resulting PCT and whole-core oxidation are not significantly different from the base EM that models Zircaloy-4.

F.6 COMPLIANCE WITH 10CFR50.46

The cases examined in this appendix were intended to show that the response of the FTI evaluation models using the M5 cladding and the associated swelling and rupture model are not significantly different from the response using Zircaloy-4 and the swelling and rupture model defined in NUREG-0630. The following subsections discuss the comparison with respect to each of the acceptance criteria for large break LOCA.

F.6.1 Peak Cladding Temperature

The first criterion of 10CFR50.46 states that the calculated peak cladding temperature (PCT) shall remain below 2200 F. The PCTs obtained using the M5 cladding and associated swelling and rupture model were similar to the PCTs obtained using the Zircaloy-4 cladding with the NUREG-0630 swelling and rupture model. Further, the overall thermal hydraulic response of the systems were shown to be unaffected by the new cladding and associated models. Therefore, the M5 cladding performance should not adversely effect core operation or operating limits.

F.6.2 Local Cladding Oxidation

The second criterion of 10CFR50.46 requires that the maximum local degree of cladding oxidation not exceed 17 percent. Compliance to this criterion is obtained by evaluating the results of the calculation of peak cladding temperature. In the OTSG calculation, local cladding oxidation is computed as long as the cladding temperature remains above 1000 F. In the RSG calculation, local oxidation is computed as long as the REFLOD3B predicted quench front has not reached the elevation.

The peak local oxidations obtained using the M5 cladding and associated swelling and rupture model were similar to the oxidations obtained using the Zircaloy-4 cladding with the NUREG-0630 swelling and rupture model. The overall thermal-hydraulic responses of the systems were shown to be unaffected by the new cladding and associated models. Further, the Baker-Just correlation is used to determine the rate of oxide growth for both models. Therefore, the M5 cladding performance should not adversely affect core operation or operating limits.

F.6.3 Maximum Hydrogen Generation

The third criterion of 10CFR50.46 states that the calculated total amount of hydrogen generated from the chemical reaction of the cladding with water or steam shall not exceed 0.01 times the hypothetical amount that would be generated if all of the metal in the cladding cylinders surrounding the fuel reacted, excluding the cladding surrounding the plenum volume.

The maximum hydrogen generation obtained using the M5 cladding and associated swelling and rupture model was similar to the hydrogen generation obtained using the Zircaloy-4 cladding with the NUREG-0630 swelling and rupture model. The overall thermal hydraulic response of the system was shown to be unaffected by the new cladding and associated models. Further, the Baker-Just correlation is used to determine the rate of oxide growth for both models. Therefore, the M5 cladding performance should not adversely affect core operation or operating limits.

F.6.4 Coolable Geometry

The fourth acceptance criterion of 10 CFR 50.46 states that calculated changes in core geometry shall be such that the core remains amenable to cooling. The calculations in Section 4 directly assess the alterations in core geometry that result from a LOCA. These calculations demonstrate that the fuel pin cooled successfully. For these analyses, the hot assembly flow area reduction at rupture is less than 60 percent. Furthermore, the upper limit of possible channel blockage for the M5 swelling and rupture model is [c,d] limit. Neither [c,d] blockage nor 60 percent blockage constitutes total subchannel obstruction. Since the position of rupture in a fuel assembly is

distributed within the upper part of a grid span, subchannel blockage will not become coplanar across the assembly. Therefore, the assembly retains its pin-coolant-channel pin-coolant-channel arrangement and is capable of passing coolant along the pin to provide cooling for all regions of the assembly.

The effects of fuel rod bowing on whole-core blockage are considered in the fuel assembly and fuel rod designs, which minimize the potential for rod bowing. The minor adjustments of fuel pin pitch due to rod bowing do not alter the fuel assembly flow area substantially, and the average subchannel flow area is preserved. Therefore, due to the axial distribution of blockage caused by rupture, no coplanar blockage of the fuel assembly will occur, and the core will remain amenable to cooling. Deformation of the fuel pin lattice at the core periphery is allowed to occur from the combined mechanical loadings of the LOCA and a seismic event. The deformations considered are limited to the outer two or three pin lattice points of the peripheral fuel assemblies of the core and do not cause a subchannel flow area reduction larger than 37 percent (fully crushed grid). The fuel pins at these lattice points do not operate at power levels sufficient to produce a cladding rupture during LOCA. Therefore, the only reduction in channel flow area is from the mechanical effect, and the assemblies retain a coolable configuration.

The consequences of both thermal and mechanical deformation of the fuel assemblies in the core have been assessed, and the resultant deformations have been shown to maintain coolable core configurations. Therefore, the coolable geometry requirements of 10 CFR 50.46 have been met and the core has been shown to remain amenable to core cooling.

F.6.5 Long-Term Cooling

The fifth acceptance criterion of 10CFR50.46 states that the calculated core temperature shall be maintained at an acceptably low value and decay heat shall be removed for the extended period of time required by the long-lived radioactivity remaining in the core. This criterion is a system level criterion which is independent of fuel design. There have been no system level changes introduced with this swelling and rupture model that would alter the long-term cooling process. Therefore, the calculations and arguments presented to license subject plants remain valid for M5 cladding.

F.7 REFERENCES

F-1. BAW-10192-P, BWNT LOCA, BWNT Loss-of-Coolant Accident Evaluation Model for Once-Through Steam Generator Plants, B&W Nuclear Technologies, Lynchburg, Virginia, 1994.

F-2. BAW-10168-A Rev. 3, RSG LOCA, BWNT Loss-of-Coolant Accident Evaluation Model for Recirculating Steam Generator Plants, B&W Nuclear Technologies, Lynchburg, Virginia, 1996.

F-3. BAW-10164-A Revision 3, RELAP5/MOD2-B&W, An Advanced Computer Code for Light Water Reactor LOCA and Non-LOCA Transient Analysis, B&W Nuclear Technologies, Lynchburg, Virginia, 1996.

F-4. BAW-10171, Revision 3, REFLOD3B -- Model for Multinode Core Reflooding Analysis, B&W Nuclear Technologies, Lynchburg, Virginia, September 1989.

F-5. BAW-10166, Revision 4, BEACH -- A Computer Program for Reflood Heat Transfer During LOCA, B&W Nuclear Technologies, Lynchburg, Virginia, October 1992.

F-6. BAW-10162P-A, Revision 0,TACO3 - Fuel Pin Thermal Analysis Computer Code, B&W Nuclear Technologies, Lynchburg, Virginia, October, 1989.

Table F-1: Summary of Mark-B FA Input Parameters

Parameter	
Core Power, MWt	1.02*2772
RCP Power per Pump, MWt	5
Hot Leg Pressure, psia	2172
Reactor Vessel T_{ave}, F	579
Min RCS Loop Flow, lbm/hr	$67.6x10^6$ (Loop B) $69.7x10^6$ (Loop A)
Percentage of SG Tubes Plugged, %	20 in SG B/ 10 in SG A
MFW Temperature, F	465.0
Pressurizer Level, in	192
CFT Pressure, psig	565
CFT Liquid Volume, ft^3	985
CFT Temperature, F	140
CFT Form Loss Factor	6.926
BWST Temperature, F	120
Max ECCS Response Time, s	36

Table F-2: Comparison of Mark-B FA BOL Results

Parameter	Zr-4 Cladding	M5 Cladding
Peak Initial Fuel Temperature, F	2263	2328
End of Blowdown, sec	20.0	20.8
Bottom of Core Recovery, sec	27.6	27.6
Rupture Time, sec	18.71	20.16
Rupture Flow Blockage, %	0.4878	0.5266
Rupture Additive Loss Coefficient	1.84	2.41
UNRUPTURED NODE:	7	7
PCT, F	1926	1922
Time, s	32.7	33.1
RUPTURED NODE	6	6
PCT, F	2031	2038
Time, s	29.5	29.7
Peak Local Oxidation, %	2.79	3.02
Whole-Core Hydrogen Generation, %	< 0.2	<0.2

Table F-3: Comparison of Mark-B FA TIL Results

Parameter	Zr-4 Cladding	M5 Cladding
Peak Initial Fuel Temperature, F	2156	2143
End of Blowdown, sec	20.0	20.8
Bottom of Core Recovery, sec	27.6	27.9
Rupture Time, sec	19.2	20.7
Rupture Flow Blockage, %	0.5773	0.4426
Rupture Additive Loss Coefficient	3.48	1.34
UNRUPTURED NODE:	6	6
PCT, F	1878	1834
Time, s	30.2	28.8
RUPTURED NODE	7	7
PCT, F	1904	1816
Time, s	30.5	30.8
Peak Local Oxidation, %	2.19	1.88
Whole-Core Hydrogen Generation, %	<0.1	<0.1

Table F-4: Summary of Mark-BW FA Input Parameters

Parameter	
Core Power, MWt	1.02*3411
RCP Power per Pump, MWt	5
Pressurizer Pressure, psig	2295
System Flow, gpm	382,000
Reactor Vessel T_{ave}, F	585.6
Percentage of SG Tubes Plugged, %	5
Pressurizer Level, %	60
MFW Temperature, F	440
Accumulator Pressure, psig	612
Accumulator Liquid Volume, gal/acc	7106
Accumulator Temperature, F	125
Accumulator Form Loss Factor	13
SI Water Temperature, F	70
Max ECCS Response Time, s	35

Table F-5: Comparison of Mark-BW FA BOL Results

Parameter	Zr-4 Cladding	M5 Cladding
Peak Initial Fuel Temperature, F	2159.0	2160.1
End of Blowdown, sec	25.255	25.810
Bottom of Core Recovery, sec	40.28	39.99
Rupture Time, sec	59.04	70.0
Rupture Flow Blockage, %	0.4878	0.5266
Rupture Additive Loss Coefficient	NA	NA
UNRUPTURED NODE	15	15
PCT, F	2151.3	2168.8
Time, sec	139.7	137.7
RUTPURED NODE	17	17
PCT, F	1756.5	1769.3
Time, sec	236.9	138.5
Peak Local Oxidation, %	7.28	8.30
Whole-Core Oxidation, %	0.76	0.76

FIGURE F-1: LARGE BREAK ANALYSIS CODE INTERFACE

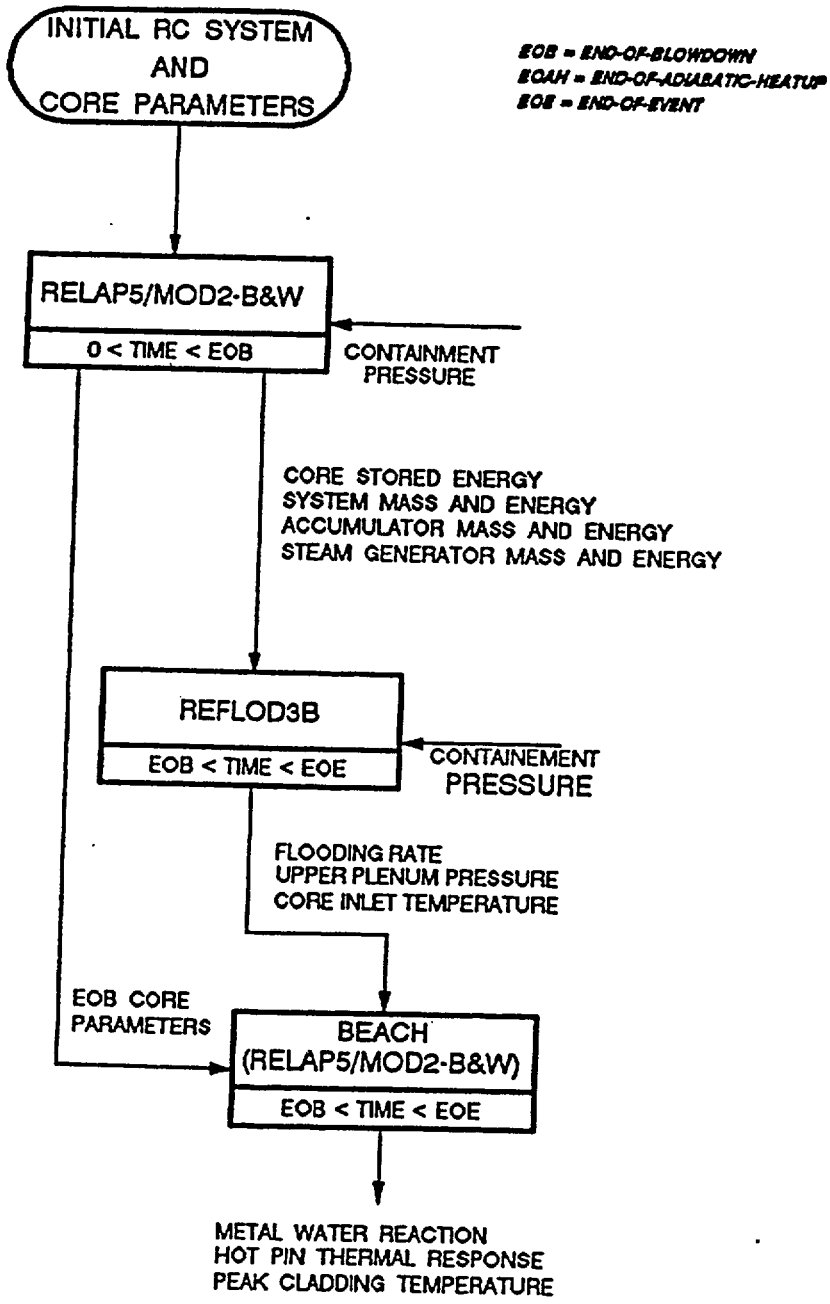

FIGURE F-2: LBLOCA LOOP NODING ARRANGEMENT (177 LL PLANT)

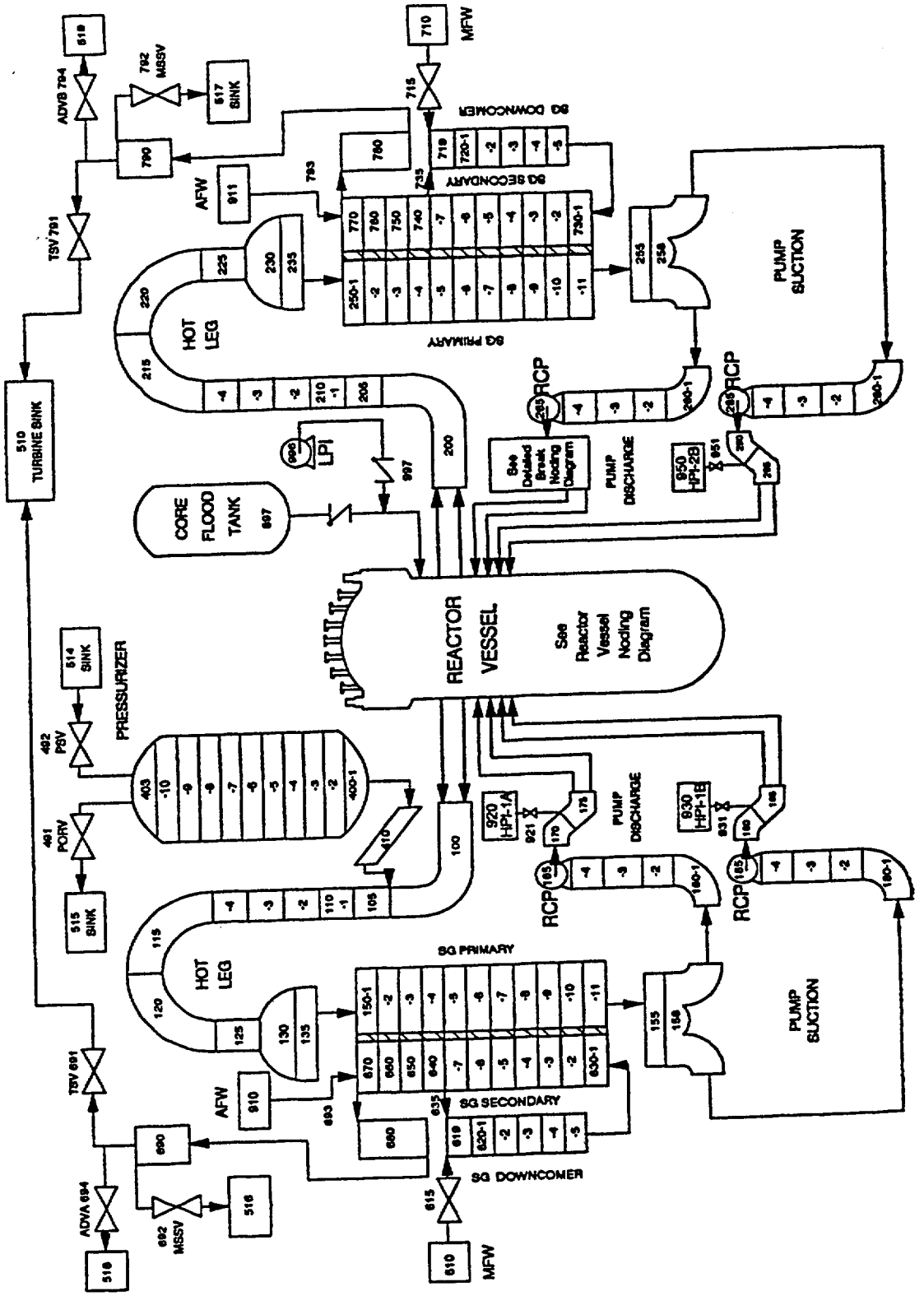

FIGURE F-3: LBLOCA REACTOR VESSEL NODING ARRANGEMENT (177 LL PLANT)

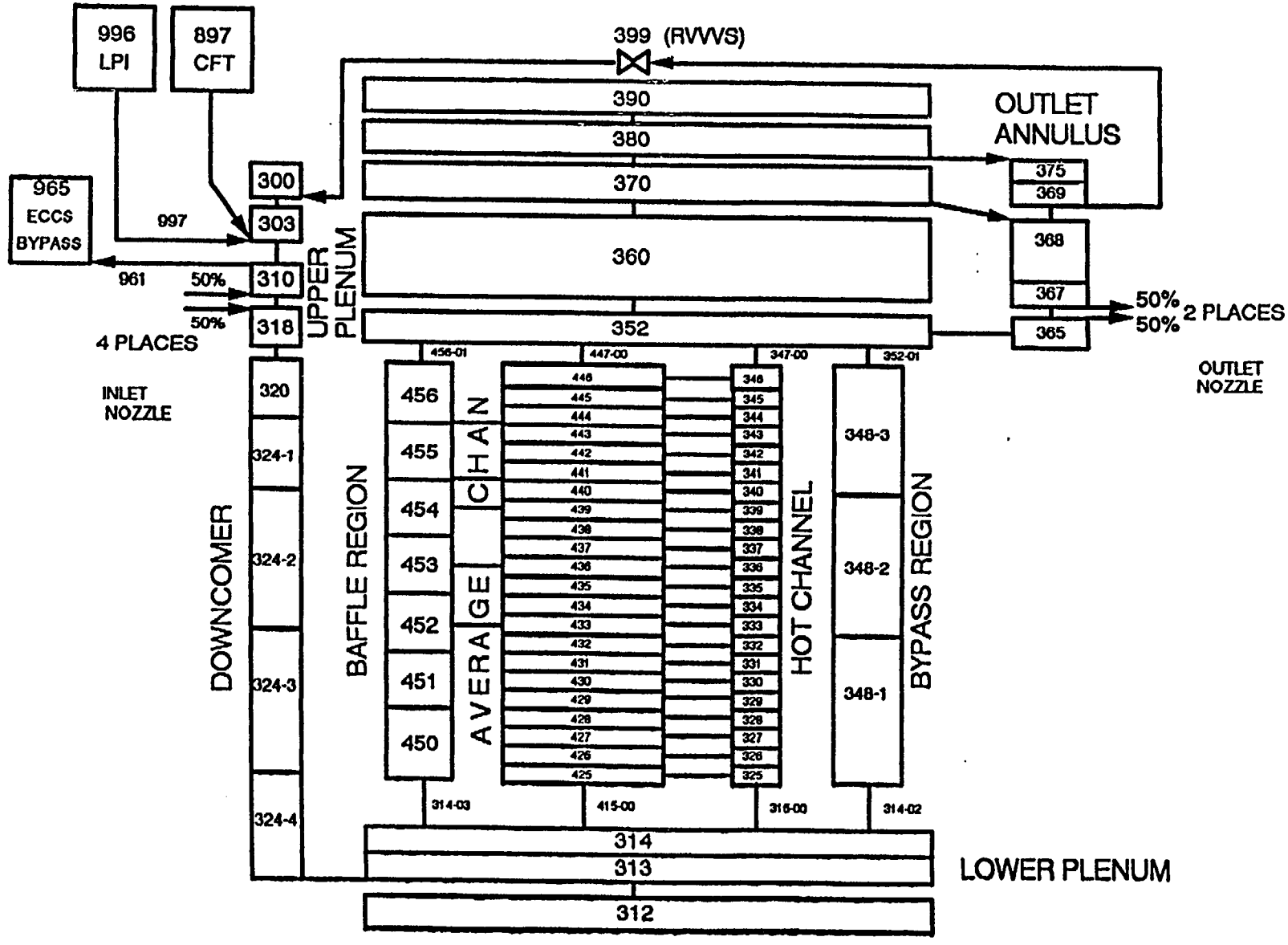

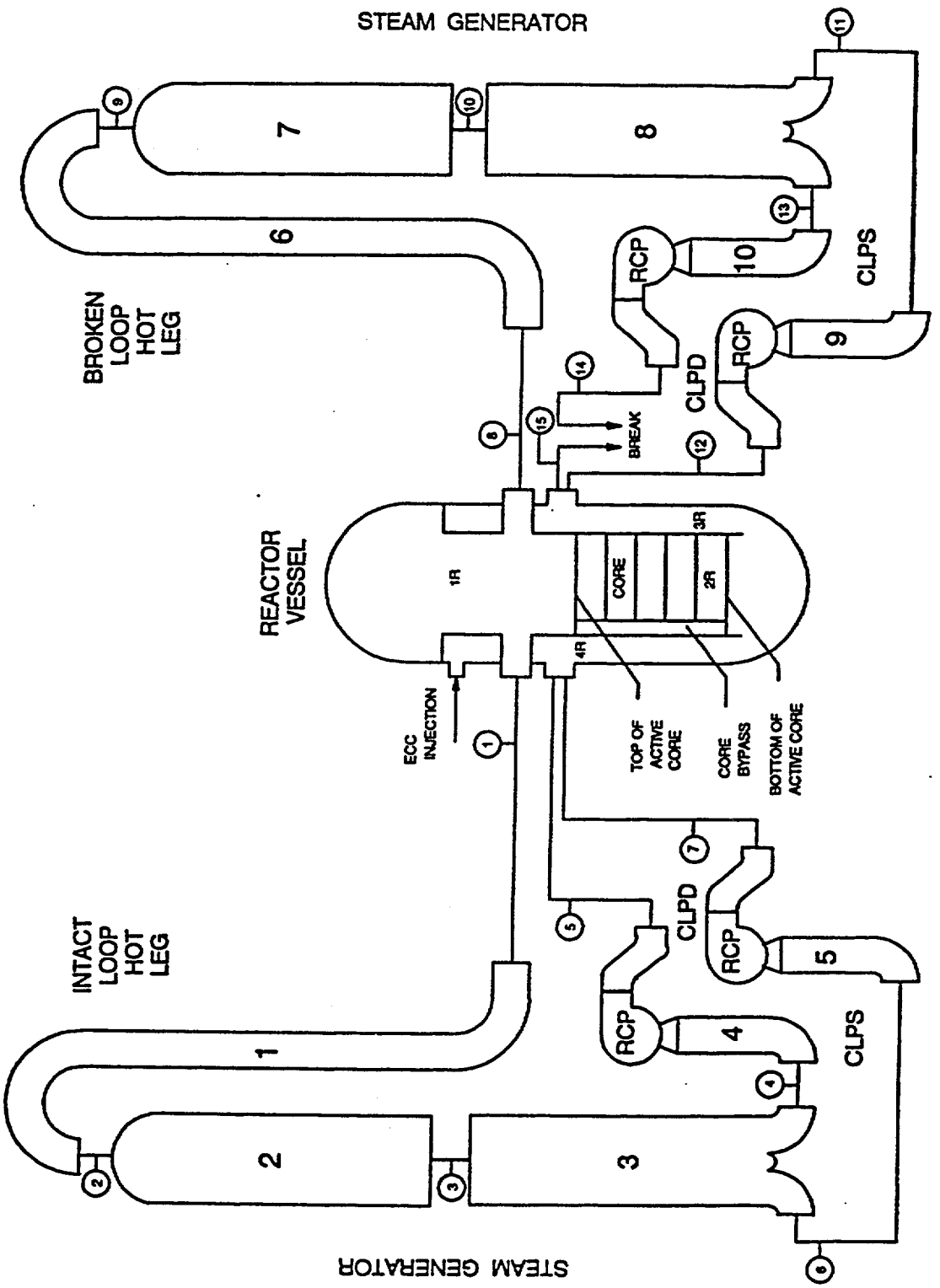

FIGURE F-4: REFLOD3B NODING ARRANGEMENT (177 LL PLANT)

FIGURE F-5: BEACH NODING ARRANGEMENT (177-LL)

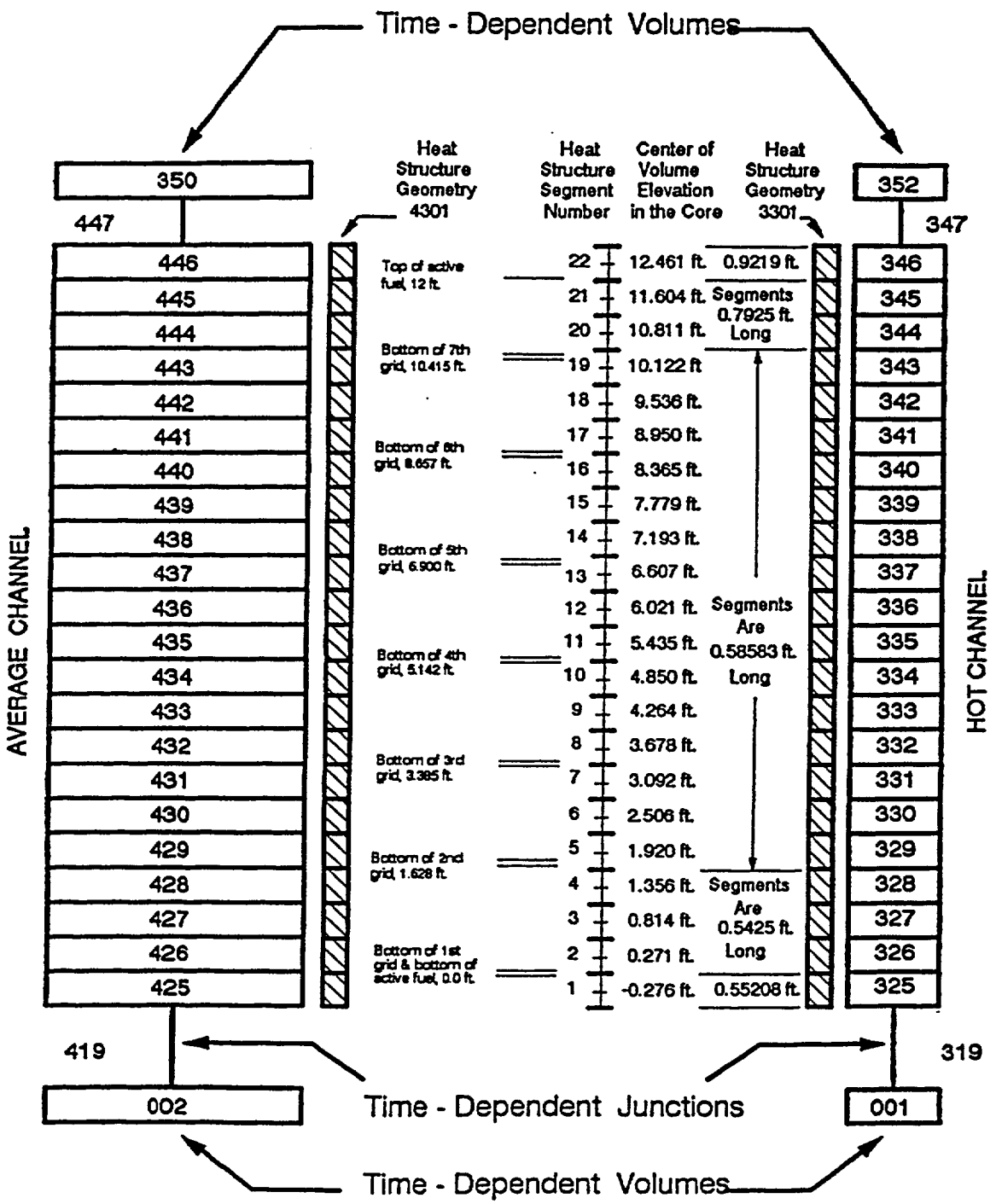

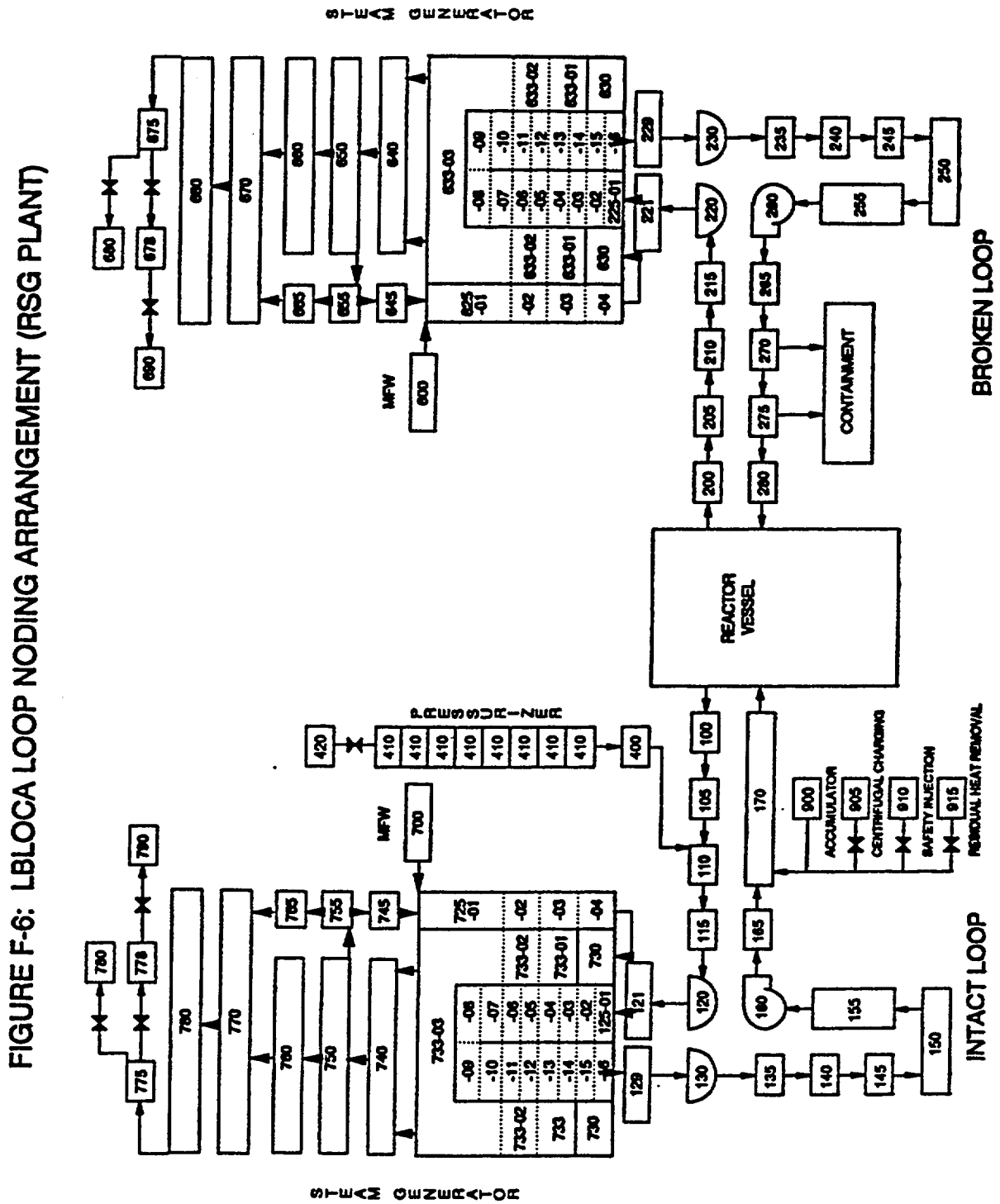

FIGURE F-6: LBLOCA LOOP NODING ARRANGEMENT (RSG PLANT)

FIGURE F-7: LBLOCA REACTOR VESSEL AND BEACH NODING ARRANGEMENT (RSG PLANT)

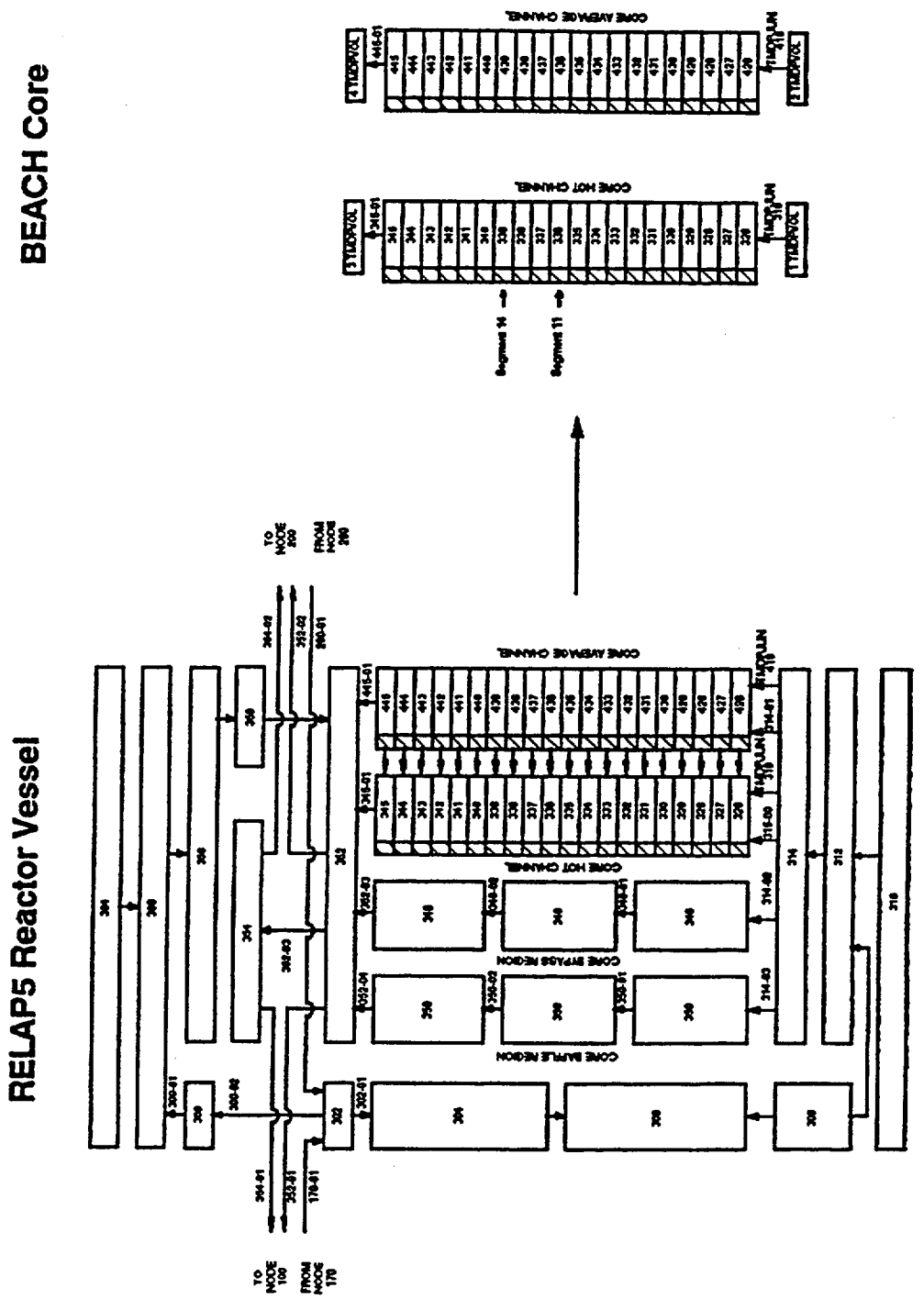

FIGURE F-8: REFLOD3B NODING ARRANGEMENT (RSG PLANT)

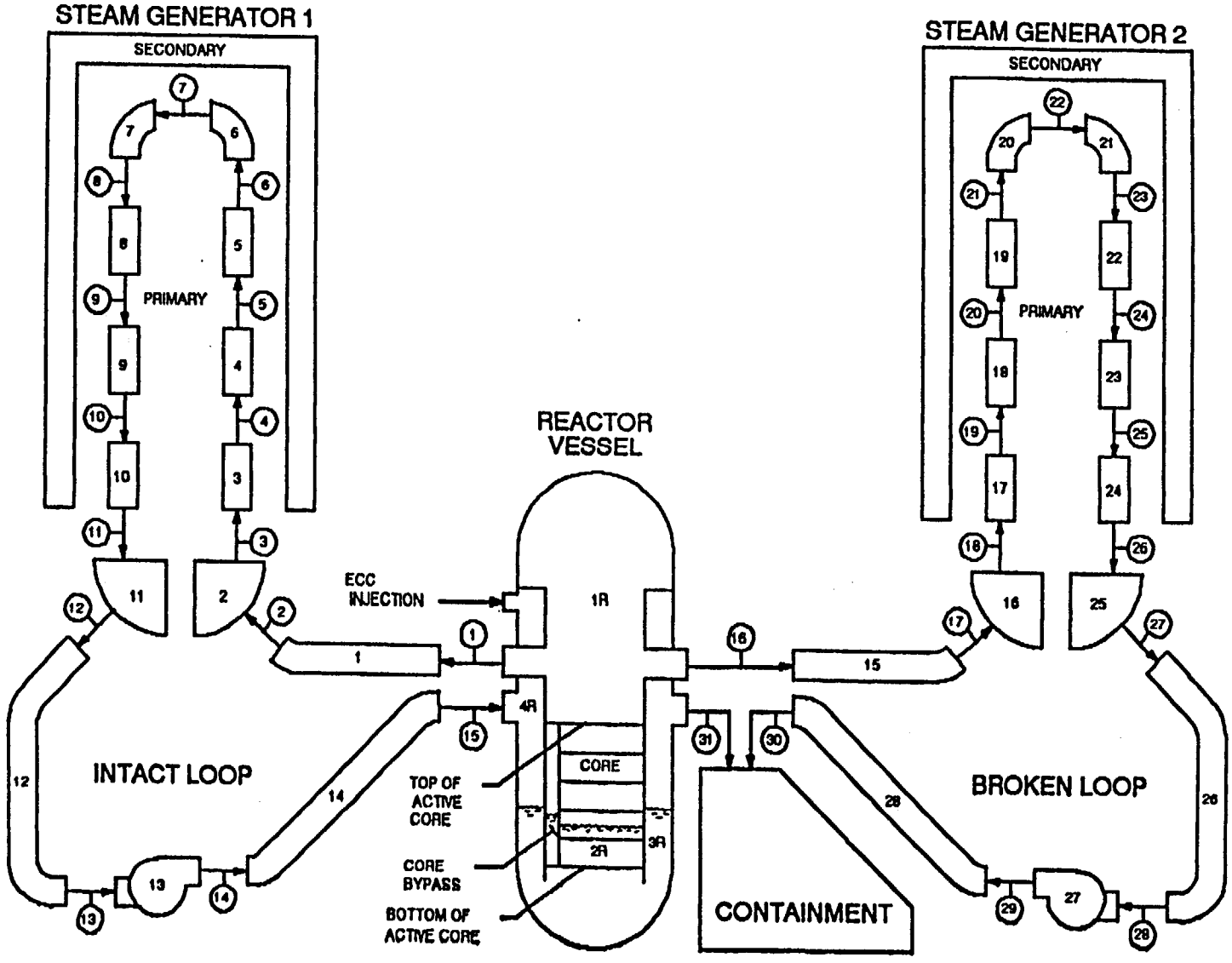

FIGURE F-9. Mk-B FA, M5 vs Zr-4 CLADDING, BOL - REACTOR VESSEL UPPER PLENUM PRESSURE.

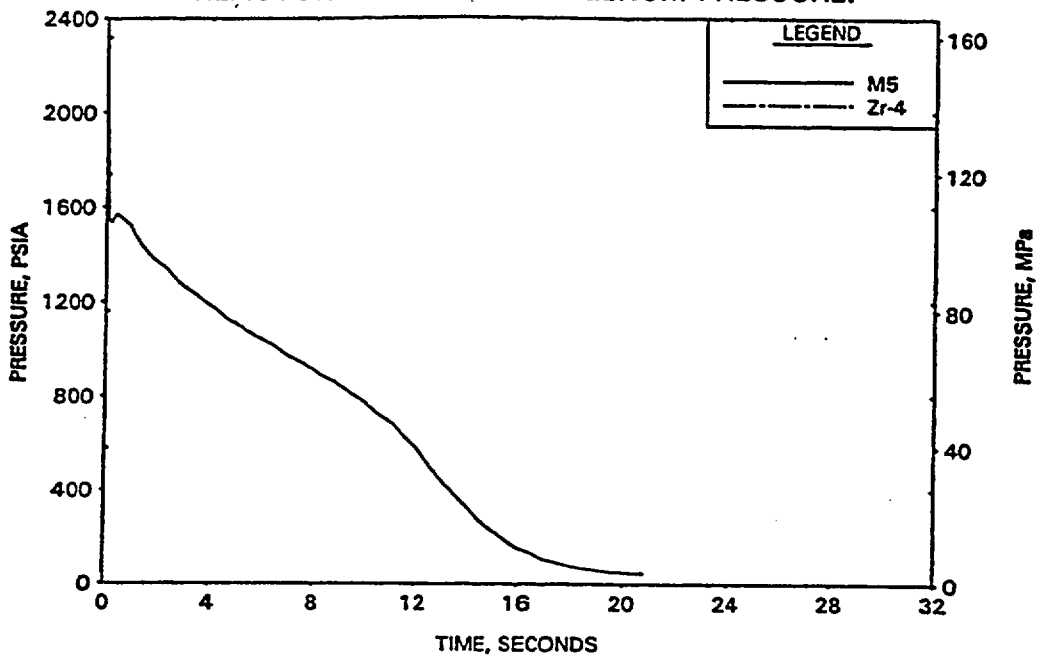

FIGURE F-10. Mk-B FA, M5 vs Zr-4 CLADDING, BOL - BREAK MASS FLOW RATE.

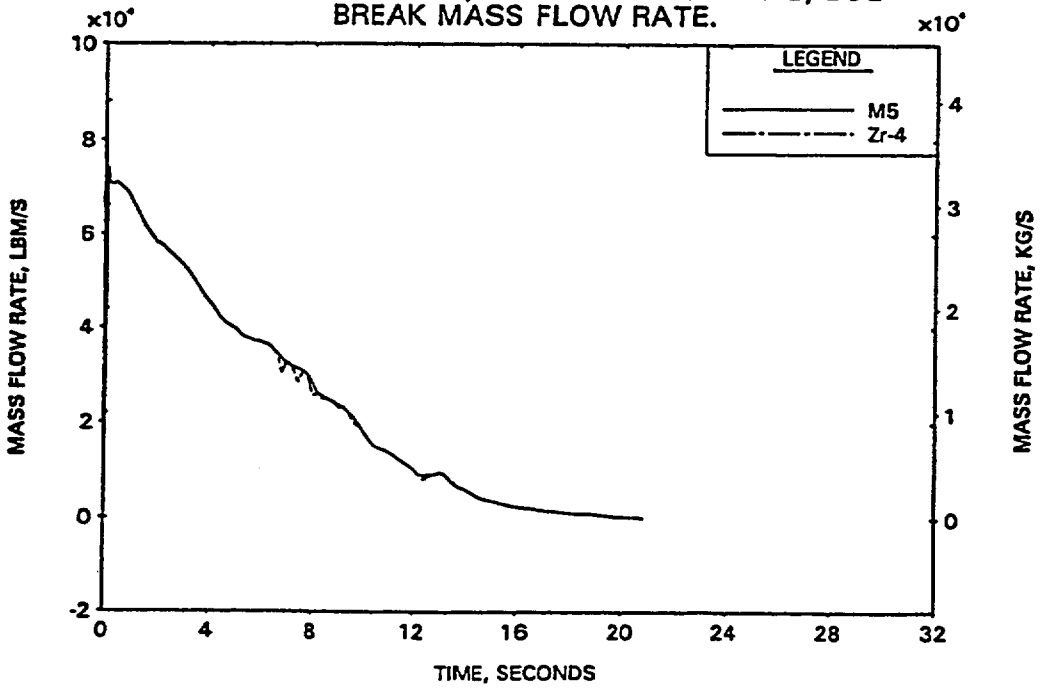

FIGURE F-11. Mk-B FA, M5 vs Zr-4 CLADDING, BOL - HC MASS FLOW RATE AT PEAK POWER LOCATION.

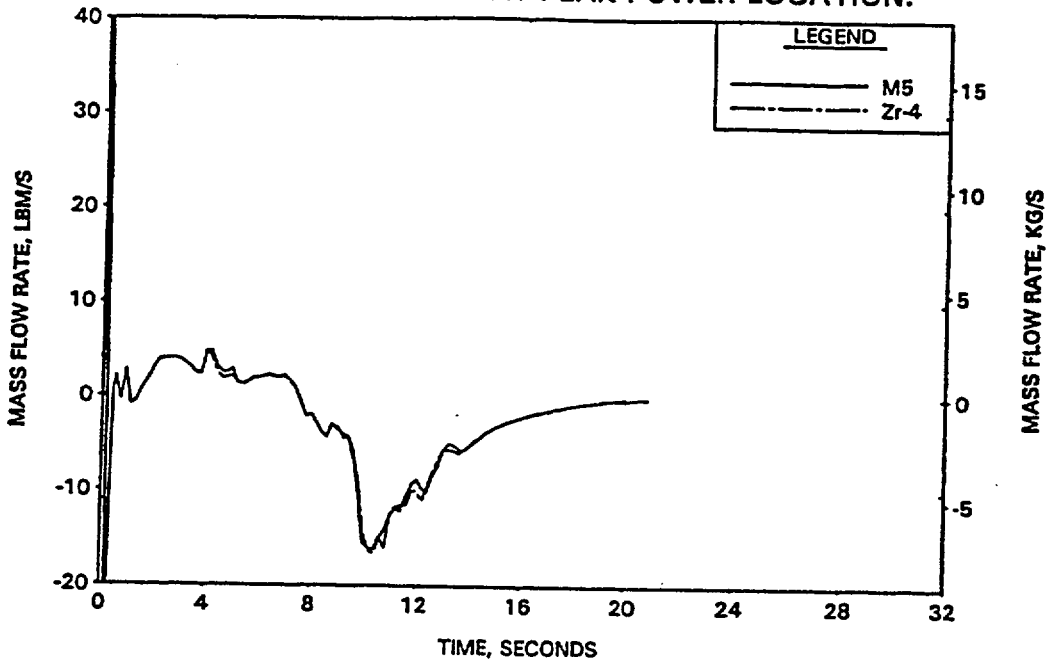

FIGURE F-12. Mk-B FA, M5 vs Zr-4 CLADDING, BOL - CORE FLOODING RATE.

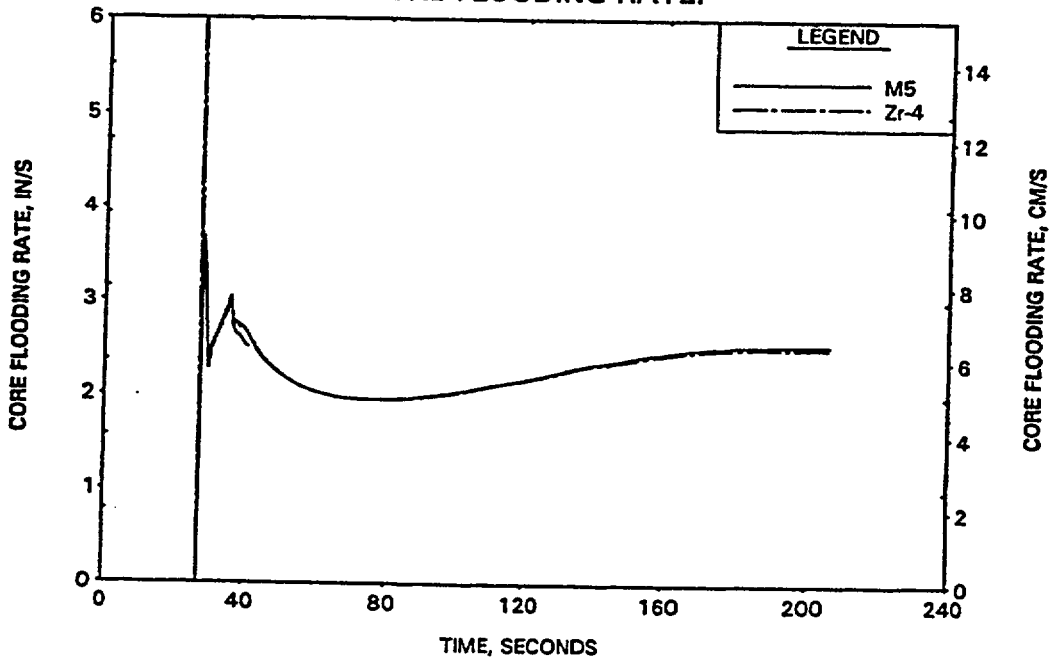

FIGURE F-13. Mk-B FA, M5 vs Zr-4 CLADDING, BOL - HC CLAD TEMP AT RUPTURED LOCATION.

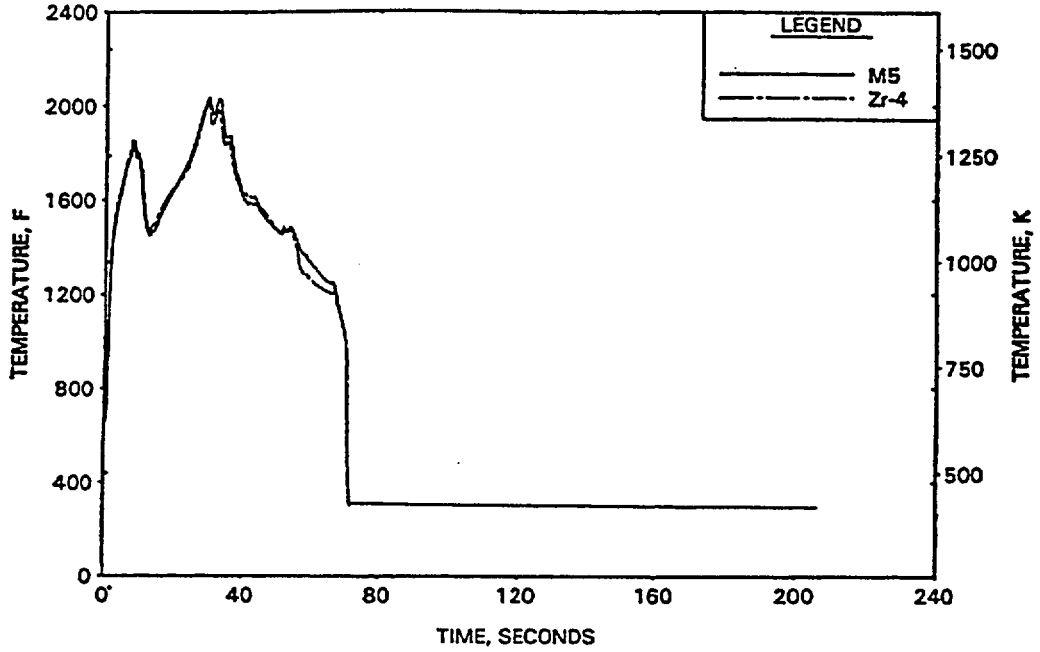

FIGURE F-14. Mk-B FA, M5 vs Zr-4 CLADDING, BOL - HC CLAD TEMP AT PEAK UNRUPTURED LOCATION.

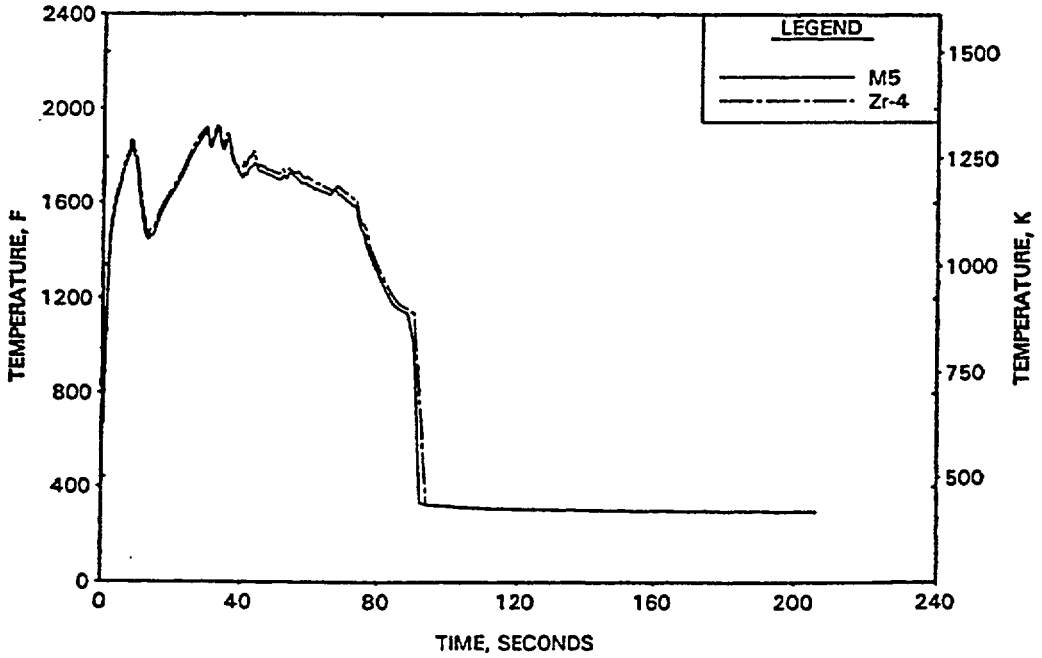

FIGURE F-15. Mk-B FA, M5 vs Zr-4 CLADDING, BOL - QUENCH FRONT ADVANCEMENT.

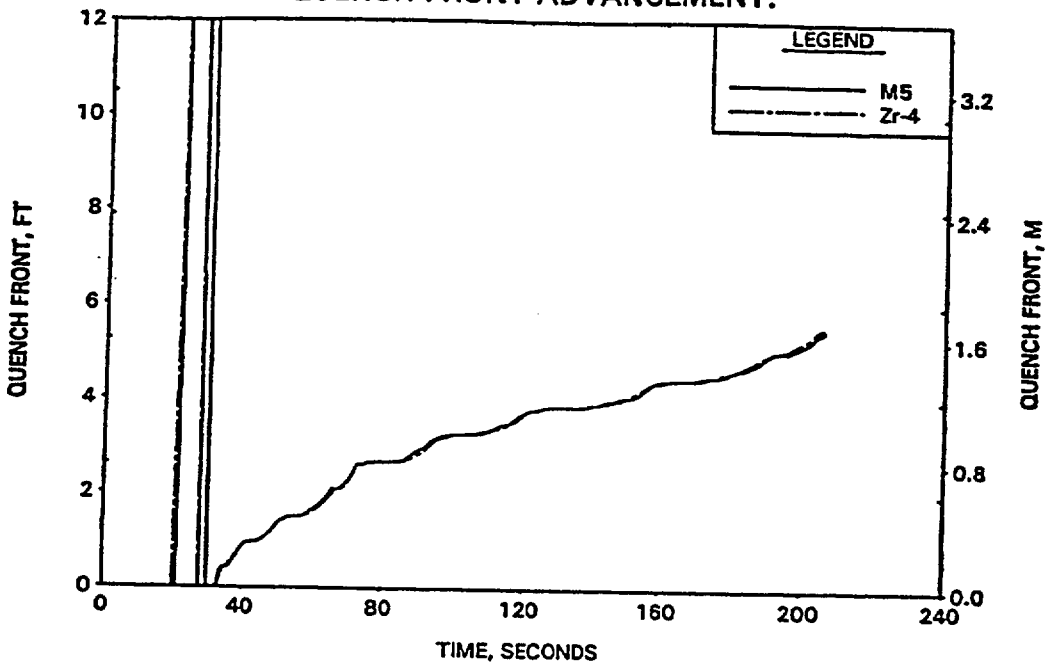

FIGURE F-16. Mk-B FA, M5 vs Zr-4 CLADDING, 40 GWd/MTU - REACTOR VESSEL UPPER PLENUM PRESSURE.

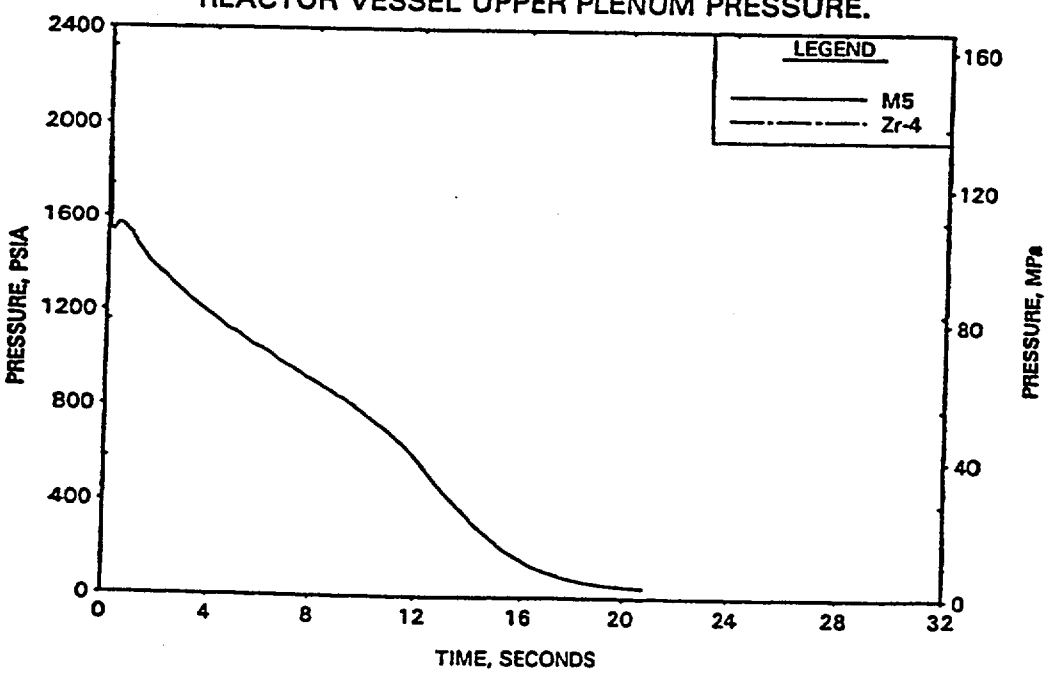

FIGURE F-17. Mk-B FA, M5 vs Zr-4 CLADDING, 40 GWd/MTU - BREAK MASS FLOW RATE.

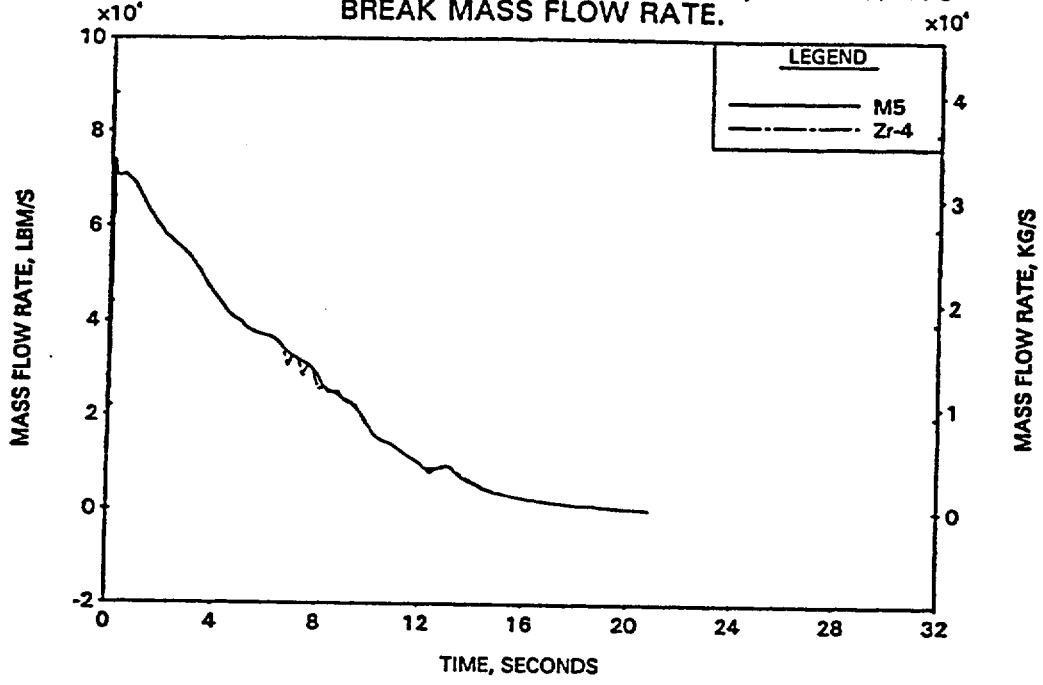

FIGURE F-18. Mk-B FA, M5 vs Zr-4 CLADDING, 40 GWd/MTU - HC MASS FLOW RATE AT PEAK POWER LOCATION.

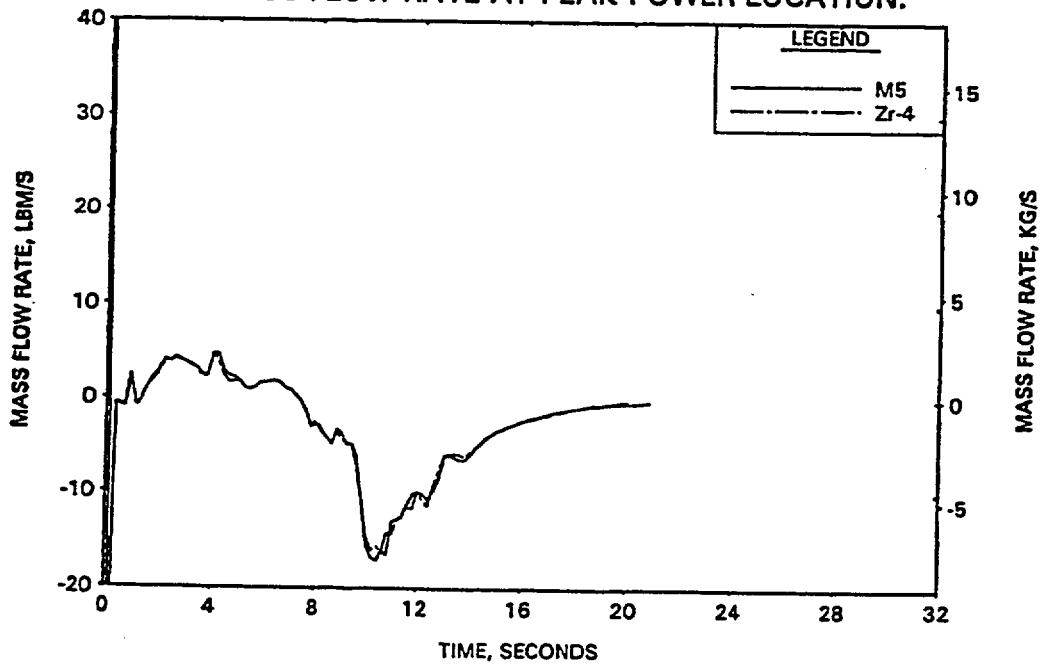

FIGURE F-19. Mk-B FA, M5 vs Zr-4 CLADDING, 40 GWd/MTU - CORE FLOODING RATE.

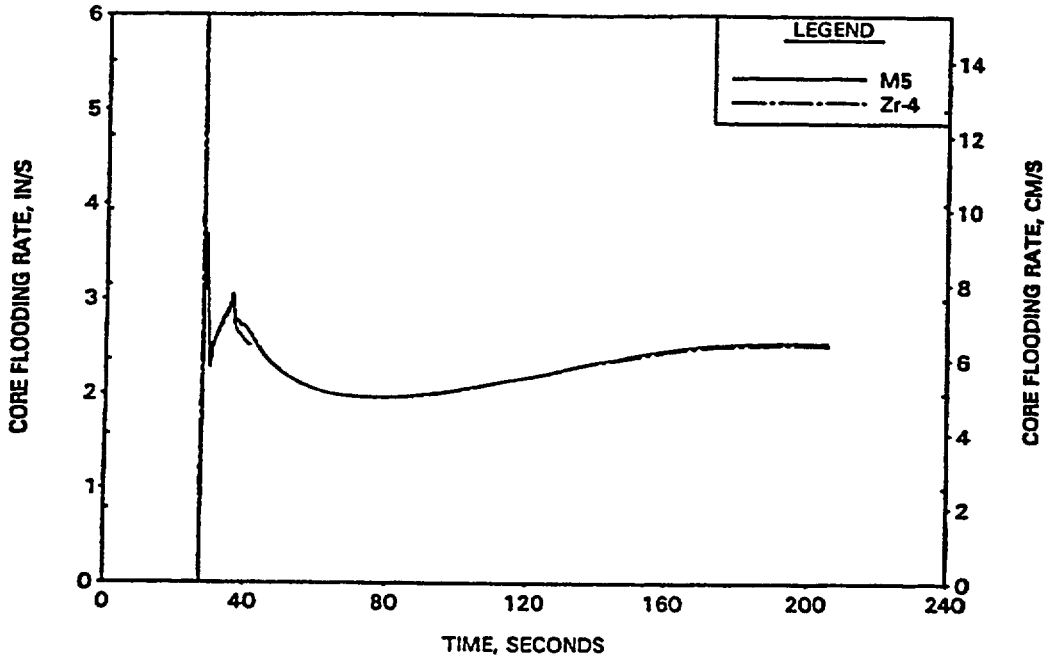

FIGURE F-20. Mk-B FA, M5 vs Zr-4 CLADDING, 40 GWd/MTU - HC CLAD TEMP AT RUPTURED LOCATION.

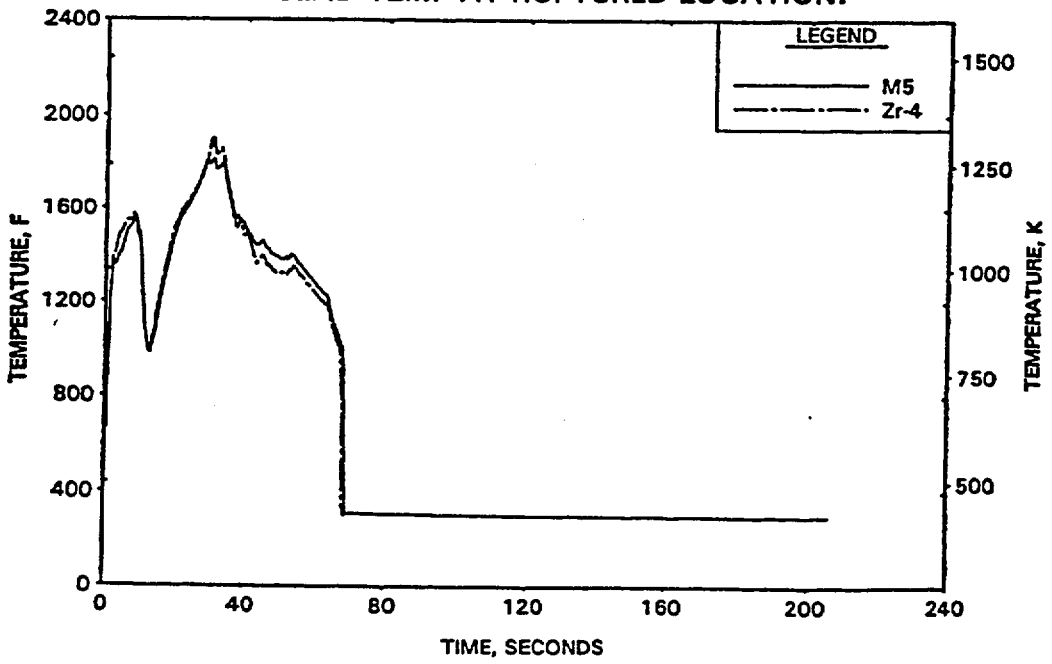

FIGURE F-21. Mk-B FA, M5 vs Zr-4 CLADDING, 40 GWd/MTU - HC CLAD TEMP AT PEAK UNRUPTURED LOCATION.

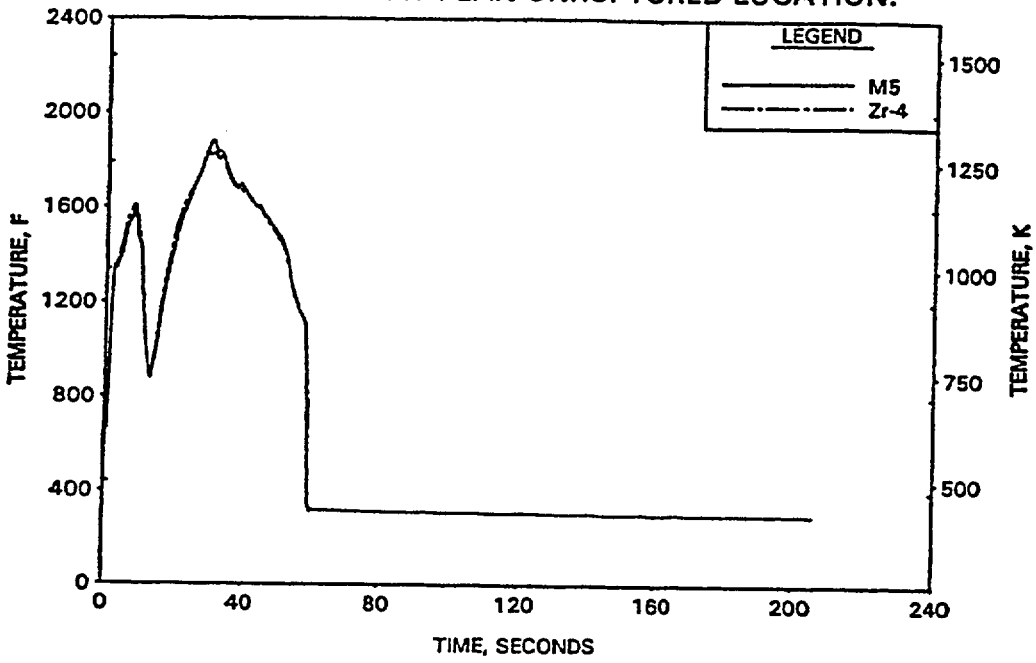

FIGURE F-22. Mk-B FA, M5 vs Zr-4 CLADDING, 40 GWd/MTU - QUENCH FRONT ADVANCEMENT.

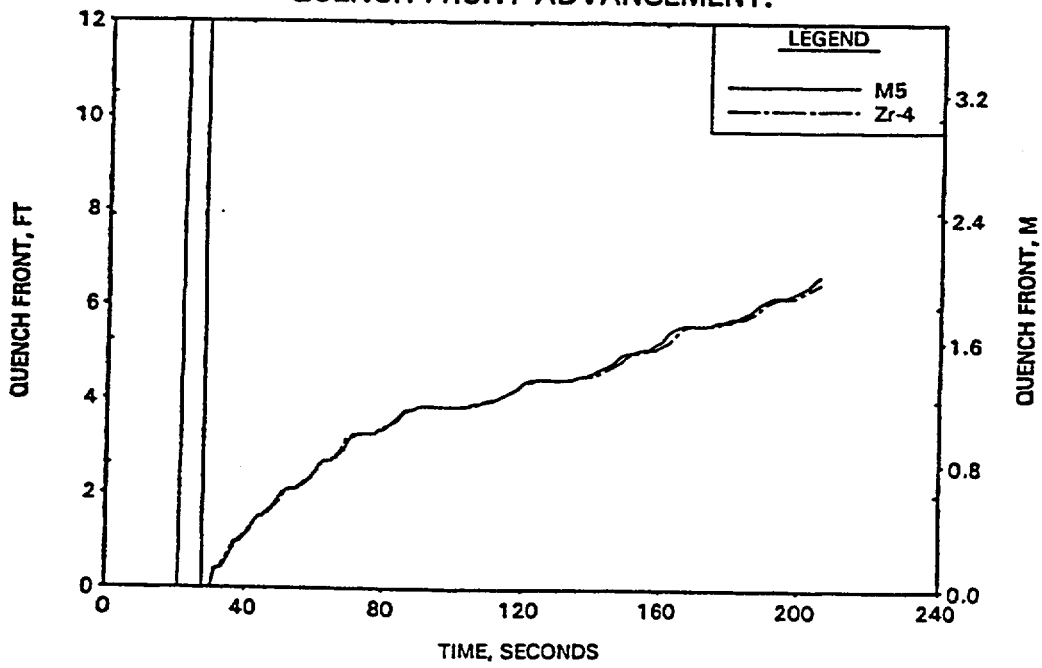

FIGURE F-23. Mk-BW FA, M5 vs Zr-4 CLADDING - REACTOR VESSEL UPPER PLENUM PRESSURE.

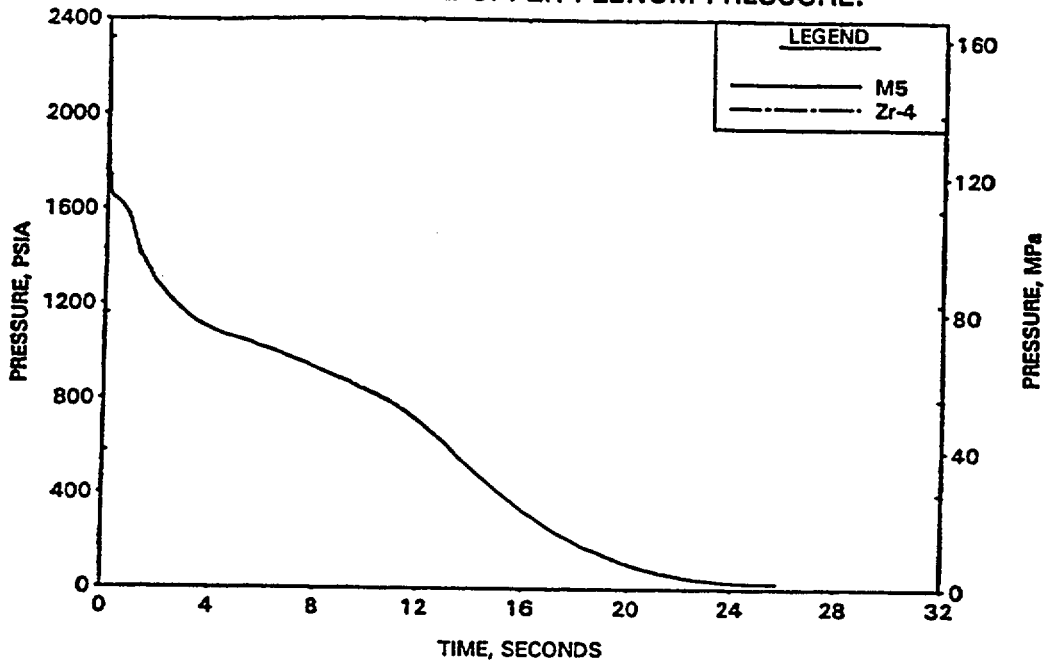

FIGURE F-24. Mk-BW FA, M5 vs Zr-4 CLADDING - BREAK MASS FLOW RATE.

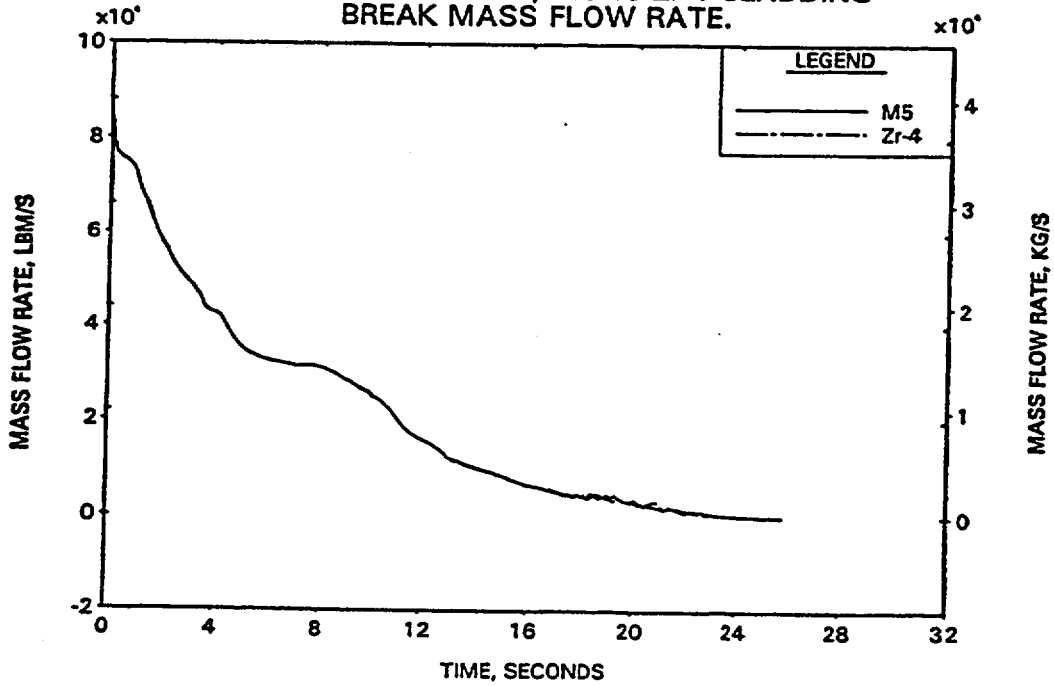

FIGURE F-25. Mk-BW FA, M5 vs Zr-4 CLADDING - HC MASS FLOW RATE AT PEAK POWER LOCATION.

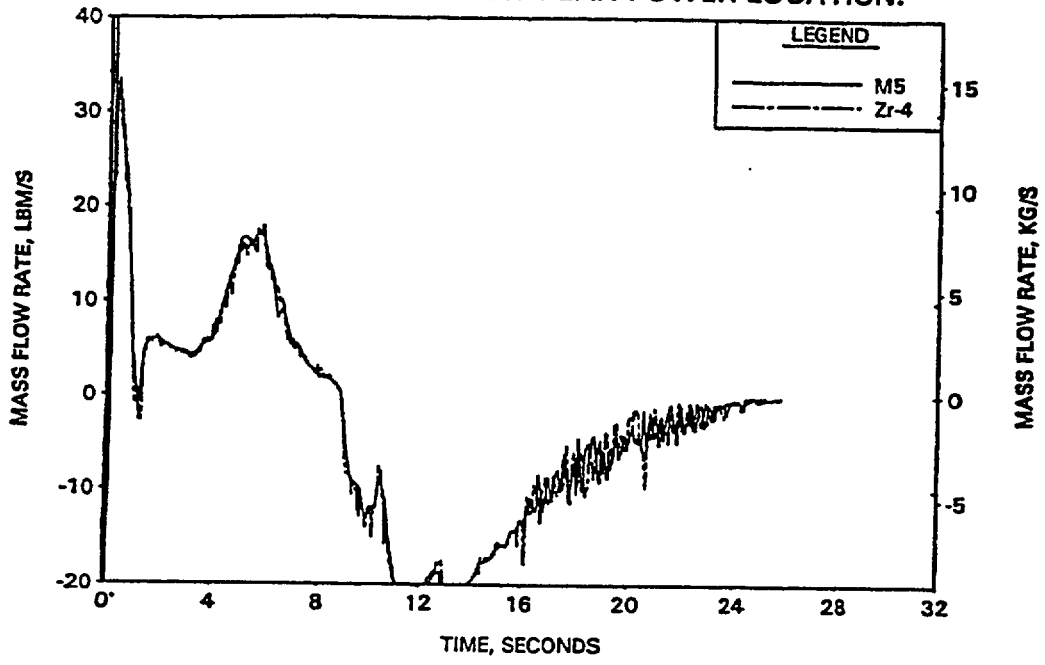

FIGURE F-26. Mk-BW FA, M5 vs Zr-4 CLADDING - CORE FLOODING RATE.

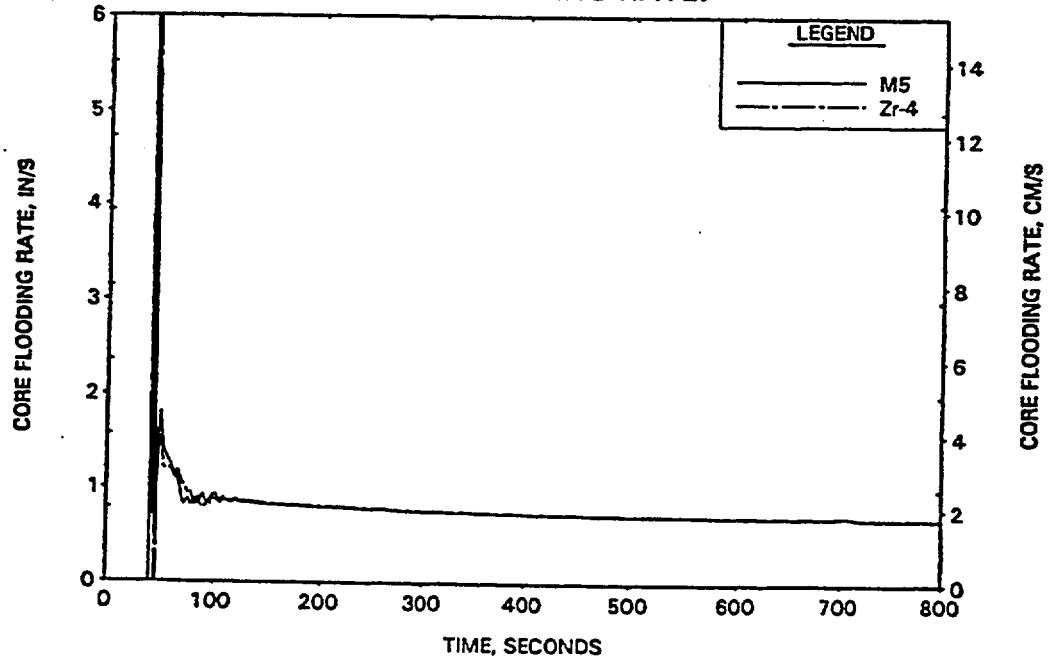

FIGURE F-27. Mk-BW FA, M5 vs Zr-4 CLADDING - HC CLAD TEMP AT RUPTURED LOCATION.

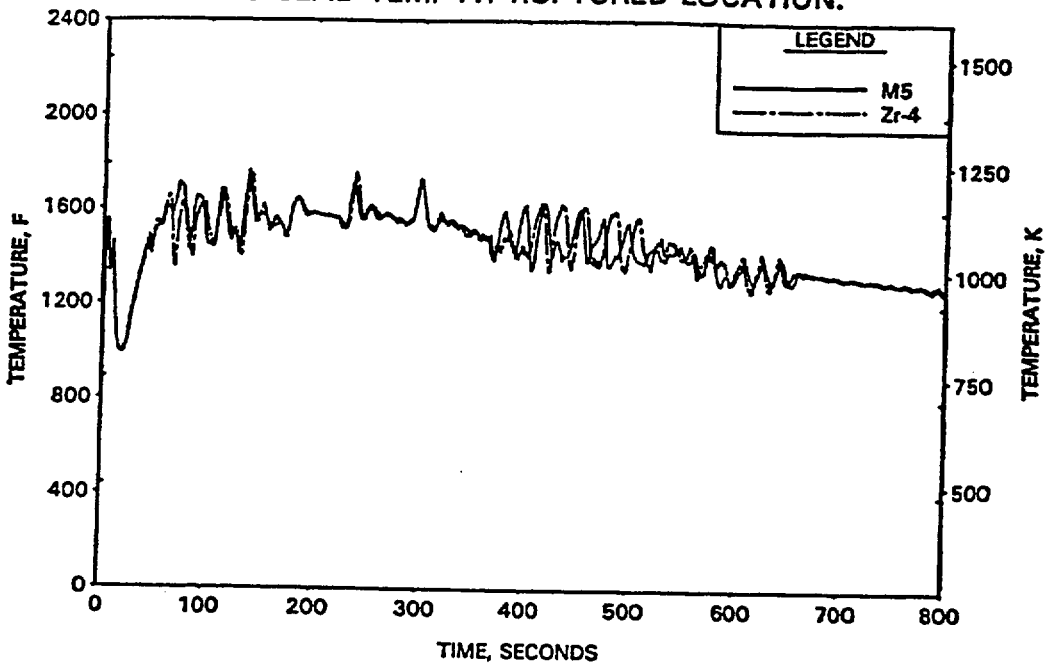

FIGURE F-28. Mk-BW FA, M5 vs Zr-4 CLADDING - HC CLAD TEMP AT PEAK UNRUPTURED LOCATION.

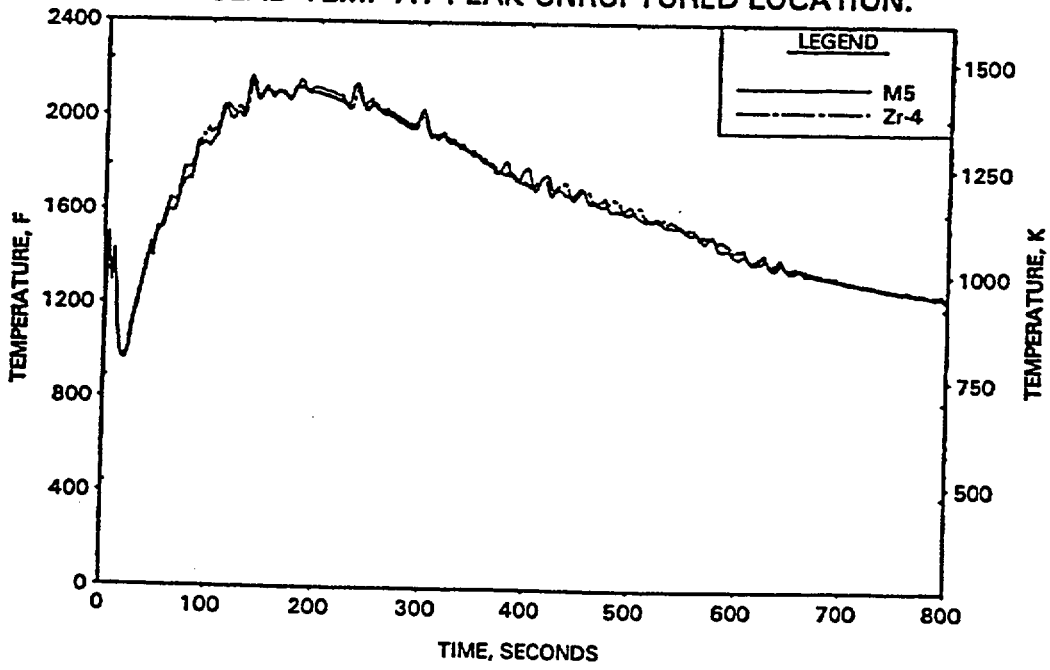

FIGURE F-29. Mk-BW FA, M5 vs Zr-4 CLADDING - QUENCH FRONT ADVANCEMENT.

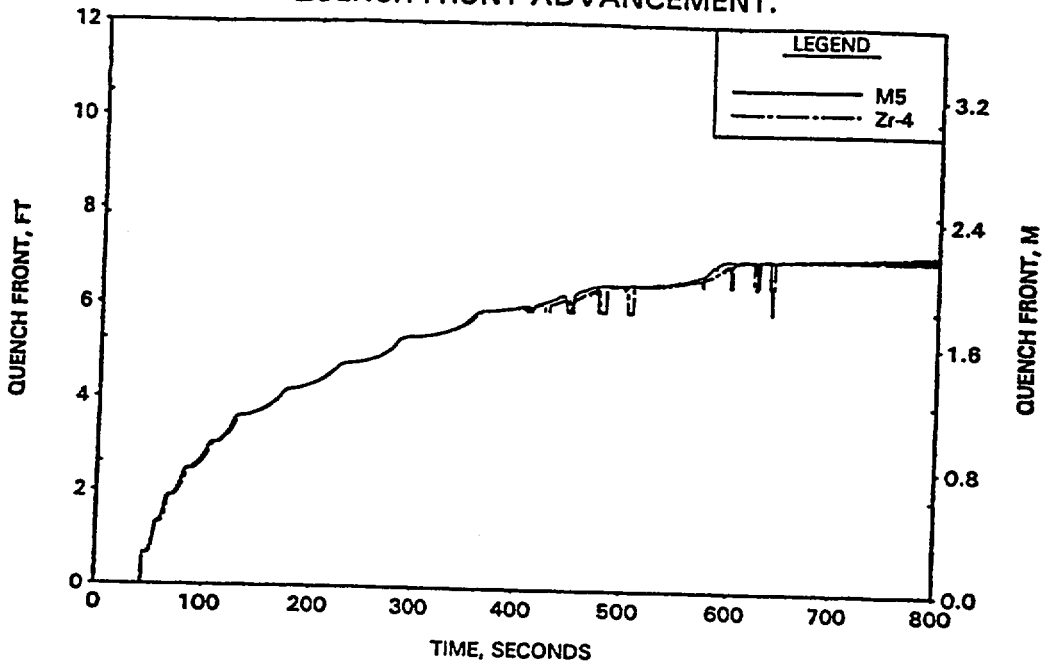

Appendix G

Applicability of 10CFR50.46 Temperature and Local Oxidation Limits

Applicability of 10CFR50.46 Temperature and Local Oxidation Limits

G.1 INTRODUCTION

10CFR50.46 requires that calculations performed with approved evaluation models, References G-1 and G-2, to support ECCS licensing demonstrate that the fuel design and plants systems meet five criteria. Of these criteria two are related to assuring cladding integrity and the remaining three to the plant systems. FTI has reviewed the considerations made in establishing the two criteria related to the fuel cladding and has determined that the criteria apply to fuel assembly designs incorporating the M5 alloy for cladding and that the same assurance of public health and safety is provided. This appendix presents the justification for the use of the existing temperature and local oxidation limits of 10CFR50.46 for M5 cladding. Briefly 10CFR50.46 limits the calculated results such that:

1. The Peak Cladding Temperature is Less than 2200 F -- This limit was established to maintain an acceptable margin against potential embrittlement of the cladding and assure a substantial margin to the true temperature at which the zirconium/water oxidation process becomes autocatalytic. The criterion was promulgated for Zircaloy claddings and must be demonstrated as applicable to the M5 alloy. Section G.3 provides an analysis in support of this criterion.

2. The Maximum Local Oxidation is Less than 17 Percent -- This limit was also imposed on the calculation to prevent the brittle fracture of the fuel pin cladding during the reflood quench. The criterion, established for Zircaloy claddings, must be demonstrated as applicable to the M5 alloy. Section G.2 provides an analysis in support of this criterion.

3. The Maximum Core Wide Oxidation is Less than 1 Percent -- This limit was imposed to prevent the accumulation of a combustible amount of hydrogen within the reactor building. The criterion is imposed to prevent a difficulty with a system removed from the cladding and is, therefore, not related to nor affected by the cladding material. No further analysis of this criterion in required.

4. The Core Geometry Remains Amenable to Cooling -- The implication of this criterion is that the core shall remain in a condition that can be readily cooled by the type of short- and long-term cooling mechanisms provided by the plant ECCS. The goal of the criterion is not directly related to the cladding material and applies equally well to all materials. No further analysis of this criterion is required.

5. Long-Term Core Cooling is Established -- This is a plant system requirement and not related to the cladding material. It is as valid for any cladding that could be used in a pressurized water reactor. No further analysis of this criterion is required.

G.2 APPLICABILITY OF 17 PERCENT OXIDATION LIMIT

The 17 percent local oxidation limit was established by the NRC to preclude the possibility that the cladding material would shatter due to thermal stresses imposed during core quench. To establish that this criterion remains applicable to the M5 alloy, a series of cold water plunge quench tests of high temperature, highly oxidized cladding were performed. These tests indicated that the limit for oxygen embrittlement of the M5 alloy lies [c, a] percent. This is the same as the range appropriate for Zircaloy determined in Reference G-3, NUREG/CR-1344 "Embrittlement Criterion for Zircaloy Fuel Cladding Applicable to Accident Situations in Light-Water Reactors."

The testing was performed at the CINOG facility (Grenoble, France) described in Appendix D. For these tests, an adaptation of the sample positioning rack was employed that allows the sample to be plunged into a cold water bath immediately following oxidation. In contrast to the oxidation kinetics testing, the sample size for the embrittlement tests is 10 cm in length. Once positioned within the heater coil the initial tests procedures follow those of the oxidation rate tests, steam flow and temperature are established and a rapid 20 C/s heating rate established until a specified temperature is reached. Temperature control is through optical pyrometer feedback to the power supply. Once the predetermined oxidation time is reached, the power supply is cut and the sample positioning rack rapidly moved downward to plunge the sample into a cold water bath. The time delay to immersion is less than 1 second. Following cooling, the sample is removed from the rack and visually examined for failure. If it is not obvious from the visual examination, the sample is pressurized to approximately 300 mbar and placed under water to look for air leaks. If leaks are present, the sample is listed as failed. Following the determination of failure or non-failure the sample is sectioned and metallographically examined to determine the amount of oxidation that it experienced.

Testing has been performed for Zircaloy-4 and for the M5 alloy at three oxidation temperatures, 1100, 1200, and 1300 C. At each temperature, five samples have been tested for progressively longer times. The oxidation times were selected to produce three unfailed tests and two failed tests for each temperature. The following tables provide the testing matrix for Zircaloy and M5.

Zircaloy-4 Alloy Brittle Fracture Test Matrix

Test Identification	Oxidation Temperature C	Time @ OT s	Result
	c, d		

M5 Alloy Brittle Fracture Test Matrix

Test Identification	Oxidation Temperature C	Time @ OT s	Result
	c, d		

The amount of oxidation that would produce cladding failure upon quench from high temperature was determined by metallographic examination of the most oxidized sample that did not fail. The following tables provide the results of those examinations for Zircaloy and for M5. Within the tables the nomenclature is:

τ ZrO_2 ext => The thickness of the outside surface layer of fully oxidized material, zirconia,

τ α Zr(O) ext => The thickness of the outside surface layer of partially oxidized material including dissolved oxygen and ZrO molecules, the alpha layer,

τ β Zr => The interior unperturbed layer of Zirconium alloy, the beta layer,

τ α Zr(O) int => The thickness of the inside surface layer of partially oxidized material including dissolved oxygen and ZrO molecules, the alpha layer, and

τ ZrO_2 int => The thickness of the inside surface layer of fully oxidized material, zirconia.

Examinations were made at 30 degree increments but only the azimuthal average of the oxide layers is presented.

Metallographic Examination Results for Zircaloy-4 Samples

Temperature of Oxidation F	Sample Identification	τ ZrO2 ext μm	τ α Zr(O) ext μm	τ β Zr μm	τ α Zr(O) int μm	τ ZrO2 int μm
		c,d				

Metallographic Examination Results for M5 Samples

Temperature of Oxidation F	Sample Identification	τ ZrO2 ext μm	τ α Zr(O) ext μm	τ β Zr μm	τ α Zr(O) int μm	τ ZrO2 int μm
		c,d				

*[c, d]

In determining the implied limit on oxidation, only the zirconia (ZrO2) regions were credited. This assumption produces some conservatism because the embrittling influence of the oxygen contained the alpha regions are not included. The calculation proceeded by determining the fraction of the original sample material that remained in the alpha and beta regions. The complement of this fraction is the amount of material that was converted to zirconia during the oxidation and, because the determination is for an unfailed sample, a suitable measure for the limit at which oxidation will produce brittle fracture of the cladding. The results for Zircaloy-4 and M5 are:

Measured Oxidation for Most Oxidized Unfailed Sample for Zircaloy-4

Temperature of Oxidation F	Sample Identification	$\tau_{unoxidized}$ μm	$F_{unodixized}$ %	$F_{oxidized}$ %
	c, d			

Measured Oxidation for Most Oxidized Unfailed Sample for M5

Temperature of Oxidation F	Sample Identification	$\tau_{unoxidized}$ μm	$F_{unodixized}$ %	$F_{oxidized}$ %
	c, d			

As can be observed, both materials are subject to brittle fracture for average local oxidations Σ c, d 7. Both materials behave in essentially the same manner and both are conservatively bounded by the 17 percent limit of local oxidation specified by 10CFR50.46.

G.3 APPLICABILITY OF 2200 F MAXIMUM TEMPERATURE LIMIT

The selection of a cladding temperature limit in the lower 2000 F range dates back to the Interim Acceptance Criteria (IAC) of June 1971, Reference G-4. In the IAC, the AEC published, "The calculated maximum fuel element cladding temperature does not exceed 2300 F. This limit has been chosen on the basis of available data on embrittlement and possible subsequent shattering of the cladding." In 1974 the AEC promulgated the Final Acceptance Criteria (FAC) and selected a peak cladding temperature limit of 2200 F. Again the AEC basis was concern about embrittlement as evidenced by the Babcock and Wilcox rebuttal of the AEC staff's ECCS Rule Making Hearing Concluding Statement, Reference G-5.

In the middle 1980's, the staff reviewed the criteria and reaffirmed that the 2200 F peak cladding temperature limit in conjunction with the 17 % limit on local oxidation was sufficient to protect the cladding from embrittlement that would cause shattering upon core quench. In this finding, the NRC staff also noted that the 2200 F limit provided margin against the occurrence of autocatalytic metal-water reaction (self maintained cladding burning in water) that had been demonstrated in the power burst facility at cladding temperatures of around 2700 F.

The basic strength of the M5 alloy at elevated temperatures is in approximate agreement with that of Zircaloy. From the phase diagrams, Reference G-6, for Zirconium/Tin alloys and Zirconium/Niobium alloys, the melting temperature of 1 to 1.5 percent tin and 1 percent niobium mixes are essentially the same at 3300 F. However, the solidus line for 1 to 1.5 percent tin (Zircaloy-4) is approximately 200 F below the melting temperature where as the solidus line for a 1 percent Niobium mix (M5) is essentially the same as the melting temperature. Thus, for high temperatures the material can be expected to maintain its strength somewhat better than Zircaloy.

The temperature at which the metal-water reaction for M5 would become autocatalytic has not been established. However, the high temperature oxidation kinetics testing, Appendix D, has demonstrated that between approximately 2000 F and 2400 F the true reaction rate of Zircaloy and M5 are essentially equal. C

C, d

the temperature at which the material enters into an autocatalytic reaction can be safely placed at or near that of Zircaloy and thus substantially above the 2200 F criterion.

That the M5 alloy does not experience embrittlement at temperatures below 1300 C (2372 F) has been demonstrated in the embrittlement testing discussed in section G.2. In these tests, the cladding was held at a constant temperature in excess of 2200 F for a sufficient time to build up an oxide layer in excess of the 17 percent limit and was then rapidly quenched. Had the material been prone to a temperature related embrittlement at temperatures at or below the 2200 F criterion, fracture would have been observed in the testing. Therefore, any concern over cladding embrittlement by exposure to high temperatures is removed by the testing provided.

The M5 cladding has been shown to: 1. Have approximately the same high temperature strength as does Zircaloy, 2. Not undergo an autocatalytic oxidation reaction prior to temperatures far above 2200 F, and 3. Not be embrittled by exposure to temperatures equal to or below at least 2400 F provided the local oxidation has been held to less than [c,d]. Therefore, the limit on peak cladding temperature of 2200 F is appropriate for the M5 cladding material and there is no need to revise the criteria of 10CFR50.46 to allow the use of this material as the cladding for nuclear fuel assemblies.

G.4 CONCLUSIONS

Applicable testing has been conducted on the M5 alloy to demonstrate that the performance criteria of 10CFR50.46 as presently promulgated offer sufficient protection of the public health and safety. In particular the performance relative to the basis for these criteria of the M5 alloy has been demonstrated as essentially equal to that of Zircaloy-4 and the applicability of the criteria have been affirmed for both materials. Therefore, the criteria for acceptance of ECCS calculations as written in 10CFR50.46 remain valid for application to M5 alloy cladding.

G.5 REFERENCES

G-1. BAW-10168-A Rev. 3, RSG LOCA, BWNT Loss-of-Coolant Accident Evaluation Model for Recirculating Steam Generator Plants, B&W Nuclear Technologies, Lynchburg, Virginia, 1996.

G-2. BAW-10192-P, BWNT LOCA, BWNT Loss-of-Coolant Accident Evaluation Model for Once-Through Steam Generator Plants, B&W Nuclear Technologies, Lynchburg, Virginia, 1994.

G-3. H. M. Chung and T. F. Kassner, NUREG/CR-1344, Embrittlement Criteria for Zircaloy Fuel Cladding Applicable to Accident Situations in Light-Water Reactors: Summary Report, U. S. Nuclear Regulatory Commission, Washington DC, January 1980.

G-4. F. N. Browder, "The ECCS Rule-Making Hearing," Nuclear Safety, Volume 15 Number 1, January-February, 1974.

G-5. N. D. Naiden, G. L. Edgar, and G. F. Doyle; "Response to Concluding Statement of the Regulatory Staff on Behalf of Babcock & Wilcox;" Docket Number RM-50-1; Morgan, Lewis, and Bockus; Washington DC; May 1973.

G-6. M. Hansen, "Constitution of Binary Alloys", Metallurgy and Metallurgical Engineering Series 2nd Edition, McGraw Hill, 1958.

Appendix H

Use of Stainless Steel Rods in Fuel Assemblies Fabricated with M5

FCF demonstrated in BAW-2149-A (Ref H-1) that FCF fuel assemblies will meet all safety criteria with up to 10 stainless steel replacement rods. The use of M5 instead of zircaloy-4 in the fuel rod cladding, end plugs, guide thimbles, guide tubes, instrument tubes and intermediate spacer grids does not change the conclusions of that report. M5 has been shown to be compatible when welded to both M5 and zircaloy-4 end plugs, and in contact with stainless steel, zircaloy-4 and inconel 718. The structural strength, available growth space and corrosion of M5 have been evaluated for compatibility.

The mass of the stainless steel replacement rods is less than the original UO_2 rods. Therefore, the fuel assembly structure has more than sufficient strength for the replacement rods. The length of the replacement rods will be sized to fit within the fuel assembly structure over the entire range of burnup. Although the growth of M5 assemblies will be less than that of the current designs, the replacement rods will fit within the available envelope. The replacement rods will be sized to account for the growth of the M5 assembly and the differential thermal expansion of the stainless steel replacement rods. Based on this, M5 structures will have sufficient strength and growth space to accommodate the use of replacement rods.

No measurable localized corrosion has been found on FCF fuel designs. In these fuel designs, contact between M5 and dissimilar metals occurs near the top and bottom of the active core where heat and neutron fluxes are low. With the use of replacement rods the concern would be the M5 material in the spacer grids which will be in contact with the replacement rods, No localized corrosion of the M5 material is expected as the heat generation in the stainless steel replacement rods is low compared to the fuel rods. In addition, these replacement rods are inserted after at least one cycle of fuel assembly operation when the M5 spacer grids will have a protective oxide layer. Based on this, the corrosion performance of the M5 spacer grids with the stainless steel replacement rods is acceptable.

[

b,c,d

]

In conclusion the results of BAW-2149-A remain valid for fuel assemblies fabricated with M5 in place of Zircaloy-4 for components such as fuel rod cladding, end caps, guide tubes, guide thimbles, and spacer grids.

REFERENCES

H-1. BAW-2149-A, Evaluation of Replacement Rods in BWFC Assemblies, Sept 1993.

I-1. Question 1: 1. The hydrogen pickup fraction used for M5 cladding (Sections 3.1 and A.4.2) appears to be low compared to the hydrogen pickup data above rod burnups of 10 GWd/MTU in Figures 3-3 and A-7. Please explain why this is acceptable. Have micrographs been taken of the hydrides in irradiated M5 cladding? What is their shape and orientation? [c,d]

Response to question 1: The hydrogen pick-up is measured by [

[b]

]

The [d] hydrogen pickup fraction was obtained at the beginning of the M5 research program. The experience gained up to now shows a hydrogen pickup fraction in the range of [d] to [d] with a mean value of about [d]. For future calculations FCF will use a pickup fraction of [d].

The attached photomicrograph in Figure I-1.1 was taken from a fuel rod with M5 cladding that was irradiated for 4 cycles in the CRUAS2 reactor. The photomicrograph is from a cladding sample with the maximum oxide thickness taken from the sixth span from the bottom of the assembly. The absorbed hydrogen, in solid solution, is in the familiar form of hydride platelets. These platelets are seen to be primarily circumferentially oriented with a distribution, density and morphology consistent with the low oxidation and low oxygen pickup fraction associated with the alloy M5 base metal.

Figure 1
Photomicrograph of 4 Cycle CRUAS 2 Fuel Rod Cladding

Outside
Diameter

Photomicrograph is proprietary
[d]

Inside
Diameter

I.2 Question 2: Please provide the yield strength (YS) and ultimate tensile strength (UTS) data along with uniform and total elongation data for irradiated and unirradiated M5 cladding. Please provide information on how the irradiated and unirradiated biaxial and axial-tensile specimens were tested (including strain rate) along with specimen sizes and shapes. Please show how the lower bound yield strength in the hoop direction was determined (Table 3-3) based on this data. Please explain why there is a difference in the stress intensity limits under compressive and tensile conditions. Please provide the temperature range that the strength models will be applied.

Table I-2.1 provides the data for yield strength, UTS and uniform elongation from various unirradiated tests of M5 cladding. Table I-2.2 provides similar data from tests of both irradiated and unirradiated cladding used in Figure 3-3.

The description of the biaxial tensile and axial tensile tests performed on M5 specimens is as follows:

Biaxial test

In the biaxial test, a tubing section is pressure loaded until it bursts. A [d] long specimen is used with cold-crimped Swagelok fittings used at both ends. The specimen is pressurized with a high temperature oil and is tested inside a resistance furnace that can heat the specimen up to 400 °C.

For irradiated specimens the zirconia (ZrO2) layer is removed at both ends by abrasive grit blasting before the Swagelok fittings are attached.

The pressurization rate is set at [d]

Axial tensile test

A [d] section of tubing is used for the test. The tubing section is machined into a standardized specimen by electrical discharge machining so that it features a reduced section in the middle and a hole near each end for a lock pin fastening. A core is inserted at each end where the lock pin fastens the specimen to the tensile test machine to

distribute the load. Figure I-2.1 shows a diagram of a test specimen. The tensile tests are then performed inside a resistance furnace that can heat the specimen up to 1,000 °C.

For irradiated specimens the Zirconia (ZrO2) layer is removed by abrasive grit blasting before machining.

The strain rate is set at a δl/l of [d]

The lower bound hoop data was determined by adjusting a relationship previously developed for Zircaloy-4 to bound all of the available M5 test data. The form of the model chosen results in a reasonable representation of yield strength up to 600 °C. It was then adjusted to match the lower range of data at all temperatures at which M5 data was available up to 400 °C. The model is plotted in Figure A-4 .

The difference in stress intensity limits for compressive and tensile modes is due to the failure mode in compression being buckling. The stress intensity limit in the compressive mode is slightly more conservative than the stress limit based on buckling. The higher stress intensity limit is required for practical design of fuel rods with RXA cladding and testing has demonstrated the applicability of higher stress limits in compression. This approach has been used in licensing M5 cladding in lead test assemblies and the design of fuel elements with compressive stress levels close to yield stress has been used previously in batch operation in US PWRs (Ref H-1).

The cladding strength correlation shown in Table 3-3 is applicable from 25 to 400 °C.

References:

H-1. WAPD-TM-1404, Ex-Reactor Deformation of Externally Pressurized Short Lengths of Fuel Rod Cladding, I.A. Selsley, May 1979.

Figure I-2.1
Axial Tensile Test Specimen.

Figure is proprietary

[b]

Table I-2.1 M5 Strength Data				
	Test	Yield		Total
	Temp	Strength	UTS	Elongation
Test	deg C	MPA	MPA	%
		[c,d]		

Table I-2.2
Irradiated and Unirradiated Mechanical Properties

Test Type	Test Temp C	FR Burnup GWd/mtU	FR Fast Fluence n/cm2	YS MPA	UTS MPA	Uniform Elongation %	Total Elongation %
			[c,d]				

I.3 Question 3: Please provide the plant coolant outlet temperatures of the M5 cladding oxidation data in Figure 3-1 and identify the data by plant and burnup. Also, please provide a plot of measured-minus-predicted corrosion as a function of burnup, oxide thickness, maximum oxide-metal-interface temperature (also end-of-life oxide-metal-interface temperature), and coolant outlet temperature (if data are at more than one outlet temperature). Please provide the oxide-metal-interface temperature range that the M5 corrosion model will be applied. Also explain how the M5 maximum oxide thickness is determined from measured data.

Response to question 3: Table I-3.1 lists the various parameters requested for the M5 data gathered to date; Plant, assembly coolant outlet temperature, rod average burnup, and maximum measured oxide thickness. The following requested plots are provided using this data:

Figure I-3.1, M-P Oxide Thickness vs. Burnup.

Figure I-3.2, M-P Oxide Thickness vs. Measured Oxide Thickness.

Figure I-3.3, M-P Oxide Thickness vs. Max Oxide-Metal Interface Temperature.

Figure I-3.4, M-P Oxide Thickness vs. EOL Oxide-Metal Interface Temperature.

Figure I-3.5, M-P Oxide Thickness vs. Assembly Coolant Outlet Temperature.

The trends in these figures show that the M5 corrosion model is conservative for high burnups and the most limiting conditions (high temperatures).

In Figures I-3.1 to I-3.5, the oxide predictions were obtained with COROS02.

In Figures I-3.3 & I-3.4, the interface temperatures are taken from the COROS02 predictions.

The range of oxide-metal interface temperature for which the models will be used is 260 - 400 °C.

The method by which the oxide thickness data is taken is follows:

Most of the data reported is poolside data. The poolside data were determined using either a line scan with an eddy current (EC) probe, or with an insertion EC probe (SABER). The data are defined as the maximum azimuthal average oxide thickness. So the data points represent the average around the circumference, and for each rod, the maximum value of the circumference average along the length of the rod is used.

Figure I-3.1

M-P Oxide Thickness vs Rod Burnup

Figure is proprietary

[c,d]

Figure I-3.2

M-P vs Measured Oxide Thickness

Figure is proprietary

[c,d]

Figure I-3.3

M-P Oxide Thickness vs Max Oxide-Metal Interface Temperature

Figure is proprietary

[c,d]

Figure I-3.4

M-P Oxide Thickness vs EOL Oxide-Metal Interface Temperature

Figure is proprietary

[c,d]

Figure I-3.5

M-P Oxide Thickness vs Assembly Exit Temperature

Figure is proprietary

[c,d]

Table I-3.1
M5 Cladding Oxide Data

Plant	MAX T OUT C	BU MWd/mtU	Max Measured Oxide um	Plant	MAX T OUT C	BU MWd/mtU	Max Measured Oxide um	Plant	MAX T OUT C	BU MWd/mtU	Max Measured Oxide um
[b,c,d]				[b,c,d]				[b,c,d]			

Table I-3.1
M5 Cladding Oxide Data

Plant	MAX T OUT C	BU MWd/mtU	Max Measured Oxide um
[b,c,d]			

Plant	MAX T OUT C	BU MWd/mtU	Max Measured Oxide um
[b,c,d]			

Plant	MAX T OUT C	BU MWd/mtU	Max Measured Oxide um
[b,c,d]			

Table I-3.1

M5 Cladding Oxide Data

Plant	MAX T OUT C	BU MWd/mtU	Max Measured Oxide um	Plant	MAX T OUT C	BU MWd/mtU	Max Measured Oxide um	Plant	MAX T OUT C	BU MWd/mtU	Max Measured Oxide um
		[b,c,d]				[b,c,d]				[b,c,d]	

Table I-3.1

M5 Cladding Oxide Data

Plant	MAX T OUT C	BU MWd/mtU	Max Measured Oxide um	Plant	MAX T OUT C	BU MWd/mtU	Max Measured Oxide um	Plant	MAX T OUT C	BU MWd/mtU	Max Measured Oxide um
	[b,c,d]					[b,c,d]				[b,c,d]	

I.4 Question 4: There is a particular concern with the M5 predictions in Figure 3-4 because they do not exhibit any indication of accelerated corrosion while experience has shown that all zirconium based alloys examined to date show accelerated corrosion given high enough cladding temperatures and/or burnups. Please provide the assumed oxide-metal-interface temperature at beginning-of-life (BOL) and the interface temperature at maximum burnup for these predictions and relate them to an assumed coolant temperature. Also, please provide CORROSO2 code predictions of M5 cladding corrosion with a 10°C higher oxide-metal-interface temperature than assumed for Figure 3-4 and extend the predictions to 70 GWd/MTU.

Response to question 4: Table I-4.1 lists the various parameters for node 14 (max oxide thickness at 112.5 inches elevation up the fuel stack) taken from the COROS02 code output using corrosion constants for M5. These include the oxide – metal interface temperature. Table I-4.2 lists the same parameters along with additional parameters for a corrosion calculation with the oxide-metal interface temperature increased by 10 °C. The oxide as a function of burnup from both tables is plotted on Figure I-4.1. Due to the thermal feedback from the increased oxide thickness corrosion experienced in the second case, the temperature increase toward end of life was greater than 10 °C.

The manufacturing process for M5 cladding has been optimized to produce a fully recrystallized and thermodynamically stable microstructure. M5 cladding is manufactured using a [

e

]. This highly refined M5 microstructure ensures optimum corrosion, hydrogen absorption, creep and growth performance in the PWR environment.

Figure I-4.1

Max Oxide Thickness vs Rod Burnup

Figure is proprietary

[d]

Table I-4.1

M5 Oxide Prediction from Figure 3-4

Time hours	Rod Average Burnup MWd/mtU	Rod Average Power kW/m	Nodal Power kW/m	Nodal Coolant Temp deg C	Metal -Oxide Interface Temp deg C	Nodal Oxide Thickness um
			[c,d]			

Table I-4.2

M5 Oxide Prediction with + 10 deg C higher oxide-metal interface temperature to 70 GWd/mtU

Time	Rod Average Burnup	Rod Average Power	Nodal Power	Nodal Coolant Temp	Nodal flux	Rod Surface Temp	Metal -Oxide Interface Temp	Nodal Oxide Thickness
hours	MWd/mtU	kW/m	kW/m	deg C	w/cm2	deg C	deg C	um

[c,d]

I.6 Question 6: What is the strength difference between the new M5 guide thimbles and guide tubes and the strength of previous Zircaloy-4 guide thimbles and guide tubes at beginning-of-life (BOL); and, if significant, how does this impact the seismic-LOCA analyses?

Response to question 6: A comparison of the strength of Zirc-4 and M5 guide thimbles, and an example of the LOCA performance of M5 guide thimbles is taken from the analyses performed for the Mark-BW X1 Lead Assemblies (LAs) in North Anna 1. The comparison of Zirc-4 and M5 guide thimbles is summarized in Table I-6.1. The strength difference is not significant.

The results of the structural integrity analysis of the X1 LAs is presented in Table I-6.2, Cold Leg Break Guide Thimble Span Maximum Axial Loads. These margins are not significantly different than would be the case for RXA Zircaloy-4 guide thimbles.

Table I-6.1
Mechanical Properties of M5 and Zircaloy-4 Tubes

	20°C			**385°C**		
Tube Material Alloy	**0.2% Y.S.**	**U.T.S.**	**% Elong**	**0.2% Y.S.**	**U.T.S.**	**% Elong**
M5	[c,d]	[c,d]	[c,d]	[c,d]	[c,d]	[c,d]
Specification Criteria (ksi)	[c,d]	[c,d]	[c,d]	[c,d]	[c,d]	[c,d]
(MPA)	[c,d]	[c,d]	[c,d]	[c,d]	[c,d]	[c,d]
Typical values (ksi)	[c,d]	[c,d]	[c,d]	[c,d]	[c,d]	[c,d]
(MPA)	[c,d]	[c,d]	[c,d]	[c,d]	[c,d]	[c,d]
	20°C			**343°C**		
	0.2% Y.S.	**U.T.S.**	**% Elong**	**0.2% Y.S.**	**U.T.S.**	**% Elong**
Zr-4 (recrytallized tube)	[c,d]	[c,d]	[c,d]	[c,d]	[c,d]	[c,d]
Specification Criteria (ksi)	[c,d]	[c,d]	[c,d]	[c,d]	[c,d]	[c,d]
(MPA)	[c,d]	[c,d]	[c,d]	[c,d]	[c,d]	[c,d]
Typical values (ksi)	[c,d]	[c,d]	[c,d]	[c,d]	[c,d]	[c,d]
(MPA)	[c,d]	[c,d]	[c,d]	[c,d]	[c,d]	[c,d]

Table I-6.2
Mark-BW X1 Lead Assembly
Cold Leg Break Guide Thimble Span Maximum Axial Loads.

Description	Maximum Load (Lbs)	Allowable Load (Lbs)	% Margin
Span 2 Span 3 Span 4 Span 5 Span 6 Span 7 Span 8	[c,d]	[c,d]	[c,d]

Notes:
1. The margins for each of the spans evaluated in the analysis are calculated as follows: % margin = 100% x [(Allowable Load – Maximum Load)/Maximum Load]
2. Span numbering starts with span 1 at the top of the assembly going to span 8 at the bottom of the assembly.

I.7 Question 7: Please provide example fuel melting (at limiting low burnups), 1% cladding strain, rod pressure (including the rod pressure limit), and fuel rod shoulder to upper tie plate gap analyses for the new M5 material along with similar analyses with low tin Zircaloy-4. Please provide the code input parameters in order that an audit calculation can be performed.

Response to question 7: A series of analyses were performed on the Mark-BW design in the North Anna-1 Reactor using both M5 and low tin zircaloy-4 cladding. The fuel rod and system inputs used in the TACO3 simulations are shown in Table I-7.1. The radial power distribution (RPD) used is shown in Table I-7.2, and the Axial Power Shapes (APSs) used are shown in Table I-7.3.

The linear heat generation rate (LHGR) at which centerline fuel melt occurs is plotted in Figure I-7.1 and shown in Table I-7.4. Also plotted in Figure I-7.4 and shown in Table I-7.1 is the LHGR where 1% cladding transient strain is reached. The results for the bounding pin pressure for both Zircaloy-4 and M5 cladding are shown in Figure I-7.2 and Table I-7.5. The burnups at which the fuel rod is subjected to transients are also plotted as triangles in Figure I-7.2. The current limiting criterion for the bounding pressure for M5 is assumed to be the same as for zircaloy-4: [c,d] above nominal system pressure. This limit will be updated as more high burnup M5 creep data becomes available. These two figures show that the operating limits for the M5 fuel rod are nearly the same as for a Zircaloy-4 fuel rod.

Since the assembly and rod growth are coupled, in the FCF methods, no rod specific analysis is performed for shoulder gap closure. Shoulder gap closure is based on trends established from post irradiation exam data (see response to question 9, Figure I-9.1). The Mark-BW X1 has a nominal shoulder gap of [c,d]inches. At an assembly burnup of 55 GWd/mtU with a peak pin of 60 GWd/mtU, the worst case (minimum) gap expected is [c,d]

Figure I-7.1

LHGR for CFM vs Burnup

Figure is proprietary

[c,d]

Figure I-7.2

Mark-BWX1 Pin Pressure vs Rod Burnup

Figure is proprietary

[c,d]

Table I-7.1
Rod Analysis Inputs

Parameter	Value	Units
Cladding Length	[c,d}	in.
Cladding OD	[c,d]	in.
Cladding ID	[c,d]	in.
Plenum Volume	[c,d]	in3.
Fuel Stack Length	[c,d]	in.
Pellet Diameter	[c,d]	in.
Pellet Density	[c,d]	%TD
Max In-core densification	[c,d]	%TD
Pellet Goemetry factor		
Enrichment	[c,d]	wt %
Backfill Pressure	[c,d]	psia
System Pressure	[c,d]	psia
Core Average Linear Heat Generation Rate	[c,d]	Kw/ft
Subchannel Flow Rate	[c,d]	lbm/hr
Hydraulic Diameter	[c,d]	in.
Coolant Inlet temperature	[c,d]	deg F
Subchannel Flow Area	[c,d]	in2.

Table I-7.2
Rod Power History

Rod Burnup MWd/mtU	Rod RPD	APS	Rod Burnup MWd/mtU	Rod RPD	APS
[c,d]					

Table I-7.3
Axial Power Shapes Used in TACO3 Simulation

Fuel Stack inches	Axial Power Shapes by Burnup Steps (Burnup as MWd/mtU)
	[c,d]

Fuel Stack inches	Axial Power Shapes by Burnup Steps (Burnup as MWd/mtU)
	[c,d]

Fuel Stack inches	Axial Power Shapes by Burnup Steps (Burnup as MWd/mtU)
	[c,d]

Table I-7.4
LHGR Limits

LHGR for Centerline Fuel Melt

	Fuel		
Rod	Melt	LHGR for CFM	
Burnup	Temp	M5	Zr-4
MWd/mtU	deg F	kW/ft	kW/ft
[c,d]			

LHGR Limits for 1 % Transient Strain

	Transient Strain	
Burnup	M5	Zr-4
MWd/mtU	kW/ft	kW/ft
[c,d]		

Table I-7.5

Rod Internal Pressure and Burnup

	M5 Cladding		Zr-4 Cladding	
	Pin Pressure		Pin Pressure	
	Best		Best	
Burnup	Estimate	Bounding	Estimate	Bounding
MWd/mtU	psia	psia	psia	psia
		[c,d]		

Table I-7.5

Rod Internal Pressure and Burnup

	M5 Cladding		Zr-4 Cladding	
	Pin Pressure		Pin Pressure	
Burnup MWd/mtU	Best Estimate psia	Bounding psia	Best Estimate psia	Bounding psia
[c,d]				

I.8 Question 8: The interpretation of Figure 3-6 is somewhat confusing. Please provide a better explanation/definition of the limiting pressures and minimum collapse delta pressures plotted on this figure. One interpolation of this figure would conclude that cladding collapse will occur above a given cladding temperature on this plot.

Response to Question 8: The information on Figure 3-6 will be separated into two figures to simplify the explanation. In Figure I-8.1 there are three lines plotted as pressure vs cladding temperature. The higher pressure line is the collapse pressure for an M5 tube calculated using Euler's Buckling equation with the following conservatisms.

This top line was calculated for a Mark-BW fuel rod with 0.374 nominal outside diameter and the following design parameters:

Minimum cladding wall, [c,d]
Maximum ovality, [c,d]
Fill pressure [c,d]

The two lower lines are the internal pressure in the fuel rod. One line (FR internal press) is for isothermal conditions with the gas pressure increasing due to temperature and volume changes. The other line (Oper FR press) is the internal pressure at BOL from a TACO3 simulation under various power levels which results in a relationship between cladding temperature and internal pressure. This shows that the fuel rod internal pressure increases with cladding temperature.

Figure I-8.2 is also a plot of pressure vs cladding temperature. The upper line is the sum of the internal fuel rod pressure and the buckling pressure. This is the pressure that the reactor coolant system (RCS) would have to reach to collapse the cladding at BOL. The other two points are the most limiting system pressure conditions[

[c,d]

] It can be observed that for both of these points there is significant margin from the RCS pressure to the collapse line.

Figure I-8.1

Mark-BW X1 Fuel Rod Internal and Buckling Pressure vs Temperature

Figure is proprietary

[c,d]

Figure I-8.2

System Pressure to Collapse vs Cladding Temperature

Figure is proprietary

[c,d]

I.9 Question 9: The upper bound model predictions for M5 shoulder gap closure in Figure 3-8 do not reflect that the statistical uncertainty of the model should be proportionately larger with increasing burnup in the burnup regime where there is little or no data. Please justify this lack of conservatism in the model where there is little or no data. Please identify the plants by legends or tabular form along with coolant outlet temperatures for each of the rod growth data provided in Figures 3-8 and 3-9.

Response to question 9: Shoulder gap closure is a function of both material performance (rod growth) and fuel assembly design. Table I-9.1 provides the data for FCF shoulder gap closure with Zirc-4 rods. Table I-9.2 provides the data for M5 rods in FCF fuel assemblies (fuel rods are seated on the bottom nozzle) Table I-9.3 provides the rod growth data for M5 rods by plant and burnup. The rod growth data for M5 now extends to 61.3 GWd/mtU (11.8E21 n/cm^2, E > 1 MeV) and is shown in Figure I-9.2. The M5 rod growth data shows M5 growth saturating at around 45 GWd/mtU. The shoulder gap closure (updated since BAW-10227P was submitted) for assemblies with seated rods is shown in Figure I-9.1. With added data from four additional assemblies with burnups > 50 GWd/mtU the trend in shoulder gap closure remains very similar and shows that the assumed shoulder gap closure rate is representative of high burnup performance.

This trend of minimal shoulder gap closure is typical of FCF fuel designs. The design features specific to current FCF designs are seating the fuel rods on the bottom nozzle and the use of fixed inconel end grids with floating intermediate zircaloy spacer grids. These design features result in a coupling of the fuel rod and assembly growth, and consequently a slow rate of shoulder gap closure.

Figure I-9.1

Shoulder Gap Closure vs Assembly Burnup

Figure is proprietary

[b,c,d]

Figure I-9.2

M5 Fuel Rod Growth

Figure is proprietary

[b,c,d]

Table I-9.1
FCF Shoulder Gap Data

FA ID	Plant	Outlet Temp deg C	Design	Assembly Burnup GWd/mtU	Shoulder Gap Avg in	Shoulder Gap Max in	Shoulder Gap Min in	Gap Closure Avg in	Gap Closure Min in	Gap Closure Max in

[b,c,d]

Table I-9.2
M5 Shoulder Gap Closure

FA ID	Plant	Outlet Temp deg C	Design	FA Burnup GWd/mtU	Rod ID	Shoulder Gap inches	Closure inches
[b,c,d]							

Table I-9.3
M5 Fuel Rod Growth Data

Plant	Outlet Temp deg C	Fast Neutron Fluence x E21n/cm2 E > 1 MeV	Growth dl/l %	Plant	Outlet Temp deg C	Fast Neutron Fluence x E21n/cm2 E > 1 MeV	Growth dl/l %

[b,c,d]

Table I-9.3
M5 Fuel Rod Growth Data

Plant	Outlet Temp deg C	Fast Neutron Fluence x E21n/cm2 E > 1 MeV	Growth dl/l %	Plant	Outlet Temp deg C	Fast Neutron Fluence x E21n/cm2 E > 1 MeV	Growth dl/l %
[b,c,d]							

Table I-9.3

M5 Fuel Rod Growth Data

Plant	Outlet Temp deg C	Fast Neutron Fluence x E21n/cm2 E > 1 MeV	Growth dl/l %	Plant	Outlet Temp deg C	Fast Neutron Fluence x E21n/cm2 E > 1 MeV	Growth dl/l %

[b,c,d]

Table I-9.3
M5 Fuel Rod Growth Data

		Fast				Fast	
		Neutron				Neutron	
	Outlet	Fluence			Outlet	Fluence	
	Temp	x E21n/cm2	Growth		Temp	x E21n/cm2	Growth
Plant	deg C	E > 1 MeV	dl/l %	Plant	deg C	E > 1 MeV	dl/l %
[b,c,d]							

I.10. Question 10: Please provide the thermal conductivity equation used for M5 material.

Response to question 10: The equation for the M5 conductivity is:

$k(w/m - C) =$ [c,d]

for T = 273 to 1573 °K

As stated in the text of BAW-10227, many of the materials properties published with BAW-10227 were extrapolated from Zircaloy in order to provide a demonstration of the analytical models for the M5 alloy. This was true for the thermal conductivity, because testing had not been completed at the time of publication. Testing has now been completed for the thermal conductivity of M5. Figure I-10.1 shows both the Zircaloy-4 LOCA and Safety Analysis thermal conductivity (labeled Zr-4 RELAP5 on Figure A-2 of BAW-10227) and the M5 conductivity fit that will be used for the LOCA and Safety Analyses. However, the LOCA and Safety Analysis codes use tabular input as given below. As with all the material properties, current values will be maintained in a controlled document at our Lynchburg Virginia Offices.

Thermal Conductivity of M5

Temperature, K	Thermal Conductivity, W/cm-K
273	[c,d]
373	[c,d]
573	[c,d]
673	[c,d]
773	[c,d]
973	[c,d]
1073	[c,d]
1173	[c,d]
1373	[c,d]
1573	[c,d]

As can be observed in Figure I-10.1 the value of conductivity for M5 is higher than for Zircaloy. This difference will promote a somewhat more efficient transfer of energy from the pellet through the cladding to the coolant and should allow a larger amount of energy to be transferred to the coolant during accident phases when cooling is present. Therefore, the effect should be slightly lower cladding and fuel temperatures. A slight benefit should be observed during LOCA. Over-heating events involve the determination of a system pressure or the occurrence of CHF as limits. These transients may experience some increase in consequence. However, the heat transfer from the fuel pellet remains limited by the fuel to clad gap coefficient, minimizing the consequence of the change. Because of this, it is not considered necessary to evaluate the change explicitly. Over-cooling transients are driven by coolant temperature. The slight increase in energy transport will again provide some benefits.

Figure I-10.1
Thermal Conductivity vs Temperature

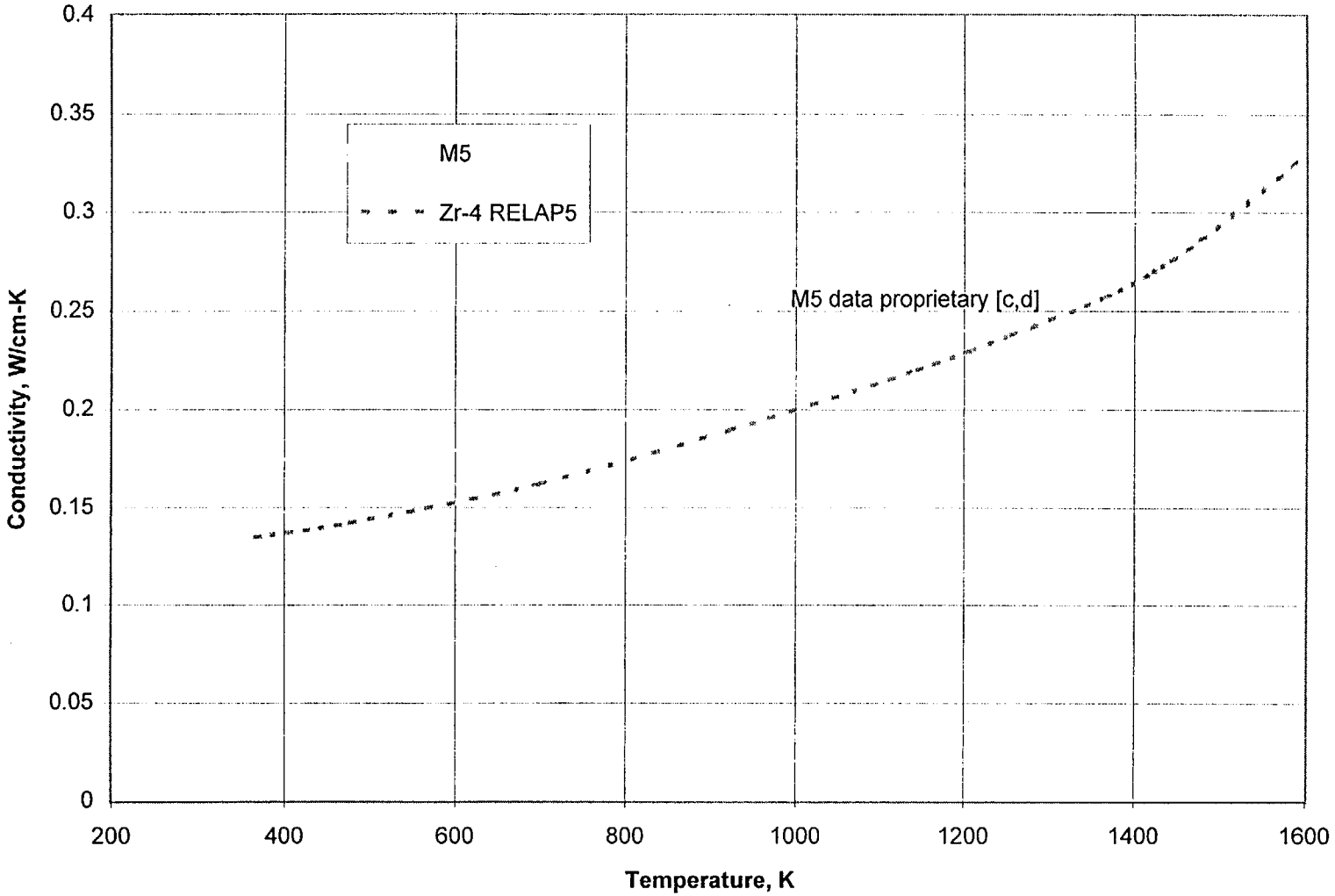

I.11 Question11 : Please provide the data used to estimate the M5 alpha-beta and beta transformation temperatures because there seems to be some differences on the start and completion of these phase transformations based on proprietary data available to NRC. What is the uncertainty in the $\alpha \Rightarrow \beta$ transformation temperatures? Also provide any assumptions used in applying these data to LOCA analyses.

Response to question 11: The response to question 11 dealing with the $\alpha \Rightarrow \beta$ transformation for M5 are taken from a joint FRA-CEA-EDF paper presented at the last ASTM meeting in Toronto in June 1998. Since these proceedings have not been published a copy of the paper is attached. The title is "Experiment and Modeling of Advanced Fuel Rod Cladding behavior under LOCA Conditions: $\alpha \Rightarrow \beta$ Phase Transformation Kinetics and Edgar Methodology." The data is on pages 6 and 7 of the paper.

The $\alpha \Rightarrow \alpha+\beta$ and $\alpha+\beta \Rightarrow \beta$ transformation temperatures for M5 are:

In equilibrium conditions (pages 10 and 11 of paper, Figures 5 and 6)

$T\alpha \Rightarrow \alpha+\beta = 750\ ^\circ C$

$T\alpha+\beta \Rightarrow \beta = 960\ ^\circ C$

In kinetic conditions (pages 10 and 11 of paper, Figure 9)

$T\alpha \Rightarrow \alpha+\beta = 750 \Rightarrow 950\ ^\circ C$ (100 °C/sec)

$T\alpha+\beta \Rightarrow \beta = 960 \Rightarrow 1030\ ^\circ C$ (100 °C/sec)

The comparison of EDGAR data with other data is shown on pages 6 and 7 of paper.

The reproducibility of the data is: $\Delta T = \pm 5\ ^\circ C$ as given on page 9 of paper.

LOCA and Safety Analysis Considerations

A key area within which the cladding phase change affects the LOCA calculations is in the prediction of clad swelling during rupture. The cladding strain, as a function of rupture temperature, is double peaked due to the fact that rupture strain is momentarily reduced as the rupture conditions transition from the alpha to the beta structure, Figures C-6, C-7, C-18, and C-19 of BAW-10227. The cladding swelling and rupture models in

Appendix C of BAW-10227 are direct fits to measured data for the M5 material, EDGAR, and contains the phase change dynamics implicitly. Therefore, these models do not depend on an independent determination of the phase change temperatures or the phase change dynamics.

The impact of temperature change dynamics (heatup rate) on the phase transformation temperature and the resulting values for cladding specific heat as a function of temperature is being evaluated by FCF. When that evaluation is complete the results will be forwarded to the NRC.

I.12 Question 12: Please provide the M5 modulus of elasticity data.

Response to question 12: The modulus data for M5 is plotted in Figure I-12.1 along with the relationship used to extrapolate the data to higher temperatures. The modulus is used in several key analyses. It is used in determining the fuel rod buckling pressure, fuel rod dimensional changes due to applied stresses in TACO3, and in LOCA and safety analysis to determine the cladding dimensions prior to the occurrence of plastic deformation at a given location.

In the LOCA evaluation, once a location of the cladding undergoes a plastic strain that exceeds the elastic strain, the degree of plastic strain is assumed to dominate any elastic dimensional changes for the remainder of the transient and no elastic strain is thereafter applied. For the Framatome evaluation model, the calculation of the plastic strain of the cladding commences when the cladding temperature has increased to within 300 F of the current cladding rupture temperature and the plastic strain has generally exceeded the elastic strain when the cladding temperature is within 200F of rupture. Because rupture for a large break LOCA consistently occurs between 1400 and 1600 F, the modulus of elasticity is normally applied up to temperatures no greater than[c,d]. An exception, however, occurs during small break LOCA (SBLOCA) or whenever a condition of low internal pin pressure is to be calculated. In these cases, the modulus of elasticity can be applied up to temperatures within 200 F of the limit temperature of 2000 F. As can be seen in Figure Q12.1, the temperature for which data is available is around 650 °F (350 °C), but the modulus has been extrapolated to 2200 F to provide for possible higher temperature applications. This extrapolation is supported by the observation that the modulus of elasticity for Zircaloy, given to 2000 F in MATPRO is nearly a constant slope over the extrapolation range. The use of an extrapolation is further supported by an

examination of the impact of the modulus during the LOCA. The maximum change in dimension, due to elastic effects, is[c,d] for temperatures as high as 2200 F. This is a negligible change in cladding dimensions and does not affect the results of SBLOCA calculations.

Figure I-12.1

Young's Modulus vs Temperature

Figure is proprietary

[b,c,d]

I.13 Question 13. What are the consequences of overpredicting M5 cladding Meyer-Hardness for the fuel melting analysis at BOL? Are there any other analyses at BOL that could be impacted due to an overprediction of Meyer-Hardness? Are there any other applications of Meyer-Hardness other than for contact conductance?

Response to question 13: The consequence of overpredicting the Meyer-Hardness for the fuel melt analysis at BOL would be a slight over prediction of the fuel temperature. If pellet cladding contact does occur when a fuel rod is ramped in power, the Meyer-Hardness affects the contact conductance between the pellet and the cladding. The hardness and surface roughness of both the cladding and the fuel pellet affect the contact conductance. Since the pellet is much harder than the cladding, with contact the cladding deforms over the surface of the pellet, increasing the area of direct contact. The harder the cladding, the less deformation of the cladding and the less surface area in direct contact. This will result in a lower contact conductance. Therefore overpredicting the Meyer-Hardness when contact occurs results in a slightly lower contact conductance and slightly higher fuel temperatures.

No other TACO3 analysis is impacted by Meyer-Hardness at BOL. LOCA initialization analysis ramps the rod to lower power levels than the fuel melt analysis and pellet clad contact does not occur. Cladding transient strain is not calculated at BOL since the fuel melt linear heat generation rate (LHGR) limits are more restrictive than the transient strain LHGR limits.

In the LOCA and safety analysis, the clad pellet gap heat transfer model in RELAP5/MOD2-B&W also employs the Meyer-Hardness to determine contact heat transport. However, the initial RELAP fuel clad gap heat transfer coefficient is normalized in order to preserve the initial fuel volume average temperature as predicted by the steady state fuel performance code (TACO). Thus, it is only the transient evolution of the gap coefficient that affects the code predictions. For Safety Analysis the gap dimensions are not generally altered significantly and the gap coefficient is essentially preserved during the transient. Thus little would be affected other than the

initial temperature. For LOCA the cladding quickly expands away from the fuel and the Meyer-Hardness no longer influences the value of the gap coefficient. Therefore, except for the initial fuel temperature, the value of Meyer-Hardness is also not significant for the LOCA predictions.

The only application of Meyer-Hardness is for contact conductance.

I.14. Question 14: Please provide information on power ramp testing of rods with M5 cladding.

Response to question 14. Framatome has performed 5 power ramps tests using M5 fuel rods with 2 cycles of irradiation (25 to 30 GWd/mtU burnup) These tests were performed in either the R2 or OSIRIS experimental reactors with a power ramp rate of [c,d]

The results were[

c,d

]

I.15. Question 15. Please provide the M5 creep data (identify source of data and relevant conditions such as stress, temperature and fluence) from which the effective creep multiplier was developed for the M5 material. Are there any independent fuel rod creep data from one and two cycles of operation with M5 cladding that can be used to verify that TACO3 with the M5 creep model can satisfactorily predict creep for the M5 cladding? Also, please provide those data and plots that demonstrate that the assumed stress, temperature and fast fluence dependencies of the creep model are applicable to the M5 cladding. What is the uncertainty in the M5 creep model as a function of fast fluence, temperature, and stress?

During the development of M5, creep data from an early variant without an optimized mircostructure was evaluated and a creep multiplier of[c,d] was obtained and used. Since then data from M5 with an optimized microstructure has been obtained. An evaluation of that data shows that a creep multiplier of [c,d] should be used. That multiplier will therefore be used for future evaluations. The four fuel rods that are used for benchmarking are shown in Table I-15.1. The measured and predicted data points are listed in Table I-15.2. The relationship between predicted and measured creep down for these rods is plotted in Figure I-15.1. In Figures I-15.2 to I-15.5, the measured – predicted creepdown is plotted as a function of local burnup, fast neutron fluence, EOL cladding temperature and BOL cladding temperature.

Table I-15
M5 Benchmark Rods

Rod	# Cycles	Rod Average Burnup MWd/mtU
4008	1	12,989
4025	1	13,002
4004	2	22,773
4053	2	19,873

M5 creep as a function of neutron fast flux, cladding temperature and stress[

c,d

] The standard TACO3 creep model with a [c,d] multiplier predicts the M5 creep down from 1,000 to 3,000 mm axial position within ± [c,d]. The impact of the creep multiplier on fuel performance is small. In the response to question 7 the impact of a [c,d] creep multiplier was evaluated. The impact was minor.

Details on the benchmarking rods can be found in Tables I-15.3 to I-15.5. Table I-15.3 lists design details and general reactor operational conditions on the benchmark fuel rods. Table I-15.4 lists the power histories for the four fuel rods and Table I-15.5 lists the axial power shapes for the rods.

Figure I-15.1

Predicted vs Measured Creepdown

Figure is proprietary

[c,d]

Figure I-15.2

Measured-Predicted Creepdown vs Local Burnup

Figure is proprietary

[c,d]

Figure I-15.3

Measured-Predicted Creepdown vs Fast Neutron Flux

Figure is proprietary

[c,d]

Figure I-15.4

Measured-Predicted Creepdown vs Clad Average Temperature at EOL

Figure is proprietary

[c,d]

Figure I-15.5

Measured-Predicted Creepdown vs Clad Average Temperature at BOL

Figure is proprietary

Table I-15.2

Measured and Predicted M5 Cladding Diameter and Creepdown

Rod 4004				
	Diameter		Creep Down	
Data	Measured	Prediction	Measured	Prediction
mm	um	um	um	um
500				
1000				
1500				
2000		[c,d]		
2500				
3000				
3500				

Rod 4008				
	Diameter		Creep Down	
Data	Measured	Prediction	Measured	Prediction
mm	um	um	um	um
500				
1000				
1500				
2000		[c,d]		
2500				
3000				
3500				

Rod 4025				
	Diameter		Creep Down	
Data	Measured	Prediction	Measured	Prediction
mm	um	um	um	um
500				
1000				
1500				
2000		[c,d]		
2500				
3000				
3500				

Rod 4053				
	Diameter		Creep Down	
Data	Measured	Prediction	Measured	Prediction
mm	um	um	um	um
500				
1000				
1500				
2000		[c,d]		
2500				
3000				
3500				

Table I-15.3

Benchmark Fuel Rod Parameters

Parameter	Value	Units
Subchannel flow rate	[c,d]	lbm/hr
subchannel hydraulic diameter	[c,d]	in
subchannel inlet temp	[c,d]	deg F
subchannel cross section	[c,d]	in2
enthalpy rise factor	[c,d]	
Outer diameter of fuel	[c,d]	in
Fuel surface roughness	[c,d]	uin.
Volume fraction in dish ends	[c,d]	
Spherical radius of dish	[c,d]	
Radius of pellet dish	[c,d]	in
Fuel enrichment	[c,d]	wt%
O to M Ratio	[c,d]	
Pellet F factor	[c,d]	
Open porosity fraction	[c,d]	
Initial fuel density	[c,d]	.TD
Resintering density change	[c,d]	.TD
Cladding OD	[c,d]	in
Cladding ID	[c,d]	in
Surface roughness	[c,d]	uin.
Cladding length	[c,d]	in
Plenum volume	[c,d]	in3
Fuel stack length	[c,d]	in
RCS pressure	[c,d]	psia
Pin fill pressure	[c,d]	psia

Table I-15.4
Fuel Rod Power Histories

Time		4004	4008	4025	4053
hours	APS	kw/ft	kw/ft	kw/ft	kw/ft
		[c,d]			

Table I-15.5
Benchmark Fuel Rods Axial Power Shapes

		Axial Power Shape (APS)										
Node	in	1	2	3	4	5	6	7	8	9	10	11
1												
2												
3												
4												
5												
6												
7												
8												
9												
10							[c,d]					
11												
12												
13												
14												
15												
16												
17												
18												

I.5. Question 5: For each of the new models for M5 cladding, e.g., growth, corrosion, hydriding, creep, thermal conductivity, high temperature oxidation, etc., in this submittal please provide the range of application of their independent variables. For example, for the cladding rupture model what is the range of engineering hoop stress and heating rate for LOCA applications?

Response to question 5. The range of application of the models is provided in Table I-5.1. The LOCA and Safety Analysis provided in BAW-10227, required the use of certain physical parameters for which, at the time of publication, actual M5 data was not available. Therefore, the values published in Appendix A for many of the M5 physical parameters were extrapolated from Zircaloy. Where such an extrapolation was made, it was clearly indicated as such within the appendix. Since the submittal of BAW-10227, continued testing of M5 has resulted in the measurement of nearly all of these parameters. Where necessary, new or revised correlations or models have been generated. The response to this question has been expanded to provide material properties data, correlations or models to update or replace the original content of Appendix A of BAW-10227. The content of Table I-5.1 is relative to the properties or models as they are herein affirmed or corrected.

Control of Properties used in LOCA or Safety Analysis

The materials properties presented in this response are a result of a comprehensive and continuing program of testing. Although the property values provided are well established, refinements are to be expected from time to time. Framatome will maintain a materials property document at our Lynchburg, Virginia office, which at any given time will contain the latest and most accurate data on materials properties for the M5 alloy. A second document will contain the material properties values approved by Framatome for use in LOCA and Safety Analysis. Framatome will apply a test on the expected sensitivity of limiting or potentially limiting calculational results to determine if an alteration of the material properties document requires a modification of the property values used in LOCA or Safety Analysis. If the calculated result of a limiting or potentially limiting parameter is expected to shift,

toward the more limiting, by greater than 2.5 percent, a change in the value of a physical parameter will precipitate an update of the design basis calculations. The values provided herein comprise the values for the thermal-physical parameters for M5 currently approved for LOCA and Safety Analysis. Should refined data become available for which a judgement is made that a limiting reported parameter would change by more than 2.5 %, the approved materials properties values will be updated and the required analysis repeated. If the judgement is that such a change would not occur, only the material properties document will be updated and no revised evaluations performed. In either case, the judgement will be recorded within the LOCA and Safety Analysis approved properties document and an assessment made as to cumulative effects or appropriateness of update when any new analysis is to be performed.

Material Composition and Condition

The material composition and condition representation provided in Appendix A were actual for the M5 alloy and not extrapolations. Therefore, sections A.1.1 and A.1.2 have not changed since the issuance of BAW-101227. The most recent version of the specification under review is shown below. Limits have been tightened and control over sulfur added to ensure uniform cladding creep:

M5 Material Specification					
	Nb wt %	Fe ppm	O ppm	C ppm	S ppm
Max	[b,c,d]				
Min	[b,c,d]				

Physical Properties

Specific Gravity (Density):

In Reference I-5.1, the specific gravity of the M5 alloy has been determined as:

6.50 g/cm^3 at 20°C (70° F).

Dimensional Controls:

These parameters are a result of the material employed and not an actual material property. The statements in BAW-10227 remain valid. The fuel assembly dimensions and dimension control will, in general, be similar to that used for Zircaloy cladding.

Surface Finish/Roughness:

The statements in BAW-10227 remain valid. Measurements of the actual surface finish of M5 cladding manufactured under the current process are similar to those for Zircaloy 4 cladding.

Thermophysical Properties

Coefficient of Thermal Expansion:

The thermal expansion model developed in BAW-10227 was based on the expectation that the expansion of M5 would be similar to that of Zircaloy. Following the issue of BAW-10227, dilatometry testing of M5, of as-manufactured tubing, has been completed. Figure I-5-1 shows the resultant base thermal expansion correlations and the average to be implemented in the LOCA and Safety Analysis. [

b,c,d]

[b,c,d] Figure I-5.1 shows the resultant thermal expansion in terms of accumulated strain from room temperature. The correlations are extracted from observation of the movement of the exterior surface of a tube in the three cylindrical dimensions. As with Zircaloy the α phase expansion rate in the rolling direction, axial for the fuel pin, differs markedly from that in the transverse dimensions. For a perfectly circular tube, there would be no difference between the radial and azimuthal expansion coefficient. The difference observed is, thus, a measure of the ovality of the tube as manufactured. Because the Framatome LOCA and Safety Analysis techniques do not include a provision for ovality during transient predictions, the radial and azmuthal coefficients will be averaged for transient analytical predictions.

Thermal Conductivity:

For BAW-10227 the thermal conductivity of M5 was assumed to be the same as that of Zircaloy-4. Testing of M5 has now been completed and the conductivity for M5 runs from [b,c,d] than that of Zircaloy. This result is also presented in the response to question 10, which includes a brief discussion of the significance of the change within LOCA and Safety Analysis (essentially no impact). The correlation for the M5 thermal conductivity is:

k = [b,c,d]

where k = conductivity, W/m-K, and
T = temperature, K.

The thermal conductivity for M5 is shown in comparison with that for Zircaloy-4 in Figure I-5-2.

Heat Capacity:

The heat capacity model developed in BAW-10227 was based on the expectation that the specific heat of M5 would be similar to that of Zircaloy except for the resonance over the phase change. Data from CEA and Russian testing on 1 percent niobium alloys (combined to form the M5 specific heat correlation) has shown this to be essentially true. The correlation for M5 given below is also compared to the standard Zr-4 correlation from Eldridge and Deem in Figure I-5-3.

[b,c,d] $273K \le T \le 1100K$

[b,c,d] $1100K \le T \le 1140K$

[b,c,d] $1140K \le T \le 1250K$

[b,c,d] $1250K \le T \le 1600K$

Where C_p = specific heat in J/g-K, and
T = temperature in K.

[

b,c,d

] As a possible explanation, the phase change kinetics for M5, Reference I-5.2, have demonstrated the beta fraction increases very slowly prior to a cladding temperature of 1050 or 1100 K for any reasonable temperature ramp. [

b,c,d

]

[b,c,d] Zr-4 in this range is based on the Eldridge and Deem investigations, which contain only two data points that lie barely, if in fact they do, within the β region. The data are so close to each other in temperature that any line could have been drawn through them. For M5, supporting data is available to temperatures beyond 1500 K.

Emissivity:

The clad emissivity of the M5 alloy has been determined from CEA testing and Russian tests of the E-110 alloy. Figure I-5-4 represents the composite result. For the LOCA and Safety Analysis, emissivity is used to determine a portion of the fuel to clad gap heat transfer and in the evaluation of the radiation term in the cladding exterior heat transfer coefficient. Because radiation is not a dominant mechanism in either process, the emissivity is implemented as a constant, non-temperature dependent, variable. Although separate values are allowed for the interior and exterior surfaces of the cladding, FTI will generally use the same value for both surfaces. (Should different values be employed, an explanation and justification will be provided with the application.) The only conditions under which the emissivity is of credible importance are those during which the cladding is approaching its peak temperature. Therefore, the emissivity to be used in the LOCA and Safety Analysis will be an average over a temperature range from 800 to 1500 K (980 to 2240 F). This gives an emissivity of [b,c,d] used for Zircaloy.

Cladding Oxide Development:

The references provided in BAW-10227, as they may have been amended elsewhere in the response to questions, are correct.

Mechanical Properties

Tensile Strength:

Ultimate Tensile Strength:

The Appendix A conclusions on ultimate tensile strength (UTS) for M5 remain valid.

0.2 % Offset Yield Strength:

The yield strength shown in Figure A-3.1.1 for both axial and biaxial conditions over the temperature range of 20 to 400 C will continue to be used to determine the appropriate stress intensity limits for stress analysis. A complete listing of data is found in the response to question 2.

Ductility:

The Appendix A conclusions on ductility remain the same. In the unirradiated condition the ductility is always greater than 10%. With irradiation the ductility decreases as the strength increases with less separation between the YS and UTS. However, irradiated cladding has ductility greater than 1%. A complete listing of data is found in the response to question 2.

Creep:

Revised data on the creep rate for the M5 alloy have become available and are discussed in the response to Question 15. The revised creep rate multiplier of [b,c,d]used in Appendix A and B, but it remains significantly lower than the creep rate for FCF SRA Zircaloy cladding.

Poisson's Ratio:

The value for Poisson's Ratio remains essentially unchanged. Further literature searches, however, have indicated that the apparent accuracy should be reduced to only two significant figures giving 0.37 instead of 0.372.

Modulus of Elasticity:

The conclusion of this subsection in the original report was that the modulus values for Zircaloy-4 could be used to represent M5. This conclusion remains valid. However, as documented in the response to Question 12, additional testing has confirmed a modulus correlation for M5, and the RELAP5 code has been reprogrammed to accept a material dependent modulus. Therefore, the LOCA and Safety Analysis evaluations of M5 cladding will use the M5 correlation:

$E = [$ b,c,d $]$

where E = modulus of elasticity, and
T = temperature, K

This correlation is compared to the Zircaloy-4 correlations that will continue to be used in TACO3 (steady state fuel performance code, Reference A-6) and CROV (Creep Collapse Code, Reference A-7) in Figure I-5.5.

Hardness (Meyer's):

The treatment of Meyer's Hardness remains as presented in Appendix A. Further discussion of this parameter is contained in the response to Question 13.

Growth:

The growth models presented in Appendix A are still valid. Additional growth data shown in the response to question 9 shows a nearly complete saturation of fuel rod growth at burnups > 40 GWd/mtU. In addition, as shown in the response to question 9, in FCF fuel assembly designs the rate of shoulder gap closure is small due to a coupling of fuel rod and fuel assembly growth.

Corrosion Effects:

Corrosion Rates:

The corrosion models presented in Appendix A are still valid. The response to question 3 provides in graphical form the performance of the corrosion model relative to data. Further information on the corrosion model was presented in the response to question 4.

Hydrogen Pickup Fraction

The hydrogen pickup fraction has been changed to [b,c,d]

Stress Corrosion Cracking:

The Appendix A conclusions on the stress corrosion cracking (SCC) performance of M5 remain valid. The testing has established that M5 fuel rod cladding has SCC threshholds the same or better than those of Zircaloy-4 cladding.

Ranges of Applications

The range of application of the models is provided in table I-5.1. For the LOCA clad swelling and rupture model the cladding heating rate is capped at 28 C/s (any heating rate greater than 28 C/s is treated as if it were 28 C/s) just as was done for Zircaloy in NuReg-0630. This is considered sufficient because the fast ramp rate strain curve saturates rapidly with heating rate and is developed as an essential bound to the aggregation of the available data.

References

I-5.1. B. Beyer & R. Juknat, "Physical and Mechanical Properties of Zirconium-niobium Alloys containing 1 & 2.4 wt % of niobium," Conference on the Use of Zirconium Alloys in Nuclear Reactors, page 55-75, Marianske Lazne, Czechoslovakia, October 1966.

I-5.2. "Experiment and Modelling of Advanced Fuel Rod Cladding Behavior under LOCA Conditions: $\alpha \Leftrightarrow \beta$ Phase Transformation Kinetics and EDGAR Methodology," 12th International Symposium on Zircomium in the Nuclear Industry, Toronto, Ontario, Canada, June 1998.

Table I-5.1 Range of Independent Variables for M5 Models									
							Fast	Fast	
							Neutron	Neutron	
						Heating	Flux	Fluence	
	Model		Temp	Stress	Time	Rate	n/cm2-s	n/cm2	Burnup
Model	Form		deg C	MPA	hours	deg C/s	E > 1 MeV		GWd/mtU
			b,c,d						

* The Baker/Just (B/J) model which is required by Appendix K is not a new model. Only the demonstration of the applicability of B/J to M5 is new.

** Heating Rates above 28 °C/s are treated as equivalent to 28 °C/s for the purpose of determining the clad swelling and rupture characteristics.

Figures I-5-1. Thermal Expansion Correlations for M5 Tubing

[b,c,d]

Figure I-5-2. Thermal Conductivity for M5 and Zr-4

[b,c,d]

Figure I-5-3. Specific Heat for M5 and Zr-4

[b,c,d]

Figure I-5-4. Emissivity for M5

[b,c,d]

Figure I-5-5. Modulus of Elasticity for M5 and Zr-4

[b,c,d]

Responses to January 1999 Questions:

Framatome Cogema Fuels (FCF) and Framatome Technologies Inc. (FTI) have recognized the need to communicate some additional material to the Nuclear Regulatory Commission (NRC) about the implementation of M5 cladding than could be done by simply responding to the questions on BAW-10227. To accomplish this, the material is organized into five sub-sections which include discussions and declarations not covered in the responses to Questions 16 through 25. The specific organization is:

1. Documentation Changes Required in Other Topical Reports (with enclosure)

2. Recalculations for Safety Analysis

3. General Response to Questions on the M5 Swelling and Rupture Model

4. LOCA Treatment of Pre-Rupture Swelling Induced Flow Diversion

5. Responses to NRC Questions 16 through 25 on BAW-10227

1. Documentation Changes Required in Other Topical Reports

The LOCA evaluation models for FTI are documented in the following set of topical reports:

BAW-10168, RSG LOCA - BWNT Loss-of-Coolant Accident Evaluation Model for Recirculating Steam Generator Plants
BAW-10192, BWNT LOCA - BWNT Loss-of-Coolant Accident Evaluation Model for Once-Through Steam Generator Plants
BAW-10164, RELAP5/MOD2-B&W - An Advanced Computer Program for Light Water Reactor LOCA and Non-LOCA Transient Analysis
BAW-10166, BEACH - Best Estimate Analysis Core Heat Transfer
BAW-10171, REFLOD3B - Model for Multinode Core Reflooding Analysis

In order to incorporate the M5 alloy into the LOCA evaluation, materials referencing the M5 topical must be added to some of these reports. This section describes the content to be added and requests NRC approval to make the modifications in the approved versions at the next convenient update of the individual reports.

BAW-10168, RSG LOCA EM Report

The following sentence will be added to page 1-1 of Volumes 1 and 2 of BAW-10168.

"For core designs employing the M5 alloy for fuel pin cladding, the material properties, inputs, methods, and correlations, described in BAW-10227 shall supercede, as appropriate, those described within this volume."

BAW-10168 describes the RSG LOCA evaluation model. This sentence merely allows the material properties and correlations for the M5 alloy to replace those for Zircaloy where those properties or correlations have been approved by the NRC as part of BAW-10227.

BAW-10192, BWNT LOCA EM Report

The following sentence will be added to page 1-1 of Volumes 1 and 2 of BAW-10192.

"For core designs employing the M5 alloy for fuel pin cladding, the material properties, inputs, methods, and correlations, described in BAW-10227 shall supercede, as appropriate, those described within this volume."

BAW-10192 describes the LOCA evaluation model for B&W-designed plants. This sentence merely allows the material properties and correlations for the M5 alloy to replace those for Zircaloy where those properties or correlations have been approved by the NRC as part of BAW-10227.

BAW-B10164, RELAP5/MOD2-B&W

The following change pages for the RELAP5 topical comprise the description of the alterations of fixed properties or correlations with input tables or input coefficients so that the materials properties and correlations described in BAW-10227 can be incorporated into the solution. It was also necessary to produce a material tracking within the code in order to provide for discrimination between Zircaloy properties and M5 properties. A change bar is supplied to indicate where on each page an alteration has been necessary. Some of the pages are included because they back a page upon which some material was altered and the figure list is altered only in that the page number for a figure has shifted.

In addition to direct M5 related changes, RELAP5/MOD2-B&W, including its BEACH routines, was updated to allow for proper supplemental pin (multiple heat structure) modeling within a fluid channel. The relationship of the pins in a common fluid channel is one in which the swell and rupture of the smaller heat structure (the supplemental pin) does not define the rupture flow blockage for the entire fluid channel. Rather, it will

define a local effect for the supplemental pin only, such that radiation heat transfer is calculated correctly for that pin. The channel droplet breakup parameters and the additive rupture form loss are controlled by the larger heat structure (primary fuel pins). The change also allows each heat structure within a fluid channel to be individually associated with a specific set of materials. These structures can be used for sensitivity studies or to determine the effects of individual dissimilar fuel pins within a fuel assembly. FTI is not, at this time asking that the LOCA evaluation models be altered to approve the use of the supplemental pin model. If this approach is used for licensing calculations it will require separate approval by the NRC.

List of RELAP Change Pages

Enclosure 1 (37 pages) contains pages from RELAP5 topical with sections to be changed indicated by a vertical line on the margin.

BAW-10166, BEACH

BAW-10166, BEACH, does not require specific modification beyond that described in the RELAP5 report to incorporate the M5 cladding material. FTI considers the instruction to be included within the EM topicals to supercede materials properties and correlations with M5 properties and correlations as dictated in BAW-10227 as sufficient to allow the use of M5 parameters in BEACH.

BAW-10171, REFLOD3B

BAW-10171, REFLOD3B, does not require specific modification to incorporate the M5 cladding material. FTI considers the instruction to be included within the EM topicals to supercede materials properties and correlations with M5 properties and correlations as dictated in BAW-10227 as sufficient to allow the use of M5 parameters in REFLOD3B.

2. Recalculations for Safety Analysis

BAW-10227 contains the following sentence on page 4-2 of Section 4.1, "It will be necessary to recalculate the temperature transients that enter or exceed the phase change range with M5 specific properties when licensing applications for M5 cladding are requested." Section 4.2 explains the non-LOCA accident analysis implications of the M5 cladding and this particular sentence commits to revisit calculations for which the cladding temperature has risen to the α to β phase change temperature range. The basis for this requirement was the expectation that the M5 specific heat would differ as a function of temperature within the phase change range from Zircaloy and that M5 cladding might therefore demonstrate altered temperature histories for high temperature transients. [

b,c,d

]

[

b,c,d

]Therefore, all non-LOCA safety analysis performed using Zircaloy materials properties apply equally to M5 cladding and there is no need to recalculate any of the non-LOCA safety analysis calculations merely because the cladding material has been changed to M5. If there are other design changes to the fuel assembly that necessitate recalculation of non-LOCA events, the recalculations will use the appropriate material properties for the fuel assembly cladding material.

3. General Response to Questions on the M5 Swelling and Rupture Model

In response to Question 19 of the first set of questions on the M5 alloy topical, FTI has elected to incorporate a small adjustment to its M5 swelling and rupture model. The change alters the temperature and value at which the peak β phase pre-rupture strains occur. The change is directed to a reviewer concern and is fully explained in the response to Question 19, herein. Although creating a model that may be more inline with available data and the current understanding of swelling and rupture phenomena, the resulting blockage curves are not significantly altered. The new M5 modeling curves have been employed throughout these responses. Thus, the M5 curves provided herein will not completely agree with those in the topical but they do represent the M5 swelling and rupture model as now proposed. None of the benchmarks performed in BAW-10227 are changed by this alteration and thus none of the conclusions of BAW-10227 are effected.

[

b,c,d

]

[

b,c,d

]

Another use of the MRBT B-1 through B-3 bundles was to benchmark the FTI model development methods. These benchmarks, Figures C-23 through C-28 of BAW-10227, are not benchmarks of the M5 swelling and rupture model. [

b,c,d

] The benchmarks only show that, if the FTI approach were used to develop a Zircaloy model using best estimate tertiary and secondary creep results, the model would reasonably predict the MRBT experiments. Figures C-29 and C-30 of BAW-10227 were intended as a benchmark of the FTI method against NUREG-0630, but used more of the NUREG-0630 base data than was implied by the FTI method. A better comparison to NUREG-0630 is made through the use of the EDGAR Zircaloy tests to replace the M5 tests in the FTI method. Such a

comparison can also be used to provide benchmarks against the JAERI tests and FRF-1, which were additional benchmarks in NUREG-0630.

[

b,c,d

b,c,d

]

[

b,c,d

]

An additional general consideration, as evidenced by the data shown in Figures I-G.3 and I-G.4, is that differing Zirconium alloys can vary considerably relative to specific physical behavior, in this case cladding swelling and rupture. If part of the M5 review is a comparison to proprietary data not available to FTI or FCF, a general description of the comparison material should be provided. Alloying makeup for elements comprising more than 0.05 % by weight along with heat treatments and cold work processes are required to establish the legitimacy of the comparison. For example, the Russian E-110 alloy and M5 are not the same materials (oxygen content and fabrication differences) relative to swelling and rupture although both are primarily 1 % Nb alloys of Zirconium.

Figure I-G.1 Fuel Pin Circumferential Strain versus Time

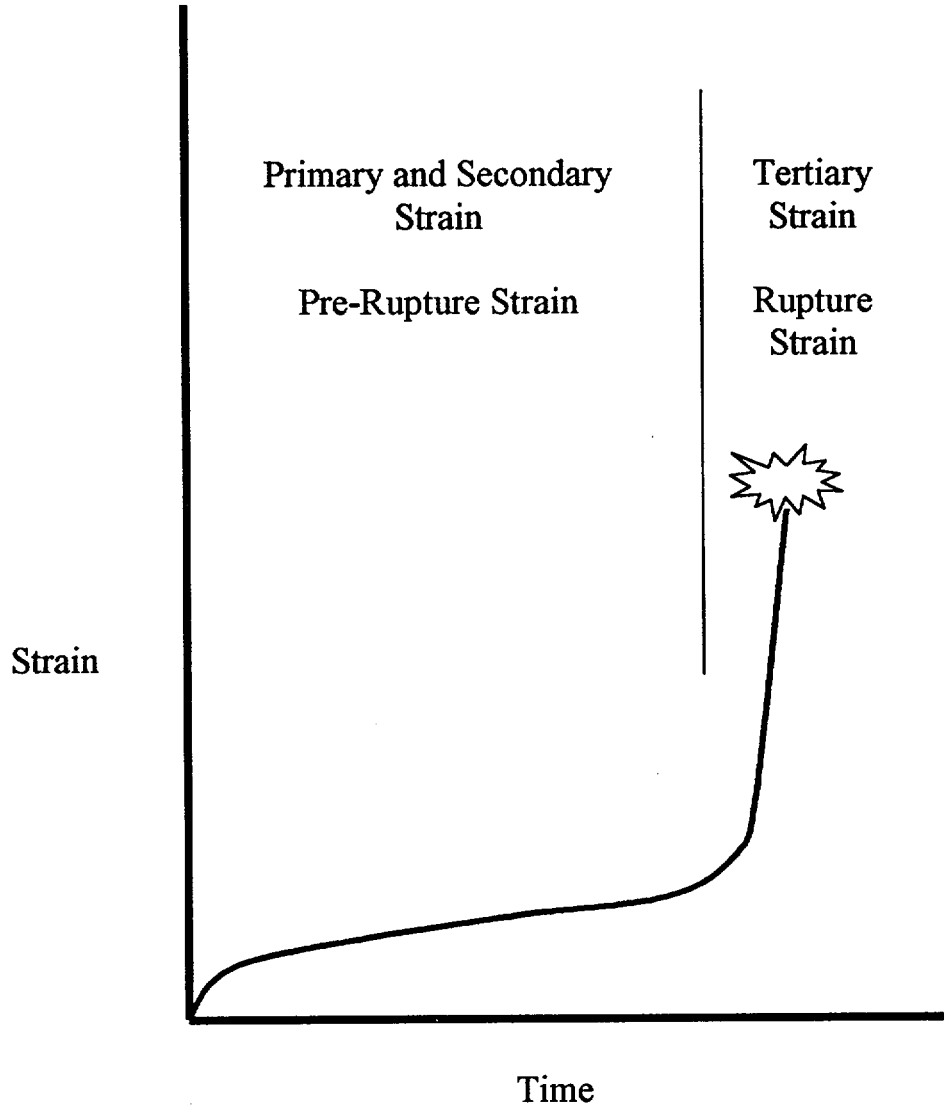

Figure I-G.2 Ruptured Fuel Pin Characterization

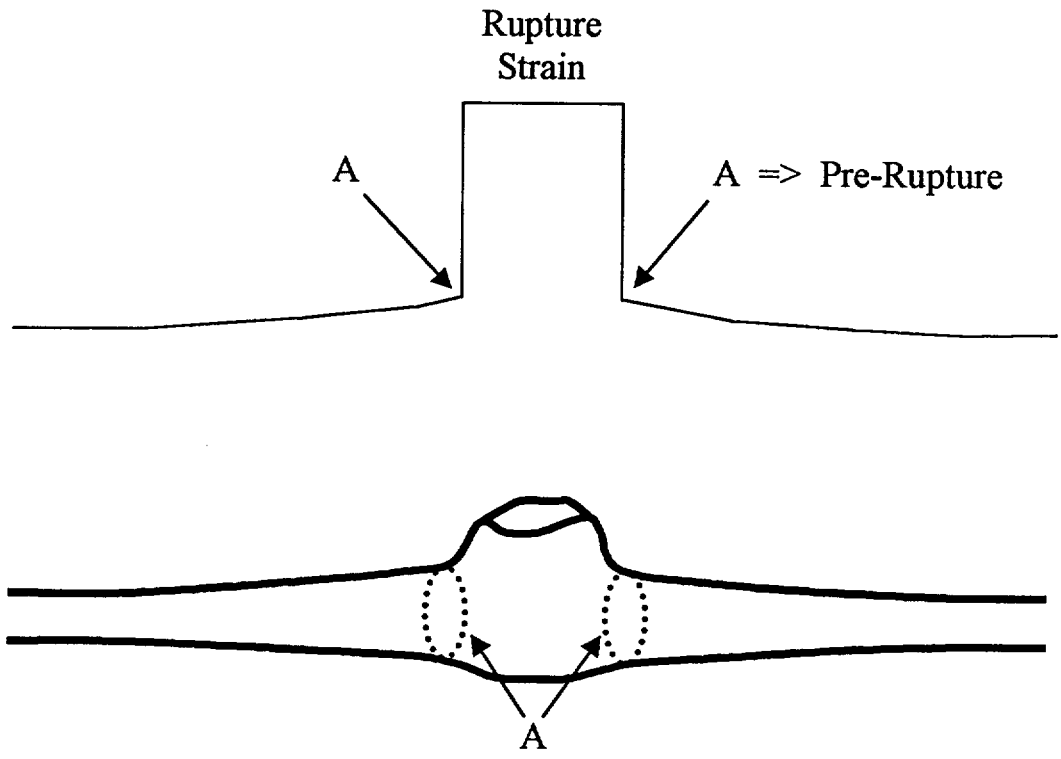

Figure I-G.3 EDGAR Slow Ramp Rupture Data and Fits for Three Alloys

[b,c,d]

Figure I-G.4 EDGAR Slow Ramp Pre-Rupture Data and Fits for Three Alloys

[b,c,d]

Figure I-G.5 EDGAR Fast Ramp Rupture Data and Fits for M5 and Zr-4 Alloys

[b,c,d]

Figure I-G.6 EDGAR Fast Ramp Pre-Rupture Data and Fits for M5 and Zr-4 Alloys [b,c,d]

Figures I-G.7 Comparison of EDGAR Based Zr-4 Blockage Model to NUREG-0630 Model
Slow Ramp

[b,c,d]

Figures I-G.8 Comparison of EDGAR Based Zr-4 Blockage Model to NUREG-0630 Model
Fast Ramp

[b,c,d]

Figure I-G.9 EDGAR Based Zr-4 Local Slow Ramp Blockage and NUREG-0630 Local Blockage with Referenced Bundle Tests

[b,c,d]

Figure I-G.10 EDGAR Based Zr-4 Local Fast Ramp Blockage and NUREG-0630 Local Blockage with Referenced Bundle Tests

[b,c,d]

4. LOCA Treatment of Pre-Rupture Swelling Induced Flow Diversion

A subject not discussed in BAW-10227 is flow diversion from the hot assembly due to pre-rupture swelling of the cladding. The FTI LOCA evaluation models (EMs) do not simulate diversion of flow out of the hot fuel assembly induced by clad swelling prior to rupture (Reference 3.1). Pre-rupture-induced flow diversion has been discussed with the NRC for pre-rupture strains up to 20 percent. Based on experimental and analytical results, which indicate that flow diversion prior to rupture is minimal and that the effects of pre-rupture swelling are beneficial to cooling the fuel rods in the hot assembly, NRC approved FTI's approach for pre-rupture strains up to 20 percent of the maximum rupture strain for Zircaloy. This section will demonstrate that pre-rupture flow diversion imposes the same consequences for the hot assembly if the cladding material is M5 as it does for Zircaloy cladding making the FTI LOCA modeling approach applicable to either cladding type.

For Zircaloy, FTI demonstrated that during the pre-rupture phase, flow blockage is limited and the geometry comprises smooth flow area changes such that any added resistance is minimized and any loss of hot assembly flow is compensated for by increases in the heat transfer processes. Calculations, Reference 3.2, showed little potential flow diversion even under a presumption that cladding strain was confined solely to the hot assembly. Heat transfer increases, primarily the increase in local fluid velocity and the pin surface area were sufficient to off set the flow diversion. Experimentally, FLECHT tests conducted with and without blockage simulations and the studies within the German REBEKA program were sited as demonstrations that the cooling process was improved for coolant channel obstructions of up to 62 percent.

In extending these conclusions to the M5 cladding evaluation, FTI is recognizes the differences in the swelling and rupture models selected for fuel pin thermal calculations and the post-rupture hot channel flow calculations between Zircaloy and M5. The Zircaloy model limits pre-rupture strain to 20 percent of rupture strain, which, because rupture strain for the FTI NUREG-0630 based swelling model peaks at 90 percent, can be no more than 18 percent. The EDGAR based M5 swelling model correlates pre-rupture

strains upto[b]percent in the α and most of the α+β temperature range and up to [b] percent in higher α+β and β temperature range. Because of this difference in the amount of pre-rupture strain, the discussion that follows will be separated into pre and post α+β regimes.

α and α+β region, rupture temperature below 950 C

The diversion of flow from the hot assembly is dependent on cross flow resistance and on the increased imbalance of axial resistances imposed by the pre-rupture strain distribution among the core assemblies. The core condition evaluated in Reference 3.2 comprised a single hot strained assembly diverting flow to cooler unstrained assemblies. The result was a diversion of 3 percent assembly flow, most of which occurred at the core inlet. The local heat transfer capability was shown to increase in a compensating fashion and the combined effect was beneficial. [

b,c,d

]the response provided in Reference 3.2 can be applied for pre-rupture strains up to those for the M5 α and α+β regions with temperatures below 950 C.

α+β and β region, rupture temperature above 950 C

[

b,c,d

]

[

b,c,d

b,c,d

]

[b,c,d]

Thus, the FTI approach to pre-rupture flow diversion is valid for both the M5 and Zircaloy cladding. It is not necessary that a direct simulation of pre-rupture strain induced flow diversion be made for conservative prediction of the LOCA transient.

References:

3.1 F.J. Erbacher, "Interaction Between Fuel Clad Balloning adn Thermal-Hydraulics in a LOCA," KfK 3880/1. pp. 299-310, December 1984.

3.2 BAW-10168P-A, "RSG LOCA - BWNT Loss-of-Coolant Accident Evaluation Model for Recirculating Steam Generator Plants," pages LA-270 to LA-290, Framatome Nuclear Technologies, Lynchburg, VA, December 1996.

3.3 F.J. Erbacher and S. Leistikow, 'Zircaloy Fuel Cladding Behavior in a Loss-of-Coolant Accident: A Review," Zircaloy in the Nuclear Industry, Seventh International Symposium, American Society for Testing and Materials, Philadelphia, Pennsylvania, 1987.

5. Responses to NRC Questions 16 through 25 on BAW-10227

I.16. Question: In order to compare the flow blockages of the FTI and NUREG-0630 models for licensing applications of full size bundles for fast and slow temperature ramp rates, Figures C-34 and C-35 from the subject topical report were compared to equivalent flow blockage curves in Figure 16 of NUREG-0630 taking into account the shift in phase transformation temperatures for M5 and Zr-4. This comparison demonstrated that the FTI model provides an overprediction of flow blockage in the β phase but an underprediction in the α phase of 5% (relative) for slow ramp rates and underprediction in the α phase of 18% (relative) for fast ramp rates relative to those for NUREG-0630. Please explain why this underprediction of flow blockage by the FTI model in the α phase in relation in NUREG-0630 is acceptable.

Response: The premise of the comparison suggested is that the change in the materials properties between Zr-4 and M5 is not important to the determination of flow blockage. As demonstrated in Figures I-G.3 and I-G.4 and below in Figures I-16.1 through I-16.6, this is not a valid premise. [

b,c,d

]

The data and preliminary fits of Figures I-16.3 through I-16.6 are limited to the α and α+β phase regions. The EDGAR data available for Zr-4 and[

b,c,d

]were not taken to support a LOCA swelling and rupture evaluation model of the breadth considered in US applications and do not include extensive β phase content. However, the deviation of the results between alloys in the α range is sufficient to establish the need to recognize alloy specific behavior in establishing a swelling and rupture model. Furthermore, this question deals specifically with the α and α+β regions. [

b,c,d

]

[

b,c,d

b,c,d

]

As seen in the figures provided, a Zr-4 model developed from EDGAR Zr-4 data using the FTI method, bounds the NUREG-0630 blockage curves. The reasons for this bound lie in the greater detail available in the EDGAR data and the fact that [

b,c,d]

[

b,c,d]Therefore, the FTI method does benchmark with NUREG-0630 and the reasons for the [b,c,d] flow blockage predicted by FTI for M5 are traceable to the differences in basic physical traits between the M5 alloy and Zr-4. Clearly the M5 blockage model should respond to differences in physical properties and should not be bound by earlier evaluations based solely on Zr-4.

Figure I-16.1 M5 Rupture Strain - Slow Ramp

[b,c,d]

Figure I-16.2 M5 Pre-Rupture Strain - Slow Ramp

[b,c,d]

Figure I-16.3 Zr-4 Rupture Strain - Slow Ramp

[b,c,d]

Figure I-16.4 Zr-4 Pre-Rupture Strain - Slow Ramp

[b,c,d]

Figure I-16.5 Zr-X Alloy Rupture Strain - Slow Ramp

[b,c,d]

Figure I-16.6 Zr-X Alloy Pre-Rupture Strain - Slow Ramp

[b,c,d]

I.17. Question: How was the magnitude of the PDF function (Figure C-16 in topical report) determined? Were the Chapman test bundle data used?

[

b,c,d

b,c,d

b,c,d

]

[

b,c,d

b,c,d

b,c,d

]

[b,c,d

]

References:

I-17.1 "Zircaloy Fuel Cladding Behavior in a Loss-of-Coolant Accident: A Review," Zirconium in the Nuclear Industry - seventh international symposium, pages 478 and 479, Conference date and place - June 1985 Strasbourg, France, ASTM Special Technical Publication 939, ASTM 1916 Race Street, Philadelphia, PA.

I-17.2 C.L. Mohr and G.H. Hessen, LOCA Rupture Strains and Coolability of Full-Length PWR Fuel Bundles, "Transactions of the 7th International Conference on Structural Mechanics in Reactor Technology, Volume C Structural Analysis of Fuel, Cladding and Assemblies," CEC The Commission of the European Communities, ANL The Argonne National Laboratory, August 1983.

I.18. Question 18: The FTI high temperature swelling and rupture model are considerably different from the NUREG-0630 model. One of the differences is the FTI pre-strain sub-model. There are some assumptions used in the development of the pre-strain sub-model that appear to be inconsistent with the data or with the general behavior of M5 and Zr-4. Some of the inconsistencies are:

Question Part: a) It is assumed that pre-strain is a function of rupture strain and a significant contributor to flow blockage. However, examination of the Chapman bundle pre-strain data show that the pre-strain data on average for each bundle do not appear to change much between those bundles with greater rupture strains (bundles B-1 and B-2 with less flow blockage) and the bundle with greater rupture strains (bundle B-3 with greater flow blockage) in the α phase. This would suggest that: 1) the amount of pre-strain is not a function of rupture strain as assumed by the FTI model, and 2) if there is an effect of pre-strain on flow blockage, it is rather constant for rupture strains greater than 40% and that significant flow blockage is primarily a function of rupture strain in the α phase.

Response: Contrary to the implication in the question, the FTI pre-rupture strain sub-model is independent of rupture strain. Pre-rupture strain, as modeled in NUREG-0630, is directly proportional to rupture strain. The implication that the pre-rupture strain is proportional to rupture strain in the FTI model was created by a publication error in Appendix C of BAW-10227. Figure C-13, "Characterization of Axial Distribution of Strain for Ruptured M5 Cladding," was intended to show how strain decreases along the fuel pin as distance from the rupture location increases. The figure was incorrectly labeled as "% of Rupture Strain" versus "Distance from Rupture," giving the understandable impression that pre-rupture strain is a function of rupture strain. The correct figure, supplied herein as Figure I-18.1, is labeled Normalized Strain versus Distance, and does not indicate any value for the strain in the ruptured zone. The normalized strain with which the figure should have been labeled is an actual local strain and has no relationship to the rupture strain. The actual value of the strain at point "A" is determined from the pre-rupture strain lines of Figures I-19.3 and I-19.4 or I-19.5 and I-19.6 (which will replace Figures C-8, C-9, C-34, and C-35 in BAW-10227) given the heating ramp rate and the rupture temperature.

The question also implies that pin strain, axially remote from the pin rupture location, is not significant in determining the degree of fuel assembly blockage. As will be demonstrated below, remote pin strain is as significant as rupture strain in the determination of fuel assembly blockage.

To determine fuel assembly blockage, NUREG-0630 multiplies the rupture strain by a ratio of average rod strain to rupture strain as derived from the Chapman testing (NUREG-0630, Reference C-1 page 28). An examination of the rupture planes from the Chapman tests (Figure 11 of NUREG-0630 or Figures C-20 through C-22 of BAW-10227) shows that no more than 3 or 4 pins have ruptured in any one plane. Using the data for the B-1 bundle provided on pages 24 through 28 of NUREG-0630, 4 pins are ruptured in the plane of maximum blockage, the average rod strain for the 15 functioning rods was 25 % in this plane and the average rupture strain was 42 %. Therefore, the average strain in the remaining unruptured rods was about 19 % for this plane. Using representative 15x15 pin and assembly dimensions, the assembly unit cell flow area is ≈ 0.18 in^2. If the blockage is based on a 15 pin array with 4 pins ruptured at 42 % strain and the remainder unruptured at 19 % strain, the total flow channel blockage would be ≈ 48 % of which 23 % is attributable to ruptured rods and 25 % to secondary strain in unruptured rods. Therefore, for this test, the secondary strain within the rods that ruptured away from the plane is as important or more so to the calculation of assembly blockage than the ruptured rod strain.

Because the applied ratio of average strain to rupture strain is held constant in NUREG-0630, the role of pre-rupture strain, essentially the amount or model of pre-rupture strain, is directly proportional to the rupture strain. [

b,c,d

]

[

b,c,d

]

The development of the FTI secondary strain model was based on secondary strains measured in the EDGAR test programs and the rate of strain drop-off measured in the MRBT program. Figure I-G.2 illustrates the condition of an individual fuel pin following rupture. A large strain, rupture strain, of the cladding is evident at the rupture site. Just to either edge of the rupture site (marked "A" in Figure I-G.2), the strain reduces dramatically. The pin strain continues to decrease slowly as distance, or remoteness, from the location of rupture increases. The strain just outside the rupture zone, "A" in Figure I-G.2, is the result of a secondary strain process that has been arrested by the release of stress when the pin ruptures. For the FTI model, it has been loosely termed the pre-rupture strain. This strain, which might be better termed the peak or maximum pre-rupture strain, is presented for M5 as data and a resulting correlation in Figures I-19.3 and I-19.4 (which will replace Figures C-8 and C-9 in the topical). Figures I-G.3, I-G.4, I-16.2, I-16.4, and I-16.6 also present this strain as data and correlation for M5 and two other alloys.

[

b,c,d

]

[

b,c,d

]

To avoid one additional source of potential confusion, it is well to explain the use of A_r in BAW-10227 as the normalizing constant for pre-rupture strain. In the EDGAR program the subscript "r" refers to the French word "reparti" and has no relation to rupture. When a parameter refers to the rupture condition the EDGAR nomenclature the subscript "t" for total is used. Thus, within EDGAR the strain or pin area at the rupture site is listed under the heading A_t and is usually referred to as the "total elongation." The matter is further complication by the frequent use of the term "burst strain" to refer not to the result of a rupture, the tertiary strain, but to the secondary strain at which rupture is imminent.

Thus, the term "burst strain" is interchangeable with "A_r" and has nothing to do with the post-rupture strain at the rupture location. In the US, however, the r subscript would most likely refer to conditions at the rupture location. In BAW-10227, FTI maintained the EDGAR nomenclature.

Question Part: b) The pre-strain values from the M5 EDGAR tests are significantly lower than those observed from the Chapman bundle tests. It would be expected that M5 and Zr-4 should give similar pre-rupture strains because both have similar rupture strain behavior at the high temperatures typical of a LOCA, as noted above in the general comment. This would suggest that there may be some problems with the single rod EDGAR tests, e.g., axial temperature gradients, that make the pre-strains non-prototypical of those in a bundle during a LOCA where cladding temperatures are more uniform. This would further suggest that the FTI pre-strain model significantly underpredicts pre-strains in the α phase resulting in an under prediction of flow blockage in the α phase for PWR bundles during a LOCA.

Response: The pre-rupture strain rates for M5, Zr-4, and [b,c,d] have been compared in Figure I-G.4. These comparisons are from EDGAR data and differ somewhat from the Chapman test results used in NUREG-0630. For the Chapman B-3 test (slow ramp), rupture occurs in the mid 700 C range indicating an EDGAR prediction of pre-rupture strain of [b,c,d] An examination of the B-3 data indicates that the average maximum secondary strain was around 32 %. (Note that the value of pre-rupture strain in the table on page C-9 of BAW-10227 is percent of rupture strain and can not be compare to the actual strains quoted herein.) The rupture temperatures for the Chapman B-1 and B-2 tests (fast ramps) lay in the mid 800 C range, indicating a pre-rupture strain of around [b,c,d] From the data for the B-1 and B-2 tests, the average maximum secondary strain was around 27 %. (Note that the table on page C-9 can not be applied.) [

b,c,d

]

[b,c,d]The mean rupture strains for the B-1 and B-2 tests were 42 %. These lie near or slightly above the mean for the single pin rupture data incorporated into NUREG-0630 but are somewhat below the fast ramp rupture strains for Zircaloy measured in EDGAR. The mean rupture strain for the B-3 test was 56 %. This value is somewhat below the mean for the data in NUREG-0630 but substantially below the slow ramp rupture strains measured in EDGAR. A direct comparison between the EDGAR Zircaloy data and the NUREG-0630 database would

show that EDGAR shows [

b,c,d

]

The comparisons provided in Figures I-G.3 and I-G.4 demonstrate that even for small alloying agents high temperature creep and rupture performance can be significantly affected. Within the alpha phase, consideration of the heat treatment and cold work of the material must also be made to determine its behavior. It is also necessary to differentiate tertiary and secondary strain performance, as similarity in alloy behavior in one does not provide assurance of similarity in the other. Therefore, the basic properties of each alloy must be measured and correlated substantially from alloy-specific data and not inferred from other alloys.

[

b,c,d

]

Question Part: c) The pre-strain FTI modeling in Figures C-8 and C-9 for slow and fast ramps, respectively, assume the same pre-strain values in the α and $\alpha+\beta$ regions. Examination of the EDGAR slow ramp data in Figure C-8 demonstrates that the α phase has higher pre-strains than the $\alpha+\beta$ phase on average. This would be expected because it is known that the latter has less strain capability than the former, and this is further demonstrated in the rupture strain data. This would suggest that the FTI pre-strain model underpredicts pre-strains of the EDGAR tests in the α phase.

Response: Figure I-18.2 presents the M5 pre-rupture strain fit and data. The solid line is the modified pre-rupture strain fit as proposed in the response to Question 19. [

b,c,d

]

Question Closure: Please comment on the above inconsistencies in the FTI modeling assumptions of M5 pre-strains and what is the impact on the calculation of flow blockage in M5 bundles (Mark B and BW designs) during a LOCA, if the assumptions regarding the FTI pre-strain model are incorrect.

Response: Within the responses to this question, the impression that the FTI pre-rupture strain sub-model correlates to the rupture strain has been corrected. The FTI pre-rupture strain is taken from data of secondary creep for the M5 alloy. It has further been demonstrated that fuel pin strain away from the pin rupture location is important to the determination of assembly blockage. [

b,c,d

] Therefore, in conjunction with the Zircaloy flow blockage comparison provided in the general response, Figures I-G.7 and I-G.8, it has been shown that small alloying differences can lead to differing creep performance and that swelling and rupture models should reflect alloy-specific data to the extent practical.

The effect of any changes to the FTI basic strain correlations would be to alter, to some extent, the resultant flow blockage model. However, these models are developed to not underestimate the amount of flow blockage and, because substantial conservatism has been incorporated within the rupture strain fit, it is doubtful that any alteration of the pre-rupture strain models would lead to an under estimation of blockage. [

b,c,d

]

Finally, both in this response and in the response to Question 19, alternate strain correlations have been evaluated without serious changes to the assembly blockage result. Therefore, it is concluded that the FTI approach to swelling and rupture modeling for the M5 cladding is fully and robustly compliant with the 10CFR50.46 requirements.

Figure I-18.1 Axial Distribution of Pre-Rupture Strain for M5 Cladding

[b,c,d]

Figure I-18.2 Slow Ramp Pre-Rupture Strain Fits

[b,c,d]

Figure I-18.3 Blockage Result with Alternate Slow Ramp Pre-Rupture Strain Fits [b,c,d]

I.19. Question19: The shape of the FTI pre-strain curve in the β phase (between 1000 to 2000°C) does not appear to be justified based on the data presented (3 data points for slow ramp rates and 2 data points for fast ramp rates). In addition, the β phase transformation is complete by 1000°C, which would suggest that perhaps the peak of the pre-strain should be at 1000°C. There is also one pre-strain data point near 1000°C for slow ramp rates that would suggest that the peak is near this temperature, but that is ignored (significantly underpredicted) by the FTI pre-strain curve. Are there additional pre-strain data to substantiate the FTI pre-strain curves?

If there are no additional data that are applicable, there are two alternatives: 1) Ignore the single rod pre-strain data altogether and adopt the NUREG-0630 methodology for determining flow blockage (based on rupture strains only -- the justification for this modeling change would be the observation in item 3-b above), or 2) assume that the pre-strain begins to peak near 1000°C and still fits the few data points that exist in the β phase. Please discuss the impact of the above two alternatives to modeling flow blockage in the β phase on M5 bundles (Mark B and BW designs) for LOCA analyses.

[

b,c,d

b,c,d

]

[

b,c,d

]

However, the consideration presented in the question may also be valid. The full transition to the β phase does occur at temperatures varying from just below 1000 C to perhaps a little above 1000 C depending on the heating rate. A general argument can be made that at high temperatures the ability of most materials to sustain strain without rupture decreases with increasing temperature. If applicable here, the hypothesis would indicate that M5 can sustain the largest secondary strains at the coldest temperature for which its crystalline structure is set. The argument may not be valid for specific alloys but when alloy-specific data are lacking it could form a reasonable physical basis for the pre-rupture curves.

[

b,c,d

]

[

b,c,d

b,c,d

b,c,d

]

[

b,c,d

]

[

b,c,d

b,c,d

]

FTI shares with the reviewer a deference to establishing the maximum pre-rupture strain near the $\alpha+\beta$ to β transition and has chosen to switch the pre-rupture curve to fit "a". The other fits, although providing useful sensitivity information, do not take sufficient accounting of all of the data to reflect a reasonable attempt at correlating the average fuel pin response in the assembly. [

b,c,d

]

To be consistent, if a physically realistic requirement is used to establish the slow ramp pre-rupture strain it should also be used for the fast ramp pre-rupture strain. Such a fit has been constructed, albeit with some license because [b,c,d] for the fast ramp beta region. The resultant slow and fast ramp rupture and pre-rupture strain fits are provided in Figures I-19.3 and I-19.4 with the measured pre-rupture data. The rupture data and fits have not been altered and reference is made to Figures C-6 and C-7 for data comparisons. Figures I-19.5 and I-19.6 present the respective strain curves along with the resultant flow blockage based on the revised pre-rupture strains. FTI proposes to

replace Figures C-34 and C-35 with Figures I-19.5 and I-19.6 for the M5 swelling and rupture model.

Figure I-19.1 Slow Ramp Pre-Rupture Strain with Alternative Beta Range Fits [b,c,d]

Figure I-19.2 Fuel Assembly Blockage Resulting from Alternative Beta Range Fits [b,c,d]

Figure I-19.3 M5 Rupture and Pre-Rupture Strain versus Rupture Temperature with Pre-Rupture Data, Slow Ramp Rate

[b,c,d]

Figure I-19.4 M5 Rupture and Pre-Rupture Strain versus Rupture Temperature with Pre-Rupture Data, Fast Ramp Rate

[b,c,d]

Figure I-19.5 M5 Strain and Blockage Curves for Slow Ramp Rates

[b,c,d]

Figure I-19.6 M5 Strain and Blockage Curves for Fast Ramp Rates

[b,c,d]

I.20. Question 20: Has the composition or specifications for the fabrication of the M5 cladding changed from that used to develop the data in the subject topical report or that used in the LTA irradiations? If so, please provide the differences and identify the data impacted.

Response to Question 20: The compositional range of Alloy M5 has not significantly changed. The data generated in the development program and documented in the topical report are from in-reactor and ex-reactor exposure of the alloy over it's full allowable range of chemical composition. In the course of the alloy's development however, the *specification* governing its constituency has been modified to tighten and optimize the allowable range for some alloying and impurity constituents. The final chemical composition of M5 was reported in the response to question 5 and a complete specification is as follows:

[	b,c,d	]
[	b,c,d	]

Impurities (ppm maximum)

[	b,c,d	]
[	b,c,d	]
[	b,c,d	]
[	b,c,d	]
[	b,c,d	]
[	b,c,d	]

The most important change in the nature of the M5 alloy during development was the [

b,c,d

] Earlier developmental precursors of

alloy M5 were [

b,c,d

]

Question 21: Please provide new M5 test and LTA data that have become available since the publication of the subject report.

Response to Question 21: New data for alloy M5 has become available. That data has been reported in responses to earlier questions where appropriate. All new data is the result of continued in-reactor exposure of LTA's containing fuel rods with alloy M5 cladding. A brief summary of new data is as follows:

- Completion of a sixth, one-year cycle in Cruas 2. [b,c,d] burnup attained. Subsequent fuel rod inspection revealed that the maximum average oxide thickness present on the M5 cladding was [b,c,d]and that the [b,c,d]The fuel rod growth showed [b,c,d] as shown in Figure I-9.2 in the response to question 9.

- Completion of a fifth, one-year cycle in Gravelines 5. Fuel rod inspection results consistent with data base.

- Completion of a fourth, one-year cycle in Doel 1. Approximately [b,c,d] burnup attained.

- Completion of the first, two year cycle in TMI 1. [b,c,d] burnup attained. The alloy performed well in this first long-cycle, higher lithium environment [b,c,d] The maximum average oxide thickness was[b,c,d] Fuel rod creep down was lower than that of the adjacent Zr-4 rods. Fuel rod growth as measured by shoulder gap closure was similar to Zr-4 rods as was shown in the response to question 9 in Table I-9.2.

- Completion of one, eighteen month cycle in North Anna 1. [b,c,d] burnup attained. Cladding oxide was not measured in the PIE campaign. The data base for first cycle oxide thickness on alloy M5 is extensive and this measurement was eliminated in favor of other PIE measurements in a limited time-frame for poolside measurements in this campaign. Fuel rod growth data were measured and were consistent with the M5 data base.

I.22. Question: Please provide cycle lengths in full power days for each of the plants listed in Table E-1. It appears that the LTA data taken to date are based on power operation that does not appear to be particularly aggressive, e.g., six cycles to achieve a burnup of 63 GWd/MTU and data from LTAs with more aggressive operation will not be obtained until calendar years 2000 to 2001. Is this observation correct?

Table I-22.1 lists the burnups and cycle lengths in EFPDs for each fuel cycle with M5 fuel rods. The highest burnup data is not particularly aggressive. However data from several plants has been obtained after operation under aggressive conditions, both for linear heat generation rate and heat flux. Those plants can be identified by the reactor conditions listed in table I-22.1. Although the burnups from these more aggressive cycles is lower, the performance trends as a function of burnup are similar as can be observed in the response to question 3.

Table I-22.1 M5 Experience

[b,c,d]

I.23. Question 23: Please provide the standard deviation and also the maximum and minimum values of the azimuthal average thicknesses quoted on page G-6 for the oxide, α and β phase thicknesses from M5 and Zr-4 samples. Also, please discuss the differences in the alpha-incursion behavior between Zr-4 and M5 samples at 1200 to 1300°C. Were equivalent cladding reacted (ECR) measurements performed on the other failed and un-failed specimens from the table on page G-5, other than those provided for the un-failed specimens with maximum oxidation? If so, please provide these values and how they were determined.

Response: The purpose of Appendix G is to demonstrate that the criteria of 10CFR50.46 are applicable to the M5 alloy. That is, they provide approximately the same degree of protection from adverse consequences when applied to M5 as they do for Zircaloy. As such, only those studies necessary to validate the criteria were performed. The following should provide most of the information requested and, where not specifically provided, an alternative is included to address the apparent concern.

Statistics have not been performed on the oxide measurements taken to support the applicability of the brittle fracture criterion. The variation of these measurements is not significant to the conclusions drawn from the tests and with only 12 measurements the standard deviation would not mean much. Tables I-23.1 through I-23.6 provide the full set of measurements taken for each of the Ziraloy-4 and M5 tests included in the tables on page G-6. In addition to the measurements, the tables provide the mean of the measurements, the deviation from the mean, and the mean of the absolute value of the deviations for each test. The procedure used to establish a measure of the oxide development, for validation of the 17 percent limit, was to combine the thickness of exterior and interior α layers with the β region thickness and subtract the result from the original cladding thickness. This simplifies the calculation because no adjustment for the growth of the zirconia layer is required and provides a conservatism in that the oxygen absorbed in the α layers is ignored. The mean is appropriate for this calculation. However, even if the combined α and β region thickness was increased by the mean of the absolute value of the measurement deviations, the resultant equivalent cladding reacted (ECR) would decrease by less than 1.5 percent and remain well above the 17 percent limit.

The measurements for the remaining samples in the brittle fracture tests are not readily available but metallographic data from the oxidation tests described in Appendix D are presented in Figures I-23.1 to I-23.12. These data are from the same testing apparatus excepting that the material was not rapidly quenched and tested for brittleness. As in the brittle fracture testing, oxidation occurs on both the outer and inner faces of the tube sample. These tests were conducted mostly at 1050 C, 1150 C, and 1250 C, making a one for one comparison with the brittle fracture testing impossible at all temperatures. Zircaloy samples, however, were also tested at 1100 C and those data demonstrate comparable development and progress of the zirconia, alpha and beta regions with the brittle fracture tests.

Figures I-23.1 through I-23.6 provide the transient development of the zirconia layer, the oxygen stabilized α layer, and the β core as determined from post-oxidation metallographic examination. The data provided are in terms of the thickness of the layers and regions and not the weight gain presented in Appendix D. Comparisons to Appendix D need to allow for the oxidation growth of the zirconia layers and the oxygen retention in the α layers. For the zirconia and the α layer, data are supplied for the layers developing from both of the tube surfaces. The data are fit to an exponential to allow easy comparison of trends. The decrease of the β region has not been fit to a curve and the data are simply connected by straight lines. ECR calculations can be reasonably performed by totaling the α and β layer thicknesses and subtracting from the cladding thickness, 559 μm for the Zircaloy samples and 601 μm for the M5 samples.

The development of the α regions for Zircaloy and M5 can also be observed in these data. Figures I-23.7 through I-23.12 compare the growth of the α regions for the two alloys and the decrease of the β regions at three oxidation temperatures. The fits provided in the figures are quite reasonable excepting the shortest duration Zr-4 data in Figure I-23.7 and I-23.10. [b,c,d

] However, there is not yet sufficient information to confirm such a

hypothesis.[

b,c,d

]

Figures I-23.10 through I-23.12 provide an alternative view of the α development in that the timing of the elimination of a β core can be observed. The M5 cladding used in the testing was thicker, 42 μm, than the Zircaloy tubes. This does not interfere with direct comparisons of the α layer development but direct comparison of the decrease of the β core is compromised. To correct this, Figures I-23.10 through I-23.12 contain a second curve for M5 which is the actual measured β thickness less 42 μm. [

b,c,d

] For higher temperature oxidation, probably above 1100 C, [

b,c,d

]

[

b,c,d

] It also shows that M5 does not require a core of prior β material to withstand brittle fracture. Further, the overall resistance to brittle fracture for M5 is comparable to that of Zircaloy and the 17 percent criterion can be applied to either material.

Table I-23.1 M5 Metallographic Examination, Oxidation Temperature 1100 C

[b,c,d]

Table I-23.2 M5 Metallographic Examination, Oxidation Temperature 1200 C

[b,c,d]

Table I-23.3 M5 Metallographic Examination, Oxidation Temperature 1300 C

[b,c,d]

Table I-23.4 Zr-4 Metallographic Examination, Oxidation Temperature 1100 C

[b,c,d]

Table I-23.5 Zr-4 Metallographic Examination, Oxidation Temperature 1200 C

[b,c,d]

Table I-23.6 Zr-4 Metallographic Examination, Oxidation Temperature 1300 C

[b,c,d]

Figure I-23.1 Zerconia (ZrO_2) Development in Zr-4

[b,c,d]

Figure I-23.2 Alpha Layer (Zr(O)) Development in Zr-4

[b,c,d]

Figure I-23.3 Beta Core (Zr) Depletion in Zr-4

[b,c,d]

Figure I-23.4 Zerconia (ZrO_2) Development in M5

[b,c,d]

Figure I-23.5 Alpha Layer (Zr(O)) Development in M5

[b,c,d]

Figure I-23.6 Beta Core (Zr) Depletion in M5

[b,c,d]

Figure I-23.7 Comparison of Alpha Layer Development in Zr-4 and M5 at 1050 C Oxidation Temperature

[b,c,d]

Figure I-23.8 Comparison of Alpha Layer Development in Zr-4 and M5 at 1150 C Oxidation Temperature

[b,c,d]

Figure I-23.9 Comparison of Alpha Layer Development in Zr-4 and M5 at 1250 C Oxidation Temperature

[b,c,d]

Figure I-23.10 Comparison of Beta Core Depletion in Zr-4 and M5 at 1050 C Oxidation Temperature

[b,c,d]

Figure I-23.11 Comparison of Beta Core Depletion in Zr-4 and M5 at 1150 C Oxidation Temperature

[b,c,d]

Figure I-23.12 Comparison of Beta Core Depletion in Zr-4 and M5 at 1250 C Oxidation Temperature

[b,c,d]

I.24. Question 24: The peak local oxidation values provided in Table F-3 (LOCA calculation at 40 GWd/MTU burnup) do not appear to include the cladding oxidation from normal operation. If so, please justify why this initial oxidation from normal operation is not included in the total amount of oxidation for LOCA to assess whether the 17% oxidation limit is exceeded. Also, for this same calculation (Table F-3), please provide the burnup level at which the gap closed for the Zr-4 clad fuel rods and for the M5 clad fuel rods.

Response: The initial oxidation thickness is included in the reported maximum local oxidation values in Table F-3. For both Zr-4 and M5 the initial oxidation was 0.2 mils on the inside of the cladding and 0.064 mils on the outside of the cladding. These accrue to a total initial oxide of about one percent of the cladding thickness. The values were determined in accordance with the FTI LOCA evaluation models (EMs), References I-24.1 and I-24.2, which control, as a function of burnup, the amount of initial cladding oxidation used in the LOCA calculations. The corrosion rates incorporated within the evaluation models were developed in the 1970s and underpredict the corrosion data available today. Underprediction is conservative for the evaluation of peak cladding temperature, and until recently, calculated maximum local oxidation was sufficiently low in comparison with the 10CFR50.46 criterion that the primary emphasis of LOCA calculations was peak cladding temperature. Therefore, because both the Zr-4 and the M5 initial oxidation, as controlled by the EMs, would be underpredicted it was not considered necessary to revise the EM correlations.

Over the last year the recognition of the degree of operational oxidation possible with new cycle designs, 18 and 24 months cycles, has prompted an industry and NRC review of EM practices in demonstrating compliance with the 17 % oxidation criterion of 10CFR50.46. The NRC has issued an information notice, IN 98-29 August 3, 1998, stating their expectation that the initial oxide thickness be included with the transient oxidation in the comparison to the criterion. This information notice does not, however, address the determination of the initial oxide layers, particularly relative to NRC approved procedures contained within the EMs. NEI has responded to the information notice with an opinion that the NRC has, in the past, accepted and perhaps directed that

only the oxidation developed during the transient be included in comparisons to the criterion. Such a position would be comparable with Japanese and French experimental results. To our knowledge all the major vendors have been actively involved with the NRC in attempts to resolve the issue. Pending resolution, FTI has made a verbal commitment to the NRC (telephone call with Ms. Margaret Chatterton of the NRC) to check the burnup dependency of the total local oxidation, initial (function of burnup) plus transient, based on realistic corrosion correlations to assure that the 17 % criterion would be met if such an approach were adopted.

As described, the procedures for demonstrating compliance with the 17 % criterion of 10CFR50.46 have become a generic issue and are being actively pursued by the NRC. The issue applies equally to Zircaloy cladding and the current round of advanced claddings. If anything, the advanced claddings moderate the issue because of their improved corrosion performance. Therefore, FTI does not believe that the generic issue should become involved with the review of M5 cladding and that the EM corrosion rates should be unaltered pending the outcome of the generic issue.

The burnup for which gap closure occurs varies as a function of pin design and is not cladding specific. Cold fill pressure, interior free volume, and operational history all participate in the determination of the gap closure. However, the M5 alloy does experience a slightly reduced creep rate from Zr-4 leading to a generalization that gap closure can be expected to take slightly longer for M5, all other considerations being equal. For the studies documented in Table F-3 this was true. The gap at the 6-foot elevation of the hot pins closed at approximately [b,c,d]for the Zr-4 pins and approximately [b,c,d] for the M5 pins.

References:

I-24.1 BAW-10168P-A, "RSG LOCA - BWNT Loss-of-Coolant Accident Evaluation Model for Recirculating Steam Generator Plants," Framatome Nuclear Technologies, Lynchburg, VA, December 1996.

I-24.2 BAW-10192P-A, "BWNT LOCA - BWNT Loss-of-Coolant Accident Evaluation Model of Once-Through Steam Generator Plants, Framatome Nuclear Technologies, Lynchburg, VA, June 1998.

I.25. Question 25: Please provide Arrhenius plots of the Zr-4 and M5 high temperature oxidation data. Please provide a discussion of the uncertainties and potential biases in the optical pyrometer temperature measurement Appendices D and G. Were independent temperature measurements performed on oxidized M5 material to confirm uncertainties and lack of bias in the optical pyrometer measurement?

Response: Figures I-25.1 and I-25.2 provide Arrhenius plots for the Ziraloy-4 and M5 data provided in Appendix D of BAW-10227. Data of the type requested are not readily available for the testing reported in Appendix G. Appendix G is intended to show only that M5 was stable upon quenching over an appropriate temperature range provided the amount of oxidation does not exceed 17 percent. The demonstration relied primarily on metallographic examination of the sample with oxidation temperature being only a secondary consideration. The information in Appendices D and G, however, is obtained from the same test apparatus with a modification of the sample size and changes in the testing procedure to produce a rapid quench for the Appendix G results. Further, for the one common oxidation temperature between the two test programs, the results are complementary. Therefore, Figures I-25.1 and I-25.2 can be applied and interpreted as applicable to the data used in both Appendices.

The oxidation process is most frequently correlated in the form:

$$WG^2 = K \cdot t \quad ,$$

where WG => weight gain during oxidation

t => time

$K = C \cdot e^{-Q/(R \cdot T)}$

C = a constant

T = temperature, K

R = the gas constant and

Q = a constant, the activation energy for the process.

Combining these and taking the logarithms gives the expression:

$$\ln(WG^2/t) = \ln(C) - \frac{Q}{R} \cdot \frac{1}{T} \quad ,$$

the Arrhenius form. Figures I-25.1 and I-25.2 validate this correlation form for both M5 and Zr-4 high temperature oxidation against the weight gain data taken during the oxidation testing for Appendix D.

The premise for the tests conducted to support the high temperature oxidation performance of M5 was to demonstrate the relative behavior of M5 versus Zircaloy-4. Particularly for the work documented in Appendix D, high temperature oxidation kinetics, there is little to gain by obtaining additional information. 10CFR50.46 Appendix K specifies the Baker/Just oxidation correlation by law. Even if it were possible to demonstrate that a material oxidized substantially more slowly than Zircaloy-4, the analysis of that material during LOCA under an Appendix K evaluation model could not credit the reduction. On the other hand, it is necessary to show that the material does not oxidize substantially faster than Zircaloy-4 so that the Baker/Just correlation remains conservative. Essentially the same is true for Appendix G. So long as the degree of brittleness experienced by M5 for oxidations between 20 and 30 percent is comparable to that of Zircaloy-4, the 17 percent limitation of 10CFR50.46 applies and the margin of safety expected from the criterion is preserved with the new material. Within Appendices D and G both of these facts are evidenced by testing that demonstrates the comparative behavior of M5 and Zircaloy-4. To do this it is only necessary that the experiments be conducted with the same apparatus, using the same procedures, and within the general range of interest. All of this is true regardless of measurement bias, if there was any, in the optical pyrometers.

Nonetheless, the experiments were not so shallow. It was determined in preliminary testing that the attachment of thermocouples to the test samples perturbs the sample

temperature distribution and oxidation distribution creating unnecessary uncertainties in the results. Therefore, optical pyrometers which require no physical connection were selected for the temperature measurement and no thermocouples used. Except for preliminary testing, there were no backup or benchmark thermocouple measurements. However, during preliminary testing comparisons were made between the thermocouples and pyrometers that validated the optical approach.

Two IRCOM MODLINE series 2000 pyrometers, a monochromatic and a bichromatic, were used for temperature measurements. Both pyrometers were calibrated on site by the vendor prior to the test program. Calibration to a reference tungsten lamp was performed prior to each test. The intrinsic measurement uncertainty for these pyrometers is 10 C between 700 and 1300 C. During each test the measurements of the two pyrometers are compared and they have demonstrated essentially perfect consistency throughout the program. Further confidence in the reasonableness of the temperature measurements is obtained from the consistency of the Zircaloy-4 results with those of other laboratories.

In addition to the direct ability to measure temperature, uncertainty arises from the testing configuration. The temperature measurement is for the exterior oxide surface. The typical correlation for the oxidation is the metal temperature, either surface or core. The temperature drop across the oxide increases as oxidation increases, building to around 10 to 15 C for a zirconia layer of 100 μm. This uncertainty could increase if the sample were to experience spalling or incipient spalling in the pyrometer measurement zone. However, such conditions would be observed in metallographic examinations and none were. Although the heat deposition in the sample will be relatively uniform throughout the α and β regions, the interior surface of the sample tube will be a little hotter than the exterior surface because there is less radiation heat loss potential from the inner surface. In combination these effects tend to create a bias toward a conservative oxidation rate on the order of 5 to 15 C. The bias will be toward the lower value for the low temperature tests and may approach the 15 C range for the 1300 C testing. Another source of uncertainty is the potential for water retention in the oxide after oxidation. This was essentially eliminated by doing the post-oxidation weighing before water pickup could

occur. In combination, the overall accuracy of the testing is judged to be within [b,c,d] with the expectation of a slight conservative bias. The measured oxidation rate is considered to be higher than that which would occur for a sample truly at the indicated temperature.

Figure I-25.1. Arrhenius Plot of Weight Gain for M5

[b,c,d]

Figure I-25.2. Arrhenius Plot of Weight Gain for Zr-4

[b,c,d]

Beginning of Enclosure 1

LISTING OF CHANGES IMPLEMENTED IN REVISION 4 OF RELAP5/MOD2-B&W TOPICAL REPORT

Page	Type/Change	Item	Reason
--	Revision	Title page	Revision & Date
i-ii	Revision	Abstract	Revision & Date
v	Addition	Revision Record	New topical version
xii	Revision	Table/Contents, etc.	New revisions
1-1	Addition	Introduction	Non-zircaloy cladding
2.1-126 to 2.1-126.2	Addition	Void-Dependent Cross-flow	New code option
2.3-25 to 2.3-28	Addition	EM Pin Model Changes	Non-zircaloy cladding
2.3-37	Addition	EM Pin Model Changes	Non-Zircaloy cladding
2.3-39 to 2.3-41	Addition	EM Pin Model Changes	Non-Zircaloy cladding
2.3-45 to 2.3-46.2.2	Addition	EM Pin Model Changes	Non-Zircaloy cladding
2.3-52	Correction	EM Pin Model	Non-Zircaloy cladding
2.3-55	Addition	Steady-State EM Pin Model	Fuel temperature convergence
5-364.1 to 5-364.2	Correction	Missing SER Page	Include missing page

(NOTE: Pages 2.1-126.1, 2.1-126.2, 2.3-27.1, 2.3-27.2, 2.3-46.2.1, 2.3-46.2.2, 5-364.1, and 5-364.2 were added in Revision 4)

BAW-10164P
Topical Report
Revision 4
April 1999

- RELAP5/MOD2-B&W -

An Advanced Computer Program for Light Water Reactor LOCA and Non-LOCA Transient Analysis

Framatome Technologies Inc.
P. O. Box 10935
Lynchburg, Virginia 24506

Framatome Technologies Inc.
Lynchburg, Virginia

Topical Report BAW-10164P
Revision 4
April 1999

RELAP5/MOD2-B&W

An Advanced Computer Program for Light Water Reactor LOCA and Non-LOCA Transient Analysis

Key Words: RELAP5/MOD2, LOCA, Transient, Water Reactors

Abstract

This document describes the physical solution technique used by the RELAP5/MOD2-B&W computer code. RELAP5/MOD2-B&W is a Framatome Technologies Incorporated (previously known as and refered to in the text as B&W or B&W Nuclear Technologies) adaption of the Idaho National Engineering Laboratory RELAP5/MOD2. The code developed for best estimate transient simulation of pressurized water reactors has been modified to include models required for licensing analysis of zircaloy or non-zircaloy fuel assemblies. Modeling capabilities are simulation of large and small break loss-of-coolant accidents, as well as operational transients such as anticipated transient without SCRAM, loss-of-offsite power, loss of feedwater, and loss of flow. The solution technique contains two energy equations, a two-step numerics option, a gap conductance model, constitutive models, and component and control system models. Control system and secondary system components have been added to permit modeling of plant controls, turbines, condensers, and secondary feedwater conditioning systems. Some discussion of the numerical techniques is presented. Benchmark

comparison of code predictions to integral system test results are presented in an appendix.

Topical Revision Record

Documentation Revision	Description	Program Change?	Program Version
0	Original issue	_____	8.0
1	Typographical corrections Replace CSO correlation with Condie-Bengston IV	yes	10.0
2	SBLOCA modifications Miscellaneous corrections	yes	18.0
3	EM Pin Enhancements Filtered Flows for Hot Channel Heat Transfer Rupture Area Enhancement for Surface Heat Transfer OTSG Improvements and Benchmarks using the Becker CHF, Slug Drag, and Chen Void Ramp	yes	19.0
4	Non-zircaloy pin changes Option for multiple pin channels in a single core fluid channel Void-dependent core cross flow option	yes	23.0

This page is intentionally left blank.

LIST OF FIGURES (Cont'd)

LIST OF FIGURES (Cont'd)

1. INTRODUCTION

RELAP5/MOD2 is an advanced system analysis computer code designed to analyze a variety of thermal-hydraulic transients in light water reactor systems. It is the latest of the RELAP series of codes, developed by the Idaho National Engineering Laboratory (INEL) under the NRC Advanced Code Program. RELAP5/MOD2 is advanced over its predecessors by its six-equation, full nonequilibrium two-fluid model for the vapor-liquid flow field and partially implicit numerical integration scheme for more rapid execution. As a system code, it provides simulation capabilities for the reactor primary coolant system, secondary system, feedwater trains, control systems, and core neutronics. Special component models include pumps, valves, heat structures, electric heaters, turbines, separators, and accumulators. Code applications include the full range of safety evaluation transients, loss-of-coolant accidents (LOCAs), and operating events.

RELAP5/MOD2 has been adopted and modified by B&W for licensing and best estimate analyses of PWR transients in both the LOCA and non-LOCA categories. RELAP5/MOD2-B&W retains virtually all of the features of the original RELAP5/MOD2. Certain modifications have been made either to add to the predictive capabilities of the constitutive models or to improve code execution. More significant, however, are the B&W additions to RELAP5/MOD2 of models and features to meet the 10CFR50 Appendix K requirements for ECCS evaluation models. The Appendix K modifications are concentrated in the following areas: (1) critical flow and break discharge, (2) fuel pin heat transfer correlations and switching, and (3) fuel clad swelling and rupture for both zircaloy and non-zircaloy cladding types.

This report describes the physical models, formulation, and structure of the B&W version of RELAP5/MOD2 as it will be applied to ECCS and system safety analyses. It has been prepared as a stand-alone document; therefore substantial portions of the text that describe the formulation and numerics have been taken directly from original public domain reports, particularly NUREG/CR-4312[1]. Chapter 2 presents the method of solution in a series of subsections, beginning with the basic hydrodynamic solution including the field equations, state equations, and constitutive models in section 2.1. Certain special process models, which require some modification of the basic hydrodynamic approach, and component models are also described. The general solution for heat structures is discussed in section 2.2. Because of the importance of the reactor core and the thermal and hydraulic interaction between the core region and the rest of the system, a separate section is dedicated to core modeling. Contained in section 2.3 are the reactor kinetics solution, the core heat structure model, and the modeling for fuel rod rupture and its consequences. Auxiliary equipment and other boundary conditions are discussed in section 2.4 and reactor control and trip function techniques in section 2.5. Chapter 3 provides an overview of the code structure, numerical solution technique, method and order of advancement, and initialization. Time step limitation and error control are presented in section 3.3.

The INEL versions of RELAP5/MOD2 contain certain solution techniques, correlations, and physical models that have not been selected for use by B&W. These options have been left intact in the coding of the B&W version, but descriptions have not been included in the main body of this report. Appendix A contains a list of those options that remain in the RELAP5/MOD2 programming but are not used by B&W and not submitted for review. A brief description of each along with a reference to an appropriate full discussion is provided in the appendix. Appendix B defines the nomenclature used throughout this report. Appendix G documents

$v_{J,3}$ not be included in the volume average (axial) velocity calculation for cell L.

The second area of numerical modification relates to the reduced form of the momentum equations to be used at a crossflow junction. In crossflow junctions, the cross product momentum flux terms are neglected, that is, there is no x-direction transport of momentum due to the y velocity.

For the case of a small crossflow junction between two axial-flow streams (J_2 in Figure 2.1.4-7) all the geometric input (AVOL, DX, DZ) for both of the volumes relates to the axial flow direction as does the wall drag and code calculated form losses. Since the crossflow has a different flow geometry and resistance (for example, crossflow resistance in a rod bundle) the friction and form losses must be user input and must be appropriate for the crossflow direction geometry. For crossflow junctions the user input form losses should include all crossflow resistance (form losses and wall drag). The normal terms representing wall drag and abrupt area change losses are not included in the formulation of the momentum equation at a crossflow junction as these refer to the axial properties of the K and L volumes.

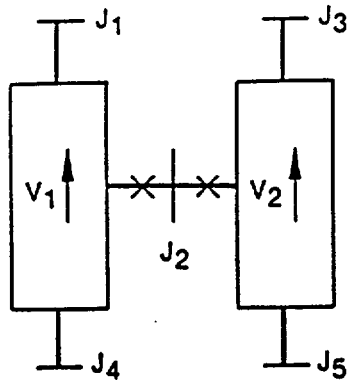

Figure 2.1.4-7. Modeling of Crossflows or Leak.

Since the connecting K and L volumes are assumed to be predominately axial-flow volumes, the crossflow junction momentum flux (related to the axial volume velocity in K and L) is neglected along with the associated numerical viscous term. In addition, the horizontal stratified pressure gradient is neglected.

All lengths and elevation changes in the one-dimensional representation are based upon the axial geometry of the K and L volumes and the crossflow junction is assumed to be perpendicular to the axial direction and of zero elevation change, thus, no gravity force term is included.

The resulting vapor momentum finite difference equation for a crossflow junction is

$$\left(\alpha_g \rho_g\right)_j^n \left(v_g^{n+1} - v_g^n \right)_j \Delta x_j = - \alpha_{g,j}^n \left(P_L - P_K\right)^{n+1} \Delta t$$

$$- \left(\alpha_g \rho_g\right)_j^n \mathrm{HLOSSG}_j^n \, v_{g,j}^{n+1} \, \Delta t$$

$$- \left(\alpha_g \rho_g\right)_j^n \mathrm{FIG}_j^n \left(v_{g,j}^{n+1} - v_{f,j}^{n+1} \right) \Delta x_j \Delta t$$

$$+ \text{ADDED MASS + MASS TRANSFER MOMENTUM.} \qquad 2.1.4\text{-}72$$

A similar equation can be written for the liquid phase. In Equation 2.1.4-72, HLOSSG_j^n contains only the user-input crossflow resistance. The Δx_j term that is used to estimate the inertial length associated with crossflow is defined using the diameters of volumes K and L,

$$\Delta x_j = \frac{1}{2} [D(K) + D(L)] \quad .$$ 2.1.4-73

A special void-dependent form loss option of the full crossflow model has been added for certain multi-core channel applications. This option allows the user to alter the input constant form loss coefficient based on the void fraction in the upstream volume. The specific applications are possibly multi-channel core analyses such as SBLOCA scenarios with significant core uncovering or future multi-channel BEACH reflooding calculations. This model allows the regions of the core covered by a two-phase mixture or pool to have a resistance that is different from that in the uncovered or steam region. The crossflow resistance changes can alter the volume-average axial velocities that are used to determine the core surface heat transfer. Any cross flow is excluded from the volume average velocity used for heat transfer.

The model uses the input form loss coefficients whenever the upstream steam void fraction is less than a user-supplied minimum void fraction value given as $\alpha_{min\text{-}Kcross}$. The model allows user input of a forward, $M_{K\text{-}forward}$, and reverse, $M_{K\text{-}reverse}$, crossflow resistance multiplier when the upstream steam void fraction is greater than the maximum user-input void fraction, $\alpha_{max\text{-}Kcross}$. Linear interpolation is used to determine the multiplicative factor when the void fraction is between minimum and maximum input void fractions as indicated in the following equations. For the forward flow direction (from Volume K to Volume L),

If $\alpha_g(K) < \alpha_{min\text{-}Kcross}$	$K_{jun} = K_{jun\ forward}$
If $\alpha_{max\text{-}Kcross} \leq \alpha_g(K)$	$K_{jun} = K_{jun\ forward} * M_{K\text{-}forward}$
If $\alpha_{min\text{-}Kcross} \leq \alpha_g(K) < \alpha_{max\text{-}Kcross}$	$K_{jun} = K_{jun\ forward} * M_{Kf\ interp}$

2.1.4-73.1

where

$$M_{kf\ interp} = 1 - (1 - M_{K\text{-}forward}) * [\ \alpha_{min\text{-}Kcross} - \alpha_g(K)\ ] / (\alpha_{min\text{-}Kcross} - \alpha_{max\text{-}Kcross})$$

and $K_{jun\ forward}$ is the user-supplied forward loss coefficient specified in this junction input.

The equation for the reverse flow direction (from Volume L to Volume K) is similar.

$$\begin{aligned}
&\text{If} && \alpha_g(L) < \alpha_{min\text{-}Kcross} && K_{jun} = K_{jun\ reverse} \\
&\text{If } \alpha_{max\text{-}Kcross} \le \alpha_g(L) && && K_{jun} = K_{jun\ reverse} * M_{K\text{-}reverse} \\
&\text{If } \alpha_{min\text{-}Kcross} \le \alpha_g(L) < \alpha_{max\text{-}Kcross} && && K_{jun} = K_{jun\ reverse} * M_{Kr\ interp}
\end{aligned}$$

2.1.4-73.2

where

$$M_{Kr\ interp} = 1 - (1 - M_{K\text{-}reverse}) * [\ \alpha_{min\text{-}Kcross} - \alpha_g(L)\ ] / (\alpha_{min\text{-}Kcross} - \alpha_{max\text{-}Kcross})$$

and $K_{jun\ reverse}$ is the user-supplied reverse loss coefficient specified in this junction input.

The code performs several input checks to ensure that the user input will not cause code failures. These checks include tests to see if the input form loss multipliers are greater than zero. The minimum void fraction must be greater than zero and less than the maximum void fraction input. The maximum void fraction must be less than or equal to one.

The crossflow option can be used with the crossflow junction perpendicular to the axial flow in Volume L (or K) but parallel

2.3.2. Core Heat Structure Model

The ordinary RELAP5 heat structures are general in nature and can be used for modeling core fuel pins; however, licensing calculations require special treatment of the fuel pin heat transfer. To accommodate these requirements, two additional models, commonly referred to as the EM (Evaluation Model) pin and core surface heat transfer models, were added to the code. The EM pin model calculates dynamic fuel-clad gap conductance, fuel rod swell and rupture using either NUREG-0630[117] or user input options (for modeling M5 cladding or other new cladding material types), and cladding metal-water reaction. The core fuel pin surface heat transfer is calculated with a flow regime-dependent set of correlations that include restrictions on which correlations can be selected per NRC licensing requirements. These new models are independent and mutually exclusive of the original system heat transfer model (described in section 2.2.2) and the existing simple gap conductance model[118] (referenced in Appendix A). The new models are explicitly coupled to the solution scheme through the modification of the gap conductance term, addition of fluid hydraulic resistance upon rupture, deposition of metal-water reaction energy in the clad, and determination of fuel pin surface heat transfer. The new EM pin model calculations are described in this section, while the EM heat transfer description is contained in section 2.3.3.

The EM pin model consists of three basic parts:

1. Dynamic fuel-clad gap conductance,
2. Fuel rod swell and rupture using NUREG-0630 or user specified swell and rupture options, and
3. Clad metal-water reaction,

which couple explicitly to the heat structure solution scheme or add fluid hydraulic resistance upon rupture. The model may be

executed either in a steady-state initialization or transient mode determined by user input.

The pin calculations are performed on single fuel rod which represent the average behavior of a large number of rods. Each rod (also termed channel) can be broken into up to ninety heat structures, each having an associated pin segment. The gap conductance, deformation mode, and metal-water reaction are determined for each individual segment based on the channel specific pin pressure.

The changes to the EM pin model included in Version 21 and later code versions are:

1. User options to model zircaloy and/or M5 cladding (or other material types) in the same problem,

2. User options to specify the pin channel as a primary or supplemental channel for additive form loss and BEACH droplet breakup calculations upon pin rupture, and

3. Integration of the NRC SER limitation (BEACH code-BAW-10166, Rev. 2 dated 8/13/90) for use of a maximum flow blockage of 60 percent in the ruptured cladding droplet breakup calculations.

The option to allow non-zircaloy cladding types requires user input to identify which pin channels are zircaloy and which are not. The non-zircaloy cladding also requires additional user input to specify the material properties necessary to calculate the transient cladding swell and rupture behavior.

The supplemental pin capability was added to improve the calculational methods that require modeling of multiple EM pin channels within a single hydrodynamic fluid channel (i.e., an

assembly or a group of assemblies) for LOCA applications. The relationship between the supplemental pin and the remainder of the pins in a common fluid channel is one in which the supplemental pin swell and rupture will not define the rupture flow blockage for the entire channel. Rather it will define a local effect that should not be used in determination of the channel droplet breakup parameters and the additive form loss due to rupture. These parameters should be controlled by the larger group of pins (i.e. primary channel) and not the smaller grouping (i.e. supplemental channel). The supplemental rod modeling is particularly useful for gadolinia or lead test pin (M5) analyses. It may also be used in future EM revisions for hot pin applications, in which the hot pin has a higher radial peak or a different initial fuel temperature.

2.3.2.1. Transient Dynamic Fuel-Clad Gap Conductance

The RELAP5 heat structure conduction scheme uses cold, unstressed geometrical dimensions for its solution technique. The dynamic gap conductance, h_{gap}, is calculated from hot stressed conditions from which an effective gap thermal conductivity, $\bar{K}_{gap}$, based on cold gap size, $\tau_{g_{cold}}$, is determined for each pin segment.

$$\bar{K}_{gap} = h_{gap} \cdot \tau_{g_{cold}} . \qquad 2.3.2\text{-}1$$

The gap conductance is determined by calculating the gap gas conductivity, temperature jump gap distance, radiation component, and dynamic fuel-clad gap from the deformation models. An additive fuel-clad contact conductance term has also been included as an option to simulate the closed gap contribution for high fuel rod burn-up applications. Two options are provided to

calculate the conductance. The first option assumes that the fuel pellet is concentric within the clad, while the second option assumes the fuel pellet is non-concentric within the clad as illustrated in Figure 2.3.2-1.

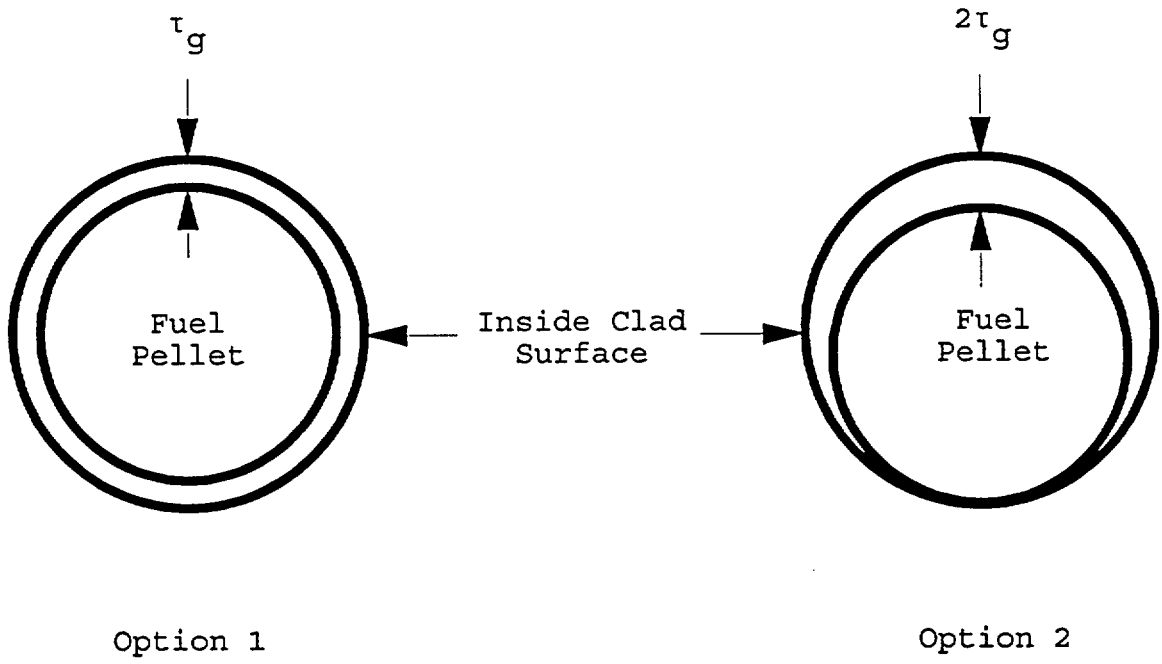

Figure 2.3.2-1. Gap Conductance Options.

Eight half-symmetrical azimuthal sections are used for determining the overall conductance for the second option without calculating an azimuthal temperature gradient. The total gap conductance is determined by

$$h_{gap} = M_g \, h_{\substack{gap \\ gas}} + h_{rad} + h_{fcc} \qquad 2.3.2\text{-}2$$

with

h_{gap} = conductance through gap gas (w/m^2-K),

M_g = user input multiplier used to acquire correct initial temperature within fuel,

$h_{\substack{gap \\ gas}}$ = gap gas conductance contribution (w/m^2-K),

h_{rad} = conductance due to radiation contribution from fuel to clad (w/m^2-K), and

h_{fcc} = gap contact conductance contribution due to fuel-cladding mechanical interaction (w/m^2-K).

The radiation gap conductance contribution is calculated by

$$h_{rad} = \frac{\sigma}{\frac{1}{e_f} + \frac{r_f}{r_{ic}}\left(\frac{1}{e_c} - 1\right)} \left[\frac{T_{fs}^4 - T_{ics}^4}{T_{fs} - T_{ics}}\right]$$

$$= \frac{\sigma(T_{fs}^2 + T_{ics}^2)(T_{fs} + T_{ics})}{\frac{1}{e_f} + \frac{r_f}{r_{ic}}\left(\frac{1}{e_c} - 1\right)}, \qquad 2.3.2\text{-}2.1$$

where

σ = Stefan-Boltzmann constant,

= 5.6697×10^{-8} $(w/m^2\text{-}K^4)$,

e_f = emissivity of fuel surface,

e_c = emissivity of clad-inside surface,

T_{fs} = fuel outside surface temperature (K), and

T_{ics} = clad-inside surface temperature (K).

The radial strain function is defined by either a user input table as a function of cladding temperature for material types other than zircaloy or a built in code correlation set for zircaloy cladding[119] consisting of

$$\epsilon_{TC} = -2.0731 \cdot 10^{-3} + 6.721 \cdot 10^{-6} \, T_C \qquad 2.3.2\text{-}22$$

for $T_C \leq 1073.15$ K (α phase), and

$$\epsilon_{TC} = -9.4495 \cdot 10^{-3} + 9.7 \cdot 10^{-6} \, T_C \qquad 2.3.2\text{-}23$$

for $T_C \geq 1273.15$ K (β phase), where T_C is the average cladding temperature (K). In the α phase to β phase transition zone, $1073.15 \text{ K} < T_C < 1273.15$ K, a table lookup is used. Some selected values are listed in Table 2.3.2-2.

Table 2.3.2-2. Thermal Strain of Zircaloy for $1073.15 \text{ K} < T < 1273.15$ K.

T(K)	Radial Strain ϵ_{TC}	Axial Strain ϵ_{ATC}
1073.15	$5.14 \cdot 10^{-3}$	$3.53 \cdot 10^{-3}$
1093.15	$5.25 \cdot 10^{-3}$	$3.50 \cdot 10^{-3}$
1103.15	$5.28 \cdot 10^{-3}$	$3.46 \cdot 10^{-3}$
1123.15	$5.24 \cdot 10^{-3}$	$3.33 \cdot 10^{-3}$
1143.15	$5.15 \cdot 10^{-3}$	$3.07 \cdot 10^{-3}$
1183.15	$4.45 \cdot 10^{-3}$	$1.50 \cdot 10^{-3}$
1223.15	$2.97 \cdot 10^{-3}$	$1.10 \cdot 10^{-3}$
1273.15	$2.90 \cdot 10^{-3}$	$1.40 \cdot 10^{-3}$

The average clad temperature is calculated via a volume weighted average.

$$T_C = \sum_{n=N_f+2}^{N_{HS}} \frac{(r_{n+1}^2 - r_n^2)}{(r_{N_{HS}+1}^2 - r_{N_f+2}^2)} \left[\frac{(T_{n+1} + T_n)}{2}\right]. \qquad 2.3.2\text{-}24$$

The maximum clad average temperature is calculated for each EM pin channel and written at each major edit and at the end of each case. The segment number and time of the peak cladding temperature is also specified. The fuel volume weighted average temperature, $\bar{T}_f$, is calculated similarly to the cladding.

$$\bar{T}_f = \sum_{n=1}^{N_f} \frac{(r_{n+1}^2 - r_n^2)}{(r_{N_f+1}^2 - r_1^2)} \left[\frac{(T_{n+1} + T_n)}{2}\right] . \qquad 2.3.2\text{-}25$$

The elastic deformation, u_e, is calculated by

$$u_e = \left[\frac{r_{N_{HS}+1} + r_{N_f+2}}{2}\right] \left[\frac{\sigma_h - \upsilon\sigma_z}{E}\right] , \qquad 2.3.2\text{-}26$$

where

E = Young's modulus for clad (Pa),

σ_h = segment clad hoop stress (Pa),

σ_z = channel clad axial stress (Pa), and

υ = Poisson's ratio for clad (dimensionless).

The channel axial stress is the same for all segments in the channel and is determined by

$$\sigma_z = \frac{P_g\, r_{ic_{cold}}^2 - P_f\, r_{oc_{cold}}^2}{r_{oc_{cold}}^2 - r_{ic_{cold}}^2} . \qquad 2.3.2\text{-}27$$

Young's modulus is given either by the code for zircaloy cladding as

$$E = \begin{cases} 1.088 \cdot 10^{11} - 5.475 \cdot 10^{7}\ T_c; & \text{for } 1090K \geq T_c \\ 1.017 \cdot 10^{11} - 4.827 \cdot 10^{7}\ T_c; & \text{for } 1240K \geq T_c > 1090K \\ 9.21 \cdot 10^{10} - 4.05 \cdot 10^{7}\ T_c; & \text{for } 2027K \geq T_c > 1240K \\ 1.0 \cdot 10^{10}; & \text{for } T_c > 2027K, \end{cases}$$

2.3.2-28

or by a user-specified cubic equation that can be used for non-zircaloy cladding

$$E = C_1 T_c^{\,3} + C_2 T_c^{\,2} + C_3 T_c + C_4 \ . \qquad 2.3.2\text{-}29$$

Poisson's ratio is a constant which is defined as 0.30 for zircaloy by the code, however, the user can over-ride this value for non-zircaloy cladding types.

The normalized heating ramp rate for the elastic mode is determined by one of two methods. The code calculates an instantaneous heating rate for one method, while the other method sets the rate to a normalized user-input value between 0 and 1. The calculated heating rate is normalized via a constant value, H_{Rnorm}, of 28 K/s for zircaloy cladding or a user input for other cladding materials.

$$H = \left\{\frac{dT_c}{dt}\right\} \Big/ H_{Rnorm}$$

$$= \left\{\frac{T_c^{\,n} - T_c^{\,n-1}}{t^{\,n} - t^{\,n-1}}\right\} \Big/ H_{Rnorm} \ . \qquad 2.3.2\text{-}30$$

The normalized heating rate is always limited to values between 0 and 1 or(0 K/s / H_{Rnorm}) $\leq$ H $\leq$ (28 K/s / H_{Rnorm} = 1) for zircaloy cladding and between ($H_{slow\ input}$ / H_{Rnorm}) $\leq$ H $\leq$ ($H_{fast\ input}$ / H_{Rnorm}) for

other cladding types. This limit is applied to H prior to using it in any subsequent checking or calculations. The superscripts reflect the current time, n, and old time, n-1, values. The non-zircaloy slow or fast ramp rate divided by the normalized rate is still limited between 0 and 1, but they do not have to be equal to 0 or 1. Values greater than 0 or less than 1 activate the slow or fast ramp curves at different normalized heating rates.

Mode 2: Unruptured Elastic and Thermal Deformation Within 166.7K (300 F) of the Rupture Temperature

When the clad average temperature is within 166.7K (300 F) of the rupture temperature, the elastic inside clad radius is calculated as shown in Mode 1. This radius is compared against the plastic inside clad radius calculated in Mode 3. If the elastic radius is greater than the plastic radius, then Mode 2 is retained and the inside clad radius is set to the elastic radius. If not, the clad becomes plastic (Mode 3) and the plastic clad calculations are used. An informative message is printed when a segment first becomes plastic. No return to elastic Modes (1 or 2) is permitted once the clad becomes plastic.

$$r_{ic} = MAX(r_{ic_{elastic}}, r_{ic_{plastic}}) . \qquad 2.3.2\text{-}31$$

If $r_{ic_{elastic}} \geq r_{ic_{plastic}}$, Mode = 2 .

If $r_{ic_{elastic}} < r_{ic_{plastic}}$, Mode = 3 .

Mode 3: Unruptured Plastic Deformation

The unruptured plastic deformation is determined by the plastic strain, ϵ_p.

$$r_{ic} = r_{ic_{cold}}(1 + \epsilon_p), \qquad 2.3.2\text{-}32$$

with

$$\epsilon_p = \epsilon_{cps} \exp[-0.02754 (T_{rupt} - T_c)], \qquad 2.3.2\text{-}33$$

where ϵ_{cps} is 0.2 * ϵ_B (ϵ_B is the burst strain) based on NUREG-0630 for maximum cladding plastic strain and on user input tables for non-zircaloy cladding. The plastic strain or burst strain is determined by a double interpolation relative to H and T_{rupt} in the user input or default NUREG-0630 burst strain Tables 2.3.2-3 and 2.3.2-4. The plastic strain behaves as a ratchet. Once a given plastic strain is reached, no decrease in its value is allowed. In other words, for plastic mode calculations

$$r_{ic} = MAX(r_{ic}^{n}, r_{ic}^{n-1}), \qquad 2.3.2\text{-}34$$

where the superscripts refer to the current and old time values.

If the plastic mode is selected, the normalized heating ramp rate is calculated from any of three user options: user input constant, average ramp rate, or plastic weighted ramp rate. The normalized average ramp rate is calculated from

$$H = \left\{ \frac{T_c^n - T_c^P}{t^n - t^P} \right\} \Big/ \quad H_{Rnorm} \quad , \qquad 2.3.2\text{-}35$$

where

t = time (s),

n = superscript defining the current time, and

p = superscript defining the time in which the clad first went plastic.

The normalized plastic weighted ramp is calculated by

$$H = \left[\frac{\int_{t^p}^{t^n} W(T) \left\{ \frac{dT_c}{dt} \right\} dt}{\int_{t^p}^{t^n} W(T)\, dt} \right] \Big/ \quad H_{Rnorm} \qquad 2.3.2\text{-}36$$

Table 2.3.2-3. NUREG-0630 Slow-Ramp Correlations for Burst Strain and Flow Blockage.

Rupture temperature, C	≤10 C/S burst strain, %	≤10 C/S flow blockage, %
600	10	6.5
625	11	7.0
650	13	8.4
675	20	13.8
700	45	33.5
725	67	52.5
750	82	65.8
775	89	71.0
800	90	71.5
825	89	71.0
850	82	65.8
875	67	52.5
900	48	35.7
925	28	20.0
950	25	18.0
975	28	20.0
1000	33	24.1
1025	35	25.7
1050	33	24.1
1075	25	18.0
1100	14	9.2
1125	11	7.0
1150	10	6.5
1175	10	6.5
1200	10	6.5

noding options) chosen by the user. The fine mesh noding option computes the inside radius as

$$r_{ic} = r_{ic_{cold}} (1 + \epsilon_B) \ . \qquad 2.3.2\text{-}39$$

With this option, the gap conductance is calculated as though there is steam in the gap. The steam thermal conductivity is evaluated at the gap temperature and used with the hot gap size to compute the conductance. This option also calculates inside metal-water reaction for the ruptured segment.

The coarse mesh noding option computes the inside clad radius as

$$r_{ic} = r_{ic_{cold}} (1 + \epsilon_{cps}) \ . \qquad 2.3.2\text{-}40$$

This option uses the regular gap gas conductance and does not consider inside metal-water reaction. It is intended for use nominally when the expected rupture length is small when compared to the total segment length. The microscopic effects at the rupture site considered with the fine mesh option are expected to be negligible when compared to the longer segment behavior. With the coarse mesh option, the overall behavior will be more closely controlled by the entire segment rather than just the rupture site conditions.

Within the ruptured channel various calculations are modified at the time of rupture. Each segment within that channel undergoes a mode change. The pin pressure becomes that of the hydrodynamic volume associated with the ruptured segment. An additive form loss coefficient is calculated at rupture based on the clad flow blockage by a simple expression for an abrupt contraction-expansion.

$$K_{add} = \frac{0.5(1 - \beta^2) + (1 - \beta^2)^2}{(\beta^2)^2}, \qquad 2.3.2\text{-}41$$

where

β^2 = fraction of the channel flow area blocked,

= $(1.0 - A_{blocked}/A_{channel})$.

The flow blockage is obtained via a double table interpolation relative to the normalized heating ramp rate and rupture temperature similarly to the clad burst strain. The table is either user supplied or default NUREG-0630 values listed in Tables 2.3.2-3 and 2.3.2-4. The additive value of the loss coefficient is edited at the time of rupture. The flow blockage loss coefficient is added automatically to the problem for a primary pin channel unless the user overrides via a new optional input. If added, the form loss is applied to the forward flow direction for the inlet (bottom) junction and the reverse flow direction for the exit (top) junction attached to the volume in which the clad ruptured. The user option to exclude this form loss addition from the junctions has been included for supplemental pin channels or for certain non-licensing sensitivity studies with multiple cross-connected channels.

Another option has been added to the EM Pin model to help minimize user burden when running EM reflooding heat transfer analyses with BEACH (BAW-10166 Section 2.1.3.8.4). This user-controlled option automatically includes code-calculated pin rupture, droplet break-up (up to 60 percent blockage) for primary pin channels and convective enhancement adjustments for primary or supplemental pin channels. The input grid parameters are modified with the ruptured values and will be retained for use in the reflooding heat transfer calculations. This model is optional and requires input to activate the calculations. If no input is specified the default is that no rupture enhancements will be calculated and no droplet

breakup calculations will be performed for any supplemental pin channels.

When this option is activated, Equations 2.3.2-41.1 through 2.3.2-41.4 will be calculated following cladding rupture for primary pin channels, only. The first calculation performed determines the midpoint elevation of ruptured segment, referenced from the bottom of the pin channel (which coincides with the bottom of the heat structure geometry or reflood stack). This midpoint elevation, Z_{grid}, is the location where the new "grid" is inserted. This elevation is used to determine the droplet break-up effects for the ruptured segment.

$$Z_{grid} = 0.5 \cdot \Delta Z_{rupt_{seg}} + \sum_{j=1}^{rupt\ seg-1} \Delta Z_{seg_j}, \qquad 2.3.2\text{-}41.1$$

where

ΔZ_{seg} = elevation change of pin segment.

The second set of calculations is to calculate rupture droplet breakup efficiency. These calculations are identical to those described in Sections 2.1.3.7. and 2.1.3.8. of Reference 123. The rupture atomization factor, η_{etamax}, is calculated as

$$\eta_{etamax} = \frac{1}{[\ 1 + \{(n^{1/3} - 1) \cdot \min(0.60\ , \epsilon_{fb})\}]}, \qquad 2.3.2\text{-}41.2$$

where

n = number of equal size droplets resulting from the split-up of the larger droplets,

= 2.7, from a droplet distribution flux, and

ϵ_{fb} = flow blockage fraction (limited to a maximum of 0.60).

The increase in the droplet surface area from that used for interface heat transfer is defined in Equation 2.1.3-105[123] as

$$\Delta a_{gf} = C_{maxDB} \Theta \ a_{gf} \ .$$

The proportionality constant, C_{maxDB}, is determined from the constant, C_1, the rupture flow blockage fraction (limited to a maximum of 0.60), and the length of the ruptured segment.

$$C_{maxDB} = \frac{C_1 \cdot \min(0.6 \ , \epsilon_{fb})}{\Delta Z_{rupt_{seg}}} \ . \qquad 2.3.2\text{-}41.3$$

The recommended value of C_1 is 1.22 meters (4.0 feet).

The velocity of the fluid at the ruptured location increases because of the flow area reduction. The physical area in the code calculations is not modified, but a velocity multiplier, used for determining the droplet Weber number, is calculated from

$$VELMULT = \frac{1}{1 - \min(0.6 \ , \epsilon_{fb})} \ . \qquad 2.3.2\text{-}41.4$$

The cladding rupture results in an increase in the pin outside heat transfer surface area. The increase in area is not directly included in the conduction solution in the code calculations. It is accounted for by using the rupture convective enhancement factor and applying it to the grid wall heat transfer enhancement factor, F_{gq}, for primary or supplemental channels. The rupture enhancement, M_{RAR}, is an multiplicative contribution determined by

$$M_{RAR} = \text{Rupture Area Ratio}$$

$$= \frac{2\pi \ r_{rupt_{oc}} \ L}{2\pi \ r_{oc_{cold}} \ L} = \frac{r_{rupt_{oc}}}{r_{oc_{cold}}} \ , \qquad 2.3.2\text{-}41.5$$

where

$r_{rupt_{oc}}$ = outside clad radius of the ruptured node given by

$$= r_{ic} + \left[r_{oc_{cold}} - r_{ic_{cold}} \right] \left[r_{ic_{cold}} / r_{ic} \right] . \quad 2.3.2\text{-}41.6$$

The total wall heat transfer convective factor then becomes

$$F_{gq_{tot}} = F_{gq_{grid}} \cdot M_{RAR} . \quad 2.3.2\text{-}41.7$$

These droplet break-up and convective enhancement terms are optionally calculated and edited at rupture by the EM pin model.

This page intentionally blank.

r_{ic_u} = inside clad radius of the top pin segment (m), and

ΔL_p = change in gas plenum length (m).

The change in gas plenum length is calculated from the net change in the fuel and clad stack lengths due to axial thermal expansions as follows. Let

ΔL_{cf} = change in gas plenum length from cold condition (m),

$$= \Delta L_c - \Delta L_f \ , \qquad 2.3.2\text{-}51.4$$

where

ΔL_c = total axial thermal expansion of clad from cold condition (m),

$$= \sum_{j=1}^{\#\ seg} (L_j\ \epsilon_{ATC_j}) \ , \text{ and} \qquad 2.3.2\text{-}51.5$$

ΔL_f = total axial thermal expansion of fuel from cold condition (m),

$$= \sum_{j=1}^{\#\ seg} (L_j\ \epsilon_{ATF_j}) \ . \qquad 2.3.2\text{-}51.6$$

Then

ΔL_p = change in gas plenum length from hot initial condition (m),

$$= \Delta L_{cf} - \Delta L_{cf}^{o} \ , \qquad 2.3.2\text{-}51.7$$

where

ΔL_{cf}^{o} = initial over-specification in gas plenum length (m), determined during pin transient initiation,

L_j = axial length of the jth segment (m),

ϵ_{ATF} = fuel strain function of Equation 2.3.2-15, evaluated at fuel volume weighted average temperature $\bar{T}_f$ of Equation 2.3.2-25, (dimensionless), and

ϵ_{ATC} = axial strain function defining clad axial thermal expansion as a function of clad volume average temperature, (dimensionless).

The axial strain for the cladding is defined by either a user-input table versus cladding temperature for non-zircaloy cladding (Note: This table replaces the cubic fit from Rev. 3 Eqn 2.3.2-51.8.) or a built in code correlation set for zircaloy cladding[119]

$$\epsilon_{ATC} = -2.506 \times 10^{-5} + (T_C - 273.15)\ 4.441 \times 10^{-6}$$
$$= -1.2381 \times 10^{-3} + 4.441 \times 10^{-6}\ T_C \qquad 2.3.2\text{-}51.9$$

for $T_C \leq$ 1073.15 K (α phase), or

$$\epsilon_{ATC} = -8.3 \times 10^{-3} + (T_C - 273.15)\ 9.7 \times 10^{-6}$$
$$= -1.0950 \times 10^{-2} + 9.7 \times 10^{-6}\ T_C \qquad 2.3.2\text{-}51.10$$

for $T_C \geq$ 1273.15 K (β phase), where T_C is the volume average cladding temperature (K) of Equation 2.3.2-24. In the α phase to β phase transition zone, 1073.15 K < T_C < 1273.15 K, a table lookup is used. Some selected values are listed in Table 2.3.2-2.

Using the assumption that both the slope of the fuel mesh point temperatures and the overall gap conductance will not change significantly, the last gap multiplier (1.0 for the first iteration) can be adjusted via a ratio to give a new multiplier,

$$M_g^{\eta+1} = \frac{\Delta T_{gap}}{(\Delta T_{gap} + \Delta \bar{T}_f)} M_g^{\eta} \quad . \qquad 2.3.2\text{-}52.3$$

After calculation of the new gap multiplier, another conduction solution iteration step is taken. The fuel volume average temperature differential is recalculated via Equation 2.3.2-52.1. If the absolute value is greater than 2 K, then another iteration step is taken after recalculating a new multiplier via Equations 2.3.2-52.2 and 2.3.2-52.3. If the absolute value is less than 2 K, then the iteration has converged and the last multiplier calculated is edited and used during the steady-state and transient EM pin calculations. Up to twenty-one iterations are allowed. If convergence is not obtained in twenty-one iterations, then the code will stop at the end of the initialization process and appropriate failure messages will be edited. Failure of the iteration to converge is generally related to poor estimates given for the initial mesh point temperature distribution. An improved estimate will normally allow the iteration to converge properly. If convergence is still a problem, user specification of the multiplier is also available.

At the completion of the EM pin steady-state calculations (i.e., after EM pin steady-state trip becomes true or during the first time step if there is no trip) several calculations are required to initiate the pin transient calculations. The user-supplied cold unstressed pin geometry input via the heat structure cards is elastically expanded using the final code calculated temperature and mechanical stresses.

$$r_{f_o} = r_{f_{cold}} + u_{TF} \qquad 2.3.2\text{-}53$$

and

$$r_{ic_o} = r_{ic_{cold}} + u_{TC} + u_e + u_{fcc}, \qquad 2.3.2\text{-}54$$

with

r_{f_o} = thermally expanded outside fuel radius (m),

r_{ic_o} = thermally and mechanically expanded inside clad radius (m),

u_e = elastic deformation due to mechanical stresses (m), and

u_{fcc} = elastic deformation from gap mechanical contact (m). This term is calculated from the user supplied input contact pressure and cladding radii during the initialization.

$$u_{fcc} = \frac{P_{fcc} \cdot r_{ic}}{E_c} \left\{ \left[\frac{r_{oc}^2 + r_{ic}^2}{r_{oc}^2 - r_{ic}^2} \right] + \nu_c + \frac{E_c}{E_f} (1 - \nu_f) \right\} \qquad 2.3.2\text{-}54.1$$

The calculated radii are compared against the input values by

$$u_{FC} = r_{f_{input}} - r_{f_o} \qquad 2.3.2\text{-}55$$

$$u_{CC} = r_{ic_{input}} - r_{ic_o}, \qquad 2.3.2\text{-}56$$

and

$$u_{cg} = \begin{cases} 0.0, & \text{for } P_{fcc_{input}} = 0.0 \\ r_{ic_{input}} - r_{f_{input}}, & \text{for } P_{fcc_{input}} > 0.0 \end{cases} \qquad 2.3.2\text{-}56.1$$

5.0 REFERENCES

1. Ransom, V. H., et. al., RELAP5/MOD2 Code Manual -- Volume 1: Code Structures, System Models and Solution Methods and Volume 2: Users Guide and Input Requirements, NUREG/CR-4312 - Volume 1, August, 1985 and NUREG/CR-4312 - Volume 2, December 1985.

2. B&W Nuclear Technologies, RELAP5/MOD2-B&W -- An Advanced Computer Program for Light Water Reactor LOCA and non-LOCA Transient Analysis, BAW-10164P, Revision 1, October 1988.

3. Letter from A. C. Thadani (USNRC) to J. H. Taylor (B&W Nuclear Technologies), Acceptance for Referencing of Topical Report BAW-10164P, Revision 1, RELAP5/MOD2-B&W, An Advanced Computer Program for Light Water Reactor LOCA and Non-LOCA Transient Analysis, April 18, 1990.

4. Code of Federal Regulations, ECCS Evaluation Models, Chapter 10, Part 50, Appendix K

5. B&W Nuclear Technologies, RELAP5/MOD2-B&W -- An Advanced Computer Program for Light Water Reactor LOCA and Non-LOCA Transient Analysis, BAW-10164P, Revision 2, August 1992.

6. B&W Nuclear Technologies, RELAP5/MOD2-B&W -- An Advanced Computer Program for Light Water Reactor LOCA and non-LOCA Transient Analysis, BAW-10164P, Revision 3, October 1992.

7. Letter from J. H. Taylor (B&W Nuclear Technologies) to R. C. Jones (USNRC) BEACH Topical Report BAW-10166P, JHT/93-214, August 31, 1993.

8. Letter from J.H. Taylor (B&W Nuclear Technologies), Response to NRC's Request for Additional Information on BAW-10164, Revision 2, August, 1992; RELAP5/MOD2-B&W, An Advanced Computer Program for Light Water Reactor LOCA and NON-LOCA Transient Analysis, JHT/93-279, November 16, 1993

9. Letter from J.H. Taylor (B&W Nuclear Technologies), Response to NRC's Request for Additional Information on BAW-10164, Revision 3, October, 1992; RELAP5/MOD2-B&W, An Advanced Computer Program for Light Water Reactor LOCA and NON-LOCA Transient Analysis, JHT/94-7, January 21, 1994

10. Letter from J.H. Taylor (B&W Nuclear Technologies), Response to NRC's Supplemental Request for Additional Information on BAW-10164, Revision 2, August, 1992; RELAP5/MOD2-B&W, An Advanced Computer Program for Light Water Reactor LOCA and NON-LOCA Transient Analysis, JHT/94-146, September 20, 1994.

This page intentionally left blank.

Appendix J

M5 Cladding Creep for Evaluation of Fuel-Clad Lift-Off

In Appendix I, question 15, FCF presented a new creep multiplier to be used with TACO3[1] for modeling M5 cladding. In this section, a creep model for M5 cladding is presented to be used when outward creep is being modeled to predict fuel clad lift-off. This is used when the fuel rod bounding internal pressure exceeds the system pressure.

Originally it was planned to use the cladding creep formulation for the FCF Zircaloy-4 cladding presented in BAW-10183-A (Fuel Rod Gas Pressure Criterion – FRGPC) for performing fuel-clad lift-off analyses with M5 cladding. However, the evaluation of fuel-clad lift-off with a recently developed M5 creep model indicated that the use of the BAW-10183P-A FCF Zircaloy-4 formulation may not provide conservative predictions for all cases. In order to ensure conservatism in the M5 fuel-clad lift-off predictions, it became necessary to develop an M5 creep model that would replace the Zircaloy-4 model in BAW-10183P-A. Due to the limited M5 creep data currently available, the following conservative formulation was selected:

[c,d]

Where:

[

c, d

]

Note that the creep rate in this formulation is [c, d .] This approach is conservative because the creep data from Franklin[2] for recrystallized cladding indicates that hardening effects substantially reduce the creep rate at higher residence times characteristic of fuel-clad lift-off.

A multilinear regression analysis was performed to determine the coefficients in the above equation using the first and second cycle creep data from the four rods listed in Table J-1:

[

c, d

]

The strain data used to develop these coefficients were obtained from diametral measurements performed in a hot cell. Thus, complete circumferential scans were performed along the entire length of the rod. Hot cell measurements eliminated any errors associated with cladding oxide formation or ovality typically encountered in poolside measurements.

The mean and standard deviation of the measured to predicted strains generated from the multilinear regression analysis are:

Mean Meas./Pred. = [c, d]
Std. Dev. Meas./Pred. = [c, d]

These statistical parameters provide the information necessary to determine the creep strain rate that would be greater than 95% of the distribution with a 95% confidence[3]:

$$\dot{\varepsilon}_{\theta\,95/95} = \dot{\varepsilon}_{\theta}(\overline{\chi} + K_1 s) = [\ c,d\ ]$$

where:

$\overline{\chi}$: Mean Meas./Pred for data set.

s: Sample standard deviation.

K_1: Factor for one sided 95%/95% tolerance limit, normal distribution [c, d]

A comparison of the measured and predicted creep strains of the first and second cycle data from the four rods used to derive the above coefficients is shown in Figure J-1.

Two data points from three cycle data are also illustrated in Figure J-1. Except near the ends of the rods, fuel clad contact had occurred in the three cycle rods. The two points illustrated in Figure J-1 were near the ends of the rods where the cladding creep was not impeded by the fuel-clad contact. The measured to predicted strains for these data were [c, d] respectively which is greater than the above uncertainty. These data further illustrate the conservatism of the approach used to derive the M5 fuel-clad lift-off creep rate formulation.

The M5 creep rate formulation will be used in place of the current FCF Zircaloy-4 creep formulation for BAW-10183P-A. Recall that a conservative factor of approximately [c,d] was used in BAW-10183P-A. This consisted of a [c,d] uncertainty in the cladding creep rate predictions and a [c,d] anisotropic factor applied to the fuel swelling rate predictions[3]; the quotient of these two values [c,d] Although the uncertainty in the above M5 creep rate predictions is [c,d], which is less than the FCF Zircaloy-4 uncertainty of [c,d], the factors of [c, d] will be retained for the M5 fuel-clad lift-off predictions in the BAW-10183P-A methodology. An internal gas pressure limit of [c,d] above system pressure will also be retained. The M5 creep rate formulation developed above will be used until the availability of additional future M5 creep data warrants the need to revise this formulation.

References:

1. BAW-10182P-A, TACO3 Fuel Pin Thermal Analysis Computer Code, November 1989.

2. D.G. Franklin, "Zircaloy-4 Cladding Deformation During Power Reactor Irradiation," American Society of Testing Materials, ASTM-STP-754, 1982.

3. BAW-10183P-A, Fuel Rod Gas Pressure Criterion, July 1995.

Figure J-1

Predicted vs Measured Cladding Deformation

Figure is Proprietary
[c, d]

Table J-1
M5 Creep Data and Average Conditions

Rod ID	Axial Position	Time Hours	Fast Neutron Flux n/cm^2-s E > 1 MeV	Hoop Stress MPA	Clad Average Temp deg C	Measured Deformation µm	Predicted Deformation µm
				c,d			

Table J-1
M5 Creep Data and Average Conditions

Rod ID	Axial Position	Time Hours	Fast Neutron Flux n/cm^2-s E > 1 MeV	Hoop Stress MPA	Clad Average Temp deg C	Measured Deformation µm	Predicted Deformation µm
				c,d			

Appendix K
Response to Questions on Appendix I

K.1 Response to verbal request for additional information on I-2.

The data from the response to Question 2 has been plotted in Figure K-1.1 with the data from Figure A-4 along with revised design strength curves. The relationship for the design curves is:

Table K-1.1
Revised M5 Design Strength Curves

[b,c,d,e]

The ductility for the Table I-2.2 tensile test at 350 °C at a fluence of 6.81E+21 n/cm^2 should be[b,c]and not 0.97%.

There are no photo-micrographs available from the test specimens in Table I-2.2. Figure K-1.2 is comprised of photographs at 10x magnification of a biaxial test specimen after testing. The bi-axial test typically gives low uniform ductility results. The irradiated M5 results are similar to those observed for irradiated Zircaloy-4.

Figure K-1.1 Yield Strength vs Temperature

[b,c,d,e]

Figure K-1.2 Post Test View of Irradiated Bi-axial Test Specimen

[b,c,d,e]

K.2 Response to verbal request for additional information on I-5.

K.2.1 PCI Testing of M5 Cladding

M5 PCI performance has been evaluated by two methods. The first is ex-core testing to determine stress corrosion cracking (SCC) sensitivity and compare it to Zircaloy-4. In these tests, cladding ring sections are exposed at 350 °C to either pure argon gas, or a mixture of argon gas and iodine vapor and placed under a tensile stress. In the test a slow tensile strain rate[b,c,d,e]is applied. The strain rate is held until failure occurs and the total ductility recorded. The change in ductility between the pure argon test and the argon gas and iodine vapor is then compared to the results obtained for Zircaloy-4. The M5 results showed a smaller change in ductility between the tests compared to Zircaloy-4.

Table K-2.1
Ring Tensile Test SCC Sensitivity Test

[b,c,d,e]

The second test is ramp testing see section K.4.

K.2.2 Fatigue Behavior of M5 Cladding

Fatigue behavior of M5 cladding has been tested at 350 °C using a[

b,c,d,e

] Results of the test are plotted as an alternating stress vs. N cycles to failure in Figure K-2.1.

The RXA state of the M5 cladding resulted in the cladding being subjected to hoop stresses greater than the bi-axial yield as shown in Figure K-1.1 (page K-2) at 350 °C. Due to low yield of the material, large strains result from the higher stress levels imposed on the cladding. With these large strains failure occurs at a lower stress level than the reference K-2.1 curve which is also shown on Figure K-2.1. However, Fatigue is really a result of an alternating strain being applied to a material. To demonstrate that the M5 has adequate fatigue strength SRA Zircaloy-4 cladding was also tested in the same test setup. The results of both the M5 and Zircaloy-4 tests are then plotted as plastic strain at failure vs. number of cycles in Figure K-2.2. It can be seen that the Zircaloy-4 material fails at a lower strain than M5. Therefore, as M5 hardens under irradiation, higher alternating stress levels can be tolerated as the imposed plastic strain is reduced.

References:

K-2.1 O'Donnell, W.J. and Langer, B.F."Fatigue Design Basis for Zircaloy Components." Nuclear Science and Engineering, Volume 20, pages 1-12.

Figure K-2.1 Fatigue Curve, Stress vs Cycles (N) to Failure

[b,c,d,e]

Figure K-2.2 Fatigue Curve, Plastic Strain vs Cycles (N) to Failure

[b,c,d,e]

K.2.3 Thermal Conductivity of M5 Cladding

The conductivity of M5, given in response to Questions 5 and 10 of the request for additional information on BAW-10227, is supported by the results of Peletsky and Musayeva, Reference K-2.2, published in 1995. Peletsky and Musayeva measured the thermal conductivity of cylinders of Zr-1% Nb alloy between 350 and 1600 K using the longitudinal steady-state heat flow. The Peletsky data, digitized from Reference K-2.2, are shown along with the Framatome conductivity fit in Figure K-2.3. The Framatome curve is given by:

$$k = 19.13 - 0.009072T + 0.00001181T^2$$

where k : thermal conductivity (W/m-K)
T : temperature (K).

The fit is applied over a range from 293 to 1600 K.

References:

K-2.2 Peletsky V.E. and Musayeva Z.A., "Effect of Oxidation on Transport Properties of Zirconium - 1% Niobium alloy," International Journal of Thermo-physics, Volume 16, No. 6, 1995, pp 1481-1487.

Figure K-2.3 M5 Thermal Conductivity Fit and Peletsky Data versus Temperature

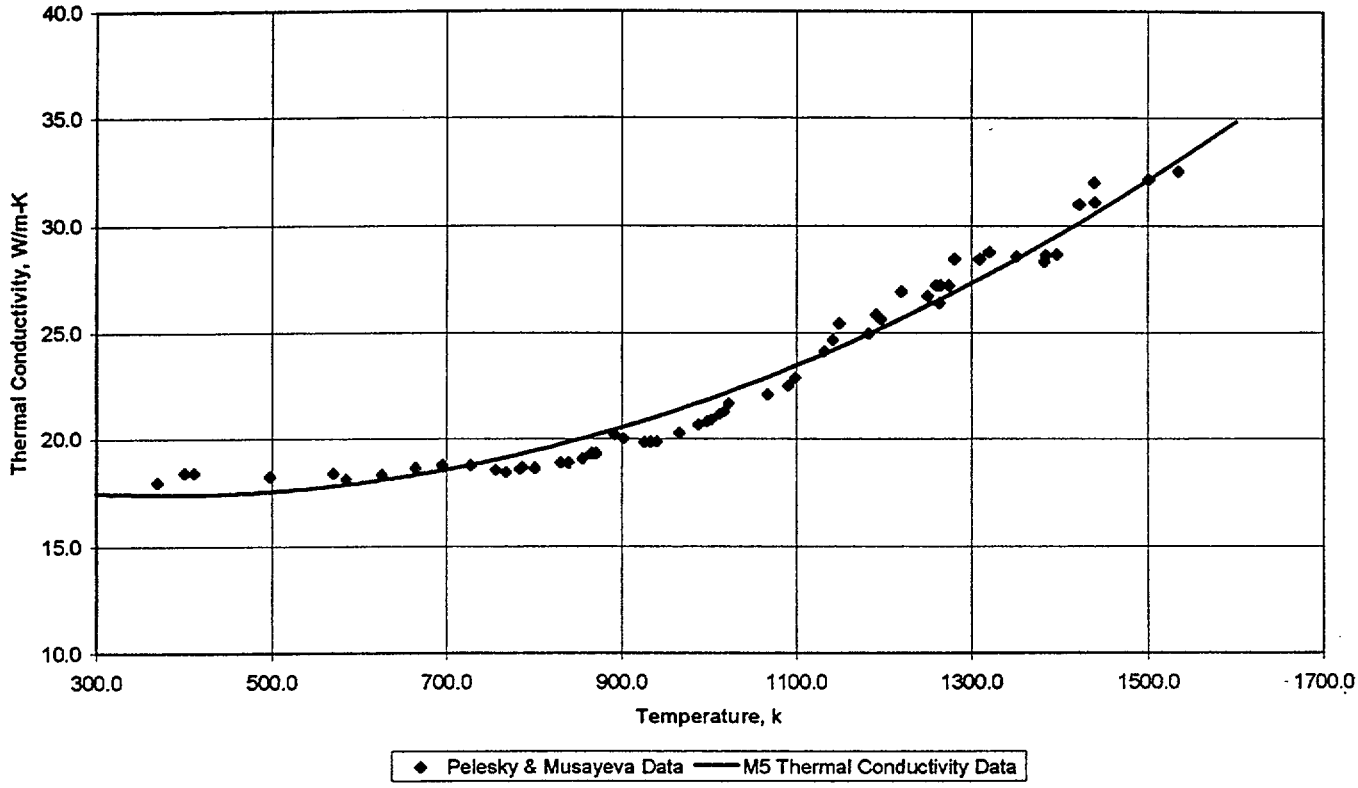

From conduct.xls

K.2.4 Thermal Expansion of M5 Cladding

Le Blanc, Reference K-2.3, and Jouen, Reference K-2.4, have experimentally determined the coefficients of thermal expansion for M5 with a quenching dilatometer. Table K-2.2 provides the series of measurements of the thermal expansion coefficients obtained for testing in the α range. All data was extracted for a temperature range of 200 to 500 C with a heating or a cooling rate of 1 C/s. The measurement results in the β range are provided in Table K-2.3. Data was extracted for a temperature decrease from 1000 C to 900 C with a cooling rate of 10 C/s. The material is isotropic in this phase such that no directional distinction was made during the measurements.

Le Blanc and Jouen have also, References K-2.3 and K-2.4, determined the contraction occurring during the transition between the α and the β phase. Extrapolating the linear expansions of both phases to 850 C, the relative contractions are[b,c,d,e]

References:

K-2.3 L. Le Blanc, Study by Calorimetry, Dilatometry and Analysis of Images of Transformation of Phase from $\alpha \rightarrow \beta$ in Zr/0.8$\rightarrow$1.2% Nb Alloys, CEA, SRMA 96-1561.

K-2.4 T. Jouen, Metallurgical Study of Zr Based Alloys (Zr-1% Nb (M5) and Zy-4-AFA2G): Correlation Between the Initial Texture nad the Dilatometric Performance, CEA, SRMA 97-1585.

Table K-2.2 Experimental Data for M5 α Region Thermal Expansion Coefficients

[b,c,d,e]

Table K-2.3 Experimental Data for M5 β Region Thermal Expansion Coefficients

[b,c,d,e]

K.2.5 Specific Heat of M5 Cladding

The specific heat model provided in Figure I-5-3 was constructed from M5 specific tests conducted by CEA in Saclay, France and open literature Russian tests on Zr-1% Nb alloys.

The CEA testing was performed by continuous calorimetry at a heating rate of 0.05 K/s between 473 K and 1423 K. Table K-2.4 Provides the CEA data obtained. The Russian tests were performed by calorimetry and by pulse heating. In 1993, Lusternik, Peletsky, and Petrova, Reference K-2.5, obtained the data compiled in Table K-2.5 for the E110 alloy. Later that year, the same authors published a paper, Reference K-2.6, containing the results of pulse heating and their correlation for specific heat in the α and β phases.

$C_p = 0.2375 + 0.0001591T$, for the α phase (300 < T < 1050 K)

$C_p = 0.1997 + 0.00012364T$, for the β phase (1200 K< T)

with Cp => J/g-K , and
T => K.

No data was provided with this paper but reference to the earlier paper as one of the sources was given.

In 1997, Peletsky and Petrova, Reference K-2.7, published the results of additional studies. Reference K-2.7 does not clearly present measurement results, data, from the studies but does provide the following correlations.

$C_p = 0.2375 + 0.0001591T$, for the α phase (500 < T < 1100 K)

$C_p = 0.2813 + 0.00006625T$, for the β phase (1250 K < T)

with Cp => J/g-K , and
T => K.

For the α phase the correlation is the same as published in 1993 but the range has been extended to 1100 K. For the β phase, the phase initiation temperature is raised by 50 K and a slightly altered correlation put forward.

Neither the 93 nor the 97 publication offer a correlation for the transition range. Both, however, include apparent correlation of data for this range in the published graphs. Within the 93 publication the integral of the specific heat over the phase change is describe as an approximate constant of 42 J/g.

These sources of data and information have been assembled to determine the FTI M5 specific heat fit as follows.

[b,c,d,e]

The results of this fitting and the various data and correlations that were used are provided in Figure K-2.4. The fit is a reasonable compromise between the various sources for a moderately slow heating transient. This is similar to the specific heat fits accepted within MATPRO, Reference K-2.8, for Zircaloy. Data for phase change kinetics have been published recently and potentially could be incorporated within the calculations. However, the studies in this area are relatively new and should be allowed to mature before the results are incorporated into nuclear safety predictions. Therefore, the moderately slow ramp correlation as determined for a heating event is applied for both heating and cooling transients and with no consideration of ramp rate.

References:

K-2.5 Lusternik VE, Peletsky VE, and Petrova II, "Experimental Study of Calorific Properties of Materials with Zirconium Base (Alloy E110) Used for Reactors," Institute of High Temperatures of the Academy of Sciences of Russia, Moscow, 1993, Volume 31, No. 4, pp. 560-564.

K-2.6 Lusternik VE, Peletsky VE, and Petrova II, "High Temperature Calorimetric Measurements of Zr-0.01Nb Alloy at Various Rates of Heating," High Temperatures - High Pressures, 1993, Volume 25, pp. 539-543.

K-2.7 Peletsky VE, and Petrova II, "Investigation of the Thermophysical Properties of the Alloy Zr-0.01Nb by a Subsecond Pulse-Heating Technique," High Temperatures - High Pressures, 1997, Volume 29, pp. 373-378.

K-2.8 NUREG/CR-0497, Tree-1280, Rev 1, "MATPRO-Version 11 (Revision 1) A Handbook of Materials Properties for Use in the Analysis of Light Water Reactor Fuel Rod Behavior," August, 1981, US Nuclear Regulatory Commission and US Department of Energy, Idaho Operations, Idaho Falls, Idaho.

Table K-2.4 CEA Specific Heat Data

[b,c,d,e]

Table K-2.5 Specific Heat Test Data from Reference K-2.6 (0.02 K/s heating rate)

Temperature, K	Specific Heat, J/g-K
298	0.282
350	0.295
400	0.32
450	0.348
500	0.349
550	0.351
600	0.362
650	0.361
700	0.35
750	0.39
800	0.41
850	0.41
900	0.418
950	0.425
1000	0.62
1050	0.41
1100	1.21
1150	0.66
1200	0.33

Figure K-2.4 M5 Specific Heat Correlations and Data

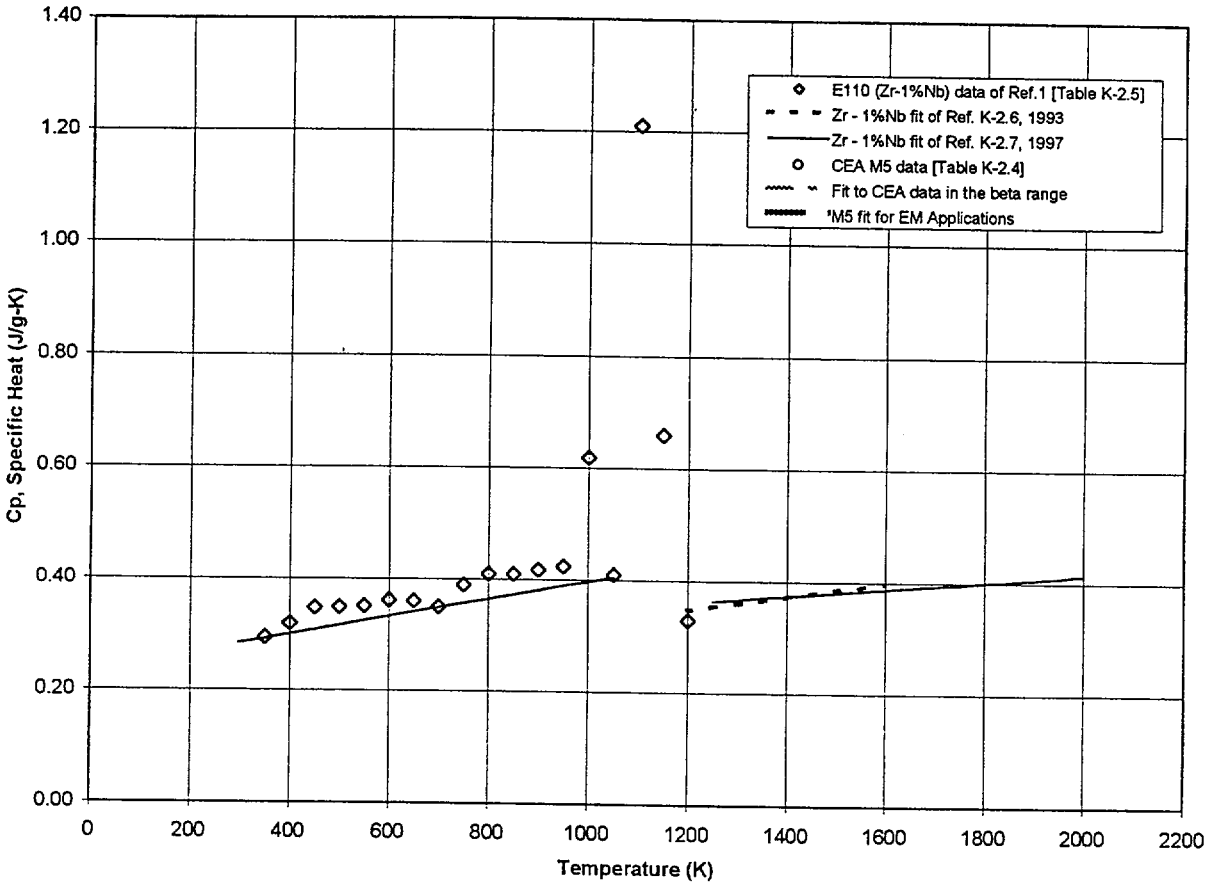

From Zrm5cp.xls

K.3 Responses to verbal request for additional information on I.12 - Young's Modulus

The elastic modulus of M5 cladding at ambient temperature (20 °C, 293 °K) was determined experimentally by tensile and burst testing to be[b,c,d,e]

The M5 model for the elastic modulus is calculated using the formula $E = E'(1 - \nu/2)$. The values of the elastic slope E' as a function of temperature are determined using burst tests at 20, 200 and 350 °C assuming[b,c,d,e]is consistent with alloy M5 and Russian alloy E-110 data shown in Figure K-3.1. [

b,c,d,e

]

By using the value of[b,c,d,e]

E (MPa) = [b,c,d,e]

This model, presented in figure I-12.1 of our M5 Alloy Topical Report, is in good agreement with the M5 and E-110 data at normal operating temperatures.

Deviation between the M5 model and the Russian E-110 and H1 data starts to become significant as the temperature increases past 400 to 500 C. However, the process by which Young's modulus was determined for the E-110 and H1 alloys, which agree with the Zr MATPRO fit (NUREG/CR-0497), is not well known and it is not readily apparent that the slope of the decrease in modulus is correct.

Further, as discussed, the deviation between the Framatome Fit and the Zr MATPRO fit is only significant for high temperature transients such as LOCA. In these cases, however, thermal expansion and high temperature creep dominate elastic expansion. As an example, thermal expansion is approximately four times that of elastic expansion. Thus thermal expansion is the primary cause of cladding gap development and gap coefficient degradation during these transients. Even severe deficiencies in the elastic modulus would not appreciably effect the analyses. When high temperature creep at cladding temperatures approaching the rupture criteria during LOCA is considered, the elastic expansion is ignored by the evaluations because it is such a small contribution.

Framatome believes that the development of the elastic modulus as described is appropriate and that for the reasons discussed M5 model as proposed is to be preferred over a direct fit to the E110 or H1 measured modulus.

Figure K-3.1 Poisson's Ratio versus Temperature

[b,c,d,e]

K.4 Responses to verbal request for additional information on I.14 - Ramp testing of M5 Fuel Rods

The failure threshold for M5 rods was the same as for Zircaloy-4 rods. For Zircaloy-4 rods the PCI/SCC failure thresh hold is:

Table K-4.1
Zircaloy-4 Failure Thresholds

[b,c,d,e]

The M5 Ramp test results were:

Table K-4.2
M5 Ramp Test Results (Note 1)

[b,c,d,e]

Based on these ramp tests results (end power level and failure or non-failure) along with the SCC testing reported in section K.2.1, it is concluded than M5 has the same or better resistance to SCC than does Zircaloy-4.

K.5 Response to verbal request for additional information on I-19 -- M5 Swelling and Rupture Curves

[

b,c,d,e

]

[

b,c,d,e

]

[

b,c,d,e

Figure K-5.1 M5 Slow and Fast Heating Ramp Rate Rupture Strain Curves

[b,c,d,e]

From: Fast_v_Slow_Rev2.xls

Figure K-5.2 Interpolated 5 C/s Heating Ramp Rate Rupture Strain with Data

[b,c,d,e]

From: Fast_v_Slow_Rev2.xls

Figure K-5.3 Interpolated 10 C/s Heating Ramp Rate Rupture Strain with Data

[b,c,d,e]

From: Fast_v_Slow_Rev2.xls

Figure K-5.4 Interpolated 15 C/s Heating Ramp Rate Rupture Strain with Data

[b,c,d,e]

From: Fast_v_Slow_Rev2.xls

Figure K-5.5 M5 Slow and Fast Heating Ramp Rate Pre-Rupture Strain Curves

[b,c,d,e]

From: M5_rev5_alpha_pre.xls

Figure K-5.6 Interpolated 5 C/s Heating RampRate Pre-Rupture Strain with Data

[b,c,d,e]

From: M5_rev5_alpha_pre.xls

Figure K-5.7 Interpolated 10 C/s Heating Ramp Pre-Rupture Strain with Data

[b,c,d,e]

From: M5_rev5_alpha_pre.xls

Figure K-5.8 Interpolated 15 C/s Heating Ramp Rate Pre-Rupture Strain with Data

[b,c,d,e]

From: M5_rev5_alpha_pre.xls

Figure K-5.9 M5 Strain and Blockage Curves for Slow Ramp Rates

[b,c,d,e]

From: BK09_15_new2.xls

Figure K-5.10 M5 Strain and Blockage Curves for Fast Ramp Rates

[b,c,d,e]

From: BK09_15_new2.xls

Figure K-5.11 Rupture Temperature versus Stress, M5

[b,c,d,e]

From: Rupture_Stress_F2.xls

Figure K-5.12 Rupture Temperature versus Stress, M5

[b,c,d,e]

From: Rupture_Stress_F2.xls

K.6 Supplemental Addition to Enclosure 1 of the April 23 Response to Questions

Supplement 1 included copies of the change pages for BAW-10164, the RELAP5 topical report, necessary to allow the manual input of materials properties necessary for M5 modeling. In the original changes, no provision was made for a revised cladding rupture temperature versus cladding stress correlation. As indicated in the supplemental response to Question 19, FTI has modified the Chapman correlation to improve its fit to the M5 data. This requires an additional code change to accept the new coefficients and override the Chapman coefficients. This section will include the topical change pages necessary to describe the altered code.

Further, all of the change pages for RELAP5 submitted in April were dated 4/99. FTI does not wish to implement a second change to the RELAP5 topical. Therefore, we will, with NRC approval, change the date on the change pages submitted in April to September such that all pages noted as Rev. 4 agree as to date of revision.

K.7 Planned Post Irradiation Exams

The following tables present the near term FCF and Framatome plans for M5 fuel rod examinations. Table K-7.1 lists near term poolside exams while Table K-7.2 lists near term hotcell exams. FCF has presented data for rod burnups up to[b,c,d,e]based on Framatome lead rod irradiations. FCF is pursuing plans to obtain additional data at burnups beyond those listed in Table 1 for FCF fuel. As higher lead rod and lead assembly burnups are achieved, FCF will perform similar scope PIEs on that lead fuel. For FCF lead rod and assembly programs going above 62 GWd/mtU, a separate submittal will be made to the NRC and it will identify the planned examinations. In FCF's yearly meeting with the NRC, a presentation updating PIEs campaigns and data will be made.

Table K-7.1
Planned M5 Poolside Related Post Irradiation Exams (PIEs)

[b,c,d,e]

Table K-7.2
Planned Near Term Hotcell Exams

[b,c,d,e]

K.8 Additional Change Pages for BAW-10164

The April 23, 1999 response to request for additional information included documentation of several changes to RELAP5 that were required to allow the input of M5 data. These changes replaced Zircaloy appropriate correlations that had been incorporated directly in the coding with input tables to alloy the use of M5 correlations and data. At that time, Framatome had not proposed any change to the Chapman cladding stress versus rupture temperature correlation. Section K.5 of this submittal alters the coefficients of the Chapman correlation to better represent the M5 alloy. This requires the incorporation of input values for the cladding stress versus rupture temperature correlation coefficients. The change page documentation for BAW-10164 in Enclosure 1 accomplishes those changes. In addition Framatome Technologies Incorporated (FTI) would like to have only one revision level to BAW-10164 for M5 application. Therefore, all of the BAW-10164 change pages submitted in April have been re-dated to September and are included in Enclosure 1. Enclosure 1 is thus a complete record of the required changes and Framatome requests the approval for these changes to BAW-10164.

K-11 Response to verbal request for additional information on fatigue of M5

The M5 data shown in Figures K-2.1 and K-2.2 (pages K-6 & K-7) showed low stresses and high strains for a given number of cycles at failure compared to the reference Zirc-4 fatigue design curve. To account for the impact of either work or irradiation hardening, the following transformation is made:

$S_a = ((\epsilon_{total\%}/100)* E)/2$

Where:

S_a : Equivalent stress amplitude (alternating stress intensity)
$\epsilon_{total\%}$: Total strain (Plastic + Elastic)
E: Young's Modulus at test temperature

Then to compare to a design curve, each data point is then modified

Mod 1, $S_a' = S_a/2$

Mod 2, $N'' = N/20$

These points are then plotted against the reference fatigue design curve. It can be observed that both populations are above the design curve.

The test data and the transformed values (Mod 1 and Mod 2 are listed in Table K-11.1. These were calculated using the modulus of M5 at 350 °C of [b,d,c,e]

Table K-11.1								
M5 Test Data								
	Mod 2			Elastic	Plastic	Total	Mod 1	Mod 2
N	N/20	Stress	Stress	Strain	Strain	Strain	Stress	Stress
Cycles	Cycles	MPA	psi	%	%	%	psi	psi
					b,c,d,e			

Figure K-11.1
Stress vs Cycles (N) to Failur

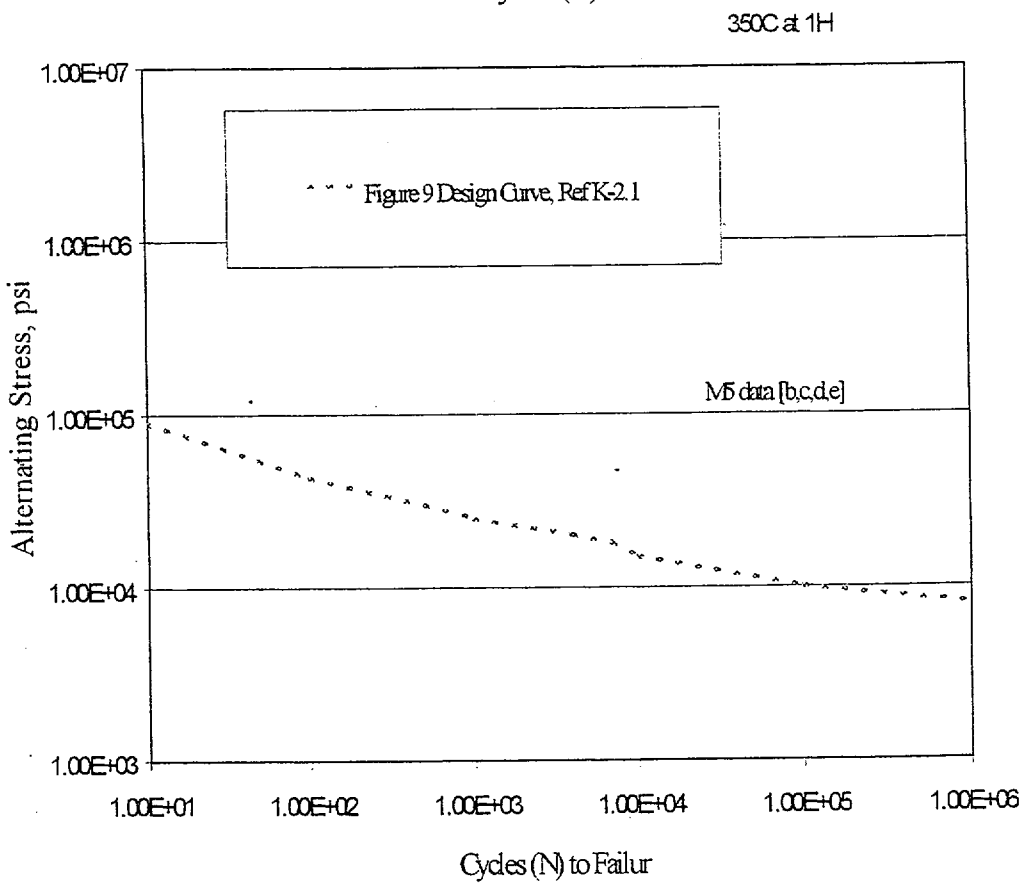

K-12 Response to request for information on growth of fuel assemblies with M5 guide tubes and on FCF method of evaluating fuel assembly shoulder gap closure.

K-12.1 Fuel Assembly Growth

The Mark-BW/X1 LTAs under irradiation in North Anna were measured for growth after the first cycle of irradiation in which they achieved a burnup of [c,d] The growth for the two fuel assemblies with the standard FCF design configuration is [c,d] These are the first assemblies irradiated with M5 guide tube/thimbles. Fuel assembly growth with M5 guide tubes is expected to behave similarly to M5 fuel rods and saturate at ~ 40 GWd/mtU. Hold down spring performance is evaluated using the following models which are expected to bound the range of growth:

For fuel assemblies with M5 fuel rods and Zirc-4 guide tubes/thimbles.

[c,d]
[c,d]

For fuel assemblies with M5 fuel rods and M5 guide tubes/thimbles.

[c,d]
[c,d]

These growth models are plotted in Figure K-12.1 along with the Mark-BW/X1 growth data. When data becomes available from batch irradiation of M5 fuel the growth models will be updated as needed .

K-12.2 Shoulder Gap Closure

For fuel assembly designs with M5 clad fuel rods and Zircaloy-4 guide tubes, the shoulder gap closure will be determined using the FCF Zircaloy-4 data base. A UTL 95/95 bound on the minimum shoulder gap closure vs assembly burnup was determined using the database presented in I-9. The relationship is:

[c,d]

This is expected to be conservative since the growth of M5 fuel rods saturates at around ~40 GWd/mtU. The Gap closure was then adjusted for M5:

[c,d]

The shoulder gap is adjusted for thermal expansion of the fuel rod and guide tube. Dimensional tolerances are [c, d].

For fuel assemblies with both M5 clad fuel rods and M5 guide tubes a similar database does not exist, therefore the gap closure for Zirc-4 fuel rods is used with a [c,d,] factor on the slope. The Gap closure was then adjusted for M5:

[c,d]

The shoulder gap is adjusted for thermal expansion of the fuel rod and guide tube. Dimensional tolerances are [c, d
c,d]

The available shoulder gap closure data for FCF fuel with M5 fuel rods is shown in Figure K-12.2. All of the data except for the Mark-BW/X1 data is for M5 fuel rods with Zirc-4 guide tubes/thimbles.

Figure K-12.1
Fuel Assembly Growth vs Burnup

Figure is proprietary

[c,d]

Figure K-12.2
Shoulder Gap vs Assembly Burnup M5 Fuel Rods with Zirc-4 Guide Tubes

Figure is Proprietary

[c,d]

K-13. Commitment to obtain requested data.

FCF plans on continuing general fuel performance meetings with the NRC on at least a yearly basis. As part of these meetings FCF will present to the NRC a summary of the performance of M5.

K-13.1 Cladding strain. Data is currently available to 43 GWd/mtU. In future PIEs irradiated M5 rods will be sent to the hotcell for destructive testing to establish mechanical properties. FCF will evaluate the data when it becomes available. For future mechanical properties testing the hotcell laboratories will be instructed to record both uniform and total strains for bi-axial burst tests. FCF will review those results along with micrographs of the fracture surface. The NRC will be informed if total strains are less than 1% and/or brittle failure surfaces are observed.

K-13.2 Oxidation. Data is currently available to 63 GWd/MTU. As new data is added to the database it will be identified in the yearly FCF/NRC fuel performance meetings.

K-13.3 Hydride formation. Data is currently available to 41 GWd/MTU. As new data is added to the database it will be identified in the yearly FCF/NRC fuel performance meetings.

K-13.4 Rod bowing . No data is currently available. FCF Plans to collect data from the Mark-BW/X1 LTAs in North Anna. As new data is added to the database it will be identified in the yearly FCF/NRC fuel performance meetings.

K-13.5 Axial Growth (rod-shoulder to upper-tie-plate gap closure). Shoulder gap data is currently available up to 54 GWd/MTU and rod growth data up to 50 GWd/MTU with 1 rod to 63 GWd/MTU. As new data is added to the database it will be identified in the yearly FCF/NRC fuel performance meetings.

K-13.6 Cladding Creep.

Good data is currently available from only 4 rods. As new data is available from first and second cycle rods where pellet-cladding-contact has not yet occurred, creep evaluations will be performed. As new data is added to the database it will be identified in the yearly FCF/NRC fuel performance meetings. If these data indicate that the creep model used for fuel-clad lift-off and for creep collapse is non conservative, then the NRC will be notified.

Beginning of Enclosure 1

LISTING OF CHANGES IMPLEMENTED IN REVISION 4 OF RELAP5/MOD2-B&W TOPICAL REPORT

Page	Type/Change	Item	Reason
--	Revision	Title page	Revision & Date
i-ii	Revision	Abstract	Revision & Date
v	Addition	Revision Record	New topical version
xii	Revision	Table/Contents, etc.	New revisions
1-1	Addition	Introduction	Zirconium-based alloy clad
2.1-126 to 2.1-126.2	Addition	Void-Dependent Cross-flow	New code option
2.3-25 to 2.3-28	Addition	EM Pin Model Changes	Zirconium-based alloy clad
2.3-33	Addition	EM Pin Model Changes	Zirconium-based alloy clad
2.3-35 to 2.3-37	Addition	EM Pin Model Changes	Zirconium-based alloy clad
2.3-39 to 2.3-41	Addition	EM Pin Model Changes	Zirconium-based alloy clad
2.3-45 to 2.3-46.2.2	Addition	EM Pin Model Changes	Zirconium-based alloy clad
2.3-52	Correction	EM Pin Model	Zirconium-based alloy clad
2.3-55	Addition	Steady-State EM Pin Model	Fuel temperature convergence
5-364.1 to 5-364.2	Correction	Missing SER Page	Include missing page

(NOTE: Pages 2.1-126.1, 2.1-126.2, 2.3-27.1, 2.3-27.2, 2.3-46.2.1, 2.3-46.2.2, 5-364.1, and 5-364.2 were added in Revision 4)

BAW-10164P
Topical Report
Revision 4
September 1999

- RELAP5/MOD2-B&W -

An Advanced Computer Program for Light Water Reactor LOCA and Non-LOCA Transient Analysis

Framatome Technologies Inc.
P. O. Box 10935
Lynchburg, Virginia 24506

Framatome Technologies Inc.
Lynchburg, Virginia

Topical Report BAW-10164P
Revision 4
September 1999

RELAP5/MOD2-B&W

An Advanced Computer Program for Light Water Reactor LOCA and Non-LOCA Transient Analysis

Key Words: RELAP5/MOD2, LOCA, Transient, Water Reactors

Abstract

This document describes the physical solution technique used by the RELAP5/MOD2-B&W computer code. RELAP5/MOD2-B&W is a Framatome Technologies Incorporated (previously known as and refered to in the text as B&W or B&W Nuclear Technologies) adaption of the Idaho National Engineering Laboratory RELAP5/MOD2. The code developed for best estimate transient simulation of pressurized water reactors has been modified to include models required for licensing analysis of zircaloy or zirconium-based alloy fuel assemblies. Modeling capabilities are simulation of large and small break loss-of-coolant accidents, as well as operational transients such as anticipated transient without SCRAM, loss-of-offsite power, loss of feedwater, and loss of flow. The solution technique contains two energy equations, a two-step numerics option, a gap conductance model, constitutive models, and component and control system models. Control system and secondary system components have been added to permit modeling of plant controls, turbines, condensers, and secondary feedwater conditioning systems. Some discussion of the numerical techniques is presented. Benchmark comparison of code

predictions to integral system test results are presented in an appendix.

Topical Revision Record

Documentation Revision	Description	Program Change?	Program Version
0	Original issue	_____	8.0
1	Typographical corrections Replace CSO correlation with Condie-Bengston IV	yes	10.0
2	SBLOCA modifications Miscellaneous corrections	yes	18.0
3	EM Pin Enhancements Filtered Flows for Hot Channel Heat Transfer Rupture Area Enhancement for Surface Heat Transfer OTSG Improvements and Benchmarks using the Becker CHF, Slug Drag, and Chen Void Ramp	yes	19.0
4	Zirconium-based alloy pin model changes Option for multiple pin channels in a single core fluid channel Void-dependent core cross flow option Zirconium-based alloy rupture temperature	yes	24.0

This page is intentionally left blank.

LIST OF FIGURES (Cont'd)

LIST OF FIGURES (Cont'd)

1. INTRODUCTION

RELAP5/MOD2 is an advanced system analysis computer code designed to analyze a variety of thermal-hydraulic transients in light water reactor systems. It is the latest of the RELAP series of codes, developed by the Idaho National Engineering Laboratory (INEL) under the NRC Advanced Code Program. RELAP5/MOD2 is advanced over its predecessors by its six-equation, full nonequilibrium two-fluid model for the vapor-liquid flow field and partially implicit numerical integration scheme for more rapid execution. As a system code, it provides simulation capabilities for the reactor primary coolant system, secondary system, feedwater trains, control systems, and core neutronics. Special component models include pumps, valves, heat structures, electric heaters, turbines, separators, and accumulators. Code applications include the full range of safety evaluation transients, loss-of-coolant accidents (LOCAs), and operating events.

RELAP5/MOD2 has been adopted and modified by B&W for licensing and best estimate analyses of PWR transients in both the LOCA and non-LOCA categories. RELAP5/MOD2-B&W retains virtually all of the features of the original RELAP5/MOD2. Certain modifications have been made either to add to the predictive capabilities of the constitutive models or to improve code execution. More significant, however, are the B&W additions to RELAP5/MOD2 of models and features to meet the 10CFR50 Appendix K requirements for ECCS evaluation models. The Appendix K modifications are concentrated in the following areas: (1) critical flow and break discharge, (2) fuel pin heat transfer correlations and switching, and (3) fuel clad swelling and rupture for both zircaloy and zirconium-based alloy cladding types.

This report describes the physical models, formulation, and structure of the B&W version of RELAP5/MOD2 as it will be applied to ECCS and system safety analyses. It has been prepared as a stand-alone document; therefore substantial portions of the text that describe the formulation and numerics have been taken directly from original public domain reports, particularly NUREG/CR-4312[1]. Chapter 2 presents the method of solution in a series of subsections, beginning with the basic hydrodynamic solution including the field equations, state equations, and constitutive models in section 2.1. Certain special process models, which require some modification of the basic hydrodynamic approach, and component models are also described. The general solution for heat structures is discussed in section 2.2. Because of the importance of the reactor core and the thermal and hydraulic interaction between the core region and the rest of the system, a separate section is dedicated to core modeling. Contained in section 2.3 are the reactor kinetics solution, the core heat structure model, and the modeling for fuel rod rupture and its consequences. Auxiliary equipment and other boundary conditions are discussed in section 2.4 and reactor control and trip function techniques in section 2.5. Chapter 3 provides an overview of the code structure, numerical solution technique, method and order of advancement, and initialization. Time step limitation and error control are presented in section 3.3.

The INEL versions of RELAP5/MOD2 contain certain solution techniques, correlations, and physical models that have not been selected for use by B&W. These options have been left intact in the coding of the B&W version, but descriptions have not been included in the main body of this report. Appendix A contains a list of those options that remain in the RELAP5/MOD2 programming but are not used by B&W and not submitted for review. A brief description of each along with a reference to an appropriate full discussion is provided in the appendix. Appendix B defines the nomenclature used throughout this report. Appendix G documents

$v_{J,3}$ not be included in the volume average (axial) velocity calculation for cell L.

The second area of numerical modification relates to the reduced form of the momentum equations to be used at a crossflow junction. In crossflow junctions, the cross product momentum flux terms are neglected, that is, there is no x-direction transport of momentum due to the y velocity.

For the case of a small crossflow junction between two axial-flow streams (J_2 in Figure 2.1.4-7) all the geometric input (AVOL, DX, DZ) for both of the volumes relates to the axial flow direction as does the wall drag and code calculated form losses. Since the crossflow has a different flow geometry and resistance (for example, crossflow resistance in a rod bundle) the friction and form losses must be user input and must be appropriate for the crossflow direction geometry. For crossflow junctions the user input form losses should include all crossflow resistance (form losses and wall drag). The normal terms representing wall drag and abrupt area change losses are not included in the formulation of the momentum equation at a crossflow junction as these refer to the axial properties of the K and L volumes.

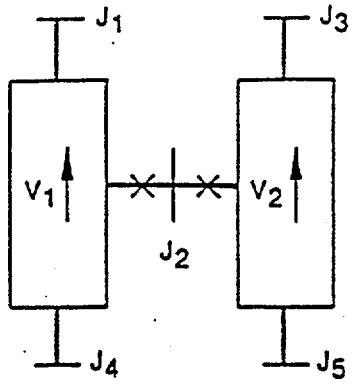

Figure 2.1.4-7. Modeling of Crossflows or Leak.

Since the connecting K and L volumes are assumed to be predominately axial-flow volumes, the crossflow junction momentum flux (related to the axial volume velocity in K and L) is neglected along with the associated numerical viscous term. In addition, the horizontal stratified pressure gradient is neglected.

All lengths and elevation changes in the one-dimensional representation are based upon the axial geometry of the K and L volumes and the crossflow junction is assumed to be perpendicular to the axial direction and of zero elevation change, thus, no gravity force term is included.

The resulting vapor momentum finite difference equation for a crossflow junction is

$$\left(\alpha_g \rho_g\right)_j^n \left(v_g^{n+1} - v_g^n\right)_j \Delta x_j = - \alpha_{g,j}^n \left(P_L - P_K\right)^{n+1} \Delta t$$

$$- \left(\alpha_g \rho_g\right)_j^n \mathrm{HLOSSG}_j^n \, v_{g,j}^{n+1} \Delta t$$

$$- \left(\alpha_g \rho_g\right)_j^n \mathrm{FIG}_j^n \left(v_{g,j}^{n+1} - v_{f,j}^{n+1}\right) \Delta x_j \Delta t$$

$$+ \text{ADDED MASS} + \text{MASS TRANSFER MOMENTUM.} \qquad 2.1.4\text{-}72$$

A similar equation can be written for the liquid phase. In Equation 2.1.4-72, HLOSSG_j^n contains only the user-input crossflow resistance. The Δx_j term that is used to estimate the inertial length associated with crossflow is defined using the diameters of volumes K and L,

$$\Delta x_j = \frac{1}{2} [D(K) + D(L)] \quad . \qquad 2.1.4\text{-}73$$

A special void-dependent form loss option of the full crossflow model has been added for certain multi-core channel applications. This option allows the user to alter the input constant form loss coefficient based on the void fraction in the upstream volume. The specific applications are possibly multi-channel core analyses such as SBLOCA scenarios with significant core uncovering or future multi-channel BEACH reflooding calculations. This model allows the regions of the core covered by a two-phase mixture or pool to have a resistance that is different from that in the uncovered or steam region. The crossflow resistance changes can alter the volume-average axial velocities that are used to determine the core surface heat transfer. Any cross flow is excluded from the volume average velocity used for heat transfer.

The model uses the input form loss coefficients whenever the upstream steam void fraction is less than a user-supplied minimum void fraction value given as $\alpha_{min\text{-}Kcross}$. The model allows user input of a forward, $M_{K\text{-}forward}$, and reverse, $M_{K\text{-}reverse}$, crossflow resistance multiplier when the upstream steam void fraction is greater than the maximum user-input void fraction, $\alpha_{max\text{-}Kcross}$. Linear interpolation is used to determine the multiplicative factor when the void fraction is between minimum and maximum input void fractions as indicated in the following equations. For the forward flow direction (from Volume K to Volume L),

If $\alpha_g(K) < \alpha_{min\text{-}Kcross}$	$K_{jun} = K_{jun\ forward}$
If $\alpha_{max\text{-}Kcross} \leq \alpha_g(K)$	$K_{jun} = K_{jun\ forward} * M_{K\text{-}forward}$
If $\alpha_{min\text{-}Kcross} \leq \alpha_g(K) < \alpha_{max\text{-}Kcross}$	$K_{jun} = K_{jun\ forward} * M_{Kf\ interp}$

2.1.4-73.1

where

$$M_{kf\ interp} = 1 - (1 - M_{K\text{-}forward}) * [\ \alpha_{min\text{-}Kcross} - \alpha_g(K)\ ] / (\alpha_{min\text{-}Kcross} - \alpha_{max\text{-}Kcross})$$

and $K_{jun\ forward}$ is the user-supplied forward loss coefficient specified in this junction input.

The equation for the reverse flow direction (from Volume L to Volume K) is similar.

$$\begin{aligned}
&\text{If} && \alpha_g(L) < \alpha_{min\text{-}Kcross} && K_{jun} = K_{jun\ reverse} \\
&\text{If } \alpha_{max\text{-}Kcross} \leq && \alpha_g(L) && K_{jun} = K_{jun\ reverse} * M_{K\text{-}reverse} \\
&\text{If } \alpha_{min\text{-}Kcross} \leq && \alpha_g(L) < \alpha_{max\text{-}Kcross} && K_{jun} = K_{jun\ reverse} * M_{Kr\ interp}
\end{aligned}$$

2.1.4-73.2

where

$$M_{Kr\ interp} = 1 - (1 - M_{K\text{-}reverse}) * [\ \alpha_{min\text{-}Kcross} - \alpha_g(L)\ ] / (\alpha_{min\text{-}Kcross} - \alpha_{max\text{-}Kcross})$$

and $K_{jun\ reverse}$ is the user-supplied reverse loss coefficient specified in this junction input.

The code performs several input checks to ensure that the user input will not cause code failures. These checks include tests to see if the input form loss multipliers are greater than zero. The minimum void fraction must be greater than zero and less than the maximum void fraction input. The maximum void fraction must be less than or equal to one.

The crossflow option can be used with the crossflow junction perpendicular to the axial flow in Volume L (or K) but parallel

2.3.2. Core Heat Structure Model

The ordinary RELAP5 heat structures are general in nature and can be used for modeling core fuel pins; however, licensing calculations require special treatment of the fuel pin heat transfer. To accommodate these requirements, two additional models, commonly referred to as the EM (Evaluation Model) pin and core surface heat transfer models, were added to the code. The EM pin model calculates dynamic fuel-clad gap conductance, fuel rod swell and rupture using either NUREG-0630[117] or user input options (for modeling M5 cladding or other zirconium-based alloy cladding material types), and cladding metal-water reaction. The core fuel pin surface heat transfer is calculated with a flow regime-dependent set of correlations that include restrictions on which correlations can be selected per NRC licensing requirements. These new models are independent and mutually exclusive of the original system heat transfer model (described in section 2.2.2) and the existing simple gap conductance model[118] (referenced in Appendix A). The new models are explicitly coupled to the solution scheme through the modification of the gap conductance term, addition of fluid hydraulic resistance upon rupture, deposition of metal-water reaction energy in the clad, and determination of fuel pin surface heat transfer. The new EM pin model calculations are described in this section, while the EM heat transfer description is contained in section 2.3.3.

The EM pin model consists of three basic parts:

1. Dynamic fuel-clad gap conductance,
2. Fuel rod swell and rupture using NUREG-0630 or user specified swell and rupture options, and
3. Clad metal-water reaction,

which couple explicitly to the heat structure solution scheme or add fluid hydraulic resistance upon rupture. The model may be executed either in a steady-state initialization or transient mode determined by user input.

The pin calculations are performed on single fuel rod which represent the average behavior of a large number of rods. Each rod (also termed channel) can be broken into up to ninety heat structures, each having an associated pin segment. The gap conductance, deformation mode, and metal-water reaction are determined for each individual segment based on the channel specific pin pressure.

The changes to the EM pin model included in Version 21 and later code versions are:

1. User options to model zircaloy and/or M5 cladding (or other zirconium-based alloy material types) in the same problem,

2. User options to specify the pin channel as a primary or supplemental channel for additive form loss and BEACH droplet breakup calculations upon pin rupture, and

3. Integration of the NRC SER limitation (BEACH code-BAW-10166, Rev. 2 dated 8/13/90) for use of a maximum flow blockage of 60 percent in the ruptured cladding droplet breakup calculations.

The option to allow zirconium-based alloy cladding types requires user input to identify which pin channels are zircaloy and which are not. The zirconium-based alloy cladding also requires additional user input to specify the material properties necessary to calculate the transient cladding swell and rupture behavior.

The supplemental pin capability was added to improve the calculational methods that require modeling of multiple EM pin channels within a single hydrodynamic fluid channel (i.e., an assembly or a group of assemblies) for LOCA applications. The relationship between the supplemental pin and the remainder of the pins in a common fluid channel is one in which the supplemental pin swell and rupture will not define the rupture flow blockage for the entire channel. Rather it will define a local effect that should not be used in determination of the channel droplet breakup parameters and the additive form loss due to rupture. These parameters should be controlled by the larger group of pins (i.e. primary channel) and not the smaller grouping (i.e. supplemental channel). The supplemental rod modeling is particularly useful for gadolinia or lead test pin (M5) analyses. It may also be used in future EM revisions for hot pin applications, in which the hot pin has a higher radial peak or a different initial fuel temperature.

2.3.2.1. Transient Dynamic Fuel-Clad Gap Conductance

The RELAP5 heat structure conduction scheme uses cold, unstressed geometrical dimensions for its solution technique. The dynamic gap conductance, h_{gap}, is calculated from hot stressed conditions from which an effective gap thermal conductivity, $\bar{K}_{gap}$, based on cold gap size, $\tau_{g_{cold}}$, is determined for each pin segment.

$$\bar{K}_{gap} = h_{gap} \cdot \tau_{g_{cold}} . \qquad 2.3.2\text{-}1$$

The gap conductance is determined by calculating the gap gas conductivity, temperature jump gap distance, radiation component, and dynamic fuel-clad gap from the deformation models. An

additive fuel-clad contact conductance term has also been included as an option to simulate the closed gap contribution for high fuel rod burn-up applications. Two options are provided to calculate the conductance. The first option assumes that the fuel pellet is concentric within the clad, while the second option assumes the fuel pellet is non-concentric within the clad as illustrated in Figure 2.3.2-1.

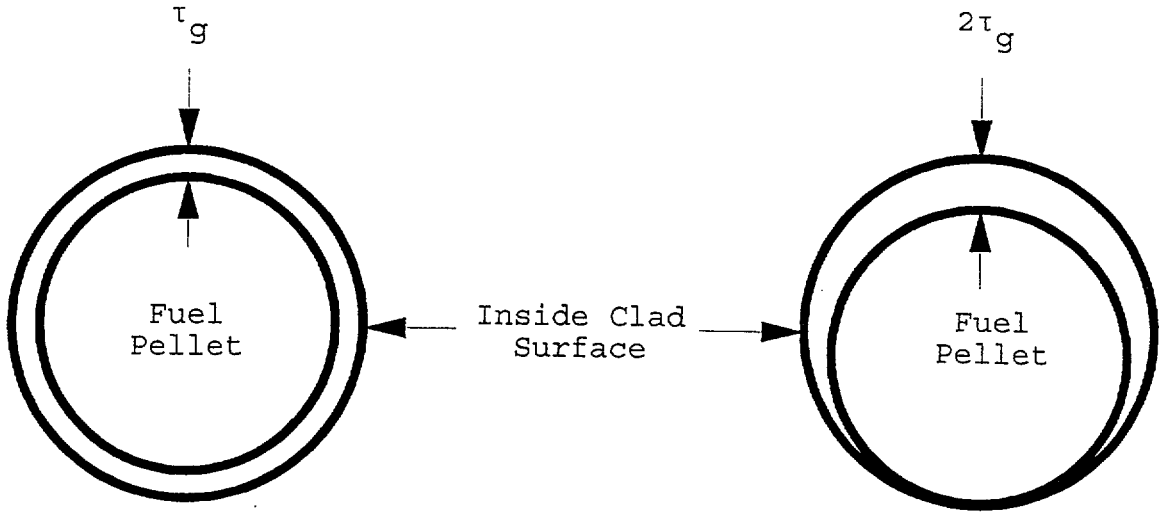

Figure 2.3.2-1. Gap Conductance Options.

Eight half-symmetrical azimuthal sections are used for determining the overall conductance for the second option without calculating an azimuthal temperature gradient. The total gap conductance is determined by

$$h_{gap} = M_g \, h_{\substack{gap \\ gas}} + h_{rad} + h_{fcc} \qquad 2.3.2\text{-}2$$

with

h_{gap} = conductance through gap gas (w/m^2-K),

M_g = user input multiplier used to acquire correct initial temperature within fuel,

$h_{\substack{gap \\ gas}}$ = gap gas conductance contribution (w/m^2-K),

h_{rad} = conductance due to radiation contribution from fuel to clad (w/m^2-K), and

h_{fcc} = gap contact conductance contribution due to fuel-cladding mechanical interaction (w/m^2-K).

The radiation gap conductance contribution is calculated by

$$h_{rad} = \frac{\sigma}{\frac{1}{e_f} + \frac{r_f}{r_{ic}}\left(\frac{1}{e_c} - 1\right)} \left[\frac{T_{fs}^4 - T_{ics}^4}{T_{fs} - T_{ics}}\right]$$

$$= \frac{\sigma(T_{fs}^2 + T_{ics}^2)(T_{fs} + T_{ics})}{\frac{1}{e_f} + \frac{r_f}{r_{ic}}\left(\frac{1}{e_c} - 1\right)}, \qquad 2.3.2\text{-}2.1$$

where

σ = Stefan-Boltzmann constant,

= 5.6697×10^{-8} $(w/m^2\text{-}K^4)$,

e_f = emissivity of fuel surface,

e_c = emissivity of clad-inside surface,

T_{fs} = fuel outside surface temperature (K), and

T_{ics} = clad-inside surface temperature (K).

$$C_1 = 1.0 \cdot 10^{-5}\ (K^{-1}),$$
$$C_2 = -3.0 \cdot 10^{-3},$$
$$C_3 = 4.0 \cdot 10^{-2},\ \text{and}$$
$$C_4 = -5.0 \cdot 10^{3}\ (K).$$

The fuel is defined by the first material type specified in the heat structure input, with the next material type being the gap and the third the clad as shown in Figure 2.3.2-2. Any deviation from the geometry will result in an error or misinterpretation of the information by the pin model. The gap can only be one mesh interval wide, while fuel or clad must be greater than or equal to one mesh interval. Currently no provisions are made for annular fuel pellets.

The calculation of the inside clad radius is not as straightforward as the fuel outside radius. Seven different calculational modes are required to cover the possible clad conditions. They are defined as:

1. Elastic and thermal expansion within an unruptured channel,
2. Elastic and thermal expansion within 166.7K (300°F) of the clad rupture temperature within an unruptured channel,
3. Plastic deformation within an unruptured channel,
4. Elastic thermal expansion within a ruptured channel,
5. Plastic deformation in a ruptured channel,
6. Ruptured segment, and
7. Fuel-cladding mechanical iteration (closed gap).

Each mode is related to the NUREG-0630 calculated rupture temperature for zircaloy cladding by the equation:

$$T_{rupt} = 4233 - \frac{20.4\sigma_h}{1 + H} - \frac{(8.51 \cdot 10^{6})\sigma_h}{100(1 + H) + 2790\sigma_h}, \qquad 2.3.2\text{-}17$$

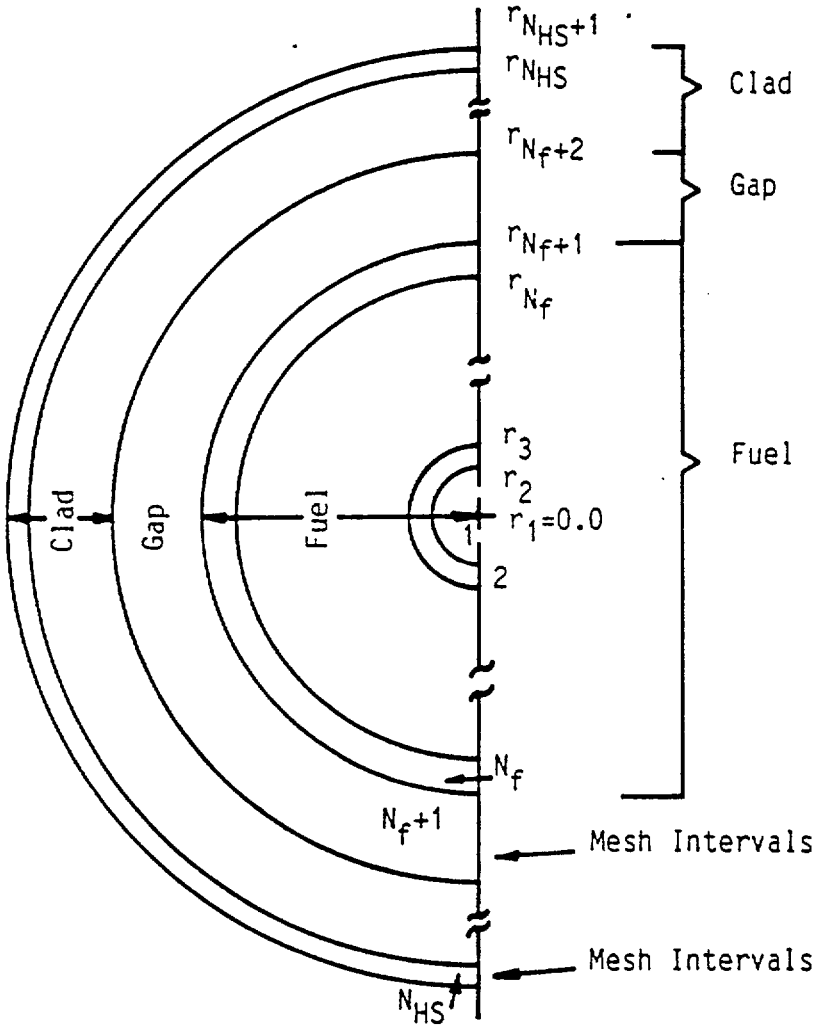

Figure 2.3.2-2. Fuel Pin Representation.

where

T_{rupt} = cladding rupture temperature (K),

σ_h = clad hoop stress (kpsi), and

H = dimensionless clad heating ramp rate, $0 \leq H \leq 1$.

The rupture temperature for other zirconium-based alloys is calculated by the following equation:

$$T_{rupt} = a1 - \frac{a2(\sigma_h - a7)}{a4 + H} - \frac{a3(\sigma_h - a7)}{a5(a4 + H) + a6(\sigma_h - a7)}, \quad 2.3.2\text{-}17a$$

where a1 through a7 are user-specified input constants. The clad hoop stress for any pin segment in either equation is given by

$$\sigma_h = C_p (P_g r_{ic_{cold}} - P_f r_{oc_{cold}})/(r_{oc_{cold}} - r_{ic_{cold}}), \quad 2.3.2\text{-}18$$

with

$r_{ic_{cold}}$ = cold unstressed inside clad radius (m),

$r_{oc_{cold}}$ = cold unstressed outside clad radius (m),

P_g = internal fuel rod pin pressure for that channel (Pa), and

P_f = external fluid pressure of the right-hand side heat structure associated volume (Pa).

$C_p = 1 / 6.894757 \times 10^6$

The heating rate can be either a user input constant or one of three additional transient-dependent algorithms discussed in detail later in this section.

At the beginning of each new time step following a successful RELAP5 time step advancement, the hoop stress and normalized heating ramp rate are computed for each pin segment. The clad average temperature is also known at this time. If the clad

average temperature is greater than the rupture temperature, then rupture occurs. Should the segment still be elastic and the rupture minus the clad temperature is less than 166.7K (300 F), then the segment stays elastic. Between these two temperatures the clad can be either elastic or plastic depending upon this temperature difference and the burst strain as described in the following paragraphs for ruptured or unruptured channels.

Mode 1: Unruptured Elastic and Thermal Deformation

Within an unruptured channel, the clad is considered purely elastic if it has never gone plastic, ruptured, or the temperature difference between rupture and clad average temperatures is less than 166.7 K (300 F). The inside clad radius for this pure elastic mode is determined by

$$r_{ic} = r_{ic_{cold}} + u_{TC} + u_{CC} + u_e \ , \qquad 2.3.2\text{-}19$$

where

u_{TC} = clad radial displacement due to thermal expansion (m), (m),

u_{CC} = clad radius over-specification factor (m), determined during pin transient initiation, and

u_e = clad radial displacement due to elastic deformation (m).

The clad thermal expansion is determined similarly to that for the fuel.

$$u_{TC} = (r_{N_{HS}+1} - r_{N_f+2}) \, \epsilon_{TC} / 2 \ , \qquad 2.3.2\text{-}20$$

with N_{HS} = total number of mesh intervals in the heat structure,

r_n = heat structure radius at the inside of mesh interval n or outside of n-1 (m), and

ϵ_{TC} = radial strain function defining fuel thermal expansion as a function of clad average temperature.

The radial strain function is defined by either a user input table as a function of cladding temperature for zirconium-based material types other than zircaloy or a built in code correlation set for zircaloy cladding[119] consisting of

$$\epsilon_{TC} = -2.0731 \cdot 10^{-3} + 6.721 \cdot 10^{-6} \; T_C \qquad 2.3.2\text{-}22$$

for $T_C \leq 1073.15$ K (α phase), and

$$\epsilon_{TC} = -9.4495 \cdot 10^{-3} + 9.7 \cdot 10^{-6} \; T_C \qquad 2.3.2\text{-}23$$

for $T_C \geq 1273.15$ K (β phase), where T_C is the average cladding temperature (K). In the α phase to β phase transition zone, $1073.15 \text{ K} < T_C < 1273.15$ K, a table lookup is used. Some selected values are listed in Table 2.3.2-2.

Table 2.3.2-2. Thermal Strain of Zircaloy for $1073.15 \text{ K} < T < 1273.15$ K.

T(K)	Radial Strain ϵ_{TC}	Axial Strain ϵ_{ATC}
1073.15	$5.14 \cdot 10^{-3}$	$3.53 \cdot 10^{-3}$
1093.15	$5.25 \cdot 10^{-3}$	$3.50 \cdot 10^{-3}$
1103.15	$5.28 \cdot 10^{-3}$	$3.46 \cdot 10^{-3}$
1123.15	$5.24 \cdot 10^{-3}$	$3.33 \cdot 10^{-3}$
1143.15	$5.15 \cdot 10^{-3}$	$3.07 \cdot 10^{-3}$
1183.15	$4.45 \cdot 10^{-3}$	$1.50 \cdot 10^{-3}$
1223.15	$2.97 \cdot 10^{-3}$	$1.10 \cdot 10^{-3}$
1273.15	$2.90 \cdot 10^{-3}$	$1.40 \cdot 10^{-3}$

The average clad temperature is calculated via a volume weighted average.

$$T_c = \sum_{n=N_f+2}^{N_{HS}} \frac{(r_{n+1}^2 - r_n^2)}{(r_{N_{HS}+1}^2 - r_{N_f+2}^2)} \left[\frac{(T_{n+1} + T_n)}{2}\right]. \qquad 2.3.2\text{-}24$$

The maximum clad average temperature is calculated for each EM pin channel and written at each major edit and at the end of each case. The segment number and time of the peak cladding temperature is also specified. The fuel volume weighted average temperature, $\bar{T}_f$, is calculated similarly to the cladding.

$$\bar{T}_f = \sum_{n=1}^{N_f} \frac{(r_{n+1}^2 - r_n^2)}{(r_{N_f+1}^2 - r_1^2)} \left[\frac{(T_{n+1} + T_n)}{2}\right] . \qquad 2.3.2\text{-}25$$

The elastic deformation, u_e, is calculated by

$$u_e = \left[\frac{r_{N_{HS}+1} + r_{N_f+2}}{2}\right] \left[\frac{\sigma_h - \upsilon\sigma_z}{E}\right] , \qquad 2.3.2\text{-}26$$

where

E = Young's modulus for clad (Pa),

σ_h = segment clad hoop stress (Pa),

σ_z = channel clad axial stress (Pa), and

υ = Poisson's ratio for clad (dimensionless).

The channel axial stress is the same for all segments in the channel and is determined by

$$\sigma_z = \frac{P_g\, r_{ic_{cold}}^2 - P_f\, r_{oc_{cold}}^2}{r_{oc_{cold}}^2 - r_{ic_{cold}}^2} . \qquad 2.3.2\text{-}27$$

Young's modulus is given either by the code for zircaloy cladding as

$$E = \begin{cases} 1.088 \cdot 10^{11} - 5.475 \cdot 10^{7}\ T_c; & \text{for } 1090K \geq T_c \\ 1.017 \cdot 10^{11} - 4.827 \cdot 10^{7}\ T_c; & \text{for } 1240K \geq T_c > 1090K \\ 9.21 \cdot 10^{10} - 4.05 \cdot 10^{7}\ T_c; & \text{for } 2027K \geq T_c > 1240K \\ 1.0 \cdot 10^{10}; & \text{for } T_c > 2027K, \end{cases}$$

2.3.2-28

or by a user-specified cubic equation that can be used for zirconium-based alloy cladding

$$E = C_1 T_c^{3} + C_2 T_c^{2} + C_3 T_c + C_4 \cdot$$ 2.3.2-29

Poisson's ratio is a constant which is defined as 0.30 for zircaloy by the code, however, the user can over-ride this value for zirconium-based alloy cladding types.

The normalized heating ramp rate for the elastic mode is determined by one of two methods. The code calculates an instantaneous heating rate for one method, while the other method sets the rate to a normalized user-input value between 0 and 1. The calculated heating rate is normalized via a constant value, H_{Rnorm}, of 28 K/s for zircaloy cladding or a user input for other zirconium-based alloy cladding materials.

$$H = \left\{ \frac{dT_c}{dt} \right\} / H_{Rnorm}$$

$$= \left\{ \frac{T_c^{n} - T_c^{n-1}}{t^{n} - t^{n-1}} \right\} / H_{Rnorm} \cdot$$ 2.3.2-30

The normalized heating rate is always limited to values between 0 and 1 or(0 K/s / H_{Rnorm}) $\leq$ H $\leq$ (28 K/s / H_{Rnorm} = 1) for zircaloy cladding and between ($H_{slow\ input}$ / H_{Rnorm}) $\leq$ H $\leq$ ($H_{fast\ input}$ / H_{Rnorm}) for

other zirconium-based alloy cladding types. This limit is applied to H prior to using it in any subsequent checking or calculations. The superscripts reflect the current time, n, and old time, n-1, values. The zirconium-based alloy slow or fast ramp rate divided by the normalized rate is still limited between 0 and 1, but they do not have to be equal to 0 or 1. Values greater than 0 or less than 1 activate the slow or fast ramp curves at different normalized heating rates.

Mode 2: Unruptured Elastic and Thermal Deformation Within 166.7K (300 F) of the Rupture Temperature

When the clad average temperature is within 166.7K (300 F) of the rupture temperature, the elastic inside clad radius is calculated as shown in Mode 1. This radius is compared against the plastic inside clad radius calculated in Mode 3. If the elastic radius is greater than the plastic radius, then Mode 2 is retained and the inside clad radius is set to the elastic radius. If not, the clad becomes plastic (Mode 3) and the plastic clad calculations are used. An informative message is printed when a segment first becomes plastic. No return to elastic Modes (1 or 2) is permitted once the clad becomes plastic.

$$r_{ic} = MAX(r_{ic_{elastic}}, r_{ic_{plastic}}) . \qquad 2.3.2\text{-}31$$

If $r_{ic_{elastic}} \geq r_{ic_{plastic}}$, Mode = 2 .

If $r_{ic_{elastic}} < r_{ic_{plastic}}$, Mode = 3 .

Mode 3: Unruptured Plastic Deformation

The unruptured plastic deformation is determined by the plastic strain, ϵ_p.

$$r_{ic} = r_{ic_{cold}}(1 + \epsilon_p), \qquad 2.3.2\text{-}32$$

with

$$\epsilon_p = \epsilon_{cps} \exp[-0.02754(T_{rupt} - T_c)], \qquad 2.3.2\text{-}33$$

where ϵ_{cps} is 0.2 * ϵ_B (ϵ_B is the burst strain) based on NUREG-0630 for maximum cladding plastic strain and on user input tables for zirconium-based alloy cladding. The plastic strain or burst strain is determined by a double interpolation relative to H and T_{rupt} in the user input or default NUREG-0630 burst strain Tables 2.3.2-3 and 2.3.2-4. The plastic strain behaves as a ratchet. Once a given plastic strain is reached, no decrease in its value is allowed. In other words, for plastic mode calculations

$$r_{ic} = MAX(r_{ic}^{\,n}, r_{ic}^{\,n-1}), \qquad 2.3.2\text{-}34$$

where the superscripts refer to the current and old time values.

If the plastic mode is selected, the normalized heating ramp rate is calculated from any of three user options: user input constant, average ramp rate, or plastic weighted ramp rate. The normalized average ramp rate is calculated from

$$H = \left\{ \frac{T_c^{\,n} - T_c^{\,P}}{t^{\,n} - t^{\,P}} \right\} \Big/ \; H_{Rnorm} \;, \qquad 2.3.2\text{-}35$$

where

t = time (s),

n = superscript defining the current time, and

p = superscript defining the time in which the clad first went plastic.

The normalized plastic weighted ramp is calculated by

$$H = \left[\frac{\int_{t^p}^{t^n} W(T) \left\{ \frac{dT_c}{dt} \right\} dt}{\int_{t^p}^{t^n} W(T)\, dt} \right] \Big/ \; H_{Rnorm} \qquad 2.3.2\text{-}36$$

Table 2.3.2-3. NUREG-0630 Slow-Ramp Correlations for Burst Strain and Flow Blockage.

Rupture temperature, C	≤10 C/S burst strain, %	≤10 C/S flow blockage, %
600	10	6.5
625	11	7.0
650	13	8.4
675	20	13.8
700	45	33.5
725	67	52.5
750	82	65.8
775	89	71.0
800	90	71.5
825	89	71.0
850	82	65.8
875	67	52.5
900	48	35.7
925	28	20.0
950	25	18.0
975	28	20.0
1000	33	24.1
1025	35	25.7
1050	33	24.1
1075	25	18.0
1100	14	9.2
1125	11	7.0
1150	10	6.5
1175	10	6.5
1200	10	6.5

noding options) chosen by the user. The fine mesh noding option computes the inside radius as

$$r_{ic} = r_{ic_{cold}} (1 + \epsilon_B) \ . \qquad 2.3.2\text{-}39$$

With this option, the gap conductance is calculated as though there is steam in the gap. The steam thermal conductivity is evaluated at the gap temperature and used with the hot gap size to compute the conductance. This option also calculates inside metal-water reaction for the ruptured segment.

The coarse mesh noding option computes the inside clad radius as

$$r_{ic} = r_{ic_{cold}} (1 + \epsilon_{cps}) \ . \qquad 2.3.2\text{-}40$$

This option uses the regular gap gas conductance and does not consider inside metal-water reaction. It is intended for use nominally when the expected rupture length is small when compared to the total segment length. The microscopic effects at the rupture site considered with the fine mesh option are expected to be negligible when compared to the longer segment behavior. With the coarse mesh option, the overall behavior will be more closely controlled by the entire segment rather than just the rupture site conditions.

Within the ruptured channel various calculations are modified at the time of rupture. Each segment within that channel undergoes a mode change. The pin pressure becomes that of the hydrodynamic volume associated with the ruptured segment. An additive form loss coefficient is calculated at rupture based on the clad flow blockage by a simple expression for an abrupt contraction-expansion.

$$K_{add} = \frac{0.5(1 - \beta^2) + (1 - \beta^2)^2}{(\beta^2)^2}, \qquad 2.3.2\text{-}41$$

where

β^2 = fraction of the channel flow area blocked,

= $(1.0 - A_{blocked}/A_{channel})$.

The flow blockage is obtained via a double table interpolation relative to the normalized heating ramp rate and rupture temperature similarly to the clad burst strain. The table is either user supplied or default NUREG-0630 values listed in Tables 2.3.2-3 and 2.3.2-4. The additive value of the loss coefficient is edited at the time of rupture. The flow blockage loss coefficient is added automatically to the problem for a primary pin channel unless the user overrides via a new optional input. If added, the form loss is applied to the forward flow direction for the inlet (bottom) junction and the reverse flow direction for the exit (top) junction attached to the volume in which the clad ruptured. The user option to exclude this form loss addition from the junctions has been included for supplemental pin channels or for certain non-licensing sensitivity studies with multiple cross-connected channels.

Another option has been added to the EM Pin model to help minimize user burden when running EM reflooding heat transfer analyses with BEACH (BAW-10166 Section 2.1.3.8.4). This user-controlled option automatically includes code-calculated pin rupture, droplet break-up (up to 60 percent blockage) for primary pin channels and convective enhancement adjustments for primary or supplemental pin channels. The input grid parameters are modified with the ruptured values and will be retained for use in the reflooding heat transfer calculations. This model is optional and requires input to activate the calculations. If no input is specified the default is that no rupture enhancements will be calculated and no droplet

breakup calculations will be performed for any supplemental pin channels.

When this option is activated, Equations 2.3.2-41.1 through 2.3.2-41.4 will be calculated following cladding rupture for primary pin channels, only. The first calculation performed determines the midpoint elevation of ruptured segment, referenced from the bottom of the pin channel (which coincides with the bottom of the heat structure geometry or reflood stack). This midpoint elevation, Z_{grid}, is the location where the new "grid" is inserted. This elevation is used to determine the droplet break-up effects for the ruptured segment.

$$Z_{grid} = 0.5 \cdot \Delta Z_{rupt_{seg}} + \sum_{j=1}^{rupt\ seg-1} \Delta Z_{seg_j}, \qquad 2.3.2\text{-}41.1$$

where

ΔZ_{seg} = elevation change of pin segment.

The second set of calculations is to calculate rupture droplet breakup efficiency. These calculations are identical to those described in Sections 2.1.3.7. and 2.1.3.8. of Reference 123. The rupture atomization factor, η_{etamax}, is calculated as

$$\eta_{etamax} = \frac{1}{\left[1 + \left\{ (n^{1/3} - 1) \cdot \min(0.60, \epsilon_{fb}) \right\} \right]}, \qquad 2.3.2\text{-}41.2$$

where

n = number of equal size droplets resulting from the split-up of the larger droplets,

= 2.7, from a droplet distribution flux, and

ϵ_{fb} = flow blockage fraction (limited to a maximum of 0.60).

The increase in the droplet surface area from that used for interface heat transfer is defined in Equation 2.1.3-105[123] as

$$\Delta a_{gf} = C_{maxDB} \Theta \; a_{gf} \; .$$

The proportionality constant, C_{maxDB}, is determined from the constant, C_1, the rupture flow blockage fraction (limited to a maximum of 0.60), and the length of the ruptured segment.

$$C_{maxDB} = \frac{C_1 \bullet \min(0.6 \; , \epsilon_{fb})}{\Delta Z_{rupt_{seg}}} \; . \qquad 2.3.2\text{-}41.3$$

The recommended value of C_1 is 1.22 meters (4.0 feet).

The velocity of the fluid at the ruptured location increases because of the flow area reduction. The physical area in the code calculations is not modified, but a velocity multiplier, used for determining the droplet Weber number, is calculated from

$$VELMULT = \frac{1}{1 - \min(0.6 \; , \epsilon_{fb})} \; . \qquad 2.3.2\text{-}41.4$$

The cladding rupture results in an increase in the pin outside heat transfer surface area. The increase in area is not directly included in the conduction solution in the code calculations. It is accounted for by using the rupture convective enhancement factor and applying it to the grid wall heat transfer enhancement factor, F_{gq}, for primary or supplemental channels. The rupture enhancement, M_{RAR}, is an multiplicative contribution determined by

$$M_{RAR} = \text{Rupture Area Ratio}$$

$$= \frac{2\pi \; r_{rupt_{oc}} \; L}{2\pi \; r_{oc_{cold}} \; L} = \frac{r_{rupt_{oc}}}{r_{oc_{cold}}} \; , \qquad 2.3.2\text{-}41.5$$

where

$r_{rupt_{oc}}$ = outside clad radius of the ruptured node given by

$$= r_{ic} + \left[r_{oc\,cold} - r_{ic\,cold} \right] \left[r_{ic\,cold} / r_{ic} \right] . \quad 2.3.2\text{-}41.6$$

The total wall heat transfer convective factor then becomes

$$F_{gq_{tot}} = F_{gq_{grid}} \cdot M_{RAR} . \quad 2.3.2\text{-}41.7$$

These droplet break-up and convective enhancement terms are optionally calculated and edited at rupture by the EM pin model.

This page intentionally blank.

r_{ic_u} = inside clad radius of the top pin segment (m), and

ΔL_p = change in gas plenum length (m).

The change in gas plenum length is calculated from the net change in the fuel and clad stack lengths due to axial thermal expansions as follows. Let

ΔL_{cf} = change in gas plenum length from cold condition (m),

$$= \Delta L_c - \Delta L_f \ , \qquad 2.3.2\text{-}51.4$$

where

ΔL_c = total axial thermal expansion of clad from cold condition (m),

$$= \sum_{j=1}^{\#\ seg} (L_j \ \epsilon_{ATC_j}) \ , \text{ and} \qquad 2.3.2\text{-}51.5$$

ΔL_f = total axial thermal expansion of fuel from cold condition (m),

$$= \sum_{j=1}^{\#\ seg} (L_j \ \epsilon_{ATF_j}) \ . \qquad 2.3.2\text{-}51.6$$

Then

ΔL_p = change in gas plenum length from hot initial condition (m),

$$= \Delta L_{cf} - \Delta L^o_{cf} \ , \qquad 2.3.2\text{-}51.7$$

where

ΔL^o_{cf} = initial over-specification in gas plenum length (m), determined during pin transient initiation,

L_j = axial length of the jth segment (m),

ϵ_{ATF} = fuel strain function of Equation 2.3.2-15, evaluated at fuel volume weighted average temperature $\bar{T}_f$ of Equation 2.3.2-25, (dimensionless), and

ϵ_{ATC} = axial strain function defining clad axial thermal expansion as a function of clad volume average temperature, (dimensionless).

The axial strain for the cladding is defined by either a user-input table versus cladding temperature for zirconium-based alloy cladding (Note: This table replaces the cubic fit from Rev. 3 Eqn 2.3.2-51.8.) or a built in code correlation set for zircaloy cladding[119]

$$\epsilon_{ATC} = -2.506 \times 10^{-5} + (T_C - 273.15)\ 4.441 \times 10^{-6}$$
$$= -1.2381 \times 10^{-3} + 4.441 \times 10^{-6}\ T_C \qquad 2.3.2\text{-}51.9$$

for $T_C \leq$ 1073.15 K (α phase), or

$$\epsilon_{ATC} = -8.3 \times 10^{-3} + (T_C - 273.15)\ 9.7 \times 10^{-6}$$
$$= -1.0950 \times 10^{-2} + 9.7 \times 10^{-6}\ T_C \qquad 2.3.2\text{-}51.10$$

for $T_C \geq$ 1273.15 K (β phase), where T_C is the volume average cladding temperature (K) of Equation 2.3.2-24. In the α phase to β phase transition zone, 1073.15 K < T_C < 1273.15 K, a table lookup is used. Some selected values are listed in Table 2.3.2-2.

Using the assumption that both the slope of the fuel mesh point temperatures and the overall gap conductance will not change significantly, the last gap multiplier (1.0 for the first iteration) can be adjusted via a ratio to give a new multiplier,

$$M_g^{\eta+1} = \frac{\Delta T_{gap}}{(\Delta T_{gap} + \Delta \bar{T}_f)} M_g^{\eta} \quad . \qquad 2.3.2\text{-}52.3$$

After calculation of the new gap multiplier, another conduction solution iteration step is taken. The fuel volume average temperature differential is recalculated via Equation 2.3.2-52.1. If the absolute value is greater than 2 K, then another iteration step is taken after recalculating a new multiplier via Equations 2.3.2-52.2 and 2.3.2-52.3. If the absolute value is less than 2 K, then the iteration has converged and the last multiplier calculated is edited and used during the steady-state and transient EM pin calculations. Up to twenty-one iterations are allowed. If convergence is not obtained in twenty-one iterations, then the code will stop at the end of the initialization process and appropriate failure messages will be edited. Failure of the iteration to converge is generally related to poor estimates given for the initial mesh point temperature distribution. An improved estimate will normally allow the iteration to converge properly. If convergence is still a problem, user specification of the multiplier is also available.

At the completion of the EM pin steady-state calculations (i.e., after EM pin steady-state trip becomes true or during the first time step if there is no trip) several calculations are required to initiate the pin transient calculations. The user-supplied cold unstressed pin geometry input via the heat structure cards is elastically expanded using the final code calculated temperature and mechanical stresses.

$$r_{f_o} = r_{f_{cold}} + u_{TF} \qquad 2.3.2\text{-}53$$

and

$$r_{ic_o} = r_{ic_{cold}} + u_{TC} + u_e + u_{fcc}, \qquad 2.3.2\text{-}54$$

with

r_{f_o} = thermally expanded outside fuel radius (m),

r_{ic_o} = thermally and mechanically expanded inside clad radius (m),

u_e = elastic deformation due to mechanical stresses (m), and

u_{fcc} = elastic deformation from gap mechanical contact (m). This term is calculated from the user supplied input contact pressure and cladding radii during the initialization.

$$u_{fcc} = \frac{P_{fcc} \cdot r_{ic}}{E_c} \left\{ \left[\frac{r_{oc}^2 + r_{ic}^2}{r_{oc}^2 - r_{ic}^2} \right] + \nu_c + \frac{E_c}{E_f} (1 - \nu_f) \right\} \qquad 2.3.2\text{-}54.1$$

The calculated radii are compared against the input values by

$$u_{FC} = r_{f_{input}} - r_{f_o} \qquad 2.3.2\text{-}55$$

$$u_{CC} = r_{ic_{input}} - r_{ic_o}, \qquad 2.3.2\text{-}56$$

and

$$u_{cg} = \begin{cases} 0.0, & \text{for } P_{fcc_{input}} = 0.0 \\ r_{ic_{input}} - r_{f_{input}}, & \text{for } P_{fcc_{input}} > 0.0 \end{cases} \qquad 2.3.2\text{-}56.1$$

5.0 REFERENCES

1. Ransom, V. H., et. al., RELAP5/MOD2 Code Manual -- Volume 1: Code Structures, System Models and Solution Methods and Volume 2: Users Guide and Input Requirements, NUREG/CR-4312 - Volume 1, August, 1985 and NUREG/CR-4312 - Volume 2, December 1985.

2. B&W Nuclear Technologies, RELAP5/MOD2-B&W -- An Advanced Computer Program for Light Water Reactor LOCA and non-LOCA Transient Analysis, BAW-10164P, Revision 1, October 1988.

3. Letter from A. C. Thadani (USNRC) to J. H. Taylor (B&W Nuclear Technologies), Acceptance for Referencing of Topical Report BAW-10164P, Revision 1, RELAP5/MOD2-B&W, An Advanced Computer Program for Light Water Reactor LOCA and Non-LOCA Transient Analysis, April 18, 1990.

4. Code of Federal Regulations, ECCS Evaluation Models, Chapter 10, Part 50, Appendix K

5. B&W Nuclear Technologies, RELAP5/MOD2-B&W -- An Advanced Computer Program for Light Water Reactor LOCA and Non-LOCA Transient Analysis, BAW-10164P, Revision 2, August 1992.

6. B&W Nuclear Technologies, RELAP5/MOD2-B&W -- An Advanced Computer Program for Light Water Reactor LOCA and non-LOCA Transient Analysis, BAW-10164P, Revision 3, October 1992.

7. Letter from J. H. Taylor (B&W Nuclear Technologies) to R. C. Jones (USNRC) BEACH Topical Report BAW-10166P, JHT/93-214, August 31, 1993.

8. Letter from J.H. Taylor (B&W Nuclear Technologies), Response to NRC's Request for Additional Information on BAW-10164, Revision 2, August, 1992; RELAP5/MOD2-B&W, An Advanced Computer Program for Light Water Reactor LOCA and NON-LOCA Transient Analysis, JHT/93-279, November 16, 1993

9. Letter from J.H. Taylor (B&W Nuclear Technologies), Response to NRC's Request for Additional Information on BAW-10164, Revision 3, October, 1992; RELAP5/MOD2-B&W, An Advanced Computer Program for Light Water Reactor LOCA and NON-LOCA Transient Analysis, JHT/94-7, January 21, 1994

10. Letter from J.H. Taylor (B&W Nuclear Technologies), Response to NRC's Supplemental Request for Additional Information on BAW-10164, Revision 2, August, 1992; RELAP5/MOD2-B&W, An Advanced Computer Program for Light Water Reactor LOCA and NON-LOCA Transient Analysis, JHT/94-146, September 20, 1994.

This page intentionally left blank.

Appendix L
Response to Questions on Pre-Rupture Swelling

ATTACHMENT

Discussion of Cladding Cooling Characteristics Under Pre-Rupture Swelling Conditions Including Potential Flow Diversion Effects

Although fuel pin cladding within a fuel assembly can swell prior to rupture creating a bulge that interferes with the local coolant passage, the Framatome LOCA evaluation models do not include flow diversion around this swelling until after a rupture has been calculated. For the Zircaloy evaluation models the justification that not including a pre-rupture flow diversion model was conservative comprised:

1. Fuel pin swelling prior to rupture generates continuously curved surfaces that are efficient in passing fluid and do not generate large pressure drops to induce flow diversion.

2. The maximum swelling of the individual fuel pins was limited in the approved Zircaloy swelling models to 20 % strain limiting channel blockages to less than 34 %.

3. Analytical evaluations indicated that cladding swelling of 20 % will decrease flow around the swelling slightly, increase the cladding heat transfer area, and increase the local fluid velocity. These effects combine to produce a net improvement in heat transfer through the swelling zone. These studies also indicated that the flow would recover rapidly downstream of the swelling such that downstream cooling is unaffected by the cladding swelling

4. Experiments modeling swelled fuel pins showed that net heat transfer from the cladding was increased for assembly blockages up to 62 %.

Because the pre-rupture swelling possible with Zircaloy was limited to 20 % strain, 34 % channel blockage, no consideration was given to larger pin strains or blockages and the EMs applicability was limited to cladding strains of 20 % or less pending additional justification. The approved M5 alloy pre-rupture swelling curves allow substantially higher pre-rupture swelling and blockages. Strains up to 56 %, blockages of 88 %, occur at the extremes of the calculations. However, even for strains and blockages this high, a more complete consideration of the available experimental and analytical results supports the conclusion that pre-rupture swelling enhances rather than degrades the heat transfer process within the affected assembly. Therefore, not including a pre-rupture flow diversion model in the LOCA evaluation models remains a neutral to conservative approach. The revised justification for not including a pre-rupture flow diversion model consists of:

1. Fuel pin swelling prior to rupture generates continuously curved surfaces that are efficient in passing fluid and do not generate large pressure drops to induce flow diversion.

2. The axial position of swelling bulges on individual fuel pins is randomly distributed within the immediate grid span such that diversion is primarily between sub-channels and not fuel assemblies.

3. Fuel assemblies adjacent to the hot assembly, to which assembly flow could be diverted, experience similar swelling providing a buffer to impede any diversion.

4. Analytical evaluations indicated that cladding swelling will decrease flow around the swelling, increase the cladding heat transfer area, increase local fluid velocities, promote turbulence, and possibly liquid droplet vaporization to reduce vapor temperatures. These effects combine to produce a net increase in heat transfer through the swelling zone.

5. Experiments, the FEBA program, directly modeling systems of partially blocked coolant channels, swelled fuel pins, adjacent to normal unblocked coolant channels, unswelled pins, indicated that the heat transfer process is more efficient in both the blocked and the adjacent unblocked channels for swelling-induced blockages up to 90 %, Reference 1.

The most significant of these factors is the FEBA program results. The FEBA simulation directly addresses flow diversion effects. Both obstructed and normal flow channels were simulated. The blockage simulators were of a conical geometry characteristic of pre-rupture swelling. An additional flow bypass around the normal channels was provided to simulate a larger test assembly. Yet no adverse impact on fuel pin cooling in either the obstructed or the unobstructed regions of the fuel was observed. Cooling in both the blocked region and the unblocked region was slightly improved for a 62 % obstruction simulation. For the 90 % blockage simulation, cooling may have been improved slightly but is essentially the same as for the completely unobstructed base line assembly until after the time of peak cladding temperature. Some delay in long term cooldown (post PCT) was indicated for the 90 % blockage case. No such effect was evident in the 62 % blockage case. The judgement as to pre-rupture cooling effects should be based on fluid conditions of low flow and high quality. Thus, the early periods of these experiments are the most representative of the conditions under which pre-rupture flow diversion would occur.

A slightly different interpretation of the FEBA results, Reference 2, was presented at the 1983 Water Reactor Safety Research Information Meeting. In a figure on page 204 of the WRSM report, the temperature rise, peak cladding temperature minus the initial temperature, for the blocked channels downstream of the blockage was compared to the temperature rise at the same elevation for reference unblocked tests. Only 3 of the 54 comparisons showed blocked cladding experiencing higher temperature rises than the base line unblocked tests. One of these had an increased rise of less than 10 C and the other two were under 25 C. One of the conclusions from Reference 1 provides a good summary, "For subchannel blockage ratios of 90 %, the mass flux reduction dominates slightly leading to a moderate increase of cladding temperatures (50K) just downstream of the blockage compared with the same axial position in the bypass {*unblocked section of same test*}. However, compared with unblocked bundle conditions {*base line test*} there is no increase of the maximum cladding temperatures for 90 % blockages for 65 mm axial length."

With the exception of droplet interactions, the arguments provided apply equally to large break simulations and to small break simulations above the core mixture height. These results verify that the Framatome approach of not including a simulation of pre-rupture flow diversion is

conservative for coolant channel obstructions up to 90 %. Therefore, the additional justification for strains in excess of 20 % has been provided and the M5 LOCA evaluations need not directly consider pre-rupture induced flow diversion effects for cladding strains up to 56 %.

Reference 1: P. Ihle and K. Rust, FEBA - Flooding Experiments with Blocked Arrays, Evaluation Report, KFK3657, March 1984.

Reference 2: Donald M. Ogden, "Review of FEBA Blockage Data," NUREG/CR-0048 Vol 1, 11th Water Reactor Safety Research Meeting, USNRC, 1983.

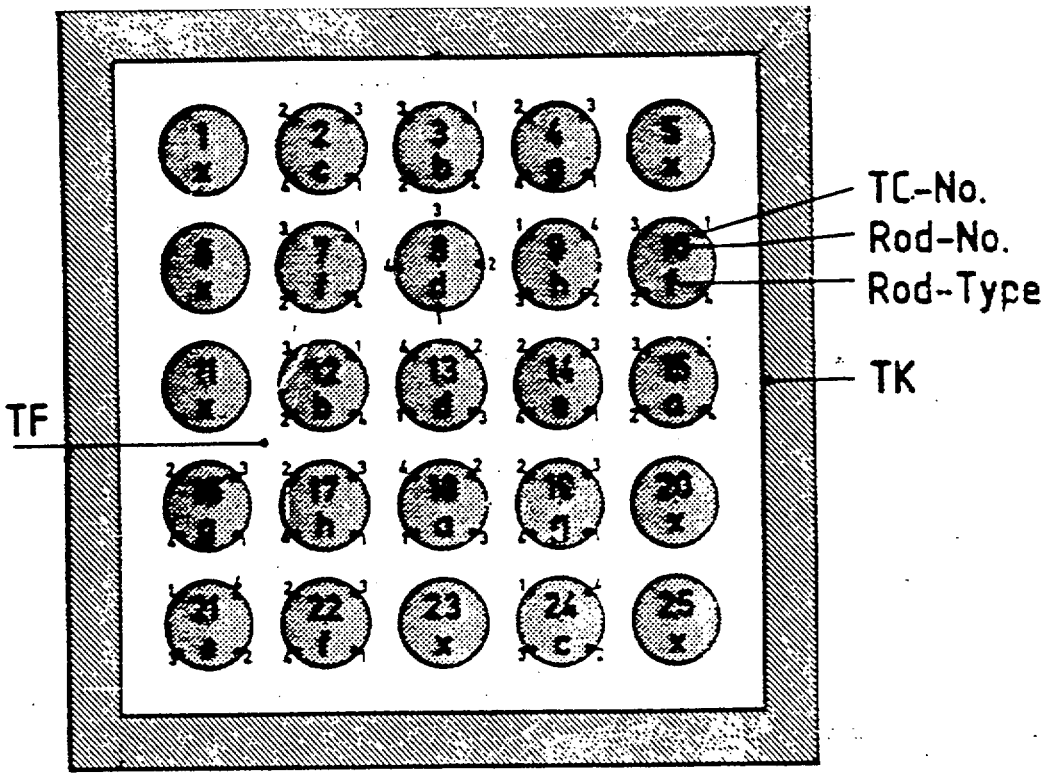

Rod Type	TC No.	Axial Level mm
a	1	2225
	2	2770
	3	3315
	4	3860
b	1	45
	2	590
	3	1135
	4	1680
c	1	3725
	2	3825
	3	3925
	4	4025
d	1	2025
	2	2025
	3	2025
	4	2025

Rod Type	TC No.	Axial Level mm
e	1	2075
	2	2125
	3	2175
	4	2225
f	1	2125
	2	2225
	3	2325
	4	2425
g	1	1625
	2	1725
	3	1825
	4	1925
h	1	1925
	2	2025
	3	2125
	4	2225

Rod Type	TC No.	Axial Level mm
x	without TC's	

Fig. 24 5x5 rod bundle: Radial and axial location of cladding, fluid and housing TC's for test series II

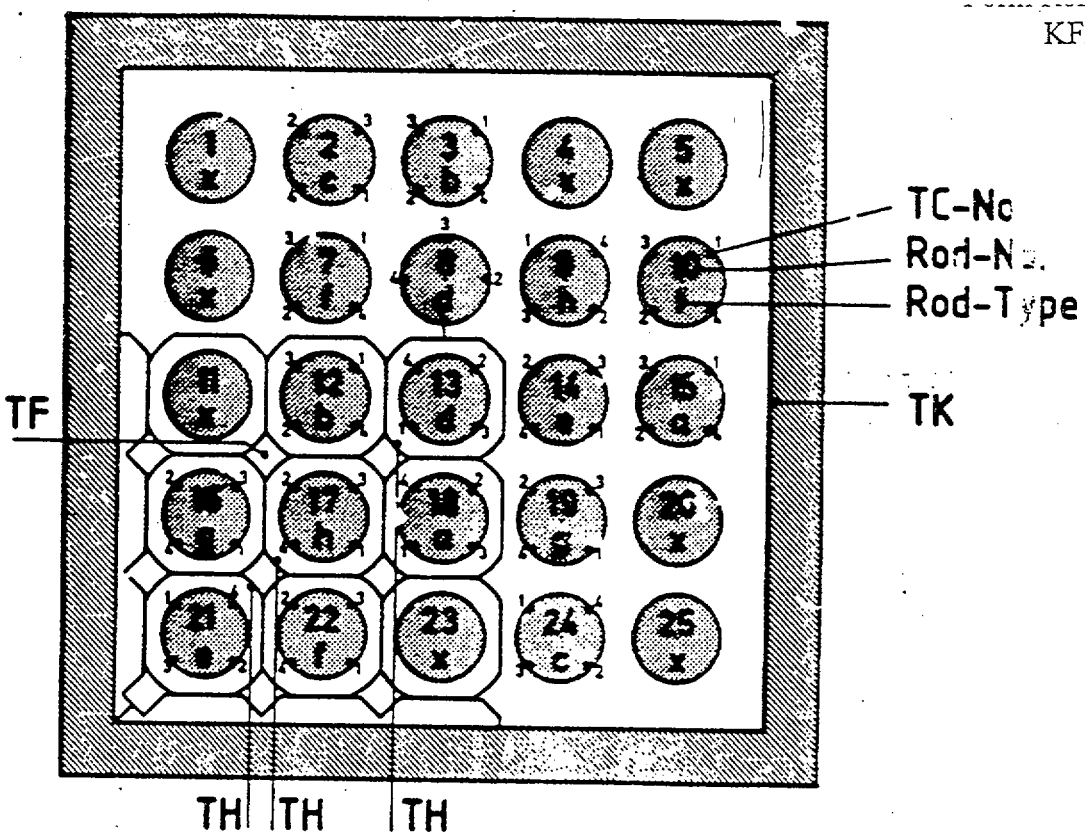

Rod Type	TC No.	Axial Level mm
a	1	2225
	2	2770
	3	3315
	4	3860
b	1	45
	2	590
	3	1135
	4	1680
c	1	3725
	2	3825
	3	3925
	4	4025
d	1	2025
	2	2025
	3	2025
	4	2025

Rod Type	TC No.	Axial Level mm
e	1	2075
	2	2125
	3	2175
	4	2225
f	1	2125
	2	2225
	3	2325
	4	2425
g	1	1625
	2	1725
	3	1825
	4	1925
h	1	1925
	2	2025
	3	2125
	4	2225

Rod Type	TC No.	Axial Level mm
x	without TC's	

Fig. 25 5x5 rod bundle: Radial and axial location of cladding, sleeve, fluid and housing TC's for test series III

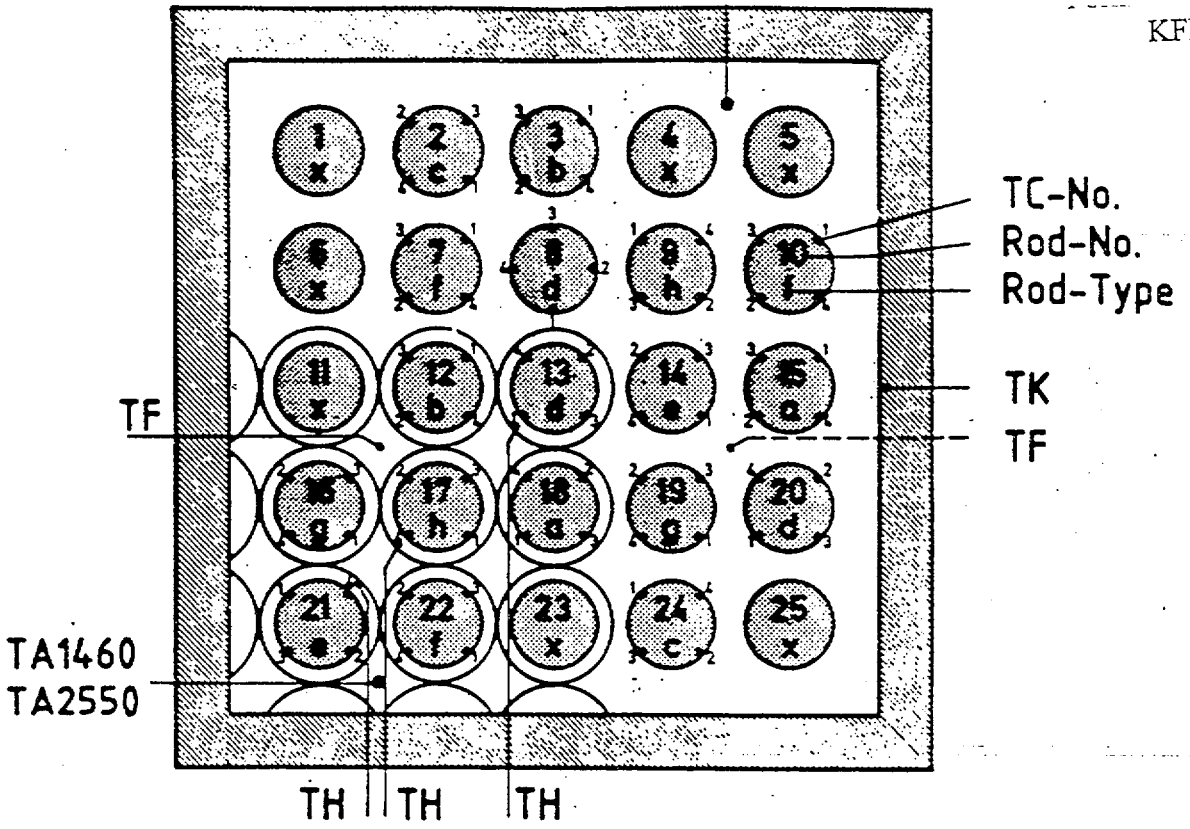

Rod Type	TC No.	Axial Level mm
a	1	2225
	2	2770
	3	3315
	4	3860
b	1	45
	2	590
	3	1135
	4	1680
c	1	3725
	2	3825
	3	3925
	4	4025
d	1	2025
	2	2025
	3	2025
	4	2025

Rod Type	TC No.	Axial Level mm
e	1	2075
	2	2125
	3	2175
	4	2225
f	1	2125
	2	2225
	3	2325
	4	2425
g	1	1625
	2	1725
	3	1825
	4	1925
h	1	1925
	2	2025
	3	2125
	4	2225

Rod Type	TC No.	Axial Level mm
x	without TC's	

Fig. 26 5x5 rod bundle: Radial and axial location of cladding, sleeve, spacer, fluid and housing TC's for test series IV

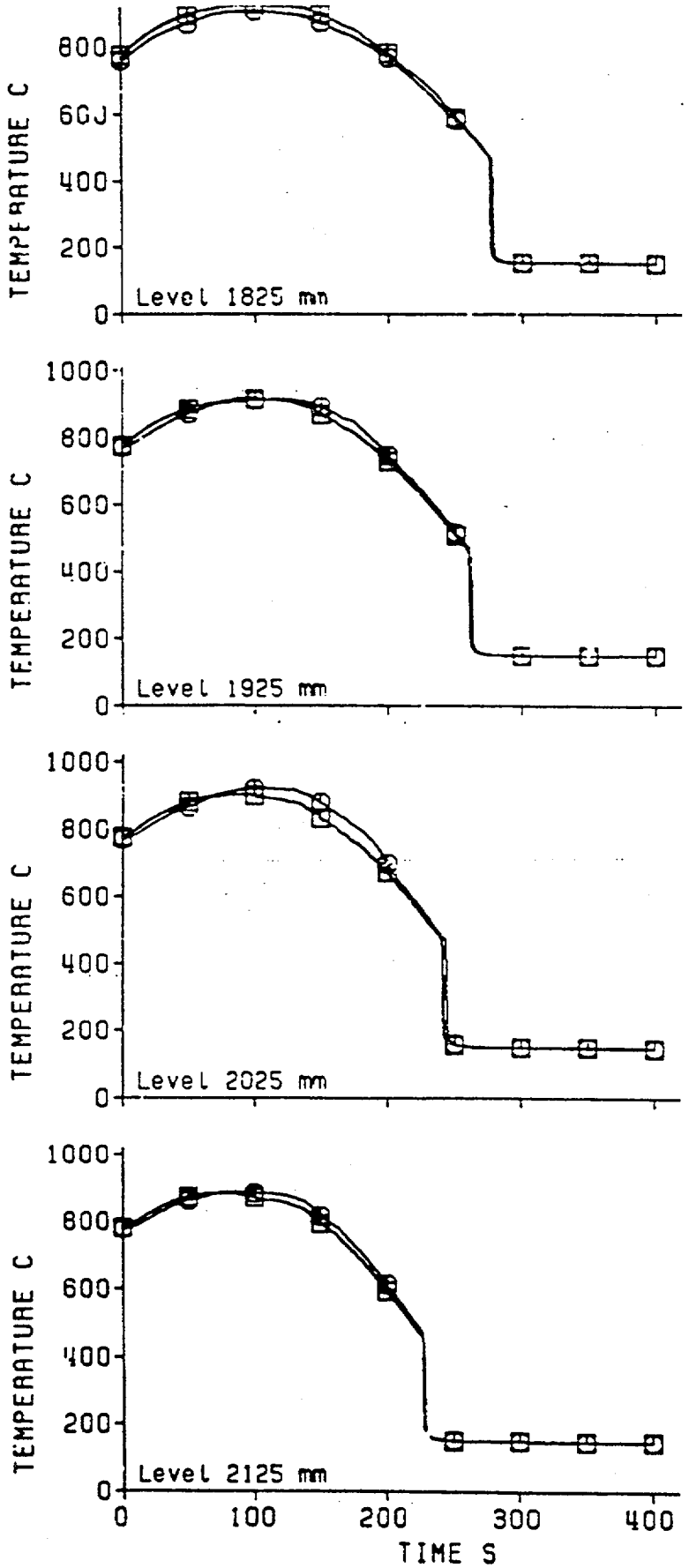

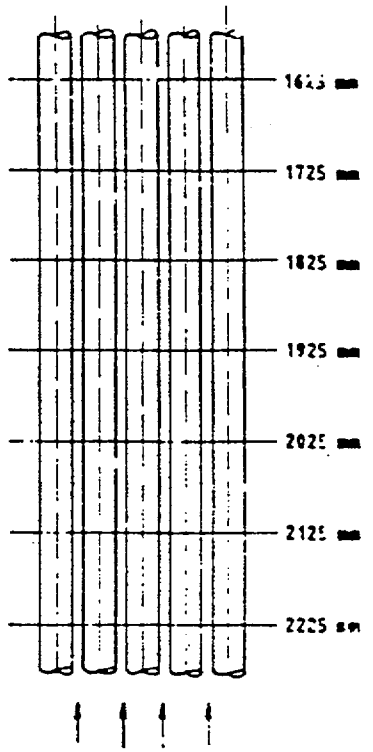

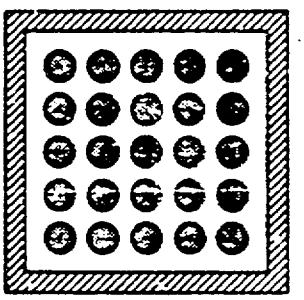

Test No. 229
6 Grid Spacers
Unblocked Bundle

Flooding Rate 3.8 cm/s
Pressure 4.1 bar

□ "Bypass Region"
⊙ "Blocked Region"

Fig. 42 5x5 rod bundle: Test series II, cladding temperatures

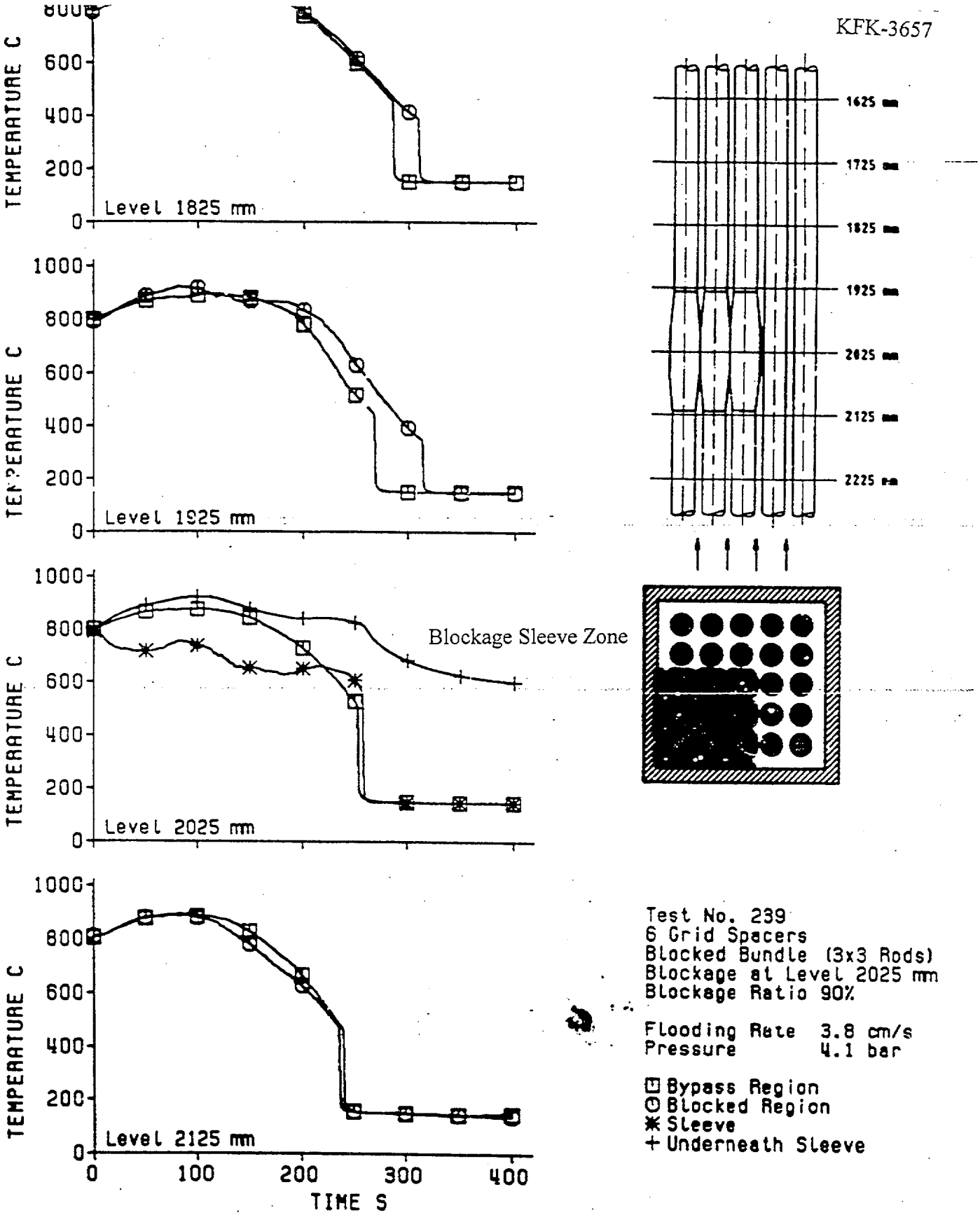

Fig. 44 5x5 rod bundle: Test series III, cladding temperatures

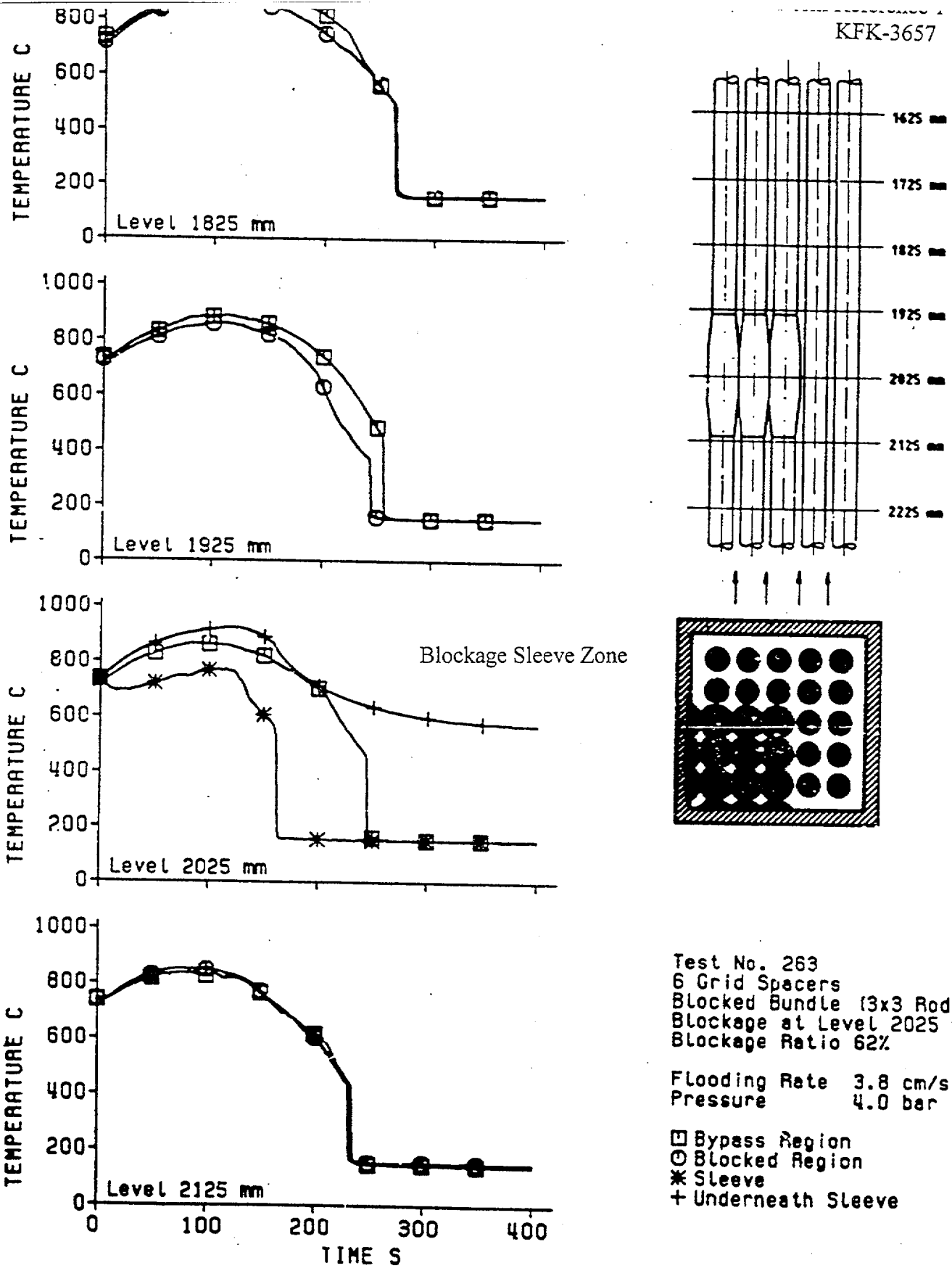

Test No. 263
6 Grid Spacers
Blocked Bundle (3x3 Rods)
Blockage at Level 2025 mm
Blockage Ratio 62%

Flooding Rate 3.8 cm/s
Pressure 4.0 bar

⊡ Bypass Region
⊙ Blocked Region
✱ Sleeve
+ Underneath Sleeve

Fig. 45 5x5 rod bundle: Test series IV, cladding temperatures

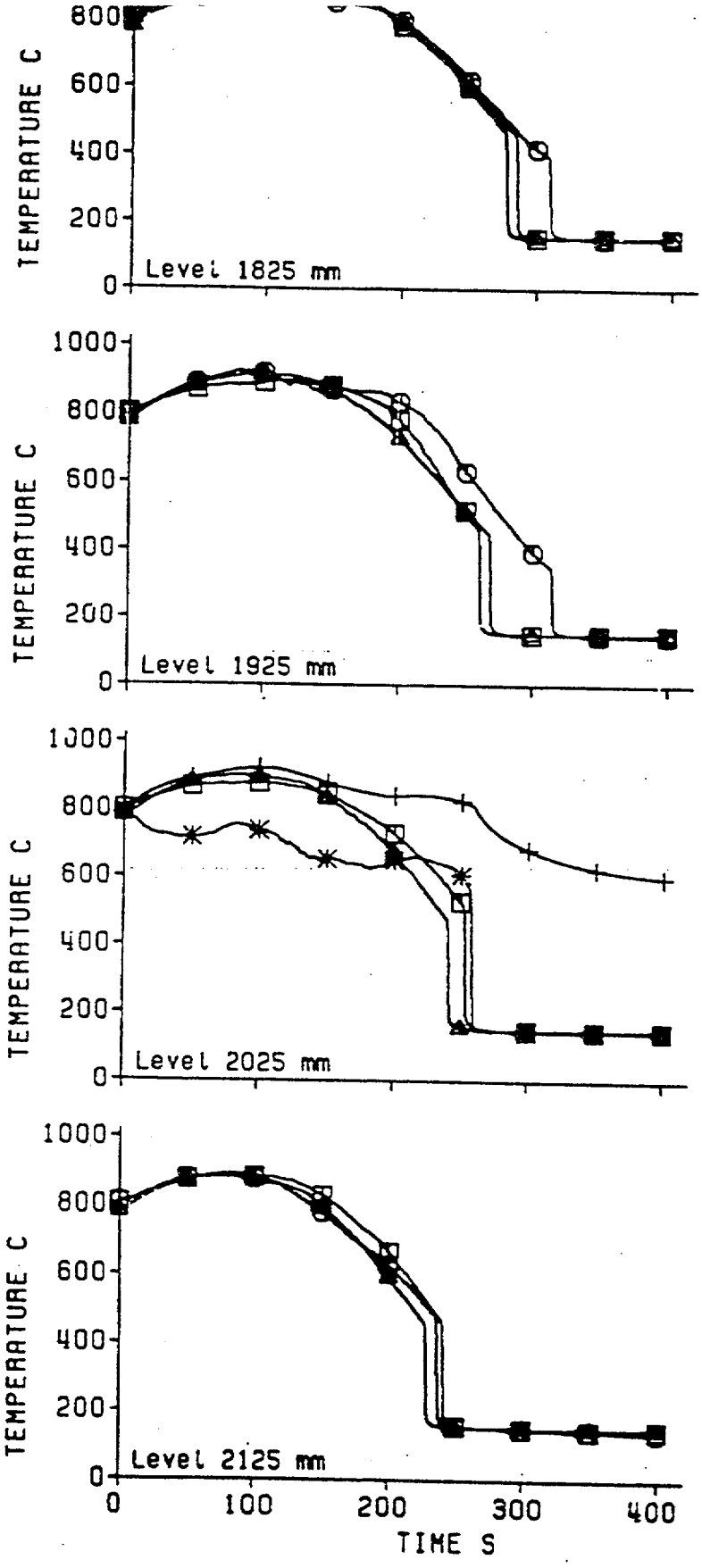

Blockage Sleeve Zone

Flooding Rate 3.8 cm/s
System Pressure 4.0 bar

Test Series II

Test No. 229
6 Grid Spacers
Unblocked Bundle

▲ Cladding

Test Series III

Test No. 239
6 Grid Spacers
Blocked Bundle (3x3 Rods)
Blockage at Level 2025 mm
Blockage Ratio 90%

⊡ Bypass Region
⊙ Blocked Region
✱ Sleeve
+ Underneath Sleeve

Fig. 57 5x5 rod bundle: Test series II + III, cladding temperatures

FEBA Comparison Tests

Blockage/ Grid Test	Test Type	Unblocked Test	Pressure (MPa)	Flooding Rate (cm/s)
241	90%	234	0.20	3.8
242	90%	234	0.20	3.8
243	90%	234	0.20	3.8
261	62%	233	0.20	5.7
262	62%	234	0.20	3.8
263	62%	229	0.39	3.8
264	62%	228	0.39	5.8
268	62%	231	0.59	3.8
269	62%	230	0.59	5.7